Distributed Energy Program
FY05 Annual Reports

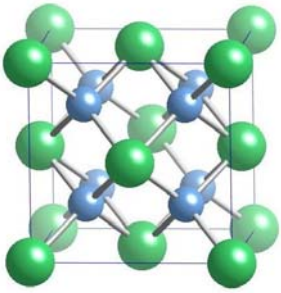

Table Of Contents


ARES

1.1 Rotating Arc Spark Plug (RASP)

Jim Parks (primary contact) and Jim Tassitano
Fuels, Engines, and Emissions Research Center
Engineering, Science and Technology Division
Oak Ridge National Laboratory
(865) 946-1527, E-mail: tassitanojb@ornl.gov; parksjeii@ornl.gov

DOE Technology Development Manager: Ron Fiskum
(202) 586-9154; fax: (202) 586-7114; e-mail: ronald.fiskum@ee.doe.gov
ORNL Technical Monitor: Tim Theiss
(865) 946-1348; fax; (865) 946-1248; e-mail: theisstj@ornl.gov

---

Objective

- Develop a working prototype rotating arc spark plug (RASP) on a natural gas engine.
- Show if there is any benefit—measured by an increase in lean limit operation or decrease in the coefficient of variation of heat release—in using the RASP concept.

Approach

- Compare the performance characteristics of the RASP (annular gap spark plug with magnet), non-rotating annular gap spark plug, and standard J-plug in a natural gas engine using the stock ignition system over the entire range of operation.
- Develop an ignition system designed to optimize RASP performance and repeat testing noting the relative and absolute improvements in performance of each configuration.

Accomplishments

- Demonstrated a RASP prototype capable of running a natural gas engine.
- Developed and evaluated an ignition system designed to improve RASP performance.
- Performed detailed evaluation of all plugs, including multiple RASP configurations, using both the stock and improved ignition systems.
- Results of our analysis showed that RASP performance was not beneficial over a standard spark plug under similar conditions. Furthermore, the performance of the non-rotating annular gap spark plug was similar or slightly better than the RASP possibly due to the energy lost in creating the rotation in the RASP.

Possible Future Research

- Based on existing results, the decision has been made not to continue RASP development in FY06.
- If additional development is performed, visual verification of rotation during engine operation using a Visio scope would be useful. Investigate the influence of rotation speed on performance to see if this will improve ignition.
- Investigate potential erosion benefits of the RASP.

Introduction

As emissions regulations become more stringent, it becomes important to be able to achieve stable operation of natural gas engines at increasingly lean air-fuel ratios. At leaner operating conditions, creating consistent ignition and combustion is difficult. To this end, the rotating arc spark plug (RASP) was developed. By using an annular gap spark plug in conjunction with a magnet, a larger spark volume can be created. The larger the spark volume, the more likely that the spark will come into contact with a combustible air and fuel mixture. This should then help reduce cycle-to-cycle variability allowing more stable operation at leaner air–fuel ratios.

Approach: Plug development

The RASP was designed to operate with a permanent magnet located near the spark, which occurs in an annular gap. This forms a magnetic field around the spark plug and as the plug discharges, the spark is propelled around the annulus at a rate that is proportional to the strength of the magnetic field and the current in the arc. Three different varieties of spark plugs were created to explore how a change in location of the spark relative to the combustion chamber and the magnet affect ignition and can be seen in Figure 1. All of the plugs were manufactured by Champion with gap sizes varying from 0.015 to 0.045 in. The performance of these plugs was then compared with and without the magnet as well as with that of the recommended spark plug for this engine: a standard J-plug with an air gap of 0.040 inches.

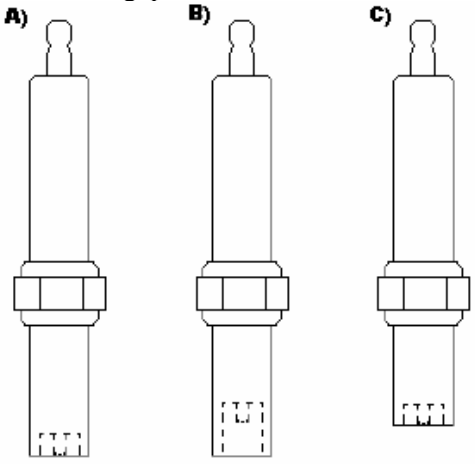

Figure 1 - A) Standard reach B) Recessed C) Short Reach

Approach: Equipment and Testing

A natural gas Kohler Command 25 generator was used to test the spark plugs. The initial tests were performed using the Kohler's stock ignition system. The Kohler generator-set is a two-cylinder four-stroke engine designed to operate at stoichiometric conditions at a steady 3600 rpm. It is rated at 11 kW and has a BMEP of 505 kPa and a compression ration of 9.0:1. The throttle was electronically controlled to maintain this speed at all attainable loads. The air-to-fuel ratio was controlled by restricting the natural gas flow with a valve and measured by an oxygen sensor placed in the exhaust stream of one of the cylinders.

Two different ignition systems were used to evaluate the performance of the plugs. The first ignition system was the stock ignition system that came on the unit. This unit provided a relatively weak spark of short duration. The second ignition system used an MSD ignition unit controlled by a Labview program. This created a strong spark with a duration roughly 4 times longer than the Kohler ignition unit. The annular gap spark plugs were then tested with and without the magnet and the J-plug was tested under identical operating conditions for comparison. The plug configurations can be seen in Figure 2.

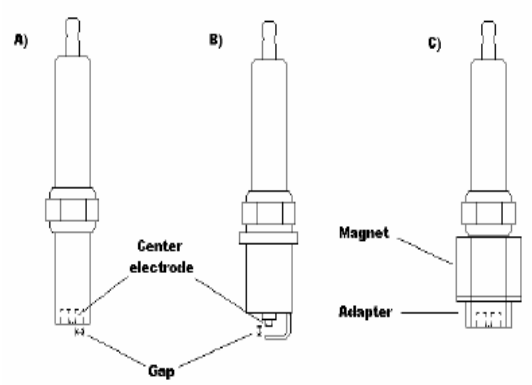

Figure 2 - A) annular gap spark plug, B) J-plug, C) RASP

Results

The evaluation of the plugs showed that the J-plug performed better than either the RASP or the annular gap plugs. The use of a higher energy ignition system extended the lean limit of the RASP and improved the performance of all the plugs slightly approaching the lean limit shown in Figure 3.

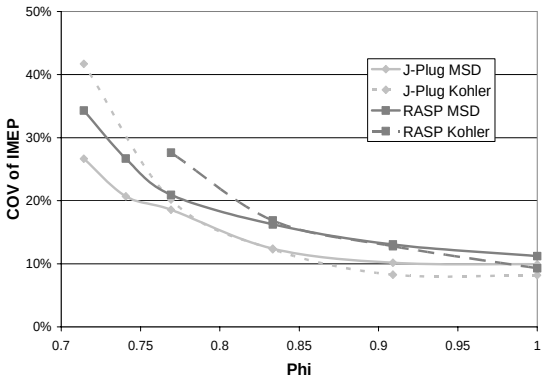

Figure 3 - Comparison of the RASP and J-plug using both ignition systems

A close look at the performance of the RASP and the annular gap spark plugs shows that their performance is nearly identical, but averaged over many runs it appears that the addition of the magnet to otherwise identical plugs may reduce performance slightly. The presence of the magnetic field may also restrict the movement of ionized gasses and be detrimental to the ignition process.

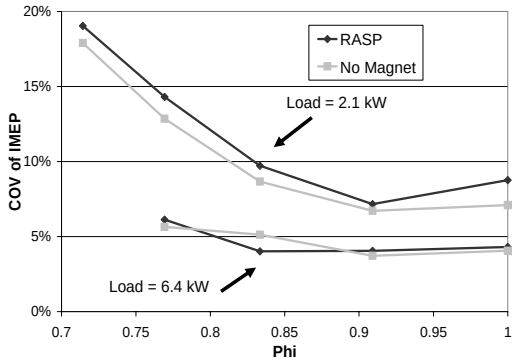

Figure 4 - Comparison of RASP vs. annular gap spark plug at different loads

Conclusions

- J-plug produced lower coefficients of variation of IMEP over all test points when compared to the RASP.
- Performance of RASP was nearly indistinguishable from the annular gap spark plug and if anything had slightly worse performance, which can be accounted for in slightly lower ignition energy possibly caused by the presence of the magnet.
- The relatively poor performance of the RASP could be mitigated by a redesign that reduces the thermal mass of the plug near the ignition point and improves the access of the spark to the combustion chamber

Unresolved Issues

- Still not certain that the RASP actually rotates the spark inside of an operating engine
- Speed of spark rotation may be too slow to make any real difference in ignition
- Adaptation of design to a ferrous engine head is non-trivial
- Industrial partners have suggested that RASP performance may improve if used in a higher BMEP engine

Publications/Presentations

1. J. B. Tassitano and J.E. Parks II, "Analysis of the Rotating Arc Spark Plug in a Natural Gas Engine", *Proceedings of Internal Combustion Engine Division of ASME 2005 Fall Technical Conference, ICEF2005-1293, 2005.*

1.2 Characterization and Development of Spark Plug Materials and Components

H. T. Lin[*] (primary contact), R.K. Richards,[**] and M. P. Brady[*]
[*]Metals and Ceramics Division
[**]Engineering Science & Technology Division
Oak Ridge National Laboratory, Oak Ridge, TN 37831-6068
Phone: (865) 576-8857; Fax: (865) 574-6098; E-mail: linh@ornl.gov

DOE Technology Program Manager: Ron Fiskum
Phone: (202) 586-9154; Fax: (202) 586-7114; E-mail: Ronald.Fiskum@ee.doe.gov
ORNL Technical Advisors: Tim Theiss and David Stinton
Phone: (865) 946-1348; Fax: (865) 946-1248; E-mail: theisstj@ornl.gov
Phone: (865) 574-4556; Fax: (865) 241-0411; E-mail: stintondp@ornl.gov

---

Objective
- Provide insight into the wear mechanisms of natural gas spark plug electrodes as a function of field exposure time and engine conditions.
- Increase the wear resistance of spark plug electrode materials to at least 1 year in advanced natural gas reciprocating engines designed to meet aggressive emission and efficiency goals.

Approach
- Characterize engine tested spark plugs to identify key erosion mechanisms and limitations of existing materials.
- Develop and optimize new electrode materials for improved erosion resistance based on results from the characterization effort.

Accomplishments
- Conducted spectroscopic and metallurgical analysis of conventional spark plugs tested over a range of time, ignition systems, and engine exposure conditions that led to new mechanistic understanding of electrode oxidation and cracking mechanisms that appear to control spark plug wear in natural gas engines.
- Received and analyzed 2 sets of unconventional plugs directly from end users, which showed a dependence of wear rate related to different engine operating conditions. These results are noteworthy i.e. they are consistent with our understanding of electrode wear, and give significant confidence in the ability of analysis protocol to provide mechanistic insight.
- Incorporated spectroscopic observations into a model of wear/erosion to aid the design of new plug materials.
- Collaborated with Federal Mogul (Champion®), to include multiple sets of natural gas engine spark plugs using ORNL developmental electrode alloys. These plugs are designed to isolate key material properties to provide a basis for improved spark plug lifetimes.
- Designed and procuring a spark plug test chamber with high temperature/high pressure capability (1200F @ 2500 psi). This capability is scheduled for delivery in early FY 2006.

Future Directions
- Spark plugs using developmental electrode alloys to be elavated in G3406 natural gas engine.
- Evaluate end-of-life and aged spark plugs in high temperature/high pressure test chamber under simulated engine conditions.
- Optimize developmental electrode alloys based on test chamber results, engine evaluations and post-test spectroscopic and metallurgical characterization.

Introduction

Natural gas (NG) reciprocating engine manufacturers have identified ignition systems as one of the key technologies to achieve cost/performance/emission characteristic goals for both lean and stoichiometric engines with exhaust gas recirculation (EGR). Spark plug erosion and subsequent failure have been identified as a major issue in long-term durability of natural gas ignition system. Current spark plug lifetimes are on the order of only ~2-6 months, which results in loss of performance and necessitates frequent, costly downtime maintenance for the plug replacement. Desired spark plug lifetimes for NG engine end users are on the order of at least 1 year. It has been recognized that as cylinder pressures, compression ratios, and ignition voltages are increased, and conditions further move towards leaner burning combustion, spark plug reliability and lifetime performance will become even more critical and could limit further advances in engine development. The goal of this effort is to identify the mechanisms of electrode wear and to design new electrode materials to improve the lifetime and reliability of NG spark plugs to meet the 1-year lifetime goal.

Approach

Microstructural and spectroscopic analysis of end-of life spark plugs from field-operated NG engines led to the identification of electrode wear phenomena driven by oxidation and cracking of the electrode material during engine operation. These findings were unexpected, as wear of spark plug electrodes is typically associated with loss of material due to sputtering, melting, ablation, and particle erosion phenomena during sparking. In FY 2005, optical spectroscopic and metallurgical investigations of field-tested NG reciprocating engine spark plugs were systematically pursued over a range of time, ignition system, and engine exposure conditions to determine the relative importance of the oxidation/cracking to electrode wear. Oxidation tests of conventional electrode materials were also carried out in conjunction with Federal Mogul and correlated with phenomena observed in field tested spark plugs. These studies have provided a basis to design new spark plug electrode alloys for improved lifetimes. To pursue this, ORNL and Federal Mogul are teaming to manufacture and evaluate conventional J-type spark plugs utilizing new electrode alloys.

Results

End of life spark plugs, acquired from a Caterpillar NG engine (G3516B), with ~6 months of field service showed extensive intergranular cracking and loss of material in the Pt-4W ground electrode insert tip and oxidation/cracking at the Ni-base ground electrode/Pt-4W interface (Fig. 1). This phenomenon significantly degrades the ignitability and performance of spark plugs, and is likely a key life-limiting step.

In collaboration with Gas Technology Institute (GTI), a series of spark plugs were run in a Cummins natural gas engine (QSV81G) and removed after short-time

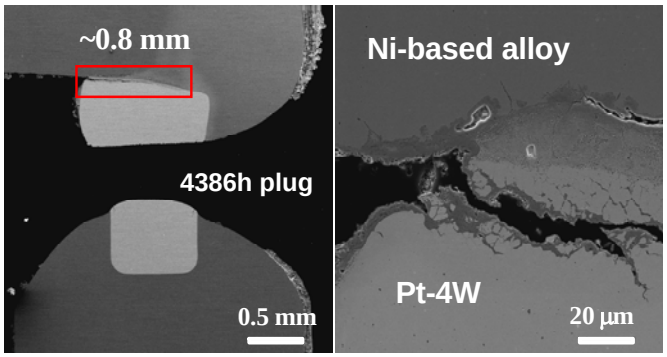

Figure 1 SEM microphotographs show crack initiation and oxidation were observed at Pt-alloy tip insert and Ni-based electrode interface after only a few days of engine operation

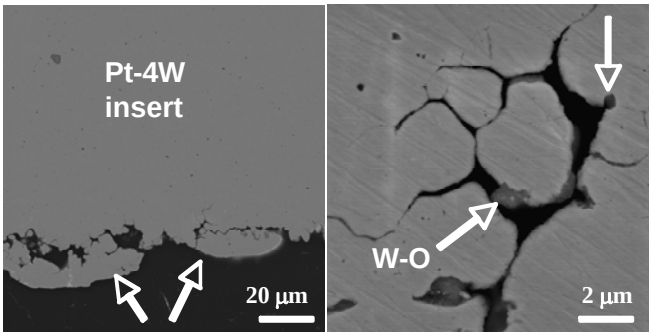

Figure 2 SEM microphotographs show substantial intergranular cracks were also observed in the Pt-W alloy electrode inserts after only a few days of field service. This cracking was found to result from internal oxidation of W additions made to the Pt

intervals to gain insight into the onset of the degradation phenomena observed in end-of-life plugs. Analysis of spark plugs tested for 108 and 188 h showed oxidation/crack initiation at the Ni

Figure 3 SEM microphotographs show extensive crack growth and oxidation at P*t-alloy tip insert and Ni-based electrode interface after 6-month lifetime.

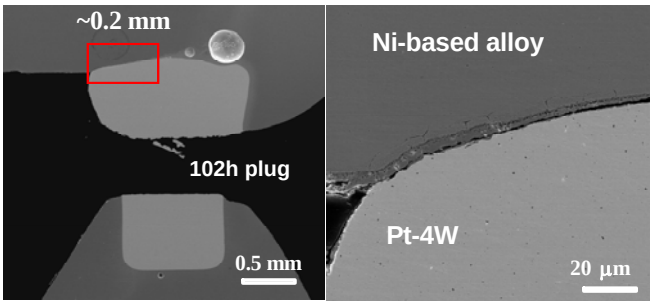

alloy ground electrode/Pt-4W insert interface, and intergranular cracking in both of the Pt-4W ground electrode and Ir center electrode inserts (Figs. 2, 3), similar to those observed in the end-of-life plugs. The extent of cracking/oxidation was less than that observed in the end-of-life spark plugs, and suggests that these degradation processes occur throughout the life of the plugs.

Spectroscopic line emissions were also used to analyze the sparking behavior of the sets of engine tested plugs in a pressurized laboratory test chamber. A comparison between a new and near end-of-life plug is illustrated in **Fig. 4**. The spectral data were used to identify line radiation from components in the arc such as the working gas (i.e., an air mixture of nitrogen and oxygen) and material being removed from the spark plug tip. For new plugs, large quantities of nickel were observed due to sputtering. For used plugs, large quantities of calcium and reduced quantities of nickel were observed. No spectral lines from the electrode insert alloys could be found, and this includes iridium, platinum, and tungsten. The absence of these materials in the spectrum would indicate that they are not eroding in a standard way such as sputtering or evaporation. This is consistent with the metallurgical observations (Fig. 3) indicative of cracking/oxidation as the dominant erosion mechanism. Fig. 5 summarizes the spectroscopic analysis of the time history of the used spark plug sets. Results show that the calcium and other impurities reach an equilibrium value after a very short time in the engine.

Metallurgical analysis of the oxides formed on Pt-4W and Ir electrode surfaces in engine tested plugs reveals Ni-Pt-O and Ni-Ir-O oxides, respectively, modified by elements including Ca, Zn, P, and S. Other elements from the Ni electrode alloys, particularly Cr, Mn, and Si have also been detected. The source of the Ca, Zn, P, and S is likely the lubricant used for NG engines. Although the electrode wear appears to result primarily from the intergranular attack of the Pt-4W electrode insert tips and the oxidation/cracking at the Ni alloy electrode/Pt-4W interface, introduction of Ca (known as glass modifiers) could significantly decrease the softening temperature and viscosity of the oxide phases, possibly further accelerating the wear of the electrode.

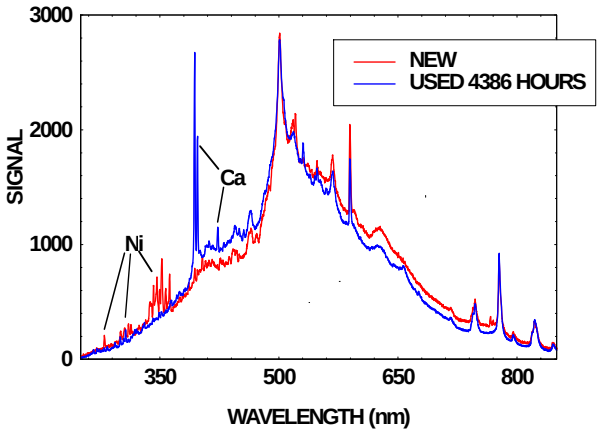

Figure 4. Spectroscopic data showing a comparison between a new and used spark plug. Spectral lines from nitrogen, oxygen, calcium, nickel and iron can be identified. Noticeably missing are lines from the electrode tip inserts; iridium, platinum and tungsten.

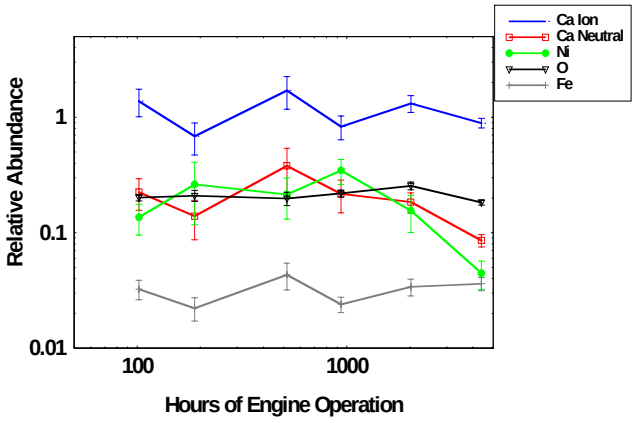

Figure 5 Summary of the spectroscopic analysis of the spark plug sets with different hours of use. Note that the values remain relatively constant after a short time in the engine.

In collaboration with Federal Mogul, laboratory gasoline engine tests and simple oxidation exposures were conducted on a range of currently used, commercially produced Ni alloy electrodes and Pt alloy

inserts. Despite the different engine and ignition conditions, the laboratory engine tested spark plugs all showed similar degradation phenomena to the field tested NG spark plugs, i.e., intergranular attack of the Pt insert alloys and cracking at the Ni alloy electrode/Pt alloy interface. These results indicate that fundamental materials related issues play a significant role in defining spark plug electrode durability.

Air oxidation tests indicated that the currently used Ni alloy electrodes were generally found to be susceptible to internal attack, due to inadequate levels of protective scale-forming elements. Intergranular attack in the Pt alloy inserts was linked to additions made to reduce breakdown voltage and/or improve manufacturability. In particular, cracking was associated with internal oxidation of W additions at Pt grain boundaries in Pt-4W alloys, and subsequent volatilization of W-oxides.

Figure 6 Photo shows the conventional J-type natural gas engine spark plugs incorporating ORNL developmental alloys.

The presence of W-oxide in the regions on intergranular attack in Pt-4W insert alloys was confirmed in the 108 h NG tested spark plug (Fig. 3).

The observed cracking/oxidation wear mechanisms establish a basis to develop new electrode alloy materials to extend spark plug lifetimes. To pursue this, ORNL and Federal Mogul are teaming to manufacture and evaluate in an NG engine the conventional J-type spark plugs utilizing new electrode alloys. Three sets of spark plugs are planned for the initial series of evaluations. The 1st set will use developmental alloys with improved oxidation resistance in the engine environments and will be tested without precious metal inserts to establish baseline behavior. The 2nd set of plugs will utilize a control, standard Pt-alloy precious metal insert with oxidation-resistant developmental electrode alloys selected for greater thermophysical compatibility with the Pt alloy to mitigate cracking at the electrode alloy/Pt insert interface. The 3rd set will utilize developmental high-melting point alloys of high corrosion resistance in place of Pt alloys for the electrode insert tip to evaluate the potential to prevent the material loss by intergranular cracking observed for the Pt alloys. In FY05, the first set of plugs were manufactured with replicates and included sixty-five spark plugs, incorporating 5 ORNL developmental alloys, and 3 control Champion® alloys (Fig. 6). Engine evaluation and post-test spectroscopic and microstructural characterization of the developmental spark plugs will be pursued in FY 2006.

Conclusions

Extensive optical spectroscopic and metallurgical investigation of field-tested NG reciprocating engine spark plugs indicated the presence of several unexpected failure modes of the spark plug electrodes, which somewhat defies conventional wisdom regarding spark plug degradation. Key degradation modes were intergranular cracking of the Pt alloy inserts, and extensive oxidation and cracking at the Ni alloy/Pt alloy insert interface. The Ni alloy electrodes were generally found to be susceptible to internal attack, due to inadequate levels of protective scale-forming elements. Intergranular attack in the Pt alloy inserts was linked to additions made to improve manufacturability and reduce breakdown voltage. The results are being used to design new alloys for spark plug electrodes for improved lifetimes in collaboration with Federal-Mogul.

FY 2005 Honors/Awards/Patents

1. M. P. Brady named to Advisory Board of the new journal *Trends in Corrosion Research*
2. M.P. Brady and H.T Lin, “Erosion Resistant Materials for Spark Plug Electrodes”, submitted to United State Patent Office Feb. 2005.

FY2005 Publications/Presentations

Publications:

1. H. T. Lin, M. P. Brady, R. K. Richards, and D. M. Layton "Characterization of Erosion and Failure Processes of Spark Plugs After Field Service in Natural Gas Engines," Wear Vol. 259/7-12 pp. 1063-1067 (2005).
2. R. K. Richards, D. M. Layton, H. T. Lin, and M. P. Brady, "Characterization of Erosion Mechanisms for Natural Gas Engine Spark Plugs," ICEF2004-875 published at Proceedings of Internal Combustion Engine Division of ASME 2004 Fall Technical Conference, October 24-27, 2004, Long Beach, CA

Presentations:

1. R. K. Richards, D. M. Layton, H. T. Lin, and M. P. Brady, "Characterization of Erosion Mechanisms for Natural Gas Engine Spark Plugs," presented at the Internal Combustion Engine Division of ASME 2004 Fall Technical Conference, October 24-27, 2004, Long Beach, CA.
2. R. K. Richards, H.T Lin, M.P. Brady, "Identification of Spark Plug Erosion Mechanisms", presented at the 2nd Annual Advanced Stationary Reciprocating Engines Conference- Moving Forward in Low Emissions and High Efficiency Technologies, March 15 – 16, 2005, South Coast Air Quality Management District Headquarters Diamond Bar, California
3. H. T. Lin, M. P. Brady, R. K. Richards, and D. M. Layton "Characterization of Erosion and Failure Processes of Spark Plugs After Field Service in Natural Gas Engines," presented at the 15th International Conference on Wear of Materials, April 24-28, San Diego, CA.
4. L R Walker, H T Lin, I Levina,* M. Brady, J. Lykowski,* "SEM and EPMA Analysis of Spark Plug Electrode Erosion", presented at Microscopy & Microanalysis 2005, July 31-August 4, 2005, Honolulu, Hawaii. * Federal Mogul (Champion®)

1.3 Adaptive Control Strategies for Clean Efficient Combustion

K. Dean Edwards, Robert M. Wagner
Fuels, Engines, and Emissions Research Center
Engineering Science and Technology Division
Oak Ridge National Laboratory
(865) 946-1239; Fax (865) 946-1248; Email: wagnerrm@ornl.gov

DOE Technology Development Manager: Ron Fiskum
(202) 586-9154; Fax (202) 586-7114; Email: ronald.fiskum@ee.doe.gov

ORNL Technical Monitor: Tim Theiss
(865) 946-1348; Fax (865) 946-1354; Email: theisstj@ornl.gov

Objective

- Extend effective combustion lean limit by employing adaptive enginecontrol.
- Demonstrate technique for estimating the potential benefits of adaptive control.
- Determine ARES representative engine platform for transitioning control technology.
- Evaluate suitability of adaptive control for spark assisted HCCI combustion (leveraged activity with OFCVT).

Approach

- Develop physics based computer model for simulating combustion and cyclic dispersion in large NG engines. Evaluate potential benefits of adaptive control using engine model.
- Characterize cyclic dispersion associated with transitioning between conventional SI and HCCI operation.

Accomplishments

- Developed model based on commercially available and industry accepted software for simulating cyclic dispersion in NG engines.
- Demonstrated ability of computer model to simulate complex cyclic dispersion and predict effect on emissions and efficiency.
- Determined and ordered large single-cylinder engine based on Waukesha Advanced Power Generation (APG) ARES engine. Engine is scheduled for delivery in November 2005.
- Characterized cyclic dispersion associated with spark assisted HCCI combustion and determined behavior is short-time predictable and consequently amenable to control.

Future Direction

- Apply benefit estimation technique to ARES size NG engine.
- Transition and evaluate advanced control system on single-cylinder NG engines.
- Transition adaptive control strategies to ARES-sized NG engine.
- Investigate spark assisted HCCI combustion on ARES sized engine platform.

Introduction

Dilute operation of internal combustion engines through lean fueling and/or high levels of EGR may be employed to increase fuel efficiency, reduce NOx emissions, and promote enhanced combustion modes such as HCCI. However, the maximum level of dilution is limited by the development of combustion instabilities that produce unacceptable levels of cycle-to-cycle variability characterized by simple or complex patterns of alternating cycles of good and poor combustion quality and increased emissions of unburned fuel (during partial burns and misfires) and NOx (produced during the succeeding enhanced-combustion events). Nonlinear feedback associated with the residual and recirculated exhaust gases exchanged between successive cycles produces small changes in the in-cylinder initial conditions. Lean operation tends to increase the sensitivity of ignition and flame propagation to these variations in initial conditions leading to the development of combustion instabilities with EGR levels as low as 5-10%. At stoichiometric conditions, the combustion process is less sensitive; however, adding high levels of EGR can produce significant fluctuations in initial conditions and lead to the development of similar instabilities.

We have previously shown that application of adaptive feedback control can reduce the severity of the cycle-to-cycle variation allowing the practical operating range of an engine to be extended [1,2]. The adaptive feedback controller observes several hundred cycles of uncontrolled behavior at a given operating condition to develop a relationship between the heat release of the current cycle and that of the following cycle. With knowledge of this relationship, the controller is capable of monitoring the heat release of the current cycle and using that information to predict the behavior of the following cycle. A control perturbation proportional to the difference between the predicted behavior and a desired target point is then applied to the following cycle to steer the system toward the desired behavior. Such control is proactive to prevent expected deviations in behavior rather than reactive to correct for deviations which have already occurred. Control perturbations may be applied to a variety of system parameters including fueling, ignition timing, and valve timing. Recent work also indicates these techniques may be applicable to HCCI combustion systems.

Estimating Benefits of Adaptive Control

In preparation for applying adaptive feedback control to lean burn or high EGR ARES-sized NG engines, we have developed a technique to estimate the expected benefit of adaptive control on a particular engine platform to address requests by industry partners. The foundation of the technique is a hybrid spark ignition (SI) engine model which combines commercially available and industry-accepted engine modeling software (WAVE from Ricardo, Inc.) with an advanced, two-zone combustion model. Detailed engine geometry information and data collected during lean or high-EGR, stoichiometric operation is used to calibrate the hybrid model to accurately simulate the behavior of the specific engine. Specifically, the model is capable of accurately predicting the development and effects of combustion instabilities that occur in highly dilute combustion. Application of adaptive control to the model through a Matlab/Simulink interface allows direct estimation of the gains in fuel efficiency and emissions reduction achievable with adaptive control.

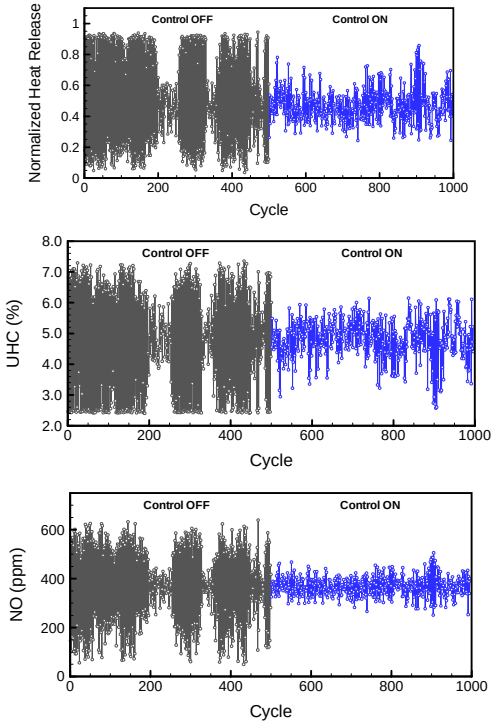

Figure 1 Example of the reductions in cyclic variation in the performance and emissions levels of the hybrid model using adaptive control and fuel perturbations

Development of Hybrid Model

We have developed a hybrid engine model by incorporating a detailed two-zone combustion model into commercially available engine-modeling software – specifically, WAVE from Ricardo, Inc. – that is

capable of predicting the development of combustion instabilities in SI engines during dilute, high-EGR operation. The behavior of specific engine platforms (including large, reciprocating, natural gas engines) can be simulated by careful calibration of the two-zone model and accurate modeling of the engine and manifold geometry in WAVE. For the current study, the model is used to simulate the behavior of a single-cylinder, 0.611-L gasoline-powered Waukesha CFR research engine and estimate the additional gains in fuel efficiency and emissions reductions which may be gained through the application of adaptive feedback control.

The primary component of the hybrid model is a WAVE engine-simulation code which can be used to model a specific SI engine geometry. To simulate SI combustion, Ricardo, Inc.'s commercial WAVE engine modeling software uses a simple function with no method of self-correction to account for the effects cycle-resolved changes in equivalence ratio and reactant temperature have on combustion performance. Therefore, in the hybrid model, results from a two-zone combustion model are used to provide feedback to WAVE to correct for these effects. The use of a more accurate and detailed combustion model that accounts for temperature effects and retains the physics of flame propagation and the ability to incorporate physical characteristics and flow dynamics of the engine through WAVE provides the hybrid model with distinct advantages over the simple model used in our previous studies [3,4].

Validation of Hybrid Model

The hybrid model was validated by modeling a Waukesha CFR gasoline engine. This engine was chosen because of our familiarity with the platform and the availability of data that exhibits the extreme cyclic variability associated with operation at lean conditions and high levels of EGR [5]. The hybrid model was programmed to match the geometry of the CFR engine and the operating conditions at which the data were collected.

Internal EGR occurred in the CFR engine due to both the trapping of residual gas and the backflow of

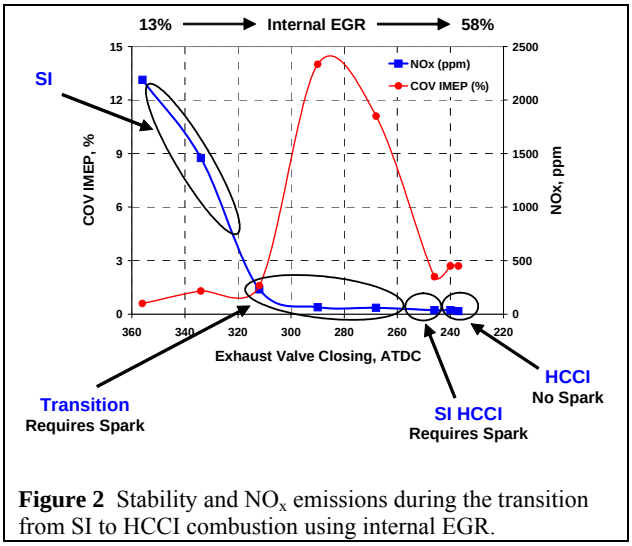

Figure 2 Stability and NO_x emissions during the transition from SI to HCCI combustion using internal EGR.

exhaust gas into the cylinder due to valve overlap. The nominal trapped residual fraction was further increased for some experiments by applying direct back pressure on the tailpipe. The combustion nstability and cyclic variability were clearly more severe at the higher EGR levels [5]. The character of the combustion oscillations also became more deterministic and complex, as would be expected for a highly nonlinear feedback process.

Overall, we observed good agreement between the hybrid model and the experimental CFR engine data. The hybrid model was able to accurately capture the general trend of the development of combustion instabilities and the onset of period-2 bifurcations in heat release with increasing EGR. We expect that further refinement of the two-zone combustion submodel and improvement of the geometric details in WAVE parameters will further improve the overall prediction accuracy. .

Application of Adaptive Feedback Control

By applying adaptive feedback control to the hybrid model, it is possible to significantly reduce the severity of the cycle-to-cycle fluctuations in performance and emission levels of NO and UHC emissions observed at dilute conditions. Figure 1 presents time series plots of heat release and the NO and UHC emissions predicted by the hybrid model (using the standard models supplied with WAVE by Ricardo, Inc.) for a particular dilute operating condition. In this example, after observing 500 cycles of uncontrolled behavior while in "learning mode", the map-based adaptive controller begins to apply control perturbations to the fuel-air ratio of the fresh charge injected each cycle.Without adaptive where it becomes briefly entrained (e.g., during the

period roughly between cycles 200 and 250 in Fig. 1). The intention of adaptive control is to stabilize the region around this fixed point making it easier to entrain the behavior and proactively predict and prevent wanderings from the fixed point which lead to the more extreme combustion behaviors. Because the period-1 fixed point lies on the system map for the given operating condition, targeting this fixed point allows control to be achieved with no net fuel penalty due to the fueling control perturbations [1,2].

With active control, the variability in predicted emission levels of NO and UHC is reduced considerably; however, there is little change in the time-averaged emission levels. This should be expected as we are targeting the unstable, period-1 fixed point which lies roughly at the center of the period-2 fixed points that correspond to partial burn (high UHC, low NOx) and enhance-combustion recovery (low UHC, high NOx). The controller acts to keep the behavior entrained near the period-1 fixed point; thus, the controlled behavior is very similar to what we see when the system becomes

briefly entrained at this point without control (e.g., during the period roughly between cycles 200 and 250 in Fig. 1). Application of control in this manner is meant to smooth operating performance at a particular equivalence ratio so that it becomes more practical to operate at higher dilution levels to achieve additional efficiency gains and emissions reductions rather than improving average efficiency and emissions at that condition.

Although not shown, control on the model has also been achieved by varying the timing of the exhaust valve closure to increase or decrease the percentage of internal EGR retained during the following cycle. This approach is especially well suited for HCCI combustion systems where a large level of internal EGR is necessary for initiating and sustaining combustion.

Spark Assisted HCCI Combustion

Homogeneous charge compression ignition (HCCI) in internal combustion engines is of considerable interest because of the potential reductions in flame temperature and nitrogen oxide emissions that can be achieved with this combustion mode. Unfortunately, it is clear that for many stationary power applications it may not be possible to sustain HCCI under all load conditions. Thus one of the most important technical developments needed to achieve wide-spread HCCI utilization is the ability to rapidly and smoothly switch between HCCI and spark ignition combustion as power demand changes. It is also clear that there are many engine conditions under which HCCI is physically possible but also typically unstable, so that the full potential of HCCI cannot be realized until appropriate stabilizing strategies are developed to maximize its practical range of implementation. Several recent publications and presentations [6-9] have begun to address the control issues but have not focused on the fundamental nature of the transition dynamics associated with switching from SI to HCCI combustion. Our main objective here is to illustrate the patterns we observed and to highlight characteristics that we believe may be potentially relevant to HCCI diagnostics and control in general. Note that this work was funded by OFCVT and is included here due to relevance and the potential role of HCCI as an enabler for clean efficient stationary power systems.

Characterization of SI HCCI Cyclic Dispersion

The experimental data discussed here were collected on a 0.5-L single-cylinder research engine operating on gasoline fuel with a full authority hydraulic variable valve actuation system. The effect of internal EGR on engine stability (as measured by COV) and NOx emissions is summarized in Fig. 2 for an operating condition of 1600 rpm and 3.4 bar IMEP. Note that in this figure, data is plotted versus the angle of exhaust valve closing rather than the explicit internal EGR

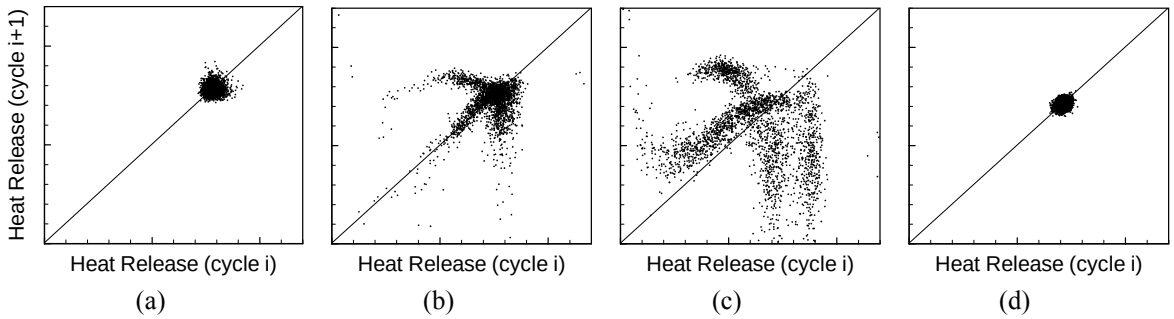

Figure 3 Experimental heat release return maps illustrating the complex dynamics when transitioning from (a) conventional SI to (e) HCCI operating using elevated levels of internal EGR.

for Convenience (both quantities trend in the same direction so that a smaller angle corresponds to higher EGR). Four distinct modes of operation were observed during this sweep and are highlighted in the figure. Mode 1 corresponds to more conventional SI operation where the coefficient of variation (COV) in IMEP is acceptable and NOx emissions are rather high. Mode 2 corresponds to a transition region where internal EGR is high and combustion is very unstable but NOx emissions are very low. A loss of efficiency was also observed in this mode along with complete misfires. Mode 3 corresponds to HCCI-like combustion where combustion is very stable and NOx emissions are very low as long as spark assist is used. Mode 4 is pure HCCI with no spark necessary for stable operation with low NOx emissions. The use of spark assist results in an expansion of the useful HCCI operating range to include Modes 3 and 4.

One method of observing the detailed combustion oscillation patterns at each level of EGR is to plot the first return maps for heat release data. Example return maps for conditions corresponding to four internal EGR levels with spark assist are shown in Fig. 3. The return map for conventional SI operation shown in Fig. 3(a) consists of a circular, unstructured cluster of data

characteristic of a fixed point that is slightly perturbed by Gaussian random noise. This pattern persists as EGR is increased until the nonlinear feedback effects from the residual gases begin to influence successive combustion events as illustrated in Figs. 3(b) and (c), which respectively correspond to increasing internal EGR level with all other engine parameters (including spark assist) maintained constant. The nonrandom patterns at the intermediate EGR levels reveal destabilization of the SI mode and the final emergence of a new fixed point for HCCI (shown in Fig. 3(d)) is indicative of a low-dimensional nonlinear process that is undergoing some type of bifurcation. The very clear repeatable patterns observable in this process suggest that it might be possible to use methods from nonlinear dynamics to characterize, model, and possibly control the SI-HCCI transition. See reference 5 for more details.

Prediction for Control

The occurrence of repeating unstable patterns in heat release is important because it suggests that future combustion events may be predictable to some degree based on recent past history. Such predictability can be potentially used for interactive control in the intermediate EGR regions where neither the SI nor HCCI fixed points are fully stable. In Fig. 4, we illustrate the potential for prediction for the intermediate combustion state similar to that represented in Fig. 3(c). In this figure we illustrate a short segment of both the observed sequential heat release values and corresponding values that have been predicted 1-cycle ahead based on recent past history. The details of the prediction method are beyond the scope of the current report, but essentially the predicted heat release values are derived from an adaptation of a symbol sequence method discussed elsewhere [5]. By observing the outcome of a limited number of previous cycles (e.g., four in this case), it is thus possible to predict the outcome of the next event with some degree of certainty as long as there are repeating non-random patterns present. In the example shown in Fig. 4, the original probability map was constructed from data measured at one time, and

then the resulting map was used to make predictions for another data set collected at a different time but for the same conditions. In effect, the analysis of the first data set constituted a 'training' process for the probabilistic model, which was then used to make predictions for another data set. While the predictions are obviously not perfect, they appear to be remarkably good considering the crudeness of the model format used in this case. We expect that considerable improvements can be made to the model construction to make prediction even more robust. Finally, the low-dimensional nature of the observed inter-mode variations suggests the possibility of developing on-line diagnostics and proactive control algorithms for expanding stable HCCI operation and improving transitions between conventional and HCCI modes.

Conclusions

We have demonstrated a hybrid model which actually captures the general trend of the development of combustion instabilities and the onset of period-2 combustion oscillations for lean burn and/or highly dilute combustion. This technique is expected to be useful for simulating the behavior of large NG stationary engines as well as estimating the potential benefits of adaptive control for lean and high EGR strategies.

The modeling and control techniques discussed here are expected to also be applicable to more extreme dilute conditions such as those used to promote HCCI combustion. The results of the HCCI portion of this study clearly indicated that cyclic dispersion associated with spark assisted HCCI combustion is short-time predictable and consequently amenable to control.

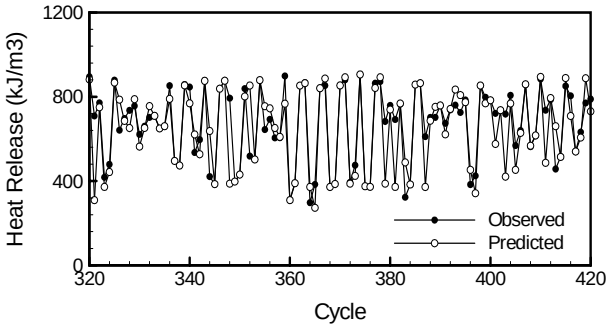

Figure 4 Example of observed and predicted heat release time series for an intermediate EGR level.

Future

ARES industry partners have expressed interest in further evaluation of our control technologies. ORNL is acquiring an ARES representative single-cylinder engine which will be installed in FY 2006. The engine is a 3.0-L single-cylinder NG engine based on the Waukesha APG ARES engine, which represents state-of-the-art in stationary power reciprocating engine technology. Collaboration is also a key part of the successful evaluation of our control technologies on large NG engines. We plan to further coordinate with industry and universities to evaluate our control and benefit estimation techniques.

We also plan to further investigate spark assisted HCCI combustion as a potential strategy for achieving clean efficient power with NG reciprocating engines. To date, this research has been performed from a transportation perspective. In FY 2006, we will begin to develop approaches for stationary power systems.

Acronyms

APG	Advanced Power Generation
ARES	Advanced Reciprocating Engine Systems
CFR	Cooperative Fuel Research
COV	Coefficient of Variation
EGR	Exhaust Gas Recirculation
HCCI	Homogeneous Charge Compression Ignition
IMEP	Indicated Mean Effective Pressure
NG	Natural Gas
NOx	Oxides of Nitrogen
ORNL	Oak Ridge National Laboratory
SI	Spark Ignition
UHC	Unburned Hydrocarbon emissions

Publications/Presentations

1. K. D. Edwards and R. M. Wagner, "Application of adaptive control to reduce cyclic dispersion near the lean limit in a small-scale, natural gas engine", ASME ICEF2004-855 (Long Beach, CA USA; October 2004).
2. R. M. Wagner, K. D. Edwards, C. S. Daw, J. B. Green, Jr., B. G. Bunting, "Enabling and expanding HCCI in PFI gasoline engines with high EGR and spark assist", 11th Diesel Engine Emissions Reduction Conference (Chicago, IL USA; August 2005)
3. K. D. Edwards, R. M. Wagner, T. J. Theiss, and C. S. Daw, "An approach for investigating adaptive control strategies to improve combustion instability under dilute operating conditions", ASME ICEF2005-1283 (Ottawa, Canada; September 2005).
4. K. D. Edwards, R. M. Wagner, V. K. Chakravarthy, C. S. Daw, and J. B. Green, Jr., "A Hybrid 2-Zone/WAVE Engine Combustion Model for Simulating Combustion Instabilities During Dilute Operation", SAE 2005-01-3801 (San Antonio, TX USA; October 2005).
5. R. M. Wagner, K. D. Edwards, C. S. Daw, J. B. Green, and B. G. Bunting, "On the Nature of Cyclic Dispersion in Spark Assisted HCCI Combustion", submitted for 2006 SAE International Congress and Exposition.

References

1. K. D. Edwards, R. M. Wagner, C. S. Daw, "Adaptive control to limit cyclic dispersion in a lean spark-ignition combustion model during fueling transients." SAE 2004-01-0895 (2004).
2. K. D. Edwards, R. M. Wagner C. S. Daw "Application of adaptive control to reduce cyclic dispersion near the lean limit in a small-scale, natural gas engine." ASME ICEF2004-855 (2004).
3. C. S. Daw, C. E. A. Finney, J. B. Green, Jr., M. B. Kennel, J. F. Thomas, F. T. Connolly, "A simple model for cyclic variations in a spark-ignition engine." SAE 962086 (1996).
4. C. S. Daw, M. B. Kennel, C. E. A. Finney, F. T. Connolly, "Observing and modeling nonlinear dynamics in an internal combustion engine." Physical Review E; 57(3), 2811-2819 (1998).
5. R. M. Wagner, J. A. Drallmeier, C. S. Daw, "Characterization of lean combustion instability in premixed charge spark ignition engines." International Journal of Engine Research; 4:1, 301-320 (2000).
6. M. Weinrotter, "Optical diagnostics of laser-induced and spark plug-assisted HCCI combustion", SAE 2005-01-0129 (2005).
7. T. Urushihara, K. Yamaguchi, K. Yoshizawa, and T. Itoh, "A study of gasoline-fueled compression ignition engine – expansion of HCCI operation range using SI combustion as a trigger of compression ignition", SAE 2005-01-0180 (2005).
8. H. Santose, J. Mathews, and W. Cheng, "Managing SI/HCCI dual-mode engine operation", SAE 2005-01-0162 (2005).
9. J. Hyvonen and B. Johansson, "Operating conditions using spark assisted HCCI combustion during com-bustion mode transfer to SI in a multi-cylinder VCR-HCCI engine", SAE 2005-01-0109 (2005).

1.4 Development of Electrodes for NO_x and Ammonia Sensors

Timothy R. Armstrong (Primary Contact), Fred C. Montgomery, and David L. West
Oak Ridge National Laboratory
1 Bethel Valley Rd.
Oak Ridge, TN 37831-6064
Phone: (865) 574-7996; Fax: (865) 241-0112; E-mail: armstrongt@ornl.gov

DOE Technology Development Manager: Ron Fiskum
Phone: (202) 586-9154; Fax: (202) 586-7114; E-mail: Ronald.Fiskum@ee.doe.gov
ORNL Technical Advisors: Tim Theiss and David Stinton
Phone: (865) 946-1348; Fax: (865) 946-1248; E-mail: theisstj@ornl.gov
Phone: (865) 574-4556; Fax: (865) 241-0411; E-mail: stintondp@ornl.gov

---

Objectives

- Develop NO_x sensors for remediation and monitoring of natural gas fired reciprocating engines.
- The sensors should have an operating temperature of 500–700 ^oC, and be able to measure NO_x concentrations from ~10–1500 ppm at oxygen levels from 5 to 20 vol%.
- Since "NO_x" refers to mixtures of NO and NO_2, it will be required to have sensors selective for either NO or NO_2, or able to measure "total NO_x" ([NO] + [NO_2]).

Approach

- Prototype sensing elements are fabricated by screen printing electrode layers onto oxygen-ion conducting (typically yttria stabilized zirconia (YSZ)) substrates.
- Elements are operated either in a "non-Nernstian" mode (where the output is a voltage) or under DC electrical bias.
- Characterize sensor in bench setting and in NG engine exhaust for NO_x sensor response, sensitivity to varying [O_2], and recovery/response kinetics.
- Develop breadboard based sensor for exhaust gas sensing

Accomplishments

- Sensing elements displaying near "total NO_x' behavior and stable in simulated long-term service have been developed.
- Sensing elements are capable of repeatedly detecting [NO_x] in the range of ~10 ppm and can operate at temperatures as high as 750 ^oC with ± 1ppm sensitivity.
- Novel techniques for applying electrical stimulus have been developed to combat drift of the sensor background output.

Future Direction

- The stability and performance of these sensing elements in real exhaust streams will be evaluated to quantify and correct for drift.
- The cross-sensitivity to other species (e.g., CO) that may be present in real exhaust streams needs to be characterized.
- Both the sensing mechanism and the cause(s) for sensor drift need to be clarified.

Introduction

Natural gas engines operated under lean (or dilute) combustion offer efficiency and maintenance advantages; however, to meet NO_x emissions targets and comply with the more stringent environmental regulations, NO_x reduction in a lean or oxygen-rich exhaust is required. To meet this challenge, NO_x remediation techniques such as the lean NO_x trap (LNT) and selective catalytic reduction (SCR) are currently being explored. The implementation of either of these techniques would be greatly simplified if a compact, robust, and low-cost NO_x sensor for *in-situ* [NO_x] monitoring of engine exhausts could be developed. This sensor could be used to monitor trap conditions in the case of the LNT and control reagent injection in the case of SCR.

The objective of this research is the development of a NO_x sensor for *in-situ* monitoring of natural gas engine exhaust. Ideally, such a sensor would operate at temperatures near 600 ^oC, measure [NO_x] in the range 10–500 ppm, be insensitive to varying [O_2] and [H_2O], and be insensitive to other oxidizible or reducible species (e.g., CO) that may be present in the exhaust. Also important for this application is the fact that "NO_x" is a mixture of NO and NO_2. NO is the dominant equilibrium form at temperatures above 600 ^oC,[1] but equilibrium conditions cannot be assumed to prevail in the exhaust.

Approach

The approach selected is to build a sensing platform on yttria-stabilized zirconia (YSZ). YSZ, an oxygen-ion conducting material, is currently widely used in [O_2] sensors for gasoline engines. This approach is not original, as two NO_x sensors based on YSZ are near commercialization and have been proven by the engine manufacturers association to not be adequate to measure NOx less than 50 ppm. In addition, both are relatively complex with multi-cavity constructions. This construction is required because in the first design [2] preliminary O_2 removal from the sampled exhaust is required before the NO_x is measured amperometrically, and in the second design[3] the sampled exhaust passes over a conversion electrode in order to convert the NO_x into NO_2 before measurement in the sensing cavity.

The lion's share of work to date has focused on the sensing *element* portion of the sensor. This is the portion of the sensor that responds to the presence of NO_x. The reason for adopting this approach is that the working characteristics of the sensing element will dictate many aspects of sensor design (operating temperature, need for catalytic overlayers, etc.).

In order to fabricate sensing elements electrodes are screen-printed and fired onto YSZ substrates (Fig. 1). These elements are then tested for NO_x response using a furnace to simulate elevated temperature service and a commercial gas mixing unit to deliver blends of N_2, O_2, NO_x (either NO or NO_2), and other species as required.

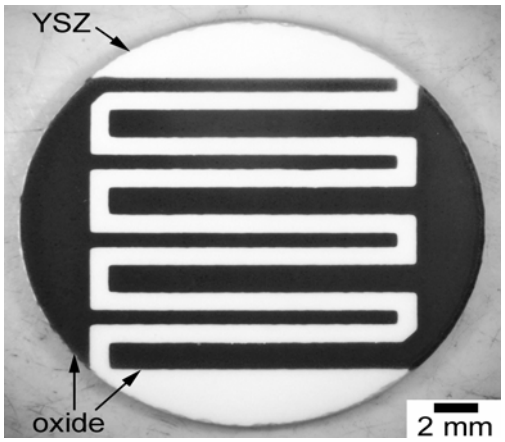

Figure 1: prototype sensing element.

Results

Much of the work on this project has been devoted to all-oxide "total NO_x" sensing elements. These sensing elements, a sample of which is depicted in Fig. 1, consist of compositionally identical oxide electrodes on a YSZ substrate. These sensing elements are attractive because the use of a single electrode material will reduce production cost and more importantly, their "total NO_x" (similar response to NO and NO_2) sensing behavior would enable measurement of [NO_x], regardless of the [NO]:[NO_2] ratio in the exhaust gas. This obviates the necessity to perform any NO_x conversion of the type described in ref. [3].

Several electrode compositions have been evaluated in order to develop a composition with large NO_x response magnitudes. The best of these, when operated at 600 ^oC and 7 vol% O_2, had responses to 77 ppm NO and NO_2 of

-37%[1] and -40% respectively. However, long term (>200 hr.) lab scale testing of this composition revealed that it was unstable in exhaust conditions, and thus the development of new compositions, stable in exhaust conditions, has been carried out.

The NO_x sensing performance of two promising new compositions is shown in Fig. 2. It can be seen that the NO_x responses are similar in magnitude over the concentration range 20–190 ppm, and efforts are ongoing to narrow the response between [NO] and [NO_2].

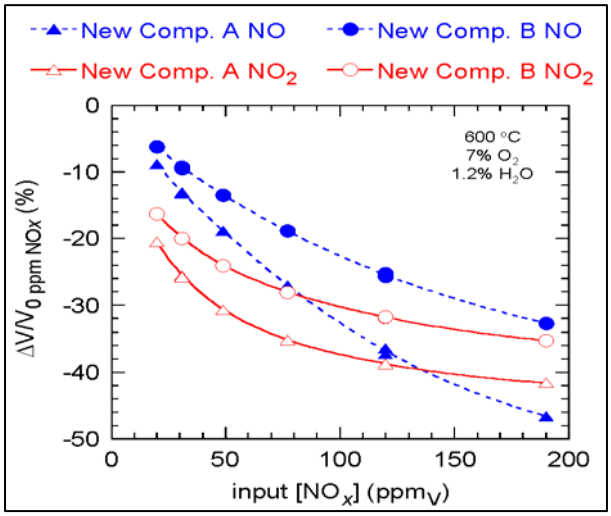

Figure 2: NO_x responses of two new electrode Compositions.

Figure 3 shows x-ray diffraction patterns from extensively tested sensing elements made with old electrode composition and the new composition. The new composition is clearly more stable as shown by the lack of decomposition products.

The data in Fig. 2 was collected at 600 °C. It may be desirable to operate the sensing element at higher temperatures, both in order to improve the response/recovery time and prevent condensation on the sensing element. The higher temperature NO sensing performance of these sensing elements is illustrated in Fig. 4, which shows sensing element performance at 750 °C. Two aspects of the sensing performance in Fig. 4 differ from that observed in Fig. 2. First, the magnitude of the changes due to

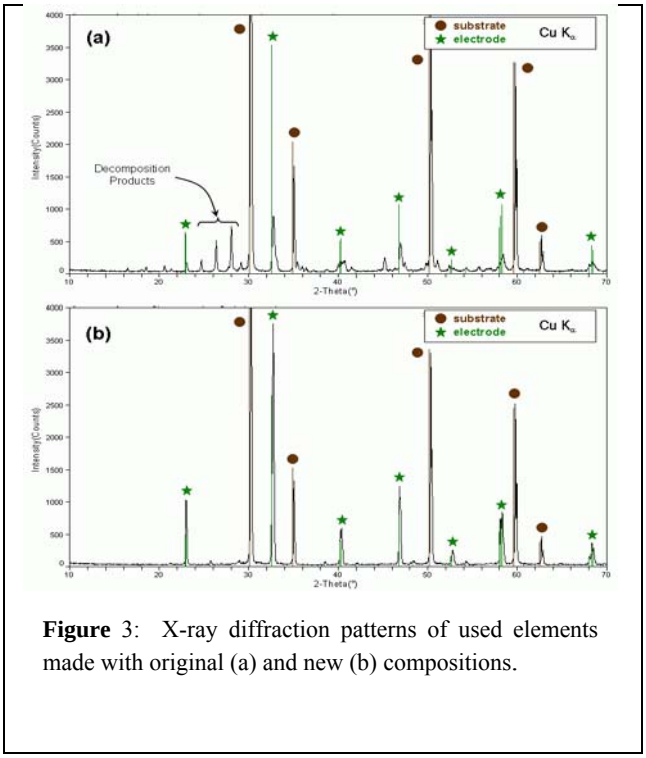

Figure 3: X-ray diffraction patterns of used elements made with original (a) and new (b) compositions.

NO are much smaller. Second, the dependence of the response on [NO] is linear. Note also that the response decreases with increasing [O_2]. This means that operation at these temperatures will most likely require lowering of the [O_2] in the sampled exhaust (by means of a pumping cell).

[1] This is the change in measured voltage when NO_x is present.

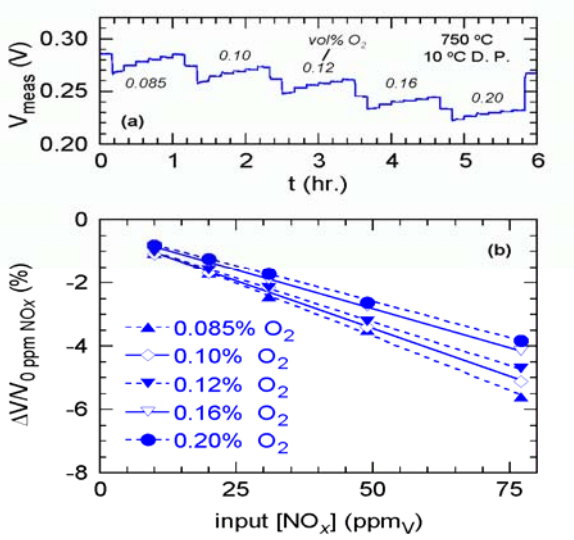

Figure 4: Sensing performance at 750 °C. In (a) [NO] is stepped through the sequence 0, 77, 49. 31, 20, 10, 0 ppm at the indicated [O_2]. Computed changes in voltage are shown in (b).

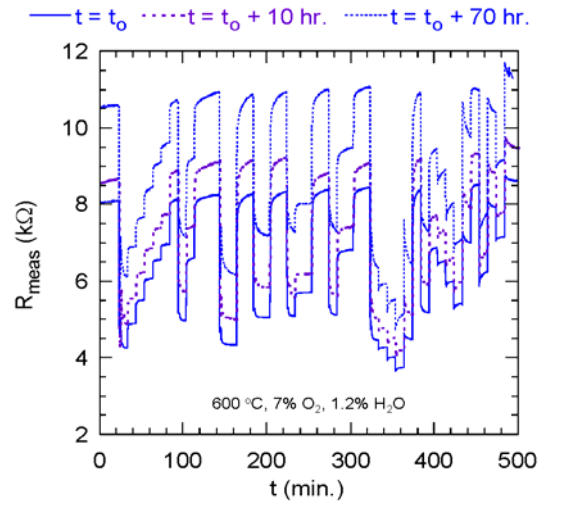

Figure 5: Response to identical changes in [NO] and [O_2] after 0, 10, and 70 hr. of continuous operation.

These sensing elements are electrochemical in nature, and electrochemical sensing elements are prone to drift. Drift is frequently observed because electrochemical sensors usually rely on charge transfer at interfaces, and these interfaces will age with use of the sensor.

Sample drift behavior observed with these sensing elements is illustrated in Fig. 5. Shown there are the element responses to identical programmed changes in [NO] and [O_2] after 0, 10, and 70 hours of continuous operation. The background resistance of the element is monotonically increasing, but the responses to the gas concentration changes are repeatable.

In order to combat this drift, we have been investigating alternate methods of applying an electrical stimulus to the sensing element. One such example is shown in Fig. 6.

The electrical stimulus was alternated between positive and negative values (only the negative values are shown in Fig. 6. During every third negative excursion, the [NO] concentration was varied systematically as indicated in Fig. 6. Operated in this manner, the sensing element is capable of repeatedly detecting [NO] changes on the order of 10 ppm over more than 10 hours of continuous operation. These are thought to be the demands that monitoring of a lean NO_x trap would place on a NO_x sensor.

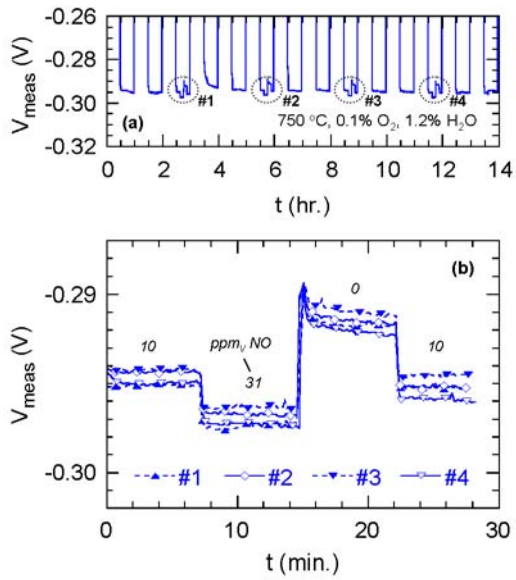

Figure 6: Element performance with alternating application of positive and negative electrical stimulus.

Conclusions

Sensing elements capable of "total NO_x" sensing behavior are under development. During the course of

this project the following accomplishments have been achieved:

- Sensing elements displaying near "total NO_x' behavior and stable in simulated long-term service have been developed.
- NO sensing elements have been demonstrated.
- Sensing elements are capable of repeatedly detecting [NO_x] in the range of ~10 ppm and can operate at temperatures as high as 750 ^oC with 1ppm sensitivity.
- Sensing elements stable for more than 1000 hrs in oxygen and steam containing environments have been developed.

The challenges ahead are fourfold: (1) the stability and sensitivity of these elements must be examined in real exhaust streams, (2) the cross-sensitivity to other species that may be present in the exhaust must be characterized, (3) techniques for combating drift must be introduced and optimized, and (4) the sensing mechanism of these elements needs to be elucidated.

This last item is important as ease of fabrication and cost may dictate changes in materials or geometry during the incorporation of these elements into sensors suitable for natural gas engines. Understanding of the sensing mechanism will be critical in predicting how such changes might affect the sensor performance.

References

1. K. B. J. Schnelle and C. A. Brown, "NO_x control," in *Air pollution control technology handbook*, CRC Press, 2001, pp. 241-255.
2. N. Kato, H. Kurachi, and Y. Hamada, "Thick film ZrO_2 sensor for the measurement of low NO_x concentration," SAE Technical Paper 980170, 1998.
3. A. Kunimoto, M. Hasei, Y. Yan, Y. Gao, T. Ono, and Y. Nakanouchi, "New total-NOx sensor based on mixed potential for automobiles," SAE Technical Paper 1999-01-1280, 1999.

Patents

1. F. C. Montgomery, D. L. West, T. R. Armstrong, and L. C. Maxey, "NO_x Sensing Devices Having Conductive Oxide Electrodes" *ORNL Docket 1348C*.

Publications/Presentations

1. D. L. West, F. C. Montgomery, and T. R. Armstrong, "'Total NO_x' sensing elements with compositionally identical oxide electrodes," accepted by *Journal of the Electrochemical Society*, Sep. 2005.
2. D. L. West, F. C. Montgomery, and T. R. Armstrong, "NO-selective NO_x sensing elements for combustion exhausts," accepted by *Sensors and Actuators B*, Feb. 2005.
4. D. L. West,* F. C. Montgomery, and T. R. Armstrong, "All-oxide "total NO_x" sensing elements," *207th Meeting of the Electrochemical Society*, 2005.
4. D. L. West, F. C. Montgomery, and T. R. Armstrong, "DC electrical-biased, all-oxide NO_x sensing elements for use at 873 K," *29th International Cocoa Beach Conference on Advanced Ceramics and Composites*, 2005.
5. D. L. West, F. C. Montgomery, and T. R. Armstrong, "High-T NO_x sensing elements using conductive oxides and Pt," *Proceedings of ICEF: Engines for Mobile, Marine, Rail, Power Generation and Stationary Applications*, 2004

1.5 Lube Oil/Catalyst Interaction Study

*John Store*y (primary contact), John Pratapas***
**Fuels, Engines, and Emissions Research Center*
Oak Ridge National Laboratory
(865) 946-1232; fax; (865) 926-1248; e-mail: storeyjm@ornl.gov
*** Gas Technology Institute*
(847) 768-0820; fax: (847) 340-2144; e-mail: john.pratapas@gastechnology.org

DOE Technology Development Manager: Ron Fiskum
(202) 586-9154; fax: (202) 586-7114; e-mail: ronald.fiskum@ee.doe.gov
ORNL Technical Monitor: Tim Theiss
(865) 946-1348; fax: (865) 946-1248; e-mail: theisstj@ornl.gov

---

Objective

- Study and quantify the contribution of natural gas engine lube oils on catalyst deactivation and useful life in achieving NOx targets.

Approach

- Secure and study field-aged catalysts and engine lube oil information. Analyze these field-aged catalysts to evaluate and quantify the types of catalyst interactions with lube oil additives. Use compositional data from catalyst analyses to determine catalyst poisoning mechanisms as a function of type of oil used and engine operating conditions.
- Characterize catalyst aging mechanisms at pilot scale utilizing a single cylinder research engine at GTI.
  - Conduct screening tests with typical base oil and different levels of additives to adequately characterize the composition, size distribution and mass of lube oil related emissions in the engine exhaust
  - Test a worst-case oil additive blend with different substrate geometries, e.g., honeycomb monolith versus wrapped metal foils, to study particle deposition rates on active sites.
- Validate key findings with a long term test on a multi-cylinder engine at ORNL (Cat G3406) equipped with three way catalyst.

Accomplishments

- Assembled a Project Technical Advisory Committee comprised of academic and engine, lube oil, and catalyst industry experts to provide guidance and feedback on our research objectives, technical approach and findings. Interacted with Committee via teleconfernce.
- Five (5) field-aged catalysts collected by GTI have been received at ORNL from engine end-users SoCal Gas Co., Coast Intelligen, and TN Pipeline. The engine conditions used and oil consumption rates were supplied for each of the catalysts. Aged catalyst foils were also received from catalyst supplier, Miratech. Each of the aged catalysts has been carefully sectioned and compositional analysis has been initiated using electron probe microanalysis to evaluate and compare the interactions between lube oil additives (P, Zn, Ca, etc.) and catalyst materials as a function of engine-aging conditions.

Future Direction

- During the next year, we plan to run screening tests using the GTI research engine to characterize exhaust emissions from different compositions of base oil and additives. Tests are targeted to begin November 2005.
- We will install some “de-greened” catalyst and begin studying the mechanisms for catalyst de-activation by lube oils

Introduction

Natural gas-fired engines are increasingly used as prime movers in gas pipeline applications, distributed generation (DG) and combined heat and power (CHP) systems. Emission regulations have led to the need to install catalytic aftertreatment to maintain or attain national ambient air quality standards in many areas, and will become more important over time.

The catalysts can be poisoned or deactivated when the precious metals bind on the catalyst with a exhaust constituent permanently and are no longer available as an active site. The pores in the catalyst substrates can become clogged, resulting in the reduced number of active sites. In addition, the exposure of catalysts and the substrates to the high temperatures in the engine exhaust can lead to thermal deactivation of the catalysts. This gradual degradation in catalyst efficiency has been seen in many different applications [1,2].

The sulfur content in natural gas is only about 0.001 % by weight, although it varies by geographic location. Therefore, the impact of sulfates on the catalyst degradation will be attributable to the lubricating oil in natural gas engines. Lube oils also contain additives and are the sources of the ash in the particulate matter (PM). Natural gas engines emit fine particulate matter, which mostly consists of organic carbon (OC) [3]. The PM also contains small amounts of elemental carbon (EC) and ash. EC would originate from incomplete combustion of natural gas and lube oil. Engine wear and cooling system leaks can also contribute to metals in the exhaust. The fine particulates that are emitted from the natural gas engine are small enough to reach the catalyst active sites and, depending on the composition of the particles, could also poison the catalyst. Over time, and depending upon oil consumption rates, the PM deposits on the catalyst and substrates, and performance degrades.

Catalyst suppliers need to have a detailed knowledge of the composition and form to know how best to mitigate the particulates' effects form of how the additives partition between the gas and particulate phase on catalyst efficiency. Engine oil manufacturers need to know what particles are formed when their product is burned. In particular, they need to determine whether oil additives that could poison catalyst end up in the small particles that can clog catalysts and reduce active sites. The GTI and ORNL team have determined that a critical need exists for data that can be utilized by gas engine companies, as well as catalyst and lube oil suppliers, to meet the reliability and maintainability goals of the three-way catalyst systems that would be required for future ARES products.

Approach

A three-phase program has been established to study and quantify the contribution of natural gas engine lube oils on catalyst deactivation and useful life in achieving NOx targets. The objective for each Phase is summarized below:

- Phase 1-Isolate and understand the physical and chemical mechanisms of catalyst degradation and failure attributable to gas engine lube oil.
- Phase 2- Conduct pilot-scale screening tests to study the influence of sulfur and ash levels in base oil, as well as additives, on the composition, size distribution and mass of lube oil related particulate emissions in the engine exhaust. Study particle deposition and chemistry on active sites as a function of catalyst geometries. Relate findings to Phase 1 results.
- Phase 3- Validate key findings from Phases 1 and 2 with a long-term test on a multi-cylinder engine equipped with a catalytic converter.

To help us ensure that the work and results meet industry needs, we have assembled a Technical Advisory Panel with representatives from suppliers of large gas engine catalysts and lube oils and lube oil experts at ARES engine manufacturers. Representatives and their affiliation (excluding ORNL and GTI) are listed below:

- Don Newburry – Miratech Corp. (catalyst supplier)
- Shazam Williams – DCl International (catalyst supplier)
- Kathleen H. Tellier – ExxonMobil (lubricant supplier)
- Subodh C. Biswas – Caterpillar (ARES member)
- Victor W. Wong - Massachusetts Institute of Technology
- William A. Paschal – Chevron Oronite (lubricant supplier)
- John Swanson – Waukesha (ARES member)
- Link Brandon – Cummins Power Generation (ARES member)
- Daniel Daly – University of Alabama

Five (5) full-size (up to 3' diameter) field-aged catalysts collected by GTI have been received at ORNL utilizing two (2) types of catalyst substrates, corrugated metal foil and porous cordierite. Details regarding the engine used for catalyst aging as well as the engine operating conditions (load, oil consumption, catalyst life, etc.) were supplied with each catalyst received. Samples were obtained from gas engines operating in non-attainment areas which require low NOx emissions. All

catalysts were three-way formulations. Of particular importance to this project are catalysts that have failed prematurely.

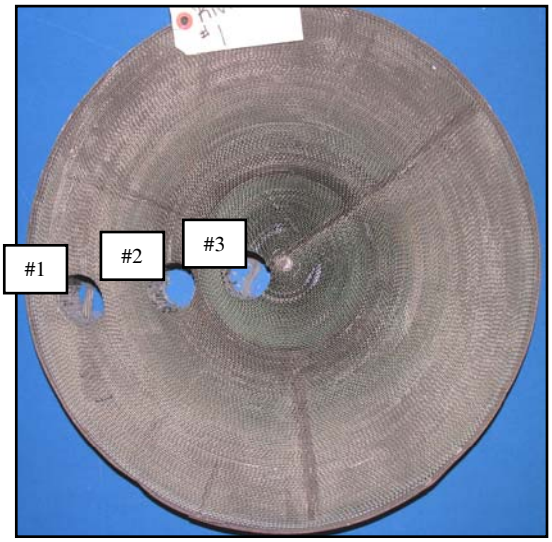

Figure 1. Typical corrugated metal foil catalyst showing where (3) core samples were removed

Sections (~1" diameter) for micro-analysis were cored from three (3) different areas of each catalyst, representing the edge, middle, and center, as shown in **Figure 1**. Polished cross-sections of the different catalyst/substrate areas were characterized using electron probe micro-analysis (EPMA) to evaluate the extent and type of catalyst interaction(s) with different lube oil additives such as P, Ca, Zn, Mn, and S.

Figure 2 - GTI's single cylinder research engine facility

To prepare for the Phase 2 pilot-scale testing, a single cylinder research engine at GTI is being modified for spark ignition with natural gas. A method for enhancing lube oil consumption in the the combustion chamber is being developed and incorporated into the test stand. The existing engine emissions bench is being modified to ensure that adequate and quality data are obtained for characterizing the contribution of lube oil to engine exhaust constituents. **Figure 2** shows the current engine and set-up.

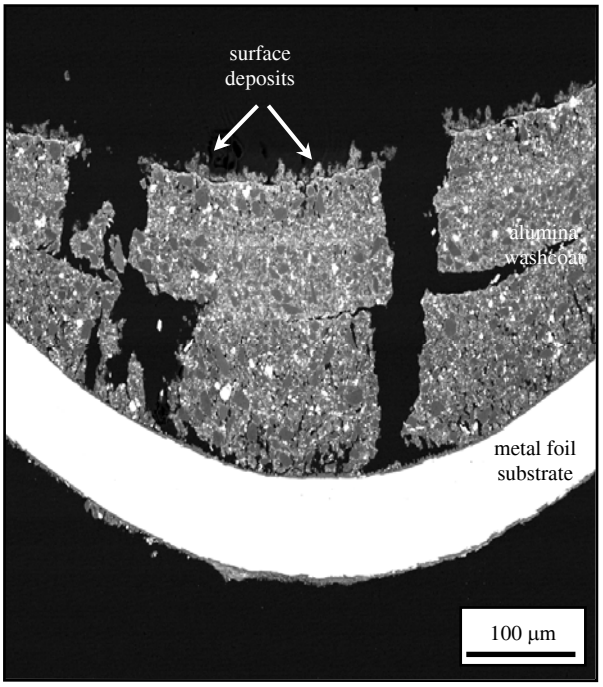

Figure 3. Low magnification SEM image showing catalyst washcoat on metal foil substrate.

Results

Preliminary cross-section images and compositional data have been accumulated for several of the field-aged catalysts using EPMA. A typical alumina washcoat (containing Pt) on a metallic foil substrate is shown in **Figure 3**. This particular catalyst was engine-aged for ~3000 h in a 250 kW synchronous CHP engine. A thin deposit (<5 µm) formed on the washcoat surface during use. Qualitative compositional analysis of the deposit shows that it is comprised of P, Ca, Zn, and O, as shown by the elemental maps in **Figure 4**. While Ca and Zn are strictly contained within the surface deposit, P is present in low concentrations throughout the washcoat. Sulfur was also found within washcoat, albeit concentrated within more localized areas than the P.

The implications of the distributions of the different lube oil poisons will become more apparent as different catalysts are microstructurally evaluated and compared. Additional characterization, primarily using transmission

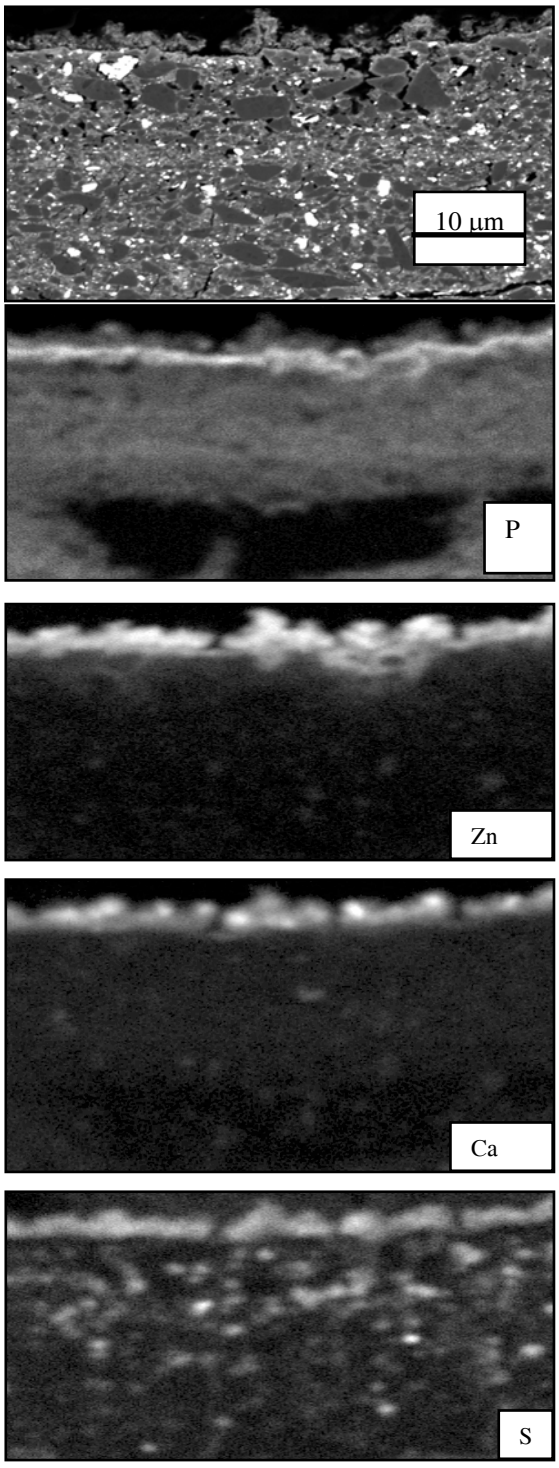

Figure 4. SEM image and associated elemental maps for P, Zn, Ca, and S, showing elemental distributions at surface of washcoat

electron microscopy, will be require in addition to bulk EPMA analyses, to determine the structural nature (integrity) of the surface deposits formed and to identify the exact nature of the elemental/phase interactions.

Because of the relatively low emissions expected in the single cylinder gas engine exhaust, we will likely have to artificially induce oil consumption to keep our test cycles within reasonable time frames. Our TAC agrees with us that the control and measurement of this artificially induced oil consumption will be an important factor in our Phase 2 test program. It was agreed that it is important that the accelerated oil consumption be introduced into the combustion chamber. Prior ORNL experience [4, 5] in applying techniques for artificially induced oil consumption with diesel engines will benefit this phase of the project.

Summary

- The project has successfully started with the formation of a Technical Advisory Committee and the acquisition of several field-aged catalyst samples.
- The single cylinder engine at GTI is installed. Exhaust characterization of the lube oil constituents in the exhaust under normal conditions and artificially-enhanced conditions will be performed.
- Preliminary microstructural analysis on one sample indicates poisons are concentrated on the surface of the catalyst, forming a glaze.

References

1. GRI Report GRI-93/0381 "Exhaust Treatment Technology for Two-Stroke Reciprocating Engines at compressor Stations."
2. GRI Report 02/0195 "Evaluation of CO or THC Emissions Control Technologies for control of Organic Hazardous Air pollutant Emissions from Natural Gas-Fired Engines."
3. SAE Transactions p. 220, SAE Paper 2002-01-0432, "Chemical Speciation of Exhaust Emissions from Trucks and Buses Fueled on Ultra-Low Sulfur Diesel and CNG
4. Phosphorous Poisoning and Phosphorous Exhaust Chemistry with Diesel Oxidation Catalysts, Bruce Bunting, et. al., Paper # 2005-01-1758, 2005 SAE International Congress, April 2005, Detroit, Michigan
5. The Development of Rapid Aging and Poisoning Protocols for the Verification of Combustion Engine Aftertreatment Devices, Paper # 007, Bruce G. Bunting & Ke Nguyen, 2005 Vietnam Society of Automotive Engineers International Conference, Hanoi, Vietnam, October 2005

1.6 Lean NOx Trap Aftertreatment for Lean Natural Gas Engines

Jim Parks
Fuels, Engines, and Emissions Research Center
Engineering, Science and Technology Division
Oak Ridge National Laboratory
(865) 946-1283, E-mail: parksjeii@ornl.gov

DOE Technology Development Manager: Ron Fiskum
(202) 586-9154; fax: (202) 586-7114; e-mail: ronald.fiskum@ee.doe.gov
ORNL Technical Monitor: Tim Theiss
(865) 946-1348; fax; (865) 946-1248; e-mail: theisstj@ornl.gov

---

Objective

- Study the feasibility of using lean NOx trap catalyst technology to reduce the NOx emissions of lean burn engines.
- Determine if natural gas can be used as the reductant for regeneration of lean NOx trap catalysts.
- Address key technical barriers for a lean NOx trap system, such as catalyst durability, sulfur poisoning, cost, etc.

Approach

- Study a lean NOx trap catalyst system installed on a lean natural gas engine (Cummins C8.3-G+) on a dynamometer test platform.
- Evaluate catalyst performance and study process chemistry with analytical tools unique to ORNL.
- In addition to the lean NOx trap catalysts, oxidation and reformer catalysts were used upstream of the lean NOx trap catalysts to enable utilization of the methane in natural gas for regeneration of the lean NOx trap.

Accomplishments

- Characterized natural gas utilization for lean NOx trap regeneration.
- Characterized partial oxidation and reforming processes of methane oxidation and reformer catalysts in lean NOx trap system with analytical tools including standard gas analyzers, FTIR spectroscopy, and SpaciMS (a unique tool developed by ORNL for exhaust measurements of H_2).
- Measured unregulated species in lean natural gas engine exhaust and the effect of the lean NOx trap catalyst system on unregulated species levels. Note: analysis of experimental data is ongoing and will continue into FY06.

Future Direction

- With performance for NOx reduction demonstrated and natural gas-based regeneration characterized, efforts will shift toward addressing durability concerns for the technology. Specifically, we plan to study potential degradation mechanisms for the technology including sulfur effects (a known catalyst poison) and thermal effects (a known catalyst degradation mechanism).
- Another area open for improvement is catalyst cost. We will continue to evaluate opportunities for cost reduction through reduction of precious metal loadings and system optimization.
- Interest has been expressed in advancing the technology from a laboratory setting to a field study or demonstration site. We plan to evaluate opportunities for field studies and design and plan for a field study if funding permits.

Introduction

Achieving the ARES goals expands the deployment of clean and efficient reciprocating engines for distributed energy production and, thereby, increases the nation's energy security. The project described in this document is focused on these goals; specifically, the goals of the project are to enable <0.1 g/bhp-hr NOx emissions from lean (high efficiency) natural gas engines.

Stoichiometric engines utilize three-way catalysts to simultaneously control carbon monoxide (CO), hydrocarbons, and NOx in exhaust; however, in lean exhaust, excess oxygen in the exhaust allows oxidation of CO and hydrocarbons without reduction of NOx when three-way catalysts are used. Traditionally, selective catalytic reduction (SCR) catalysis with an ammonia reductant has been used to control NOx in lean exhaust conditions; the ammonia is typically supplied from a urea solution which is injected into the exhaust upstream of the SCR catalyst. While urea-based SCR is a commercially available NOx reduction technology, the requirement for urea storage is a deterrent in some applications, and upcoming regulations may contain NOx emission levels that are difficult to obtain cost effectively with urea-based SCR.

The focus of the study presented here is the application of lean NOx trap catalysis to NOx reduction in lean natural gas engine applications. In lean NOx trap catalysis, NOx is stored on the catalyst under lean exhaust conditions; then, under rich exhaust conditions the NOx is released and reduced to harmless nitrogen (N_2). The technology is also known as "NOx adsorber" catalysis, "NOx storage and reduction" catalysis, etc. In FY04, a lean NOx trap catalyst was installed and studied on a dynamometer-based engine platform. The natural gas supplying the engine was used as the source of catalyst reductant. NOx emissions less than 0.1 g/bhp-hr (~0.3 lb/MW-hr) were demonstrated downstream of the lean NOx trap catalyst.[1] This level of NOx meets the ARES program target of 0.1 g/bhp-hr NOx. Fuel penalties for the catalyst system were 1-5% and were dependent on the actual engine conditions used during evaluation. These fuel penalties are low enough to maintain the fuel efficiency benefits of the lean burn engine.

During FY04 studies, the catalyst was evaluated under a variety of conditions, and emission measurements were made upstream and downstream of the catalyst to characterize the catalyst performance and process chemistry. Important technical issues and challenges were identified. Efficient utilization of the natural gas, which is primarily methane, is one the significant challenges in this application since methane is difficult to react catalytically. Another key technical issue is the temperature range of lean exhaust from natural gas reciprocating engines since the NOx storage capacity of the lean NOx trap catalyst varies with temperature.

In FY05, studies focused primarily on addressing the technical challenge of utilizing natural gas for regeneration of a lean NOx trap catalyst on a lean burn natural gas reciprocating engine. Lean NOx trap catalysts are not typically efficient at regenerating with a methane reductant, which is the primary component of natural gas; so, methane is typically partially oxidized and/or reformed into hydrogen (H_2) and/or carbon monoxide (CO) which are much more effective at regenerating the lean NOx trap. Efficient conversion of methane into H_2 and CO reductants is important to minimize fuel penalties associated with the NOx reduction process and minimize methane emissions associated with introducing the natural gas into the exhaust stream for catalyst regeneration.

In the work presented in this report, the utilization of natural gas across oxidation, reformer, and lean NOx trap catalysts is analyzed by measuring methane, CO, and H_2, etc. upstream and downstream of the catalysts. The results give an improved understanding of the chemistry occurring in the catalytic exhaust system. The greater understanding of the chemistry should enhance further research and development of the lean NOx trap as well as other natural gas technologies that may utilize methane partial oxidation and reforming such as lean NOx catalysis and H_2-assisted combustion.

Lean NOx Trap System and Engine Platform

The experimental apparatus for the study presented here has been described previously and will be reviewed here with the addition of specific instrumentation utilized for the study presented here.[1] Experiments were performed on an in-line 6-cylinder 8.3-liter natural gas engine (Cummins CG-280) with a peak torque of 1153 Nm (850 ft-lb) at 1400 rpm and a peak power of 209 kW (280 hp) at 2400 rpm. The engine load and speed were controlled by a 600-hp dynamometer system (General Electric Model 42G61). All experiments were performed at 1800 rpm and steady-state conditions to simulate gen-set speeds. Intake air conditions were controlled to approximately 23.9ºC (75^{o}F) with a relative humidity of 55%.

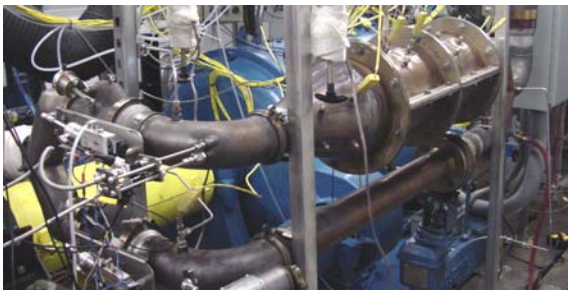

Figure 1. Picture of the lean NOx trap catalyst system installed on the ORNL engine-dynamometer platform.

The catalyst system mounted to the engine exhaust consisted of a two-chamber system with two exhaust brake valves (US Gear) controlling the flow to both chambers (see **Figures 1 and 2**). One chamber simply consisted of an empty pipe and will be referred to as the "bypass leg". The second chamber contained the oxidation, reformer, and lean NOx trap catalysts and will be referred to as the "catalyst chamber" or "leg". Downstream of the bypass and catalyst legs, the exhaust from the two legs combined again to exit the system.

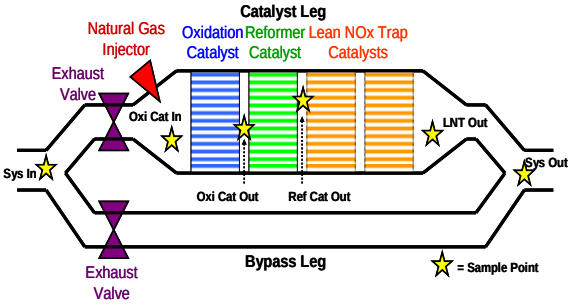

Figure 2. Lean NOx trap catalyst system.

The volumes of catalysts in the catalyst chamber were 7 liters, 7 liters, and 14 liters for the oxidation, reformer, and lean NOx trap catalysts respectively. The order from upstream to downstream of the catalysts in the catalyst chamber was oxidation, reformer, and then lean NOx trap catalysts. All catalysts were supplied by EmeraChem LLC.

Exhaust was sampled for analysis by emissions analyzers at several locations in the exhaust including positions between catalyst monoliths as described in **Fig. 2**. Exhaust samples were made at various points in the system as indicated by the abbreviations "Sys In", "Oxi Cat In", "Oxi Cat Out", "Ref Cat Out", "LNT Out", and "Sys Out".

The combination of standard emission analyzers, FTIR gas cell analysis, and a novel tool developed by ORNL for H_2 analysis known as "SpaciMS" enabled the measurement of the major species of interest for methane partial oxidation and reforming processes.[2] **Figure 3** shows a schematic of the exhaust analysis system with reference to the analyzers employed and the gas species measured.

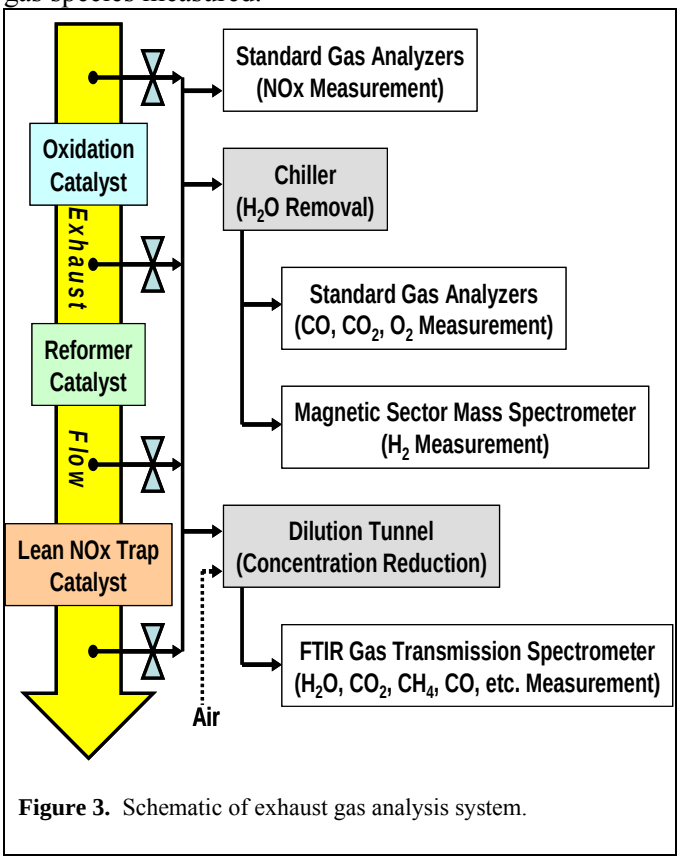

Figure 3. Schematic of exhaust gas analysis system.

Results

NOx Reduction and Fuel Penalty

The lean NOx trap system was operated with different fueling rates during regeneration for all engine loads evaluated. NOx reduction efficiencies obtained for the different fueling rates are shown in **Figure 4**. As fueling rates increased, the minimum excess air ratio during regeneration decreased. NOx reduction efficiencies generally increased as more fuel was added during regeneration, but performance became level as excess fuel was added. NOx reduction efficiencies greater than 90% were obtained for the 10% and 25% loads, but the NOx reduction efficiency at 50% load was approximately 70-75%. The higher NOx emission rate from the engine coupled with the lower NOx storage of the lean NOx trap catalyst at 560ºC caused the lower NOx reduction performance at 50% load.

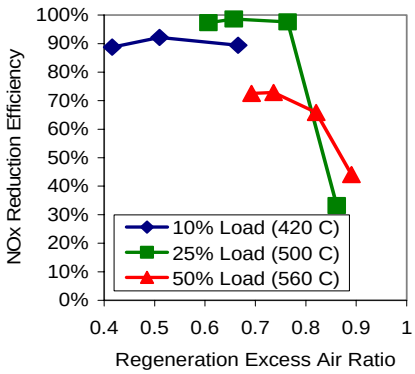

Figure 4. NOx reduction efficiency as a function of excess air ratio (%) during regeneration.

The fuel penalty associated with the excess air ratios obtained during regeneration is shown in **Figure 5**. As expected, the fuel penalty increases with increasing fueling rate and decreasing excess air ratio. The fuel penalty required to obtain a given excess air ratio is a function of the oxygen mass flow into the catalyst leg during regeneration as well as the amount of fuel injected into the catalyst system. The oxygen mass flow into the catalyst leg varies with engine load due to differences in exhaust composition and exhaust backpressures that lead to different leakage rates through the exhaust valve. Furthermore, the fuel penalties reported represent the fraction of fuel injected into the exhaust system per regeneration event relative to the engine fueling rate; thus, fuel penalties differ for different engine loads due to a variety of issues.

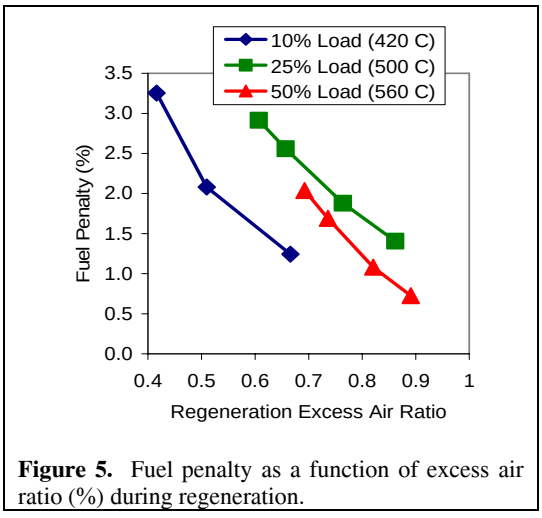

Figure 5. Fuel penalty as a function of excess air ratio (%) during regeneration.

Methane Utilization

Full exhaust species data (H_2, CO, CH_4, O_2, CO_2, H_2O) as a function of catalyst temperature and excess air ratio were obtained during lean-rich cycling of the lean

NOx trap catalyst. Results are shown in **Figure 6**. Here data from one regeneration period for each exhaust sample position is shown. As observed in the data, methane and oxygen are the only constituents going into the oxidation catalyst as expected (**Fig. 6.a**.). Then methane is partially oxidized over the oxidation catalyst and CO and H_2 are produced at the same time that O_2 is depleted (**Fig. 6.b**.). The reformer catalyst increases the H_2 level in the exhaust dramatically indicating that reforming processes are occurring (**Fig. 6.c**.). CO is also increased over the reformer catalyst indicating some partial oxidation may also be occurring over the reformer catalyst. Finally, CO and H_2 are partially depleted over the lean NOx trap catalyst as these reductants are consumed in the process of NOx reduction over the lean NOx trap catalyst (**Fig. 6.d**.).

Data shown in **Fig. 6** was analyzed by integrating the peak signals for each reductant chemistry. The integrated data allows a better view of the chemistry occurring over each catalyst in the system. **Figure 7** shows the integrated data for the three catalyst temperatures (engine loads) examined. The excess air ratios during regeneration were 0.67, 0.76, and 0.74 for temperatures 420ºC, 500ºC, and 560ºC, respectively. These excess air ratios gave optimal NOx reduction performance per fuel added for regeneration.

At 420ºC (**Fig. 7.a.**), methane levels decrease across all catalysts to some degree indicating oxidation or reforming functions occur for all catalysts, and there is a significant increase in H_2 produced by the reformer catalyst. The specific increase of H_2 relative to CO suggests reforming processes are occurring on the reformer catalyst. Furthermore, the magnitude of the rise in H_2 corresponding with a significant drop in CH_4 suggests that steam reforming is occurring. In contrast, at 560ºC (**Fig. 7.c.**), methane oxidation only occurs across the oxidation catalyst, and only a small increase in H_2 occurs over the reformer catalyst. Here the rise in H_2 level corresponds with a decline in CO which suggests water gas shift reforming is occurring. At 500ºC (**Fig. 7.b.**), the maximum production of H_2 occurs with a sharp increase in H_2 observed after the reformer catalyst. For all catalyst temperatures, total methane

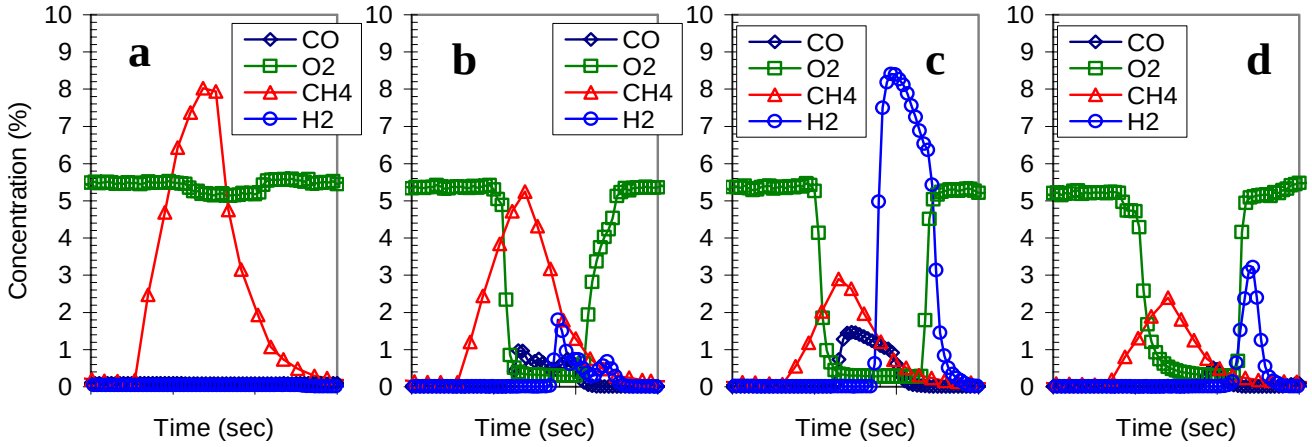

Figure 6. Exhaust species data obtained at (a) Oxi Cat In, (b) Oxi Cat Out, (c) Ref Cat Out, and (d) LNT Out sample positions. The x-axis for all plots is time in seconds with a range of 0-60. The y-axis represents concentration and is the same scale for all plots.

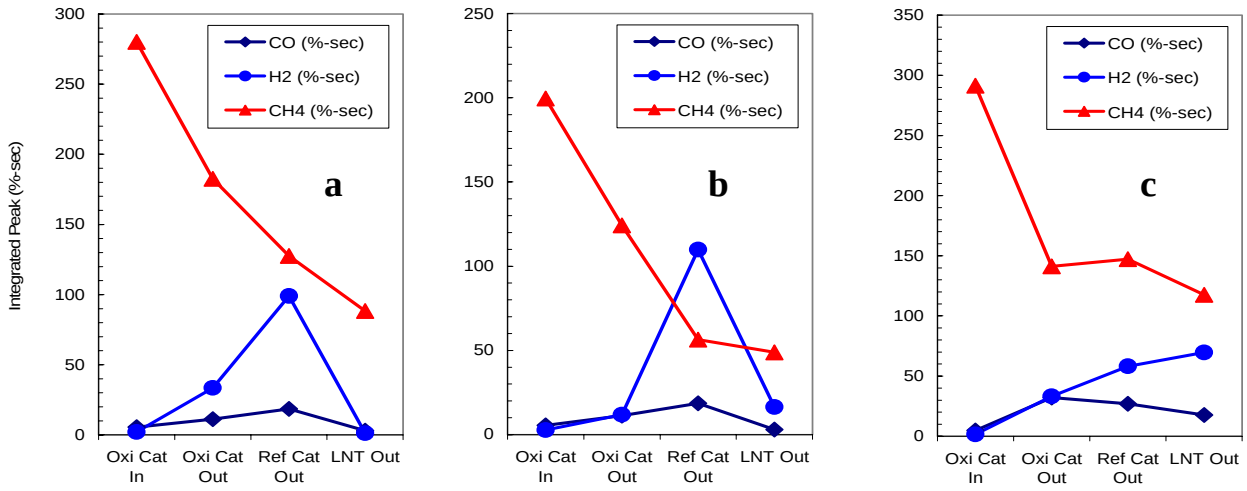

Figure 7. Integrated reductant peaks obtained at catalyst temperatures of (a) 420ºC, (b) 500ºC, and (c) 560ºC. Note the different scale for the y-axis in each plot.

conversion is similar. Higher temperatures cause more rapid methane conversion via oxidation in the oxidation catalyst, and lower catalyst temperatures convert methane via a combination of oxidation and reforming processes throughout all catalysts in the system. Although the total methane conversion is similar for all catalyst temperatures, the efficiency of methane conversion into useful products for LNT regeneration differs. The reforming function of the reformer catalyst appears to peak in efficiency at 500ºC where the greatest concentration of H_2 is produced.

A drop in H_2 level occurs across the LNT catalyst at 420ºC and 500ºC indicating that the H_2 is being used to regenerate the lean NOx trap. The absence of a drop in H_2 across the LNT catalyst at 560ºC is likely due to the fact that low amounts of NOx are stored on the LNT at that temperature. Overall, the results indicate that both oxidation and reforming processes are important in producing reductant streams suitable for regeneration of lean NOx trap catalysts, and the oxidation and reforming processes are highly dependent on catalyst temperature.

Conclusions

Natural gas injected directly into exhaust can be utilized to regenerate lean NOx trap catalysts. The high methane content of natural gas requires catalytic treatment of the methane to generate suitable reductants for the lean NOx trap such as carbon monoxide and hydrogen. Characterization of exhaust samples obtained

downstream of methane oxidation and reformer catalysts in a lean NOx trap system shows that carbon monoxide and hydrogen are produced at significant levels. Furthermore, after initial partial oxidation of methane by the oxidation catalysts, a significant amount of hydrogen is produced in reforming processes across the reformer catalyst. Both oxidation and reformer catalysts contribute significantly to the lean NOx trap regeneration process, and both processes are dependent on temperature.

The lean NOx trap catalyst technology must meet cost and durability targets for successful commercialization in lean natural gas engine applications. Based on the results presented here, the fuel requirements for catalyst operation are minimized by the fuel processing occurring on the oxidation and reforming catalysts in the system. Thus, cost optimization for minimal operating cost indicates the additional capital cost of the oxidation and reforming catalysts are worthwhile. The strict durability requirement of >10,000 hours of operation remains the critical challenge for the lean NOx trap technology. Future work will address the durability issues including the sensitivity to sulfur poisoning which adversely affects lean NOx traps.[9]

Acknowledgements

Oak Ridge National Laboratory (ORNL) would like to acknowledge EmeraChem LLC for supply of the catalysts. This work is a part of the U. S. Department of Energy (DOE) Advanced Reciprocating Engine System (ARES) Program within the Office of Distributed Energy Resources. The ARES program, under the leadership of Ron Fiskum, is in cooperation with representatives from Caterpillar, Cummins, and Waukesha. Jim Tassitano performed work under a subcontract with Oak Ridge Associated Universities. ORNL is managed by UT-Battelle LLC for the US Department of Energy under subcontract DE-AC05-00OR22725.

FY2005 Presentations/Publications

1. Jim Parks, Doug Ferguson, John Storey, "NOx Reduction with Natural Gas for Lean Large-Bore Engine Applications Using Lean NOx Trap Aftertreatment", *Gas Technology Institute Conference and Exposition,* Orlando, FL, January 30-February 2, 2005.
2. Jim Parks, Jim Tassitano, John Storey, "Lean NOx Trap Catalysis: NOx Reduction for Lean Natural Gas Engine Applications", *2nd Annual Advanced Stationary Reciprocating Engines Conference*, Diamond Bar, CA, March 15-16, 2005.
3. Jim Parks, Jim Tassitano, John Storey, "Lean NOx Trap Catalysis: Recent Studies on Methane Utilization for Lean NOx Trap Regeneration", *ARES Catalysis Workshop*, Knoxville, TN, April 27-28, 2005.
4. J. E. Parks II, J. Tassitano, "Natural Gas Partial Oxidation and Reforming for Lean NOx Trap Catalysis Regeneration", *Proceedings of ASME Internal Combustion Engine Division: 2005 Fall Technical Conference* ICEF2005-1287 (2005).

References

1. James E. Parks II, Aaron M. Williams, H. Douglas Ferguson III, John M. E. Storey, "Lean NOx Trap Catalysis for NOx Reduction in Natural Gas Engine Applications", *Proceedings of ASME Internal Combustion Division: 2004 Fall Technical Conference* ICEF2004-871 (2004).
2. W. P. Partridge, J. M. E. Storey, S. A. Lewis, R. W. Smithwick, G. L. DeVault, M. J. Cunningham, N. W. Currier, and T. M. Yonushonis, "Time-Resolved Measurements of Emission Transients by Mass Spectroscopy", *SAE Transactions – Journal of Fuels and Lubricants* **109**, p. 2992, Paper No. 2000-01-2952 (2000).

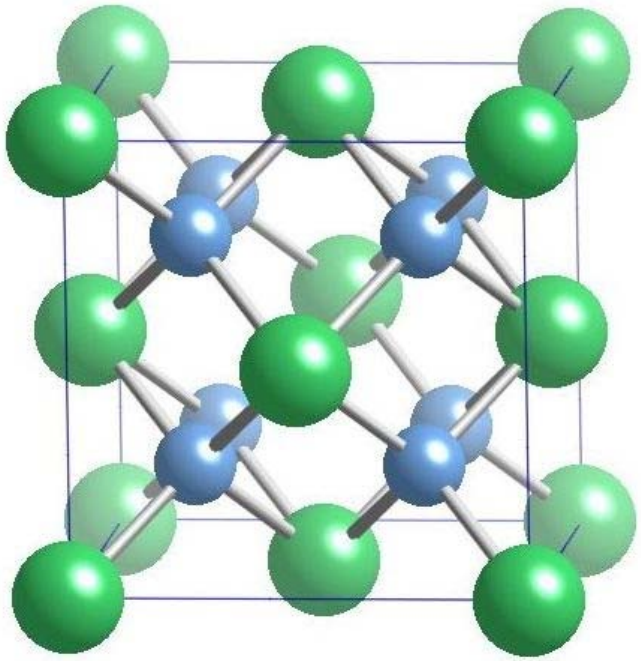

2.1.1 Advanced Alloys for High-Temperature Recuperators

P.J. Maziasz
Metals and Ceramics Division
Oak Ridge National Laboratory
P.O. Box 2008, MS-6115
Oak Ridge, TN 37831-6115
(865) 574-5082; fax: (865) 754-7659; e-mail: maziaszpj@ornl.gov

DOE Technology Development Manager: DebbieHaught
(202) 586-2211; fax: (202) 586-7114; e-mail: debbie.haught@ee.doe.gov
ORNL Technical Advisor: Karren More
(865) 574-7788; fax: (865) 576-5413; e-mail: *morekl@ornl.gov*

Objectives

- Determine creep- and oxidation-resistance of cost-effective commercial high-temperature recuperator alloys.
- Provide commercial sheets and foils of AL20-25+Nb alloy to OEMs for recuperator manufacturing, and modify processing to optimize creep-resistance (Phases I and II).
- Characterize recuperator aircells made from advanced stainless alloys (HR120 and AL20-25+Nb).

Approach

- Build a unique data base of creep- and oxidation-resistance data of commercial sheets/foils of advanced heat/corrosion resistant alloys for improved performance and reliability at 700-750^{o}C.
- ORNL established a joint program with Allegheny-Ludlum to produce and deliver commercialization of AL20-25+Nb alloy to recuperator OEMs.
- ORNL is performing creep-rupture tests and microcharacterization of the same Phase I and II foils/sheets of AL20-25-+Nb alloy to verify product performance and compare with other advanced alloys.

Accomplishments

- ORNL testing of Phase I foils/sheets of AL20-25+Nb alloy showed creep-rupture strength much greater than 347 steel at 650-750^{o}C, and better than HR120 and HR230.
- ORNL testing of Phase II sheets/foils of AL20-25+Nb alloy show that modified processing of sheet increased the uniform grain size to almost double creep-rupture life at 750^{o}C.

Future Directions

- Complete sheet/foil Phase II effort on AL20-25+Nb in support of commercialization.
- Continue overlapping characterization of all commercial advanced alloys in ORNL's Microturbine Recuperator Test Facility (MRTF).
- Complete microcharacterization of creep-tested foils/sheets of AL20-25+Nb and HR120 alloys, and alloy 625 to better understand performance differences and provide better lifetime predictions for advanced recuperator applications.

Introduction

Recuperators for industrial turbines and microturbines have traditionally been made from 347 stainless steel (SS), but problems with performance and durability are becoming evident for such steels as temperatures approach or exceed 650-700°C, particularly in moist air.[1] Economic and efficiency advantages have pushed microturbine engine sizes up from 30-70 kW to 200-250 kW, for both stand-alone power generation and CHP applications. If microturbines are used to generate power during peak demand, then cycling will further challenge the recuperator with thermal shock during rapid heat-up. Even more challenging will be switches from clean natural gas to alternate gaseous fuels (flare, land-fill or sewer gases), or even liquid fuels (diesel). Durable, reliable recuperators (and packaging/ducting) are critical components for any attractive microturbine systems. Previous ORNL work to date has identified HR120 and 625 alloys as being higher performance (creep and oxidation) foil/sheet alternatives to 347 SS at 650-750°C.[1,2] Foil testing in the ORNL MRTF has further shown that HR120 is vastly superior to 347 SS, and better than HR230 in this temperature range.

In 2003-2004, ATI Allegheny-Ludlum introduced a new high temperature alloy, AL 20/25+Nb (Fe-20Cr-25Ni–Mo,Nb,N), which was developed together with Solar Turbines earlier for foil recuperator applications.[4-6] This alloy is another in a group of improved alloys based on the austenitic stainless alloy composition of Fe-20Cr-25Ni, which includes Nippon Steel Corp.'s NF709 and Sandvik's 12R72HV, for fossil energy boiler tubing with more corrosion resistance and creep strength than 17-14CuMo and 347H stainless steels [7-10]. ORNL made lab-scale foils, rolled from slit and flattened NF709 boiler tubing, and performed creep and oxidation testing in 2001-2003 [11,12]. Based on these preliminary results, on interest from the microturbine recuperator manufacturers, and on the potential for pricing between the cost of 347 SS and alloy 625, ORNL and ATI Allegheny-Ludlum defined a new joint project in 2004 to expand commercial foil and sheet development specifically for microturbine recuperator manufacturers. This annual report summarizes progress made on this project during FY2005.

Approach

This collaborative project was divided into two phases. Phase I of this project involved production of a broad range of commercial foils and sheets of AL 20/25+Nb alloy using the standard processing employed for previous work with Solar Turbine.[4,5] Phase II of this project would involve smaller quantities of specific foils or sheets with changes in processing parameters to modify the grain size for improved creep resistance. The creep properties and microstructure of samples of these various sheet and foil products for both Phase I and II were characterized at ORNL. Foil samples of Phase I and II AL 20/25+Nb were also introduced into the lab-scale corrosion tests and into test probes for the MRTF at ORNL.

Phase I of this project reduced about 5000 lb of original hot-band into over 1000 lb of foils (0.004, 0.005 and 0.008 inch gage thickness), and 800 lb of sheets (0.010 and 0.015 inch gage thicknesses) with standard processing conditions. These foils and sheets products were delivered to Ingersoll Rand Energy Systems (IRES) in 2004/2005 to produce the various pieces required for making brazed plate-and-fin (BPF) air cells for recuperators for their new 250 kW PowerWorks microturbine.

Phase II of this effort produced several hundred pounds of 0.0032 inch foil for Capstone Turbines (CT) manufacturing trials for welded primary-surface (PS) air-cells for recuperator application in support of their 200 kW microturbine. The Phase II effort also included new experiments for modified processing on 0.005 inch thick foil and 0.010 inch thick sheet to further enhance the creep resistance.

Results

Creep-rupture testing of the 0.004, 0.005 and 0.008 inch thick foils and 0.010 and 0.015 inch thick sheets of the AL20-25+Nb alloy (Phase I) at 750°C and 100 MPa were completed this year. Creep rupture tests of the same Phase I foils and sheets is in progress at 704°C and 152 MPa. Creep testing also began of the AL 20/25+Nb alloy (Phase II) 0.010 inch thick sheet at 750°C and 100 MPa. Testing of Phase II foils made from this sheet by Allegheny-Ludlum will follow. Allegheny-Ludlum also supplied 0.004 inch thick foils of alloy 625 for comparison testing in FY2005.

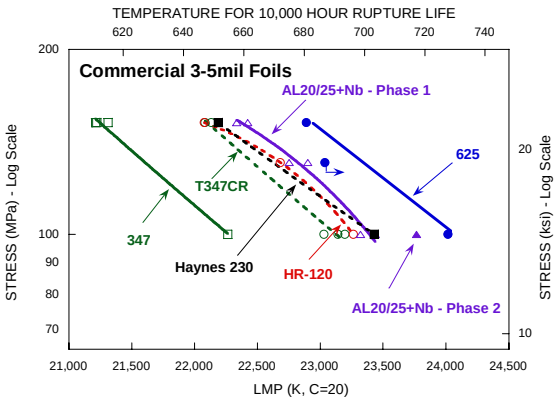

Figure 1 ORNL creep-rupture data for 0.003 – 0.005 inch thick foils of the various stainless steels, stainless alloys and Ni-based superalloys tested in air at 700-750°C. Data are plotted as creep-rupture stress as a function of Larson-Miller parameter, calculated using rupture life and creep test temperature.

Figure 1 shows a plot of creep-rupture stress versus Larson-Miller parameter (calculation combining creep-rupture time and test temperature into one unifying parameter) for foils of the AL 20/25+Nb alloy compared to 347 SS and several other alloys including HR120, HR230 and 625. Clearly the new AL 20/25+Nb alloy foils are much stronger than standard 347 SS at 700-750°C. AL 20/25+Nb alloy is somewhat stronger than 347 SS foils with modified processing for enhanced creep resistance (T347CR) developed by ORNL and ATI/Allegheny-Ludlum earlier.[13] The Phase I foils of AL 20/25+Nb are stronger than HR120 and HR230, and the limited data so far on Phase II AL 20/25+Nb comes closer to the strength of alloy 625 foils than any of the other alloys. This is significant for recuperator applications at or above 700°C, because with similar good resistance to moisture-enhanced oxidation and the potential for significantly lower cost, the AL 20/25+Nb is the most cost-effective performance upgrade for this application.

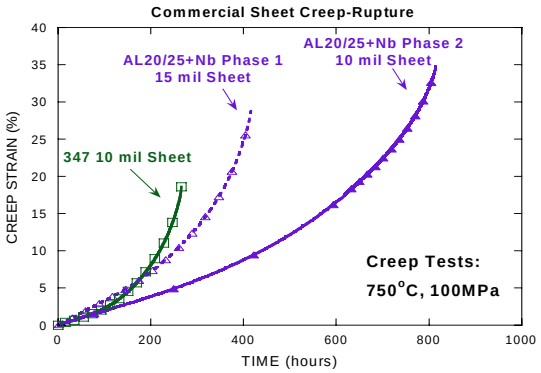

Figure 2 Creep rupture strain versus time plots for creep tests in air at 750°C and 100 MPa, for sheets of 347 steel and the Phase I and Phase II processing runs of AL 20/25+Nb stainless alloy.

Figure 2 shows plots of creep-rupture strain versus time at 750°C and 100 MPa, to show the benefits of the Phase II processing on creep resistance of sheets of the AL 20/25+Nb alloy. While PSR air cells are constructed mainly of foils, BPF air cells require sheets and foils for manufacturing, with the sheet being the main stress-bearing member of the air-cell. If sheets are intermediate products for making foils rather than final products, they will tend to have a finer grain size for maximum ductility during rolling to foil. Metallography of 0.010 inch sheet of Phase I material is shown in Fig. 3, together with quantitative grain size data showing the size distribution as well as the average grain size. The average grain size for Phase I sheet is 12.8 µm, with a higher population of small grains <10 µm. In contrast with Phase II, processing conditions were modified to a higher annealing temperature to coalesce the smallest grains and uniformly increase the grain size without making it too large. The result of this careful change in microstructure produced almost double the creep-rupture life and a slight increase in rupture elongation at 750°C and 100 MPa (Fig. 2). Both rupture life and elongation of the Phase II AL 20/25+Nb are significantly greater than 347 SS, and more ductility may also be an advantage for this alloy in cyclic recuperator/microturbine operation.

Finally, the initial input from Ingersoll-Rand indicated that the new foils and sheets of AL 20/25+Nb possess similar or better manufacturing characteristics compared to 347 SS, including weldability and good brazing behavior. Future work includes ORNL characterization of as-brazed and service-exposed BPF air-cells made using AL 20/25+Nb.

A)

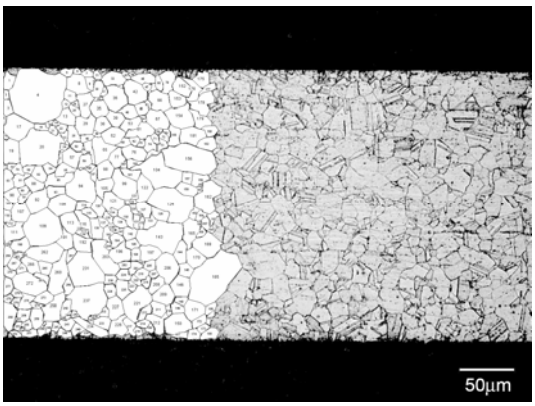

B)

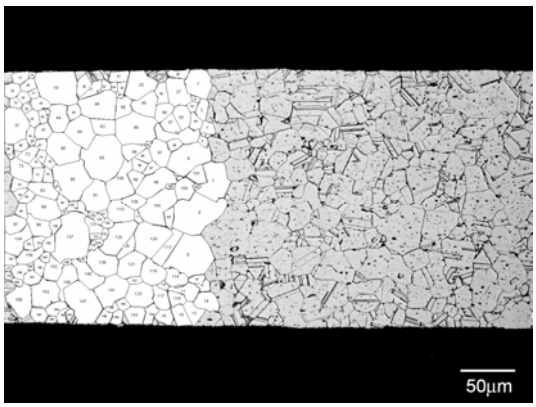

C)

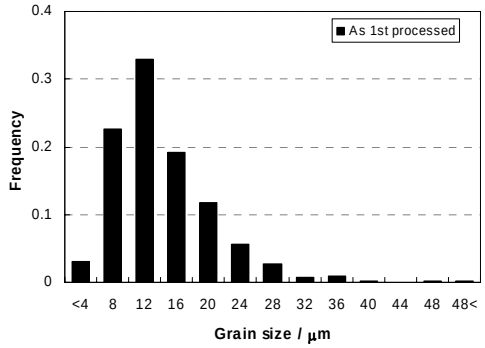

D)

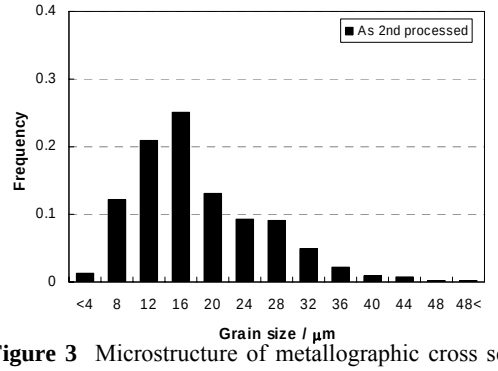

Figure 3 Microstructure of metallographic cross sections of 0.010 inch AL 20/25+Nb alloy sheets of (a) Phase I and (b) Phase II processing, together with histograms of grain size distribution obtained from quantitative analysis of both images (c, d), respectively. Dotted lines in histograms correspond to the average grain size.

Conclusions

A collaborative project by ORNL and ATI Allegheny-Ludlum in Phase I has produced a wide range of commercial foils and sheets of the new AL 20/25+Nb alloy for recuperator air-cell manufacturing with upgraded performance relative to 347 SS. These foils and sheets show better creep resistance than 347 SS at 700-750^{o}C, and Phase I foils meet or exceed the creep-rupture strength of HR120 and HR230. Phase II processing increased the average grain size and eliminated the smallest grains to boost the creep-resistance significantly. Phase II foils come closer to the strength of alloy 625. Next year, creep-testing will be expanded, and microstructural analysis of creep-tested specimens will begin.

References

1. P.J. Maziasz, J.P. Shingledecker, B.A. Pint, N.D. Evans, Y. Yamamoto, K.L. More and E. Lara-Curzio, "Overview of Creep Strength and Oxidation of Heat-Resistant Alloy Sheets and Foils for Compact Heat-Exchangers," GT2005-68927, Proc. 2005 ASME Turbo Expo, Am. Soc. Mech. Engin., New York, NY (2005).
2. Pint, B.A., and More, K.L., "Stainless Steels With Improved Oxidation Resistance for Recuperators," ASME paper GT2004-53627, Am. Soc. Mech. Engin., New York, NY (2004).
3. Lara-Curzio, E., Trejo, R., More, K.L., Maziasz, P.J., and Pint, B.A., "Evaluation and Characterization of Iron- and Nickel-Based Alloys for Microturbine Recuperators," ASME paper GT2005-68630, Am. Soc. Mech. Engin., New York, NY (2005).
4. Rakowski, J.M., Stinner, C.P., Lipschutz, M., and Montague, J.P., "The Use and Performance of Oxidation and Creep-Resistant Stainless Steels in an Exhaust Gas Primary Surface Recuperator Application," ASME paper GT2004-53917, Am. Soc. Mech. Engin., New York, NY (2004).
5. Rakowski, J.M., Stinner, C.P., Bergstrom, D.S., Lipschutz, M., Montague, J.P., "Performance of Oxidation and Creep Resistant Alloys for Primary Surface Recuperators for the Mercury 50 Gas Turbine," ASME paper GT2005-68313, Am. Soc. Mech. Engin., New York, NY (2005).
6. Stambler, I., "Mercury 50 Rated at 4600 kW and 38.5% Efficiency With 5 ppm NOx," 2004, Gas Turbine World (Feb.-Mar.), pp. 12-16.
7. Staubli, M., et al., "Materials for Advanced Steam Power Plants: The European COST522 Action," in Parsons 2003: Engineering Issues in Turbine Machinery, Power Plants and Renewables, The Institute of Materials, Minerals and Mining, Maney Publishing, London, U K, pp. 305-324.
8. Kikuchi, M., Sakakibara, M., Otoguro, Y., Mimura, H., Araki, S., and Fujita, T., 1987, "An Austenitic Heat Resisting Steel Tube Developed For Advanced Fossil-Fired Steam Plants," in High Temperature Alloys, Their Exploitable Potential, Elsevier Science Publishing Co., New York, NY, pp. 267-276.

9. Takahashi, T., et al., 1988, "Development of High-Strength 20Cr-25Ni (NF709) Steel for USC Boiler Tubes," Nippon Steel Technical Report No. 38 (July 1988), Nippon Steel Corp., Tokyo, Japan.

10. Quality and Properties of NF709 Austenitic Stainless Steel for Boiler Tubing Applications, 1996, Nippon Steel Corp., Revision 1.1, Tokyo, Japan.

11. Maziasz, P.J., Swindeman, R.W., Shingledecker, J.P., More, K.L., Pint, B.A., Lara-Curzio, E., and Evans, N.D., 2003, "Improving High Temperature Performance of Austenitic Stainless Steels for Advanced Microturbine Recuperators," in Parsons 2003: Engineering Issues in Turbine Machinery, Power Plants and Renewables, The Institute of Materials, Minerals and Mining, Maney Publishing, London, UK, pp. 1057-1073.

12. Maziasz, P.J., Pint, B.A., Shingledecker, J.P., More, K.L., Evans, D.E., and Lara-Curzio, E., "Austenitic Stainless Steels and Alloys With Improved High-Temperature Performance for Advanced Microturbine Applications," ASME paper GT2004-54239, Am. Soc. Mech. Engin., New York, NY (2004).

13. Stinner, C., "Processing to Improve Creep and Stress Rupture Properties of Alloy T347 Foil," 2003, Allegheny Ludlum Technical Center internal report, Brackenridge, PA, available upon request.

14.

FY2005 Awards/Patents

None

FY2005 Publications/Presentations

1. N.D. Evans, P.J. Maziasz, Y. Yamamoto, and J.P. Shingledecker, "Electron Microscopy of Heat-Resistant Alloy Sheets and Foils Being Considered for Use in Recuperators," *Microscopy and Microanalysis,* **11** (Supplement 2) (2005) 1714-1715.

2. P.J. Maziasz, J.P. Shingledecker, B.A. Pint, N.D. Evans, Y. Yamamoto, K.L. More and E. Lara-Curzio, "Overview of Creep Strength and Oxidation of Heat-Resistant Alloy Sheets and Foils for Compact Heat-Exchangers," GT2005-68927, Proc. 2005 ASME Turbo Expo (6-9 June, 2005, Reno, NV), Am. Soc. Mech. Engin., New York, NY (2005).

3. B.A. Pint and P.J. Maziasz, "Development of High Creep Strength and Corrosion-Resistant Stainless Steels," paper 05449, Corrosion 2005, NACE-International, Houston, TX (2005).

4. E. Lara-Curzio, R. Trejo, K.L. More, P.J. Maziasz, and B.A. Pint, "Evaluation and Characterization of Iron- and Nickel-Based Alloys for Microturbine Recuperators," GT2005-68630, Proc. 2005 ASME Turbo Expo (6-9 June, 2005, Reno, NV), Am. Soc. Mech. Engin., New York, NY (2005).

5. L. Chen and P.J. Maziasz, "Clad Metal Strips and Foils Engineered for High-Temperature Performance," GT2005-68613, Proc. 2005 ASME Turbo Expo (6-9 June, 2005, Reno, NV), Am. Soc. Mech. Engin., New York, NY (2005).

6. *Overview of Creep Strength and Oxidation of Heat-Resistant Alloy Sheets and Foils for Compact Heat Exchangers*, invited talk at Symposium on Fuel Cells: Materials Processing and Manufacturing Technologies, ASM Materials Solutions 2004, 18-20 October, 2004, Columbus, OH.

7. *Overview of Creep Strength and Oxidation ofHeat-Resistant Alloy Sheets and Foils for CompactHeat Exchangers,* presentation at IGTI TurboExpo2005, 6-9 June, 2005, Reno, NV.

Acronyms

AL – Allegheny-Ludlum

ORNL – Oak Ridge National Laboratory

OEM – original equipment manufacturer

CT – Capstone Turbines, Inc.

IRES – Ingersoll-Rand Energy Systems

ASM – ASM International

LMP – Larson-Miller Parameter

SS – stainless steel

2.1.2 Oxidation/Corrosion Characterization of High-Temperature Recuperator Alloys and Field-Exposed Recuperators

K.L. More
Metals & Ceramics Division
Oak Ridge National Laboratory
Oak Ridge, TN 37831-6064
(865) 574-7788; e-mail: morekl1@ornl.gov

DOE Technology Development Manager: Debbie Haught
(202) 586-2211; (202) 586-7114 (fax); e-mail: debbie.haught@ee.doe.gov
ORNL Technical Advisor: Karren More
(865) 574-7788; (865) 576-5413 (fax); e-mail address: morekl1@ornl.gov

Objectives
- Conduct extensive microstructural analyses on recuperator alloy foils exposed in the laboratory (elevated H_2O at 650°C, 750°C, and 800°C)) and to microturbine operating environments, both field-aged and in ORNL's Microturbine Recuperator Test Facility (MRTF), to understand alloy oxidation behavior.
- Interact with Principal Investigators for Subtasks 2.1.1, 2.1.3, and 2.1.4, to conduct critical microstructural characterization and coordinate research efforts.
- Collaborate with external microturbine recuperator manufacturers to evaluate their recuperators before and after field-exposures to assist in the optimization of alloy structure(s) and properties (primarily Capstone Turbines and Ingersoll Rand).

Approach
- Coordinate characterization effort to best compare recuperator alloys exposed in different environments (i.e., field-aged vs. laboratory aged vs. MRTF).
- Utilize appropriate characterization methods for direct comparison of structural and compositional data (i.e., electron probe microanalysis (EPMA), scanning electron microscopy (SEM), transmission electron microscopy (TEM)).

Accomplishments
- Ongoing collaboration with Capstone Turbines Inc. to evaluate field-aged recuperators; Wendy Matthews visited ORNL 4 times in FY2005 to conduct microstructural evaluation of microturbine-aged recuperators fabricated from 347 stainless steel (SS) and alloy 120. These results have been compared to ORNL's studies on the same alloys exposed in the laboratory and MRTF.
- Completed microstructural analyses of 347 SS, Haynes alloy 120, Haynes alloy 214, Haynes alloy 230, and alloy AL 20/25+Nb exposed for 1000 h in ORNL's MRTF. ORNL-modified 347 SS compositions have also been evaluated after 500 h in ORNL's MRTF.

Future Directions
- Continue to characterize recuperator alloys after laboratory exposures and exposure in ORNL's MRTF for comparison with previously-exposed foils.
- Compare extensive microstructural analyses from laboratory and MRTF exposures to microturbine-aged recuperator foils.
- Begin evaluation of recuperators exposed in microturbines run using alternative fuels.

Introduction

Commercially-available alloys for high-temperature microturbine recuperators (operating between 650°C-750°C) are being mechanically tested, microturbine-aged, and laboratory-exposed (corrosion-tested) as part of 3 separate ORNL Advanced Recuperator Materials Subtasks;

2.1.1 "Advanced Alloys for High Temperature Recuperators,"

2.1.3 "Composition Optimization for Corrosion Resistance to High Temperature Exhaust Gas Environments,"

2.1.4 "Recuperator Testing and Evaluation."

Microstructural characterization plays a critical role in each of these Subtasks (please see individual Annual Reports for each Subtask). Understanding the corrosion/oxidation behavior of the different alloys in H_2O-containing environments is important for the identification of an improved alloy for use in this application at the higher temperatures required. Microstructural characterization is used to determine the extent of oxidation, to identify the reaction products formed, to evaluate changes in the base alloy, and most importantly, to elucidate alloy degradation mechanisms.

Approach

Microstructural analysis data is extremely important in order to determine the structural and compositional factors that have the greatest impact on alloy stability in corrosive environments, such as that experienced by alloy foils in the microturbine exhaust gas (recuperator). This data, coupled with weight change data (accumulated during long-term laboratory exposures), creep strength, and residual mechanical properties data (measured after exposure in MRTF), provide the quantitative information required to model/estimate alloy lifetimes in a recuperator.

To this end, extensive microstructural analysis has been conducted on candidate high-temperature recuperator alloys exposed under a series of different exposure conditions (laboratory and microturbine) to evaluate and compare the high-temperature properties of the different commercial alloys. Cross-sections of exposed foils are prepared to characterize the foil surfaces for oxidation/corrosion performance. Elemental analyses (including maps and line profiles) and SEM imaging are conducted for each sample in a similar manner such that all data can be compared.

Results

During FY2005, microstructural analyses were conducted on the following alloy compositions and exposure conditions to correlate with alloy weight change data and residual mechanical properties:

• 347 SS	500 h MRTF Capstone C30 microturbine Capstone C60 microturbine 500 h air+10% H_2O
• Haynes 120	500 h, 1000 h MRTF Capstone C60 microturbine 1000 h, 10k h air+10% H_2O 1000 h vacuum annealed
• AL 20/25+Nb	500 h MRTF 1000 h air+10% H_2O 1000 h vacuum annealed
• Haynes 230	500 h MRTF
• Haynes 214	500 h, 1000 h MRTF
• ORNL-mod 347	500 h MRTF 1000 h air+10% H_2O
• Inconel 625	500 h, 1000 h MRTF 10,000 h air+10% H_2O

Additional exposures are currently being conducted such that there are direct comparisons between the different experimental conditions (laboratory vs. MRTF) in terms of exposure time and temperature. It is well-known that 347 SS is not stable in H_2O-containing exhaust at microturbine operating (exit) temperatures above 600°C. This is shown by the cross-section SEM images from 500 h MRTF-exposed 347 SS in Figures 1-4, where Figure 1 is the lowest exposure temperature (650°C) and Figure 4 is the highest temperature (785°C). After only 500 h exposure in the MRTF, significant oxidation of the 347 SS has occurred, especially at the 2 highest temperatures. Compare the low oxidation-resistance of the 347 SS (alloy typically used in recuperators) to that of Haynes alloy 120, as illustrated in the cross-section SEM images in Figures 5-8. Clearly, alloy 120 has much better oxidation-resistance (higher Cr reservoir) compared with 347 SS at the higher exposure temperatures. Strength retention of this alloy compared with 347 SS (after 500 h

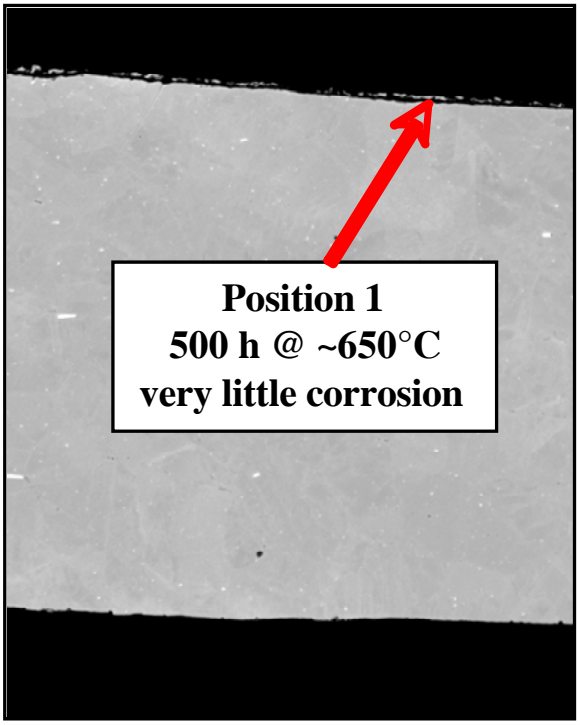

Figure 1. Cross-section of 347 SS exposed in ORNL MRTF 500 h at 650°C.

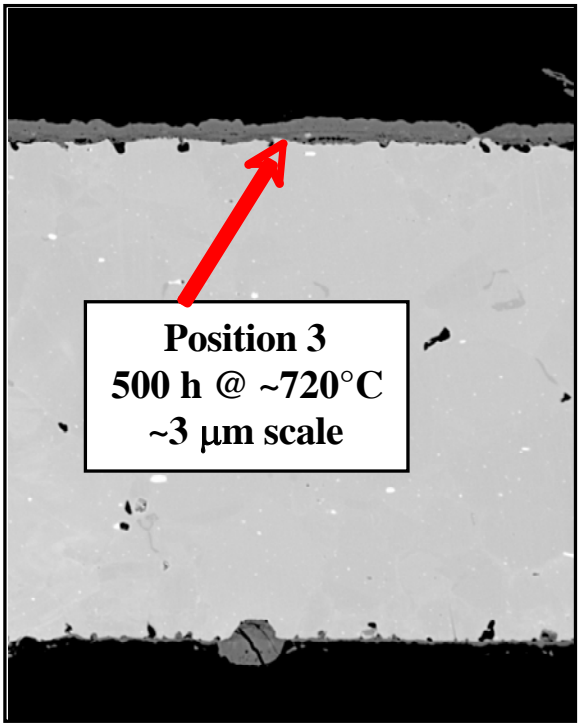

Figure 3. Cross-section of 347 SS exposed in ORNL MRTF 500 h at 720°C.

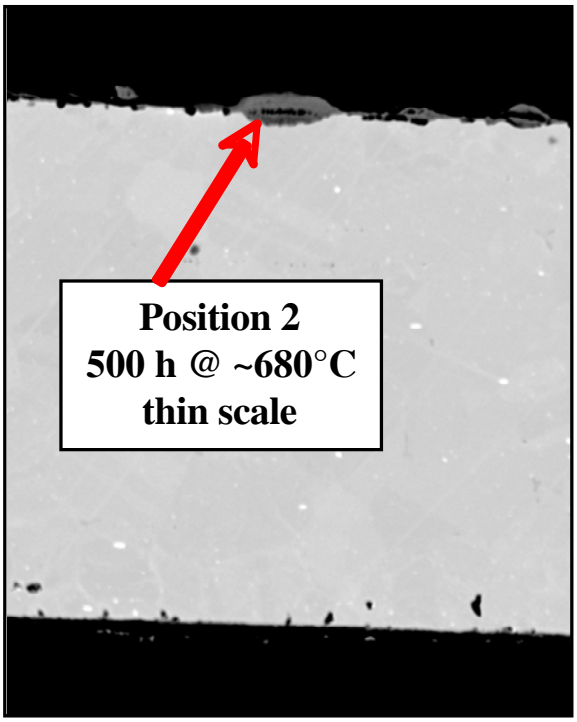

Figure 2. Cross-section of 347 SS exposed in ORNL MRTF 500 h at 680°C.

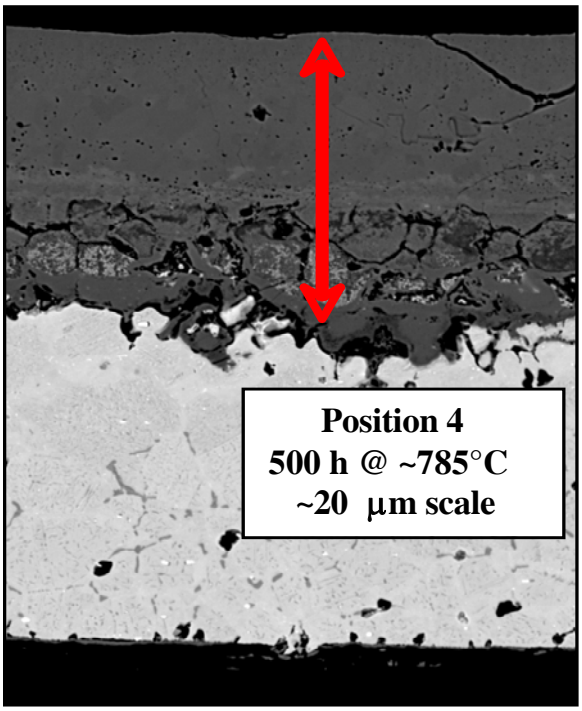

Figure 4. Cross-section of 347 SS exposed in ORNL MRTF 500 h at 785°C.

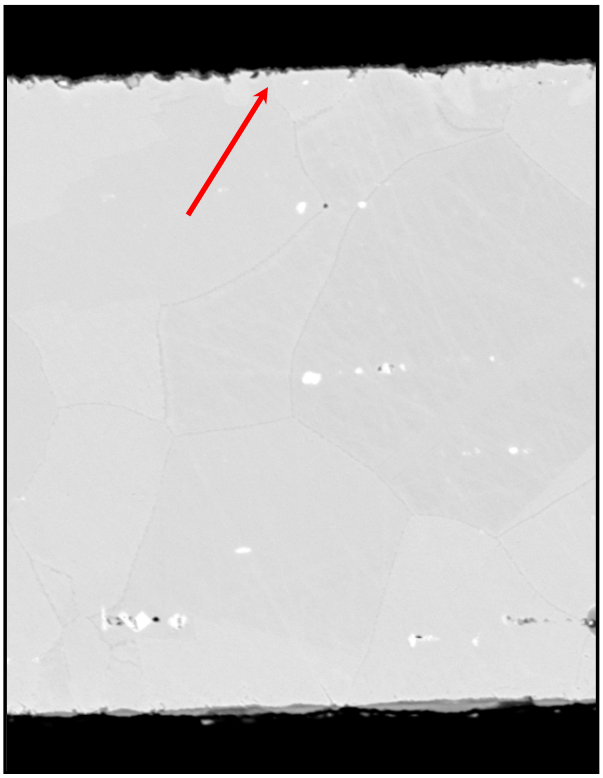

Figure 5. Cross-section of alloy 120 exposed in ORNL MRTF 500 h at 650°C.

Figure 6. Cross-section of alloy 120 exposed in ORNL MRTF 500 h at 680°C.

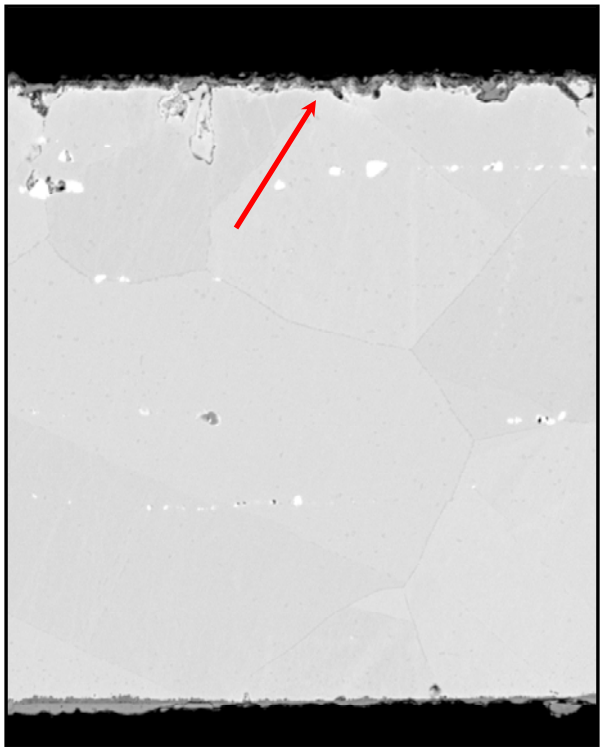

Figure 7. Cross-section of alloy exposed in ORNL MRTF 500 h at 720°C.

Figure 8. Cross-section of alloy exposed in ORNL MRTF 500 h at 785°C.

cross-section SEM images in Figures 5-8. Clearly, alloy 120 has much better oxidation-resistance (higher Cr reservoir) compared with 347 SS at the higher exposure temperatures. Strength retention of this alloy compared with 347 SS (after 500 h @ ~750°C in the MRTF) was also much higher, ~10% drop in ultimate tensile strength for alloy 120 compared with a nearly 40% drop for 347 SS.

It is not the intent of this report to detail the microstructural characteristics of each alloy exposed during the course of these research efforts. The microstructural research supports each of the individual Subtasks involved in high-temperature recuperator alloy development by providing the critical structural and compositional data required to understand observed alloy degradation and to explain life prediction models. The mechanism by which this is achieved is by working closely with each of the Subtask investigators and coordinating research efforts amongst the tasks.

Conclusions

- Extensive microstructural characterizations, including structural and compositional analyses, have been conducted on alloy foils exposed to elevated H_2O in the laboratory and compared with similar alloy compositions exposed in the MRTF.
- Field-aged recuperators from Capstone Turbine Co., Ingersoll Rand, and Honeywell have also been evaluated using similar characterization methods and compared with the ORNL exposure results.
- Results from the ongoing Capstone/ORNL collaboration have been incorporated in a 2005 IGTI paper comparing 347 SS to Haynes alloy 120 (see #5 listed below).

Awards/Patents

ASME/IGTI Microturbines & Small Turbomachinery Committee 2004 Best Paper Award, B.A. Pint and K.L. More, "Stainless Steels with Improved Oxidation Resistance," ASME Paper #GT2004-536627.

Publications/Presentations

1. K.L. More, "The Fundamental Role of Microstructural and Microchemical Analysis in High-Temperature Oxidation Science," invited presentation at 206thMeeting of The Electrochemical Society, October 2004, Honolulu, HI.
2. 2. K.L. More, B.A. Pint, E. Lara-Curzio, P.J. Maziasz, P.F. Tortorelli, and L.R. Walker, "The Effect of Water-Vapor on the Microstructural and Compositional Stability of Recuperator Alloys at Temperatures > 600°C," presented at Microscopy of Oxidation 6, April 2005, Birmingham, UK.
3. 3. E. Lara-Curzio, R. M. Trejo, K. L. More, P. J. Maziasz, and B. A. Pint, "Evaluation and Characterization of Iron- and Nickel-Based Alloys for Microturbine Recuperators," Paper #GT-2005-68630, presented at IGTI TurboExpo 2005, June 2005, Reno, NV.
4. 4. P.J. Maziasz, J.P. Shingledecker, B.A. Pint, N.D. Evans, Y. Yamamoto, K.L. More and E. Lara-Curzio, "Overview of Creep Strength and Oxidation of Heat-Resistant Alloy Sheets and Foils for Compact Heat-Exchangers," ASME Paper #GT2005-68927, presented at IGTI TurboExpo 2005, June 2005, Reno, NV.
5. 5. W.J. Matthews, T. Bartel, D.L. Klarstrom, and L.R. Walker, "Engine Testing of an Advanced Alloy for Microturbine Primary Surface Recuperators," Paper #GT-2005-68781, presented at IGTI TurboExpo 2005, June 2005, Reno, NV.

Acronyms

ORNL – Oak Ridge National Laboratory

MRTF – Microturbine Recuperator Test Facility

SS – stainless steel

EPMA – electron probe microanalysis

SEM – scanning electron microscopy

TEM – transmission electron microscopy

2.1.3 Composition Optimization for Corrosion Resistance to High Temperature Exhaust Gas Environment

Bruce A. Pint
Metals and Ceramics Division
Oak Ridge National Laboratory
Oak Ridge, TN 37831-6156
(865) 576-2897, E-mail: pintba@ornl.gov

DOE Technology Development Manager: Debbie Haught
(202) 586-2211; (202) 586-7114 (fax); e-mail: debbie.haught@ee.doe.gov
ORNL Technical Advisor: Karren More
(865) 574-7788; fax (865) 576-5413; e-mail: morekl1@ornl.gov

Objective

- Determine minimum Cr and Ni contents needed for corrosion resistance in exhaust gas to assist in the development of a cost-effective replacement for type 347 stainless steel in microturbine recuperators operating at 650°-700°C.
- Develop an improved understanding of the role of water vapor on the accelerated corrosion of stainless steel foil including mechanistic and mathematical lifetime models.

Approach

- Study the corrosion behavior of model and commercial alloys in foil and sheet form in laboratory tests designed to simulate the water content in microturbine exhaust gas
- Characterize the growth of reaction products and loss of Cr from the substrate to quantify the rate of recuperator alloy degradation.

Accomplishments

- Completed quantification of Cr consumption from foil specimens of advanced recuperator alloys that had reached 10,000h in laboratory testing at 650°, 700° and 800°C in humid air.
- Using classical gas transport theory and new NASA thermodynamic data, Cr consumption rates for Fe-20Cr-25Ni foils were calculated which matched experimental values and predictions were made for conditions expected in a microturbine recuperator.

Future Direction

- Compare Cr consumption rates from laboratory oxidation specimens to results from specimens exposed to microturbine exhaust in order to improve the lifetime model predictions
- Explore possible mitigation strategies that could reduce the Cr consumption rate in advanced austenitic alloys.
- Continue testing of commercial advanced austenitic alloy foil specimens to compare to previous results for laboratory made foils.

Introduction

In order to boost the efficiency of current microturbines, higher engine temperatures are needed. However, increasing the recuperator or heat exchanger temperature from ~600°C to 650°-700°C results in a drastic loss in durability for type 347 stainless steel thin section (75-125µm) components. The problem is caused by accelerated corrosion attack due to the presence of water vapor in the exhaust gas.[1] This problem is now widely recognized and engine manufacturers have switched to advanced austenitic alloys such as alloy 625 in the Solar Turbine Mercury 50 4.6MW turbine and alloy 120 in some Capstone microturbines. Likewise, an alloy manufacturer (Allegheny Ludlum) is now marketing Fe-20Cr-25Ni (AL20/25+Nb) foil for this application.

While these alloys do not undergo accelerated attack as readily as type 347 stainless steel, they are still affected by the presence of water vapor, resulting in increased volatilization of Cr due to the formation of $CrO_2(OH)_2(g)$. This leads to Cr consumption from the metal at a linear rate, which is much faster than the parabolic kinetics of simple oxidation in dry air. For example, the Cr loss from 1 00µm alloy 709 (Fe-20Cr-25Ni+Nb) foil during exposure in laboratory air at 800° C is much slower than that observed in air + 10% H_2O, Figure 1. Thus, the goals of this work are to better understand the mechanistic effect of water vapor and quantify this effect on the advanced

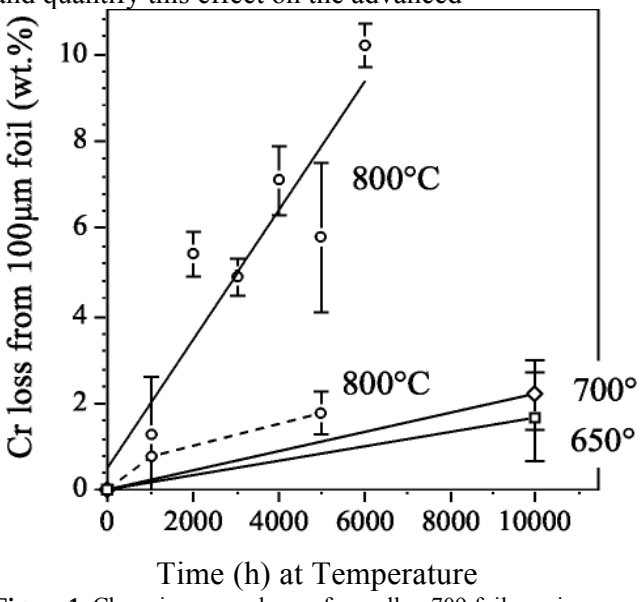

Figure 1. Chromium mass losses from alloy 709 foil specimens as a function of time after exposures to air + 1 0%H_2O (solid lines) at 650°-800°C. Values for 800°C exposures in laboratory air (dashed line) are shown for comparison.

austenitic alloys in laboratory experiments. As the first step in developing a lifetime model for these materials, classical gas transport theory and recent thermodynamic data have been used to calculate Cr consumption rates for alloy 709, which matched experimental values.

Approach

Commercial foil specimens were obtained from alloy and engine manufacturers or rolled to foil from thicker starting materials and exposed in the as-rolled condition. Model alloys were vacuum induction melted and cast in a water-chilled copper mold, followed by hot forging and rolling to 2.5mm. The sheets were then cold rolled to 1.25mm and annealed under Ar + 4%H_2 for 2 min at 1000°C. Sheet specimens (12mm x 17mm x 1.2mm) were polished to 600 grit SiC finish. Chemical compositions were measured by combustion and plasma analysis after casting, Table I. The oxidation tests were done in air + 10±1 vol.% water vapor flowing at 850cc/min with 100h cycles at 650°, 700° and 800°C. After oxidation, selected specimens were Cu-plated and sectioned for metallographic analysis and electron probe microanalysis (EPMA) to determine Cr depletion profiles.

Results

Oxidation Testing

As previously reported, testing at 650°, 700° and 800°C has been completed to 10,000h on the first series of advanced austenitic alloy foils. The next generation of commercial materials, e.g. batches of alloy 120 and AL20/25+Nb, started during the past year. An example of the mass gain data is shown in Figure 2. The new batches of commercially rolled material are showing similar mass gain behavior as the previous laboratory rolled foils with similar compositions, Table I. However, the information that can be learned from the specimen mass gain data is limited because it is the summation of several mechanisms, including growth, evaporation and

Table I. Alloy chemical compositions (weight %) and average grain sizes (µm) of the foil and sheet materials. (Balance Fe)

	Cr	Ni	Mn	Si	Other	Grain Size (µm)
Type 347	17.8	9.9	1.6	0.5	0.5Nb	5
709	20.3	24.7	1.0	0.4	1.5Mo,0.2Nb	16
AL20/25+Nb	20.3	25.4	1.1	0.3	1.5Mo,0.4Nb	n.d.
120	24.7	37.6	0.7	0.2		13,23*
Fe-16/20+2Mn	15.8	19.7	1.7	0.2		26

* ORNL- and commercial-rolled foils, respectively

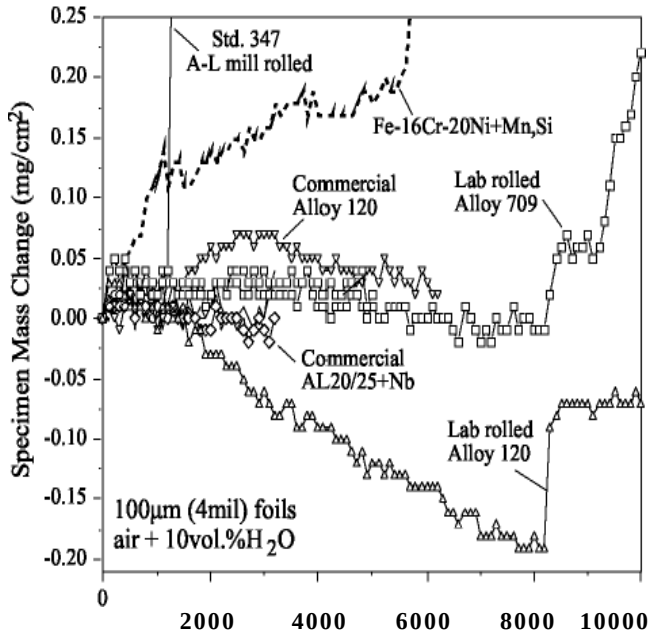

Figure 2. Specimen mass gains for various foil (100µm thick) materials during 1 00h cycles in humid air at 650°C.

spallation of the reaction product:

$$DM_{specimen} = {}^{DM}_{oxide\ growth} - {}^{DM}_{evap.} - {}^{DM}_{spall}$$

Thus, while mass gain can be used to differentiate the onset of accelerated attack (AA) it is not very useful in quantifying the extent of attack because of competing factors. Thus, additional compositional characterization is necessary.

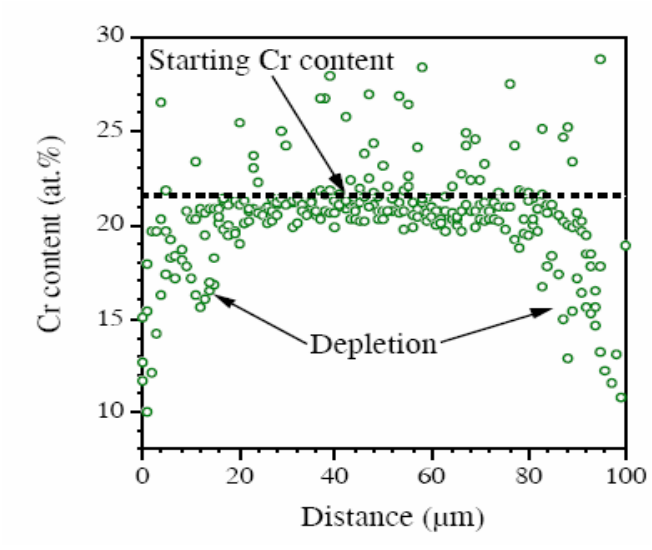

Figure 3. EPMA Cr profiles from three scans across the cross-section of alloy 709 foil after 10,000h at 700°C in humid air. The Cr depletion appears to be only ª20µm from the surface.

Characterization of Cr depletion

In order to quantify the extent of attack, composition maps and profiles were measured across polished foil specimen cross-sections exposed for 10,000h using EPMA. An example profile is given in Figure 3. Due to the relatively slow diffusion of Cr in the alloy at 650°-700°C, the depletion is concentrated near the surface (10-20µm) of the foil. The center of the foil is relatively unaffected. The local variations in the center of the profile are due to the formation of Cr-rich carbides (e.g. M_6C and $M_{23}C_6$).[2] The localized depletion explains why increasing the foil thickness will not prevent nodule formation. The diffusion of Cr is too slow at 650°-700°C for Cr from the center of the foil to diffuse to the surface and prevent localized depletion. It also explains the formation of nodules on even the higher Cr content alloy 120 foils. No matter how high the starting Cr content, the surface will eventually become depleted as Cr is selectively removed due to the combined oxidation and evaporation. The mass gain increases for alloy 709 and 120 after 8,000h at 650°C (Figure 2) indicate nodule formation. The continued mass increase for the alloy 709 foil after 8,000h suggests that the nodule formation is more severe in this material with only 20%Cr compared to 25% in alloy 120.

One problem with line profiles and a source of their variability is that they do not accurately quantify the localized Cr depletion on the alloy grain boundaries near the surface. The grain boundaries become selectively depleted because of the higher boundary Cr diffusivity compared to the interior of the grains. Depletion associated with grain boundaries near the foil surface were the most likely location for nodule (FeO_x) nucleation. As an

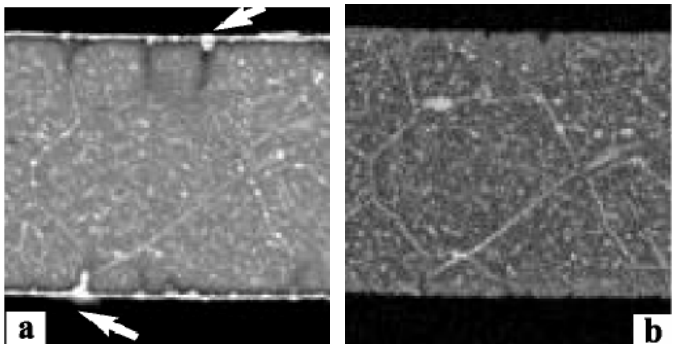

Figure 4. EPMA maps of 90µm thick commercial alloy 120 foil after a 10,000h exposure in humid air at 700°C (a) Cr, and (b) Mo. A grain-boundary phase containing Cr, Mo and Si marked the large grains within the metal and Cr depletion was observed on grain boundaries near the surface.

example, the coarser-grained commercial 1 00µm alloy 120 foil (Table I) at 700°C showed more nodule formation, arrows in Figure 4a, than the finer grained material. With fewer grain boundaries, there was an overall slower Cr flux to the foil surface in this material and the Cr depletion was more localized in the coarser-grained material resulting in more nodules. The maps in Figure 4 also illustrate that while the alloy grain boundaries are depleted (darker) at the surface, they are enriched in Cr near the center due to carbide precipitation. The Mo map in Figure 4b shows the same correlation as does the Si map (not shown). Note that the grain boundaries are not enriched with Mo near the foil surface as the carbides have dissolved where the Cr has been selectively depleted.

A summary of the Cr depletion results for the various alloys and temperatures is given in Table II. The absolute Cr depletion values are similar for all of the materials and virtually independent of starting Ni, Cr or Mn contents, Table I. Thus, the Ni-base alloys lost Cr at the same rate as the Fe-base alloys. Most surprisingly, the 1% Mn addition did not suppress Cr loss for alloy 709 as suggested by prior work by Quadakkers.3 The evaporation may be decreased due to the Mn addition but the increased scale thickness with Mn additions resulted in no net effect on the remaining Cr content in the metal compared to the alloys with less Mn.

The role of Cr and Ni content on nodule formation has been more carefully studied by the use of model alloys. Figures 5 and 6 show results from a model Fe-16Cr-20Ni+Mn,Si alloy sheet specimen exposed to humid air at 65 0°C for 7,000h. This 1mm thick specimen which started with a lower than normal Cr content began to show nodule formation near 6,000h, Figure 2. Figure 5 shows an area where a nodule formed with an area prior to nodule formation on the left. Prior to nodule formation,

Table II. Remaining Cr (% of starting content) and the actual amount of Cr consumed (wt.%) for various foil materials oxidized in humid air for 10,000h (except where noted).*

Alloy	650°C	700°C	800°C
709	92±5%	89±4%	51±2% (6,000h)
	-1.7±1.0wt%	-2.2±0.8wt%	-10.2±0.5wt%
120 (ORNL)	94±1%	91±2%	
	-1.6±0.3wt%	-2.3±0.6wt%	
120 (Comm)		92±4%	53±1% (1 0 , 0 00h)
		-2.1±0.9wt%	-11.8±0.5wt%
625	94±4%	89±2%	77±4% (6,000h)

* The Standard deviation for three EPMA profiles is indicated

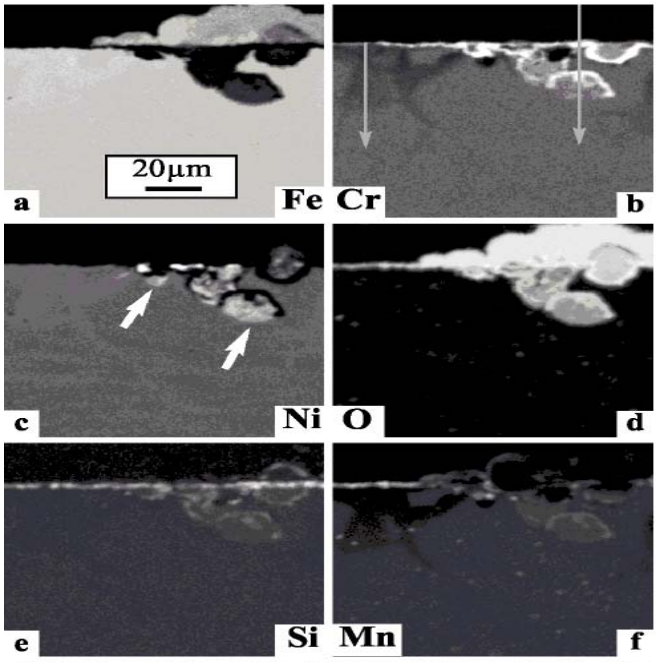

Figure 5. EPMA maps of Fe-16Cr-20Ni+Mn,Si after 7,000h at 650°C in humid air: (a) Fe, (b) Cr, (c) Ni, (d) O, (e) Si and (f) Mn. Surface oxide nodules form which have a Ni-rich center, Cr-rich underlayer and Fe-rich outer layer.

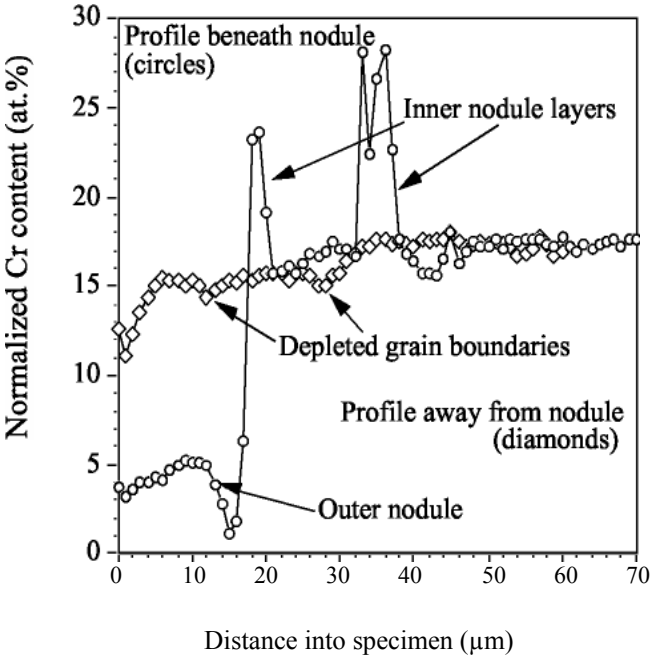

Figure 6. EPMA Cr profiles from two scans (shown in Fig. 5b).

Cr-rich scale shows a clear layer of Si- and Mn-rich oxide. The Cr map in Figure 5b and the associated line profile in Figure 6 show that the alloy grain boundaries near the surface in this area were Cr depleted. Note that without Mo or C additions in this model alloy, no Cr enrichment was observed deeper in the alloy, as in Figure 4a. The outer Fe-rich oxide nodule has an underlying inner oxide with various Cr-rich layers, profile in Figure 6. The beneficial role of Ni may be attributed to the formation of Nirich oxide beneath the nodule (Figure 5c) that may have assisted in slowing the growth of the nodule, along with the Cr-rich layers. With only ~10%Ni in type 347 stainless steel, compared to 20% Ni in this model alloy, faster-growing Fe-rich oxide likely would form beneath a nodule formed on type 347 stainless steel.

Model Development

With the expertise of Prof. David Young, ORNL visiting scientist from the Univ. of New South Wales, Australia, the first step in the development of a model was completed by applying classical gas transport theory to the Cr evaporation. Details of this analysis are available elsewhere.[4] The experimental Cr depletion results for alloy 709 foil specimens were compared to calculations based on recent thermodynamic data from E. Opila at NASA Glenn Research Center. By using the experimental gas composition, specimen length *(l)* and velocity (v), a good match was obtained between the calculation and the experimental results, Figure 7.

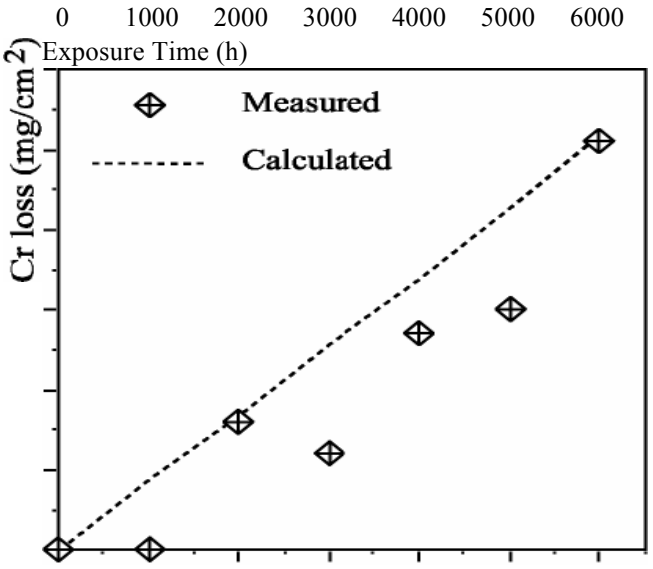

Figure 7. Comparison of the calculated and measured Cr loss from alloy 709 foils exposed to humid air at 800°C.

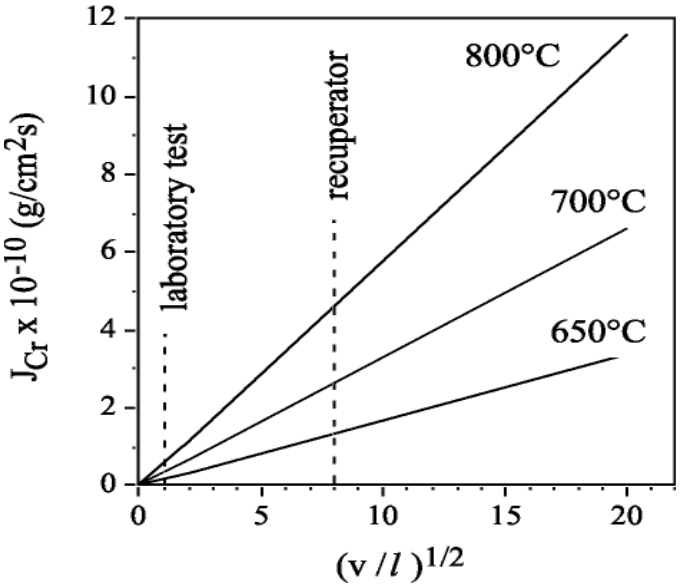

Figure 8. Calculated Cr loss fluxes as a function of $(v/l)^{1/2}$ for air+5%H_2O at 650°-800°C. Dashed lines mark conditions in the laboratory test compared to the approximate conditions in a recuperator.

The next step in the model development was to perform the same calculations based on the recuperator conditions. One of the most important variables for this calculation was the v/*l* ratio and its effect on the Cr loss flux, $_{JCr,}$ at several temperatures, as shown in Figure 8. The expected ratio in the recuperator is marked as well as the conditions for the laboratory test. The other differences between the two conditions are the water vapor content (10% in the laboratory test is nominally twice that expected in the engine exhaust) and that only one side of the foil is exposed to the exhaust gas in the recuperator. The net is an expected factor of 2 increase in Cr loss in the recuperator compared to the laboratory test. This result needs to be confirmed by comparing specimens tested in the ORNL microturbine facility to those tested in the laboratory.

Conclusions

Work has continued on studying the effect of water vapor on the corrosion of commercial, laboratory scale and model stainless steels at 650°-800°C. The rate of Cr loss due to evaporation as a function of temperature was very similar for each of the alloys tested, independent of Cr, Ni and Mn content. At 650°C, the Cr depletion was concentrated near the alloy surface due to the relatively slow diffusion of Cr in the metal. The Cr depletion, particularly on alloy grain boundaries at the surface, leads to accelerated oxidation and Fe-

rich nodule formation, even for highly alloyed austenitic alloys. Calculated Cr loss rates based on classical gas transport theory show a good match with experimental values for alloy 709. Similar calculations were made based on the expected conditions in a microturbine recuperator. The next step will be confirming the model predictions by measuring Cr losses in commercial foils exposed in the ORNL microturbine test facility.

References

1. B. A. Pint and J. M. Rakowski, (2000) NACE Paper 00-259, Houston, TX, presented at NACE Corrosion 2000, Orlando, FL, March 2000.
2. P. J. Maziasz, R. W. Swindeman, J. P. Shingledecker, K. L. More, B. A. Pint, E. Lara-Curzio and N. D. Evans, in *Parsons 2003, Engineering Issues in Turbine Machinery, Power Plant and Renewables,* A. Strang, et al. eds., Maney, 2003, London, pp.1057-73.
3. W. J. Quadakkers, T. Malkow, J. Piron-Abellan, U. Flesch, V. Shemet and L. Singheiser, in *Proc. 4th Eur. Solid Oxide Fuel Cell Forum,* Vol. 2, A. J. McEvoy ed., Elsevier, 2000, Amsterdam, pp.827-36.
4. D. J. Young and B. A. Pint, submitted to Oxidation of Metals, 2005.

FY 2005 Awards/Patents

IGTI Best Paper Award for the Microturbines & Small Turbomachinery Committee from the 2004 Turbo Expo, for ASME Paper GT2004-53627 "Stainless Steels with Improved Oxidation Resistance for Recuperators" by B. A. Pint and K. L.More, awarded in June 2005.

FY 2005 Publications/Presentations

1. B. A. Pint, (2005) "The Effect of Water Vapor on Cr Depletion in Advanced Recuperator Alloys," ASME Paper #GT2005-68495, presented at the International Gas Turbine & Aeroengine Congress & Exhibition, Reno-Tahoe, NV, June 6-9, 2005.
2. B. A. Pint and P. J Maziasz, (2005) "Development of High Creep Strength and Corrosion-Resistant Stainless Steels," NACE Paper 05-449, Houston, TX, presented at NACE Corrosion 2005, Houston, TX, April 2005.
3. D. J. Young and B. A. Pint, "Chromium Volatilization Rates from Cr_2O_3 Scales Into Flowing Gases Containing Water Vapor," submitted to Oxidation of Metals.

2.1.4 Recuperator Materials Testing and Evaluation

Edgar Lara-Curzio, Karren L. More, Rosa M. Trejo and Sebastien Dryepond
Metals & Ceramics Division
Oak Ridge National Laboratory
Oak Ridge, TN 37831-6069
(865) 574-1749; laracurzioe@ornl.gov

DOE Technology Development Manager: Debbie Haught
(202) 586-2211; (202) 586-7114 (fax); e-mail: debbie.haught@ee.doe.gov
ORNL Technical Advisor: Karren L. More
(865) 574-7788; fax (865) 576-5413; e-mail: morekl1@ornl.gov

Objectives

- Screen and evaluate candidate alloys for the next generation of advanced microturbine recuperators
- Evaluate the evolution of mechanical and physical properties and microstructure of candidate. microturbine recuperator alloys as a function of time and temperature of exposure in a microturbine environment, ORNL's Microturbine Recuperator Test Facility (MRTF).
- Identify the structural mechanisms responsible for their degradation.

Approach

- In collaboration with Capstone Turbines, Inc. a 60kW microturbine was modified to operate at recuperator inlet temperatures as high as 850°C and to allow the placement of test specimens at the entrance of the recuperator. During exposure tests, specimens are subjected to mechanical stresses that simulate the stresses associated with the flow of compressed air and exhaust gases on opposite sides of the recuperator cells.
- The durability of candidate recuperator materials is determined by characterizing the evolution of the material's mechanical properties and microstructure as a function of time and temperature of exposure in the MRTF.
- Candidate materials for evaluation in ORNL's MRTF are selected in collaboration with other tasks in the Advanced Recuperator Materials Program and with microturbine recuperator manufacturers.

Accomplishments

- The effect of temperature and time of exposure in the MRTF on the mechanical properties, corrosion resistance and microstructure of ORNL-modified stainless steels and alloys 625LCF, HR120®, HR214®, HR230®, FeCrAl and AL 20/25+Nb was determined during FY05.
- A device (sample holder) was instrumented for the MRTF to investigate the effect of microturbine intermittent operation on the durability of candidate materials for microturbine recuperators.

Future Direction

Continue evaluation of candidate alloys in ORNL's MRTF for exposures of up to 5000 h and compare results with those obtained during long-term cyclic testing performed in the laboratory at ORNL.

Introduction

The challenging performance targets for the next generation of microturbines include fuel-to-electricity efficiency of 40%, capital costs less than $500/kW, fuel flexibility, NOx emissions reduced to single parts per million and service life of 40,000 hours [1]. Significant increases in microturbine efficiency can be achieved by increasing engine-operating temperatures, and in turn, these could be realized through the use of advanced metallic alloys and ceramics for microturbine components.

One of the critical components of low-compression ratio microturbines is the recuperator, which is responsible for a significant fraction of the overall efficiency of the microturbine [2]. Conventional recuperators are thin-sheet metallic heat exchangers that recover some of the waste heat from the exhaust stream and transfer it to the incoming air stream. Most of today's compact recuperators are manufactured using 300 series (e.g.- 347) stainless steels (SS) which are used at exhaust-gas temperatures ≤ 600°C [3]. At higher temperatures, these materials are susceptible to creep deformation and oxidation, which lead to structural deterioration and leaks, reducing the effectiveness and life of the recuperator. The engine-operating temperature requirements for the next generation of microturbines have prompted efforts to identify, screen and evaluate candidate materials with the required creep and corrosion resistance.

A microturbine recuperator test facility (MRTF) was established at Oak Ridge National Laboratory (ORNL) in 2001. The objective of the MRTF is to screen and evaluate candidate materials for the next generation of microturbine recuperators. By determining how the mechanical and physical properties and microstructure of the materials under evaluation evolve as a function of time and temperature of exposure to microturbine exhaust gases, it will be possible to identify the mechanisms responsible for their degradation. Furthermore, that knowledge could be used to identify ways to modify those alloys to make them more resistant or to identify alternative materials with the required properties.

Approach

In 2001, ORNL acquired a 60kW Capstone microturbine and in collaboration with its manufacturer, the microturbine was modified to achieve higher turbine exit temperatures (TET). The microturbine was also modified to allow the placement of foil test specimens, attached to sample holders, at the entrance of the recuperator. During exposure tests, the sample holders are subjected to internal pressurization to reproduce the state of stress that recuperator cells experience during normal microturbine operation when compressed air flows inside air cells while exhaust gases flow on their outer surface. During exposure tests, the samples along the length of the sample holder are subjected to a temperature gradient. For a nominal TET value of 800°C, temperature variation along the length of the sample holder spans between 650°C and 760°C. The temperature gradient, which results from the configuration of the microturbine, turned out to be a nice feature because it allows for the evaluation of materials over a wide range of temperatures during the same test. A detailed description of ORNL's MRTF can be found elsewhere [4-5].

At the end of test campaigns, which last hundreds of hours, the residual physical and mechanical properties of the foils are determined and their microstructure analyzed using scanning electron microscopy and chemical analysis using an electron probe micro-analyzer (EPMA). The results from these tests and characterizations are compared to the baseline properties of these materials to quantify degradation and to identify the mechanisms responsible for it.

Results

During FY05, ORNL-modified SS (Tables I and II), Special Metals' alloy 625, Haynes alloys 120 (Table III), 214 (Table IV), and 230, EDM's FeCrAl and Allegheny Ludlum's (AL) AL 20/25+Nb were evaluated in ORNL's MRTF. At the time when this report was written, test specimens of some of these materials had accumulated more than 3000 h of exposure at temperatures as high as 750°C.

The materials evaluated were selected in collaboration with other tasks in this program and with microturbine recuperator manufacturers. The selection was guided to achieve the objectives of the Advanced Microturbines Program (i.e.- achieving higher temperature of operation, longer service life and lower cost) in incremental steps. The materials selected represent a wide range of capabilities from ORNL-modified stainless steels, which provide improved thermomechanical performance, compared to 347 SS, to

nickel-base alloys that rely on the formation of an aluminum oxide layer for corrosion resistance.

Table I. Composition of ORNL-modified stainless steel SS18115 (wt. %)

Element	Concentration
Ni	12.6
Cr	19.3
N	0.25
Mo	0.25
Mn	**4.55**
Si	0.36
Fe	balance
Nb	0.37
C	0.03
Cu	4.0

Table II. Composition of ORNL-modified stainless steel SS18116 (wt. %)

Element	Concentration
Ni	12.5
Cr	19.3
N	0.14
Mo	0.25
Mn	**1.8**
Si	0.38
Fe	balance
Nb	0.38
C	0.03
Cu	4.0

Table III. Composition of HR-120® alloy (wt. %) (Haynes International, Kokomo, IN 46904)

Element	Concentration
Ni	37
Cr	25
W	2.5 (max)
Co	3 (max)
N	0.2
Mo	2.5 (max)
Mn	0.7
Si	0.6
Fe	33 (balance)
Al	0.1
C	0.05
Cb	0.7
B	0.004

Table IV. Composition of HR-214® alloy (wt. %) (Haynes International, Kokomo, IN 46904)

Element	Concentration
Ni	75 (as balance)
Cr	16
Mn	0.5 (maximum)
Si	0.2 (maximum)
Fe	3.0
Y	0.01
Al	4.5
C	0.05
B	0.01 (maximum)
Zr	0.1 (maximum)

ORNL-modified stainless steels.

100-µm thick foils of ORNL-modified SS were evaluated at 650°C and 700°C in ORNL's MRTF. The pressure in the sample holder was maintained constant at 4 atm for the duration of the exposure tests. These materials were found to retain 90% of their as-processed tensile strength after a 500 h exposure at 700°C, in contrast to 347 SS, which lost 18% of its ultimate tensile strength after a similar exposure. Furthermore, these materials did not experience degradation of strength or ductility at 653°C. Figure 1 is a plot of the ultimate tensile strength of ORNL-modified SS as a function of temperature for exposure in ORNL's MRTF for 500 h. The results are normalized by the as-received ultimate tensile strength of the material at 20°C. The plot also includes results for 347 SS, which demonstrates the better performance of ORNL-modified SS compared to this material.

The chemical and microstructural analysis of these materials revealed the presence of a uniform scale on the surface of the foils that had been exposed to the microturbine exhaust gases. Figure 2 shows compositional analysis results for two ORNL-modified SS after a 500 h exposure in ORNL's MRTF. It was found that the thickness and degree of uniformity of the scale depended on the original concentration of Mn, with greater Mn concentration resulting in a thicker and more uniform scale. This scale was comprised of oxide layers of Mn, Cr, and Si, but mixed oxides of Mn and Fe were also found in the scale that had formed on ORNL-modified SS with higher concentrations of Mn.

The microstructural and chemical analysis also revealed that the grain boundaries of the base alloy had been depleted of Cr. The loss of Cr at the grain boundaries

within ~10 µm of the surface resulted from the diffusion of Cr to the surface to form Cr_2O_3, whereas the depletion of Cr at the grain boundaries in the bulk foil was due mostly to the formation of chromium carbides. It is known that the formation of these carbides leads to the degradation of the microstructure of the material and its mechanical properties.

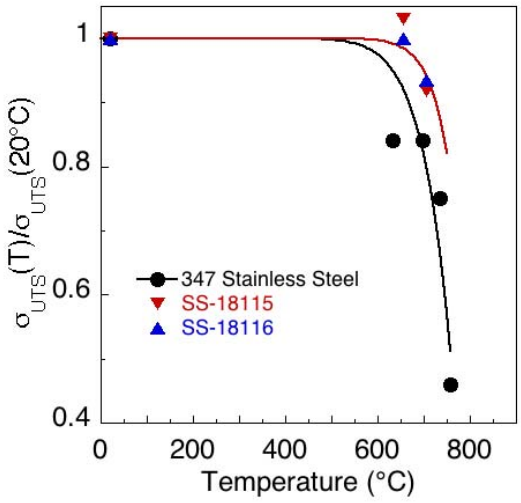

Figure 1. Effect of temperature on the ultimate tensile strength of two ORNL-modified SS after 500 h exposure in ORNL's MRTF. Results for 347 SS are included for comparison.

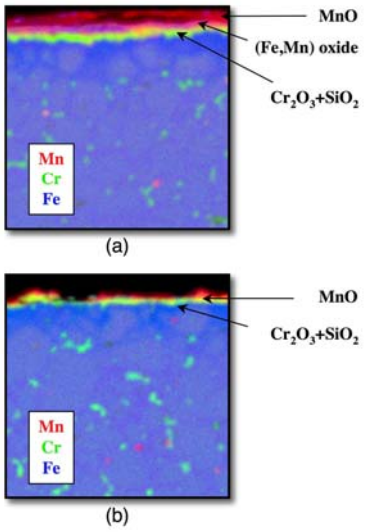

Figure 2. Effect of Mn concentration on the composition of scale formed on the surface of ORNL-modified SS exposed to the microturbine exhaust gases after 500 hours at 700°C; (a) SS-18115 (4.55 wt% Mn); (b) SS-18116 (1.8 wt% Mn).

Haynes 120

During FY05, work continued on the evaluation of Haynes alloy 120. Foils 89 µm thick were evaluated at temperatures as high as 750°C. It was found that the ultimate tensile strength and ductility of the material decreased with both temperature and time of exposure. Figure 3 is a plot containing sets of tensile stress versus strain curves obtained from the evaluation of miniature dog-bone shape test specimens at ambient temperature after 500 h and 1000 h exposures at 745°C in ORNL's MRTF. The ultimate tensile strength was found to decrease with time of exposure from 697± 3.5 MPa in the as received condition to 594 ± 32 MPa after 500 h and 512 ± 51 MPa after 1000 h. The decrease in both tensile strength and ductility as a result of time of exposure are evident in this plot. Figure 4 is a plot of ultimate tensile strength, normalized by the as-received tensile strength of the material, as a function of temperature of exposure for 500 h and 1000 h exposures in ORNL's MRTF. Equation 1, which corresponds to the trend curves in Figure 4, was found to describe well the temperature dependence of the ultimate tensile strength. With respect to Equation 1, T is the exposure temperature and T_a and b are constants.

$$\frac{\sigma_{UTS}(T)}{\sigma_{UTS}(20)} = 1 - \left(\frac{T}{T_a}\right)^b \qquad (1)$$

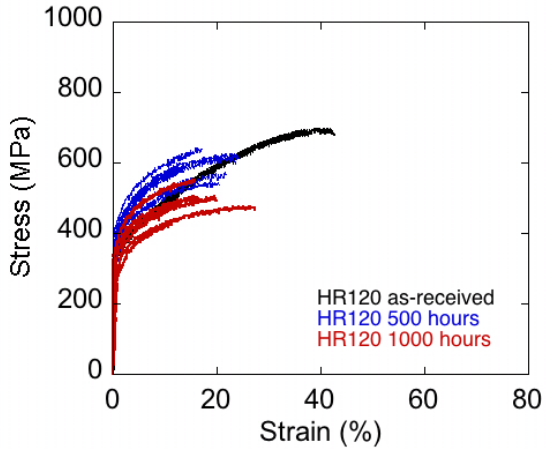

Figure 3. Effect of time of exposure at 745°C in ORNL's MRTF on the stress-strain behavior of Haynes alloy 120.

Allegheny Ludlum's AL 20/25+Nb

During FY05, ORNL procured 5000 lb of 127µm thick foils of alloy AL 20/25+Nb. In collaboration with Allegheny Ludlum, which is the material manufacturer, the foils were subjected to a high-temperature treatment to promote a microstructure that would provide both creep resistance and retention of strength at elevated temperatures.

After a 500 h exposure at 731°C in ORNL's MRTF this material was found to retain 90% of its ultimate tensile strength. Furthermore, its performance was found to be superior to those of 347 SS and Haynes alloy 230® and comparable to that of Haynes alloy 120®. Figure 5 compares the normalized ultimate tensile strength of several materials that were exposed in ORNL's MRTF in FY05, including foils of AL 20/25+Nb. At the time of the preparation of this report test specimens of this materials were on track to complete 3000 h of exposure in ORNL's MRTF.

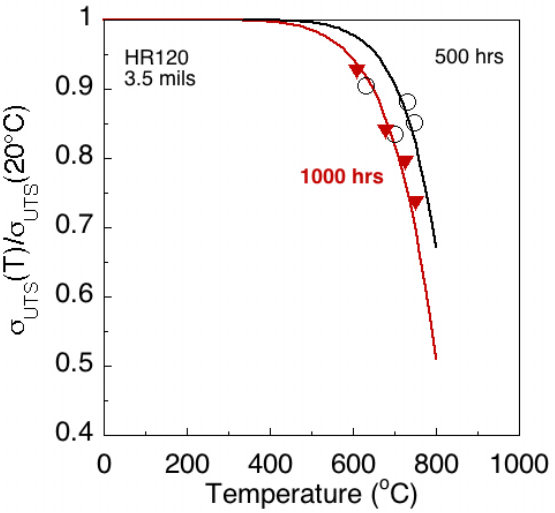

Figure 4. Effect of time and temperature of exposure in ORNL's MRTF on the ultimate tensile strength of alloy Haynes 120.

Haynes alloy 214

The Haynes® 214™ alloy is a Ni-Cr-Al-Fe alloy designed to provide the optimum in high-temperature oxidation resistance for a wrought austenitic material at temperatures of 950°C and above [6]. The excellent oxidation resistance of this alloy is attributed to the formation of a tightly adherent Al_2O_3 scale, which forms in preference to Cr_2O_3 scales at these high temperatures. At temperatures below 950°C, alloy 214 develops an oxide scale that is a mixture of Cr and Al oxides.

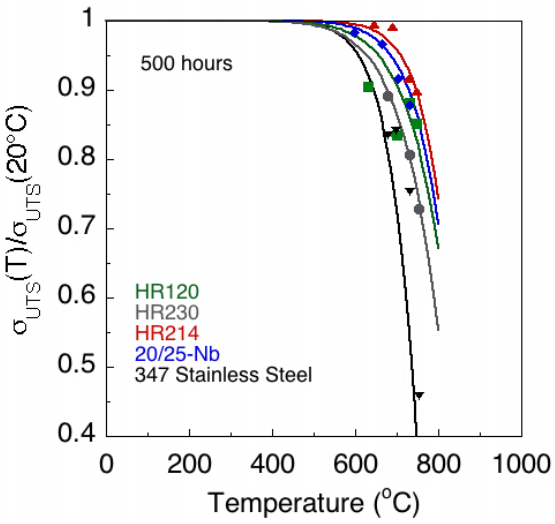

Figure 5. Effect of temperature on the ultimate tensile strength of different alloys after 500 h exposure in ORNL's MRTF.

As-received and pre-oxidized foils of alloy 214 were exposed in ORNL's MRTF for 500 and 1000 h, respectively. The pre-oxidation treatment (1 h at 1100°C in air) was carried-out to promote the formation of an aluminum oxide scale.

It was found that after a 500 h exposure at 747°C, test specimens of alloy 214 retained 90% of their ultimate tensile strength. Among all the materials that have been exposed and evaluated in ORNL's MRTF, alloy 214 has exhibited the best durability and retention of mechanical properties, as demonstrated by the results presented in Figure 5.

An analysis of the cross-section of foils of alloy 214 after a 500 h exposure in ORNL's MRTF revealed the existence of a layered scale comprised of an outward-growing scale of mixed oxides of Ni, Fe and Cr, an inward-growing scale of mixed oxides of Al, Cr and Ni, and a Cr_2O_3 scale on the surface of the base metal (Figure 6). It was also found that Al and Cr segregated to the grain boundaries of the base metal.

Pre-oxidation of alloy 214 foils resulted in a 90% retention of the ultimate tensile strength after a 1000 h exposure in ORNL's MRTF at 710°C. Analysis of the

foil surfaces (Figure 7) after exposure revealed the surface exposed to the microturbine exhaust gases had a uniform scale comprised of layers of mixed oxides of Al, Cr, Mn and Si. Furthermore, Cr-rich particles were observed both within grains and at grain boundaries.

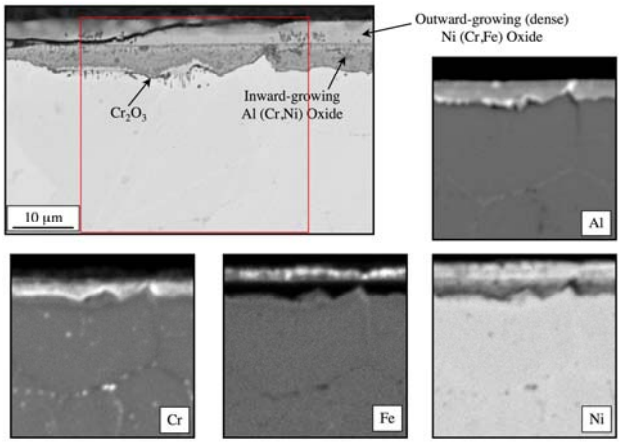

Figure 6. Backscattered electron image and corresponding elemental maps of Haynes alloy 214 after 500 h exposure at 747°C in ORNL's MRTF.

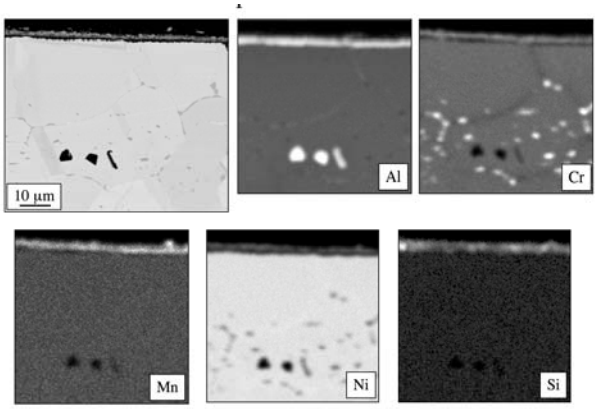

Figure 7. Backscattered electron image and corresponding elemental maps of pre-oxidized Haynes alloy 214 after 1000h exposure in ORNL's MRTF at 710°C (exhaust gas surface).

Intermittent Operation

Thermal cycling is known to be a severe operating condition for high temperature components. Under thermal cycling conditions oxide scales that would form at high temperatures are prone to spalling during cooling because of the mismatch in thermoelastic properties between the oxide scale and the base metal. This process results in a fresh surface of the base metal that becomes oxidized during the next heating cycle, just to be spalled again during subsequent cooling. Thermal cycling is a major concern for components such as microturbine recuperators, which are fabricated with thin metallic foils. To investigate the susceptibility of candidate recuperator materials to thermal cycling, a device was designed and assembled to place test specimens at the entrance of the recuperator and retrieve them after a prescribed period of time without having to stop the operation of the microturbine. Figure 8 shows a picture of the device, which consists of a pneumatic actuator, which is operated using a personal computer, and a bellow to allow the reciprocating motion of the test specimen while preventing leakage of the exhaust gases. The test specimen is mechanically attached to the end of the pneumatic actuator.

Figure 9 is a plot of the temperatures recorded along a sample holder containing foils of Haynes alloy 120 as a function of time. The duration of each cycle was 110 minutes. At the end of a predetermined number of thermal cycles, the test specimens are retrieved from the microturbine and their microstructure and mechanical properties are subsequently characterized following the same procedure employed for the characterization of test specimens that had been subjected to static exposures inside ORNL's MRTF. Results from these tests will be reported in future reports.

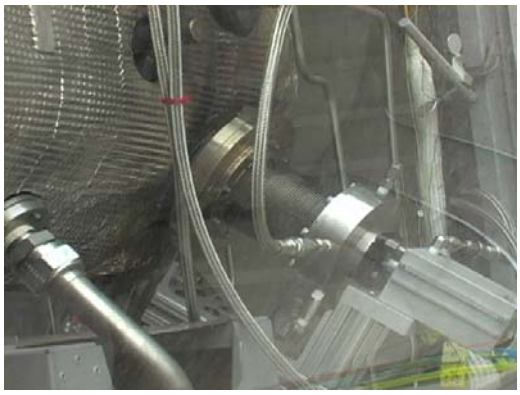

Figure 8. Device used to simulate the intermittent operation of a microturbine to evaluate the resistance of materials to thermal cycling.

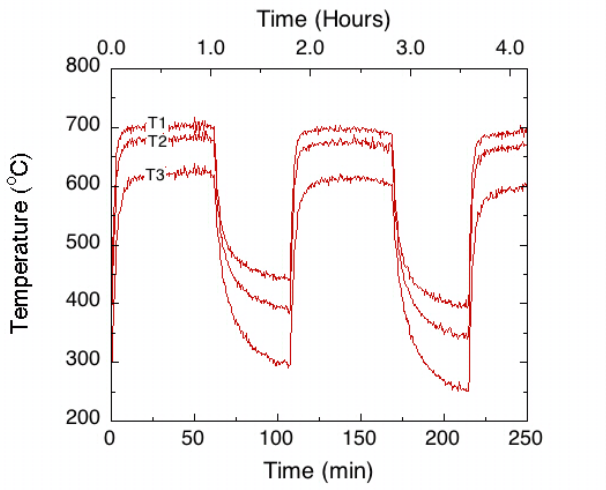

Figure 9. Temperature values along sample holder (T_1, T_2, T_3) attached at the end of pneumatic actuator as a function of time.

Conclusions

The effect of time and temperature of exposure in ORNL's MRTF on the mechanical properties and microstructure of candidate materials for the next generation of microturbine recuperators was investigated during FY05. It was found that ORNL-modified SS had greater durability than 347 SS after 500 h exposure at temperatures of 654°C and 700°C. It was also found that higher concentrations of Mn led to the formation of thicker and more uniform scales comprised of oxides of Mn, Cr, Fe and Si. Alloy AL 20/25+Nb exhibited performance comparable to that of Haynes alloy 120, retaining 90% of its ultimate tensile strength after a 500 h exposure at 731°C in ORNL's MRTF. Haynes alloy 214, pre-oxidized for 1 h at 1100°C, was found to exhibit the best performance strength retention among all the materials evaluated.

A device was instrumented to investigate the resistance of candidate materials to thermal cycling. Its operation was demonstrated with the evaluation of alloys 120 and AL 20/25+Nb.

References

1. "Advanced Microturbine Systems Program, Plan For Fiscal Years 2000 Through 2006," U.S. Department of Energy, Office of Energy Efficiency and Renewable Energy, Office of Power Technologies. March 2000.
2. C. F. McDonald, "Heat Recovery Exchanger Technology for Very Small Gas Turbines," Intl. Journal of Turbo and Jet Engines," vol. 13 (1966) pp. 239-261.
3. O. O. Omatete, P. J. Maziasz, B. A. Pint, and D. P. Stinton, "Assessment of Recuperator Materials for Microturbines," ORNL/TM-2000-304.
4. Lara-Curzio, E., Maziasz, P. J., Pint, B. A., Stewart, M., Hamrin, D., Lipovich, N. and DeMore, D., 2002, "Test Facility for Screening and Evaluating Candidate Materials for Advanced Microturbine Recuperators," ASME Paper #2002-GT-30581, presented at the International Gas Turbine & Aeroengine Congress & Exhibition, Amsterdam, Netherlands, June 3-6, 2002.
5. E. Lara-Curzio, R. M. Trejo, K. L. More, P. J. Maziasz, and B. A. Pint, "Screening and Evaluation of Materials for Advanced Microturbine Recuperators," Proceedings of ASME Turbo Expo 2004, June 14-17, 2004 Vienna, Austria, Paper GT-2004-54255.
6. Haynes 214 Alloy, Product Brochure, Haynes International (2005), Kokomo, IN 46904.

Awards/Patents

None

Publications/Presentations

1. E. Lara-Curzio, R. M. Trejo, K. L. More, P. J. Maziasz, and B. A. Pint, "Evaluation and Characterization of Iron- and Nickel-Based Alloys for Microturbine Recuperators," Proceedings of ASME Turbo Expo 2005, June 6-9, 2005, Reno-Tahoe, Nevada, USA. Paper #GT-2005-68630.

Acronyms

MRTF - Microturbine Recuperator Testing Facility

ORNL – Oak Ridge National Laboratory

AL – Allegheny Ludlum

TET – turbine exit temperature

EPMA – electron probe microanalyzer

SS – stainless steel

2.2.1 High Pressure, High Temperature Exposures of Ceramics In Water-Vapor-Containing Environments

P.F. Tortorelli, K.L. More, J.R.Keiser
Metals and Ceramics Division
Oak Ridge National Laboratory
Oak Ridge, Tennessee 37831-6156
(865) 574-5119, E-mail: tortorellipf@ornl.gov

DOE Technology Development Manager: Debbie Haught
(202) 586-2211; (202) 586-7114 (fax); e-mail: debbie.haught@ee.doe.gov
ORNL Technical Advisor: Richard Lowden

Objective
Provide the means to evaluate the long-term effects of oxidizing species, particularly water vapor, on monolithic ceramics, ceramic composites, and environmental barrier coatings at elevated pressures and temperatures.

Approach
Use specialized gas handling and pressurized high-temperature systems to:

- simulate the principal corrosive effects of a combustion environment for first-stage screening of ceramics in terms of microstructural stability and permeation resistance at prototypic water vapor pressures and temperatures
- evaluate the fundamental volatilization resistance of ceramics by conducting exposures at very high water-vapor pressures

Accomplishments
Approximately 94,000 specimen-hours of high-temperature, high-pressure exposures were achieved in support of efforts to develop reliable and durable ceramics and protective coatings for use in combustion and other high-water-vapor-pressure environments.

Future Direction
Continue to improve availability and experimental versatility to meet exposure testing needs for ceramic materials under appropriate conditions of high temperature, high pressure, and gas composition.

Introduction

This task covers the operation of the ORNL slow-flow, high-pressure mixed-gas (Keiser) rigs used for the exposure part of the evaluation of the effects of high-temperature environments on monolithic ceramics, ceramic composites, and environmental barrier coatings targeted for use in various distributed generation schemes employing combustion or steam. It involves ongoing maintenance and operation of the rigs as well as continuous upgrading to improve operational and scientific reliability as well as extending environmental simulation capabilities. Scientific results are reported as part of the Distributed Energy Materials projects on Oxidation/Corrosion Characterization of Microturbine Materials and Microstructural Characterization of CFCCs and Protective Coatings or through material suppliers or other institutions that provide materials for exposures in these facilities.

Approach

Water vapor has well-documented deleterious effects on the high-temperature environmental resistance of Si-containing ceramics.[1,2] For combustion turbines operating at moderate-to-high pressure ratios, water vapor pressures can be appreciable – on the order of 1 atm or more. At these levels, oxidation is markedly accelerated and volatility rates of SiO_2 are unacceptably high. To evaluate these effects – on Si-bearing materials as well as other ceramics – a facility to conduct high-temperature, high-pressure exposure of materials in mixed gases was developed. These exposures have been shown to accurately simulate the degradation modes related to accelerated oxidation at high water-vapor pressures found in combustion turbines with high pressure ratios.[3,4] However, because these rigs operate at low gas-flow velocities, volatilization rates of SiO_2 typically observed in turbines cannot be reached. More recently, operation of one of these rigs at very high water-vapor pressures (~18 atm) was shown to induce significant volatility of SiO_2.[5] Based on these results, this mode of operation was used to screen candidate materials for use as protective coatings for volatilization resistance in combustion environments.

Results

In FY 2005, two Keiser rigs were used for three types of exposures. Three 1000-h runs were made with a mixed gas (N_2-10%O_2-10%H_2O-6%CO_2, by volume) at 1250°C and a total pressure of 10 atm to simulate a microturbine combustion environment. Twenty-four specimens of the A/N720 CMC (alumina fiber-reinforced alumina composite) were exposed under these conditions for up to 3000 h (eight each for 1000, 2000, and 3000 h of total exposure). A single 500-h run, with the standard screening environment[3] of Ar-15% H_2O at 10 atm total pressure and 1200°C, was made with eleven specimens of developmental Si-based monolithic compositions.

Seven Keiser Rig runs (500 h each) were used to screen for volatilization tendencies at 18 atm of H_2O vapor and 1250°C. Specimens representing up to 37 different EBC variants were exposed under these conditions for up to 2000 h for a total of 36,000 specimen-hours (spec-h) at temperature and pressure. Seven specimens of silica/SiC (5500 spec-h) were included in these runs as standards for the volatility measurements and two coupons of an oxide/oxide composite were also exposed (2500 spec-h).

Conclusions

The Keiser Rigs reliably provided the means to screen a variety of ceramic materials for high-temperature thermal stability and permeation and volatilization resistance at high water-vapor pressures as part of efforts to develop reliable ceramics and protective coatings for use in combustion other high-water-vapor-pressure environments.

References

1. N.S. Jacobson, "Corrosion of Silicon-Based Ceramics in Combustion Environments," *J. Am. Ceram. Soc.*, 76 (1993) 3-28.
2. E.J. Opila, "Variation of the Oxidation Rate of Silicon Carbide with Water-Vapor Pressure," *J. Amer. Ceram. Soc.*, 82 (1999) 625-36.
3. K.L. More, P.F. Tortorelli, L.R. Walker, N. Miriyala, J.R. Price, and M. van Roode, "The High-Temperature Stability of SiC-Based Composites in High Water-Vapor Pressure Environments," *J. Am. Ceram. Soc.* 86 (2003) 1272-81.
4. P.F. Tortorelli and K.L. More, "Effects of High Water-Vapor Pressure on the Oxidation of SiC at High Temperature," *J. Am. Ceram. Soc.* 86 (2003) 1255-62.
5. P.F. Tortorelli and K.L. More, "Use of Very High Water-Vapor Pressures to Evaluate Candidate

Compositions for Environmental Barrier Coatings," paper GT2005-69064 in Proc. Turbo Expo 2005, ASME International, 2005.

Acronyms

CFCC: continuous fiber-reinforced ceramic composite

CMC: ceramic matrix composite

2.2.2 Microstructural Characterization of CFCCs and Protective Coatings

K.L. More and P.F. Tortorelli
Metals and Ceramics Division
Oak Ridge National Laboratory
Oak Ridge, TN 37831-6064
(865) 574-7788; morekl1@ornl.gov

DOE Technology Development Manager: Debbie Haught
(202) 586-2211; (202) 586-7114 (fax); e-mail: debbie.haught@ee.doe.gov
ORNL Technical Advisor: R.A. Lowden
(865) 576-2769; (865) 574-6918 (fax); lowdenra@ornl.gov

Objectives

- Characterization of CFCC/EBC materials and CFCC combustor liners after exposure to simulated (ORNL's Keiser Rig) and actual (Solar Turbines engine test) combustion environments.
- Exposures of candidate environmental barrier coatings (EBCs) to very high water-vapor pressures (in Keiser Rig) to determine thermal stability, volatility-resistance, and protective capability (permeation-resistance).
- Work with CFCC and EBC suppliers/manufacturers to evaluate new/improved ceramic fibers, protective coatings, and composite materials.

Approach

- Conduct short- and long-term Keiser Rig exposures of candidate CFCC and EBC compositions at high H_2O pressures (1.5-18 atm) to evaluate the coating's H_2O permeation-resistance, volatility-resistance, and thermal stability at temperatures greater than 1200°C
- Work with Solar Turbines to evaluate long-term engine-tested EBC/CFCC combustor liners for materials microstructural and mechanical stability in combustion environments

Accomplishments

- Completed study of the microstructural and mechanical stability of a Nextel 720 continuous-fiber reinforced alumina matrix composite (A/N720 CMC) after exposure to high H2O pressure and 3 temperatures, 1135°C, 1200°C, and 1250°C, for 3000h.
- Continued collaborations with Ceramatec, St. Gobain, and UTRC to expose experimental EBC compositions (>30) in ORNL's Keiser Rig at very high H_2O pressures for times up to 2000h.
- Completed microstructural and mechanical characterization of 3 separate (Solar Turbines) engine-exposed EBC/CFCC combustor liners with experimental EBC combinations (including SAS).

Future Directions

- Continue collaboration with Solar Turbines to evaluate field-exposed EBC/CFCC liners, including ~20,000h oxide/oxide liners (A/N720 CMC with FGI) currently running in Centaur 50S engine at Bakersfield test site and a GE pre-preg inner liner
- Conduct extensive study of volatilization results from ORNL Keiser Rig such that volatilization mechanisms are understood and candidate EBC compositions are screened for volatilization and ranked/compared
- Continue collaborations with external EBC producers/processors to evaluate new/improved EBC compositional stabilities at elevated H_2O pressures in ORNL Keiser Rigs

Introduction

Continuous fiber-reinforced ceramic matrix composites (CFCCs) have been developed to replace several metal components in stationary gas turbine engines. One such application is the uncooled CFCC combustor liner, the use of which can significantly decrease CO and NO_x emissions at increased combustor wall temperatures (~1200°C and higher).[1] Two engine tests were initially conducted on a Solar Turbines Centaur 50S engine fitted with SiC/SiC CFCC combustor liners, however, as a result of the accelerated attack of SiC-based materials (especially CFCCs) in environments containing H_2O, such as found in combustion gases, excessive surface recession of the CFCC was observed.[2] In order to increase the lifetimes of the CFCC components, EBCs must be used on the CFCC liner gas-path surfaces. SiC/SiC liners with a BSAS-based EBC ran for ~15,000 h in a single engine test.[3]

In order to attain significantly longer lifetimes (>30,000 h) in combustion environments, alternative materials for the currently-used, commercially-available SiC/SiC+BSAS system are being evaluated for the combustor liner application for use in both gas turbine and microturbine engines. A promising option is the oxide/oxide ceramic matrix composite (CMC), based on continuous Nextel 720 (alumina+mullite) fibers in a porous alumina matrix (designated commercially as A/N720 CMC). This CFCC material has demonstrated little loss in mechanical performance when exposed to water-vapor at temperatures up to 1200°C for 1000h.[4] However, microstructural instabilities of Nextel 720 fibers used in alumina- or aluminosilicate-matrix CMCs have been reported following thermal aging at temperatures >1200°C.[5] Recently, a 76cm X 18cm A/N720 CMC outer combustor liner (with a friable gradient insulator (FGI) coating) has been running for >17,000 h in a Solar Turbines engine test (at the ChevronTexaco test site in Bakersfield, CA).[6]

Approach

During FY2005, specimens of the A/N720 CMC, similar to that currently running in the Solar Turbines engine test, were exposed to a simulated combustion environment (10% H_2O) in ORNL's Keiser Rig to evaluate the CMC's microstructural and mechanical degradation as a function of temperature (1135°C, 1200°C, and 1250°C) and exposure time (up to 3000h). These results will be compared with microstructural and mechanical data from characterization of the A/N720 CMC outer combustor liner after it is removed from engine service in FY2006.

Results

The typical as-processed microstructure of the A/N720 CMC is shown by the images in Figure 1. The bulk structure was characterized by an inter- and intra-tow microcracked alumina matrix. The porous alumina matrix had an alumina grain size ranging from ~0.1-0.5 μm, with many of the smaller alumina particles adjacent to the fiber surfaces. No interfacial fiber coating was employed and, in the as-processed state, no interactions/reactions were observed between the fibers and α alumina matrix phase.

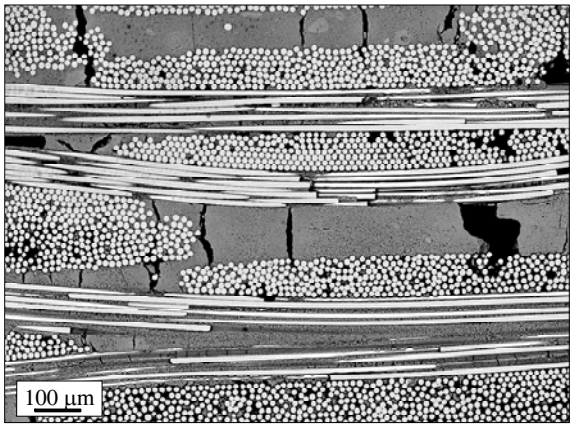

Figure 1. Backscatter electron images of bulk, as-processed A/N720 CMC showing network of micro-cracks and porous α-alumina matrix.

The continuous thermogravimetric (TGA) data for the A/N720 CMC exposed in dry air and air+10% H_2O at 1135°C, 1200°C, and 1250°C are compared in Figure 2. The TGA results show a very slow mass gain during the exposure period for all the samples. The rates of mass gain were very low and virtually the same for both dry air and air+10% H_2O at all three temperatures and 1 atm, showing that there was little overall effect of either oxidizing environment on the A/N720 CMC for the specimen exposure time. The slight mass gains observed, however, do indicate the formation of a reaction (oxidation) product or oxygen uptake during exposure.

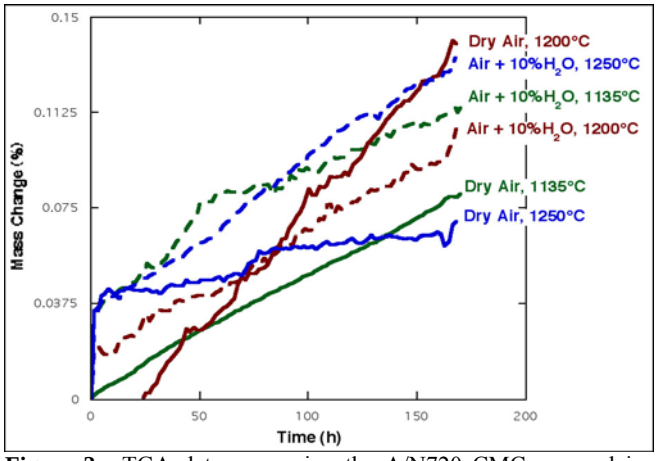

Figure 2. TGA data comparing the A/N720 CMC exposed in a microbalance for ~170h in air or air+ 10% H_2O 1135°C, 1200CMicrostructural changes within the A/N720 CMC were observed following exposure for 3000h at 1135°C.

The surfaces of the fibers had clearly roughened, as shown by the SEM images in Figures 3a and 3b, comparing a fiber surface in the as-processed composite to that from the A/N720 CMC exposed for 3000h in the Keiser Rig, respectively. The fiber surfaces had roughened by ~0.05μm after exposure for 3000h. No change in fiber or alumina matrix grain sizes were observed and no reaction between the α-alumina matrix and Nextel 720 fibers had occurred after exposure at 1135°C for 3000h.

Fiber surface roughening was much greater when the A/N720 CMC was exposed for 3000h at 1200°C and 1250°C, as shown in Figures 4 and 5, respectively. The degree of roughness of the fiber surfaces had increased by nearly an order of magnitude to ~0.3-0.5μm. The surface roughness in both cases was accompanied by a noticeable increase in the fiber grain size (both alumina and mullite grains - compare fiber structure in Figures 3a, 4, and 5) but there was no evidence for any fiber-matrix reaction/bonding after 3000h at 1200°C or 1250°C in the Keiser Rig. The microstructure of Nextel 720 fibers has been shown to become unstable when exposed to temperatures >1200°C.[4] Excessive grain growth was observed previously when these fibers were incorporated in either an alumina or aluminosilicate matrix and exposed to higher temperatures. In the case of the aluminosilicate matrix composites, the grain growth was accompanied by fiber-matrix interface reactions due primarily to simultaneous mullite grain growth in both fiber and matrix. When incorporated in an alumina matrix (as in the A/N720 CMC), Nextel 720 fiber degradation due to grain growth and increased surface roughness were the primary microstructural changes at 1200°C and 1250°C; the α-alumina matrix grains remained unchanged. The TGA data (Figure 2) clearly showed that the presence of H_2O in the environment had no effect on changing the rate of mass gain for the A/N720 CMC at any exposure temperature. Thus, the observed changes in the fiber structure are likely thermally driven and independent of the presence of water vapor. However, the small measured mass gains at 1200°C and 1250°C indicate that some uptake of oxidant may accompany fiber degradation.

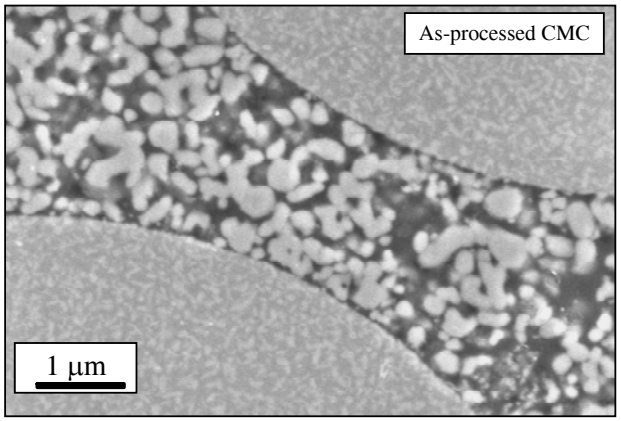

(a)

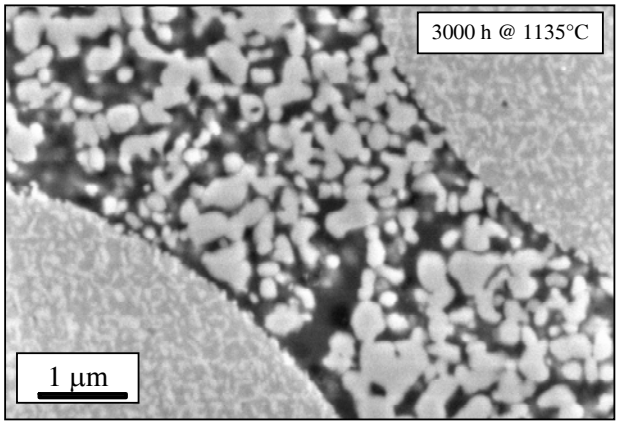

(b)

Figure 3. SEM images showing differences in Nextel 720 fiber surface roughness between (a) as-processed A/N720 CMC and (b) A/N720 CMC exposed 3000h at 1135°C in Keiser Rig.

The retained ultimate tensile strength (UTS) was determined for the A/N720 CMC (six tensile specimens were tested for each time/temperature condition) exposed for 1000, 2000, and 3000h at 1135°C, 1200°C, and 1250°C. The UTS data are shown in Figure 6. The strength results clearly show little effect of long-term exposure of the A/N720 CMC at 1135°C in the Keiser Rig's high H_2O pressure environment. While there appears to be a downward trend of average strength with time for A/N720 CMC exposure at 1200°C, which would be consistent with the microstructural changes experienced by the fibers, an analysis of variance showed that the differences among the mean values for the as-processed and exposed test specimens was not significant at the 90% confidence level. After only 1000h at 1250°C, a strength loss of ~25% was observed.

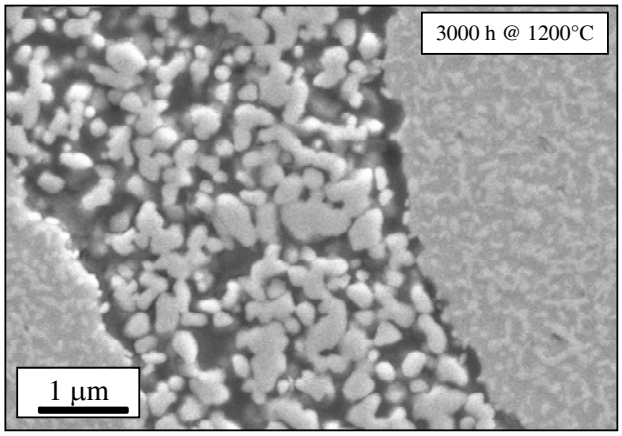

Figure 4. SEM image showing Nextel 720 fiber surface roughness in A/N720 CMC exposed 3000h at 1200°C in Keiser Rig.

Thermal degradation of Nextel 720 fibers leads to grain growth and can result in decreased strength and/or composite embrittlement.[5] In the present work, fiber surface roughening was observed, particularly during the 1200°C and 1250°C exposures in the Keiser Rig. Numerous studies have described the effects of surface roughness on debonding and fiber sliding properties in composites. These studies have shown that rougher fiber surfaces decrease the ability of the matrix to separate from the fiber, resulting in large interfacial shear strengths, higher tensile strengths, and lower strain to failure, none of which were observed in the present work at temperatures ≥ 1200°C. Clearly, the fiber surface roughness increases observed after exposure at temperatures ≥ 1200°C had not yet reached the point where the sliding of the fibers was inhibited or fiber-matrix bonding had occurred. The observed grain growth within the fibers after long-term exposure at 1250°C had the greatest impact on the A/N720 CMC strength loss.

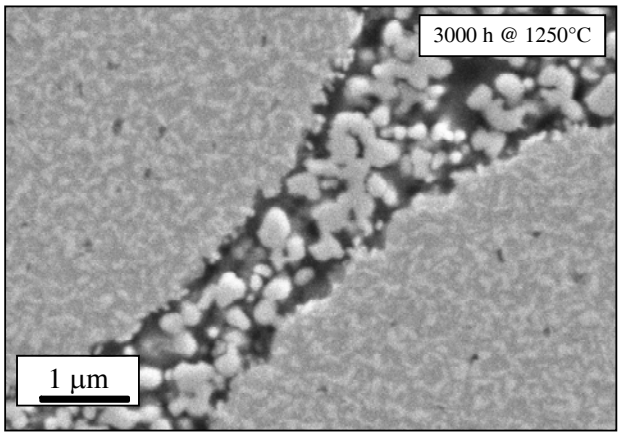

Figure 5. SEM image showing Nextel 720 fiber surface roughness in A/N720 CMC exposed 3000h at 1250°C in Keiser Rig.

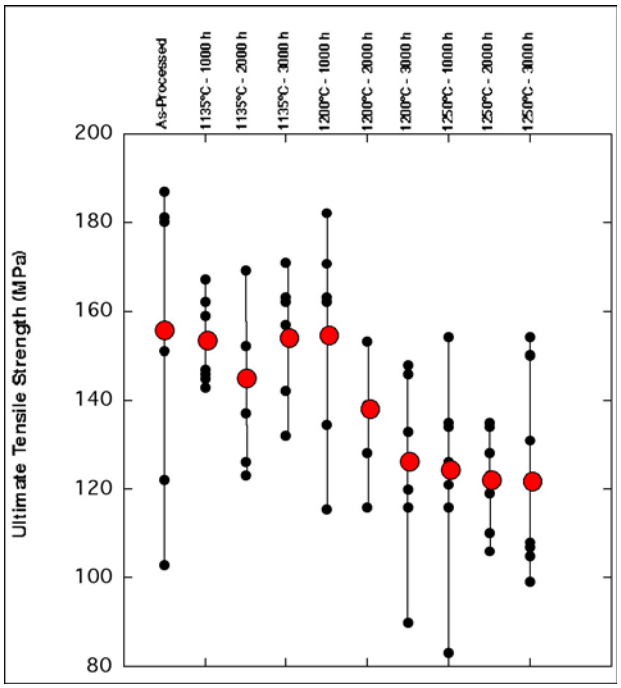

Figure 6. Summary of UTS values for A/N720 CMC exposed for 100, 2000, and 3000h at 1135°C, 1200°C, and 1250°C.

Conclusions

An oxide/oxide composite material, A/N720 CMC, was exposed to high temperatures and pressures like those in advanced gas turbine combustor environments. Results have shown minimal effect of long-term (3000h) exposures at 1135°C on the composite microstructure and strength. However, more severe degradation of the Nextel 720 fibers was observed following exposure of the A/N720 CMC at 1200°C and 1250°C. This included significant grain growth of both alumina and mullite grains within the fibers and an order of magnitude greater degree of fiber surface roughness (from <0.05μm to ~0.5μm). The observed fiber degradation, however, did not result in an obvious loss in the tensile strength of the composite after exposure at 1200°C (at the 90% confidence level) but did result in an ~25% drop in UTS following exposure at 1250°C. There was little evidence for any effect of water vapor on composite degradation.

References

1. N. Miriyala, J.F. Simpson, V.J. Parthasarathy, and W.D. Brentnall, "The Evaluation of CFCC Liners After Field-Engine Testing in a Gas Turbine," ASME Paper 99-GT-392 (1999).
2. N. Miriyala and J.R. Price, "The Evaluation of CFCC Liners After Field Testing in a Gas Turbine - II," ASME Paper 2000-GT-648 (2000).
3. K.L. More, P.F. Tortorelli, L.R. Walker, J.B. Kimmel, N. Miriyala, J.R. Price, H.E. Eaton, E.Y. Sun, and G.D. Linsey, "Evaluating EBCs on Ceramic Matrix Composites After Engine and Laboratory Exposures," ASME Paper GT-2002-30630 (2002).
4. L.P. Zawada, J. Staehler, and S. Steel, "Consequence of Intermittent Exposure to Moisture and Salt Fog on the High-Temperature Fatigue Durability of Several CMCs," *Journal of The American Ceramic Society*, **86**[8] pp. 1282-91 (2003).
5. M.G. Holmquist and F.F. Lange, "Processing and Properties of a Porous Oxide Matrix Composite Reinforced with Continuous Oxide Fibers," *Journal of The American Ceramic Society* **86**[10] pp. 1733-40 (2003)
6. A. Szweda, S. Butner, J. Ruffoni, C. Bacalski, J. Layne, J. Morrison, G. Merrill, M. van Roode, A. Fahme, D. Leroux, and N. Miriyala, "Development and Evaluation of Hybrid Oxide/Oxide CMC Combustor Liners," ASME Paper #GT2005-68496 (2005).

Awards/Patents

None

Publications/Presentations

1. K.L. More, P.F. Tortorelli, E. Lara-Curzio, and A. Szweda, "The High-Temperature Stability of an Oxide/Oxide Composite at High Water-Vapor Pressures," ASME Paper #GT2005-69065. Presented at IGTI TurboExpo 2005, June 2005, Reno, NV.
2. K.L. More, P.F. Tortorelli, E. Lara-Curzio, and A. Szweda, "High Temperature Stability of an Oxide/Oxide Composite Material at High Water-Vapor Pressures," presented at the 107th Annual Meeting of The American Ceramic Society, April 2005, Baltimore, MD.

Acronyms

CFCC – continuous fiber-reinforced ceramic composite

CMC – ceramic matrix composite

EBC – environmental barrier coating

ORNL – Oak Ridge National Laboratory

UTRC – United Technologies Research Center

BSAS – barium strontium alumino-silicate

FY – fiscal year

FGI – friable graded insulator

UTS – ultimate tensile strength

2.2.4 Oxidation/Corrosion Characterization of Microturbine Materials

K.L. More and P.F. Tortorelli
Metals and Ceramics Division
Oak Ridge National Laboratory
Oak Ridge, TN 37831-6064
(865) 574-7788; email: morekl1@ornl.gov

DOE Technology Development Manager: Debbie Haught
(202) 586-2211; (202) 586-7114 (fax); e-mail: debbie.haught@ee.doe.gov
ORNL Technical Advisor: R.A. Lowden
(865) 576-2769; (865) 574-6918; email: lowdenra@orml.gov

Objectives

- Characterization and corrosion analyses of ceramic materials (Si_3N_4, SiC, etc.) provided to ORNL from external collaborators as part of the Microturbine Materials Program.
- Exposures of candidate ceramic materials to high water-vapor pressures (in Keiser Rigs) to simulate high-temperature, high-pressure environmental effects associated with microturbines.
- Evaluate the reliability of candidate environmental barrier coatings (EBCs) on Si_3N_4 in Keiser Rigs for selected microturbine applications.

Approach

- Conduct short- and long-term Keiser Rig exposures of candidate ceramic materials and EBCs at elevated temperatures (1135°C-1315°C) and H_2O pressures (0.3-2.0 atm) to evaluate oxidation performance.
- Conduct very high H_2O-pressure exposures (~18 atm) of ceramic materials, including oxides, EBCs, CFCCs, monolithics, to evaluate and rank susceptibility of material to volatilization in combustion environments.
- Perform extensive post-exposure microstructural analyses to elucidate oxidation (degradation) mechanisms and kinetics at elevated H_2O pressures.
- Provide performance data to individual material's manufacturer for process optimization.

Accomplishments

- Calculations and experimental results from exposures of selected oxides and Si-based materials definitively demonstrated that very high H_2O pressures (~20 atm) could offset low gas velocities in the Keiser Rigs so as to differentiate volatilization resistance among various candidate EBCs.
- Collaborated with Ceramatec and Saint Gobain to expose and rank candidate EBC compositions for Si_3N_4. To date, ~14 compositions have been evaluated. Hot-pressed coupons of rare-earth oxides have also been exposed to very high water-vapor conditions.

Future Directions

- Continue collaboration with Ceramatec and Saint Gobain to expose new EBC/Si_3N_4 materials in Keiser Rigs and optimize oxidation-resistance of NT-154 Si_3N_4 for microturbine applications
- Expose new EBC materials to high water-vapor pressures (~20 atm) to evaluate and rank volatilization-resistance. Continue external collaborations to evaluate new/improved EBC compositions for Si_3N_4 in the Keiser

Introduction

It is well documented that the high-temperature corrosion resistance of Si-based ceramics is particularly sensitive to water vapor in the environment in terms of accelerated oxidation and/or mass loss by volatilization.[1-7] These coupled reactions can be life-limiting for the use of these materials in combustion environments, where high temperatures, elevated water-vapor pressures, and moderate to high gas-flow velocities exacerbate the process. This degradation mode has been shown to be of specific relevance for SiC and Si_3N_4, where SiO_2 forms by (accelerated) oxidation and then readily reacts with environmental H_2O to form volatile species.[2,5,6] Of the various volatilization reactions, the one forming $Si(OH)_4$,

$$SiO_2 + 2H_2O = Si(OH)_4 \quad (1)$$

has been shown to be predominant in combustion environments.[4] Consequently, there is concern about the use of these materials as hot-section components in gas turbine and microturbine engines because, to achieve the highest energy efficiencies and lowest emission levels, the required temperatures and water-vapor pressures in the combustion zones will be such that rapid degradation of Si-based ceramics will occur. Therefore, to take advantage of the high-temperature mechanical properties of these materials for turbine engine applications, environmental barrier coatings (EBCs) [8] will be required on surfaces exposed to combustion gases. The application of a BSAS-based EBC to SiC/SiC composite combustor liners in a Solar Turbines natural-gas turbine engine significantly increased the life of the SiC/SiC composite material. However, the long-term phase stability and oxidation/volatilization resistance of current state-of-the-art EBCs (including BSAS and SAS) are not sufficient to achieve desired engine lifetimes at temperatures ≥1200°C.[9] Therefore, the development and future implementation of improved EBCs for use in high water-vapor-containing environments has become critical for consideration of Si-based ceramic and composite materials for long-term use as hot-section components in gas turbines or microturbines.

In order to be effective for extended periods in combustion environments, an EBC must not only be substantially more volatilization resistant than the Si-based ceramic it is protecting, but also provide a permeation barrier so that oxidizing species do not readily react with the substrate and compromise properties (prevent accelerated oxidation in the presence of water vapor). In addition, the EBC must be thermally stable and relatively non-reactive with its substrate for long times at the expected use temperature (1100°C-1350°C). Efforts to develop coatings to meet these demanding characteristics have been ongoing for a number of years. A high-temperature, high-pressure exposure facility combined with detailed post-exposure microstructural analysis, has been used for first-stage evaluation of various candidate EBCs at prototypic H_2O pressures (0.3-2.0 atm) and temperatures.[10] Such an approach has been effective in screening potential EBCs in terms of permeation resistance and phase and interfacial stabilities, but not volatilization tendencies because, under normal operating conditions of low gas-flow velocities in the Keiser Rigs (3-20 cm/min.), the mass flux of volatile species was too low to be measured.

Approach

During FY05, an extremely high H_2O pressure (18 atm) and elevated temperature (1250°C) have been utilized to experimentally validate that (1) very high water vapor-pressures can be used to compensate for slow-flow gas velocities and induce volatility in the Keiser Rig and (2) measure relative volatilization rates of candidate EBCs. To accommodate the much higher water-vapor pressures used in this study, several modifications were made to the Keiser Rig's gas supply and exhaust systems.

There were several proof-of-principle specimens included in the initial high water-vapor-pressure exposures to demonstrate and measure volatilization in the Keiser Rig. High purity SiC (produced by chemical vapor deposition (CVD)) and fused quartz have been well-characterized after exposure to elevated water vapor-pressures[6,7] and were included as standards in the Keiser Rig runs. Also, since the primary purpose of these experiments was to measure volatilization of currently-used, state-of-the-art EBCs, hot-pressed BSAS, barium aluminosilicate (BAS), and strontium aluminosilicate (SAS) materials were exposed simultaneously with the Si-based standards. These hot-pressed oxides were prepared UTRC. All of

the samples to be exposed in the ORNL furnace had their surfaces mechanically ground flat and parallel and polished with 6 μm diamond paste. The mass and dimensions of each were determined before and after each exposure period (365, 500, 1000, and 1500 h). The BSAS, BAS, and SAS coupons were heat treated at 1350°C for 48 h and microstructurally characterized prior to high-temperature exposure for comparison with the same material after each exposure period in the Keiser Rig. Pre- and post-exposure cross-section specimens were imaged in a scanning electron microscope (SEM) and compositionally analyzed using an electron probe microanalyzer (EPMA). In this way, reaction products (or lack thereof) that formed during exposure, as well as any other microstructural changes, were identified and characterized with respect to their spatial dimensions.

Results

Calculations based on generalized volatility reactions and mass flux of volatilized species showed that, in terms of the Keiser Rigs, high H_2O pressures can be used to compensate for the low gas-flow velocities. The mass flux, J, of the volatile product $A_xO_{y+z}H_{2z}$ associated with the reaction

$$A_xO_y\,(s) + zH_2O\,(g) = A_xO_{y+z}H_{2z}\,(g) \qquad (2)$$

can be described as

$$J \propto v^{1/2} \bullet \exp(-\Delta G_{AxOy+zH2z}/RT) \bullet p^{z}_{H2O} \bullet a_{AxOy}/(p_{tot})^{1/2} \qquad (3)$$

where v is the gas-flow velocity, $\Delta G_{AxOy+zH2z}$ is the free energy of formation of $A_xO_{y+z}H_{2z}$ (equation (2)), p_{H2O} is the partial pressure of water vapor, p_{tot} is the total system pressure, a_{AxOy} is the thermodynamic activity of the oxide, T is the absolute temperature, and R is the universal gas constant. A flux equation of the form shown in equation (3) has been shown to describe SiC and Si_3N_4 recession controlled by volatilization of SiO_2 quite well.[5] However, at low gas-flow velocities and low-to-modest pressures, as employed in most laboratory experiments, specimen mass losses due to volatilization are small and, thus, difficult to measure, particularly because of large mass gains from accelerated solid-state oxidation at elevated p_{H2O}.[3,6,7] This was the case for most of the experiments conducted in the Keiser Rigs, which focused on the effects of elevated H_2O pressures (typically 0.3-2.0 atm) on the oxidation of Si-based ceramics and composites and EBCs to evaluate permeation resistance and thermal stability.[6,7] However, as shown by Equation (3), mass fluxes for a given P_{tot} can be increased substantially by using higher H_2O pressures, particularly if $z > 1$.

An example of how higher water-vapor pressures can be used to generate more readily measurable mass fluxes can be determined from the volatilization of SiO_2 in the presence of H_2O (Equation (1)), where, from Equations (2) and (3)

$$J \propto v^{1/2} \bullet \exp(-\Delta G_{Si(OH)4}/RT) \bullet p^{2}_{H2O} \bullet a_{SiO2}/(p_{tot})^{1/2} \qquad (4)$$

and $a_{SiO2}=1$. Relatively high fluxes of $Si(OH)_4$ can be achieved by increasing p_{H2O} since J is proportional to the square of p_{H2O} at constant p_{tot}. Therefore, if there is no change in mechanism, low gas-flow velocities can be offset by higher p_{H2O}. This is illustrated in Figure 1, which plots J/J_o versus p_{H2O} for the case represented by Equation (4) where J_o is the $Si(OH)_4$ flux for typical combustor liner conditions in land-based gas turbines (n=35 m/s, p_{H2O}=1.5 atm, T=1200°C) and J is for the same temperature with v = 6 X 10^{-4} m/s (typical gas-flow velocity in the Keiser Rigs). Note from Figure 1 that the normalized flux can be increased by approximately two orders of magnitude by increasing p_{H2O} from 1.5 atm (pressure typically used in the Keiser Rigs) to 20 atm.

The results in Figure 1 show that the high-temperature, high-pressure capability offered by a Keiser Rig (or similar exposure facility) can be used to yield relatively high volatility fluxes by conducting experiments at substantially higher water-vapor pressures (p_{H2O}). As such, this approach can be used to screen the volatility resistance of candidate ceramic compositions for use in combustion environments as bulk materials or protective surface coatings (such as needed for EBCs). However, such use is predicated on no change in the rate-controlling volatilization mechanism as the water-vapor pressure is increased. Given the nature of the process described above (diffusion of volatile product(s) across a laminar gas-boundary region), it is not expected that changes in pressures over the range indicated in Figure 1 would result in a change in mechanism. To test this approach of using high H_2O pressures to compensate for low gas-flow velocities, long-term exposure of SiO_2, SiC, and currently-used EBC compositions are being conducted in a Keiser Rig under these conditions.

This research demonstrate the utility of using this approach in evaluating the various factors involved in volatilization under oxidizing conditions as part of studies that are aimed at developing and characterizing materials that are stable at the high water-vapor pressures associated with turbine combustion conditions.

The gravimetric data for bulk specimens of BSAS, BAS, SAS, CVD SiC, and SiO_2, after exposures at 1250°C and 18 atm H_2O, are shown in Figure 2. All three alumino-silicates exhibited similar kinetic behavior and had significantly lower total mass losses and rates of volatilization than the SiO_2 and CVD SiC. At times > 500 h, the rate of mass loss of the SiO_2 was approximately an order of magnitude greater than that for the mixed oxides. This difference is approximately that expected based on results from combustor liner exposures.

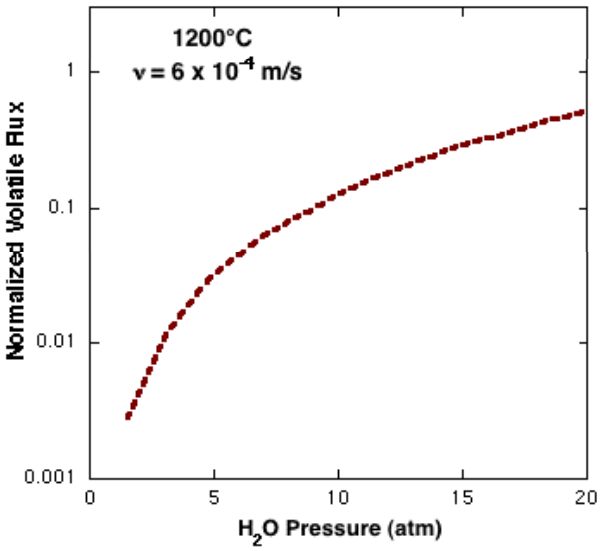

Figure 1. Plot of flux of $Si(OH)_4$ due to volatilization of SiO_2 in an H_2O-containing environment at 1200°C, a total pressure of 20 atm, and v=6X10^{-4} m/s as a function of p_{H2O}.[11]

Quantitative estimates of recession rates under conditions where there is a significant flux of volatile species will require more detailed tracking of specimen dimensions and accompanying microstructural analyses, as will a mechanistic understanding of the volatilization process in multiphase ceramics structures. Nevertheless, the volatilization trends are clearly differentiated using the gravimetric data in Figure 2. In support of the theoretical treatment, summarized by Equations (2) and (3), these results provide an experimental proof-of-principle of using very high-pressure, low-gas-velocity exposures for qualitative differentiation of volatilization resistance among different candidate materials being developed for EBC applications. An added benefit of doing such at high H_2O pressures (versus low pressures, but high gas velocities) is that permeation resistance can also be evaluated (using greater-than-worst-case conditions because the p_{H2O} is so high) when coatings on Si-based ceramic substrates are exposed.[10]

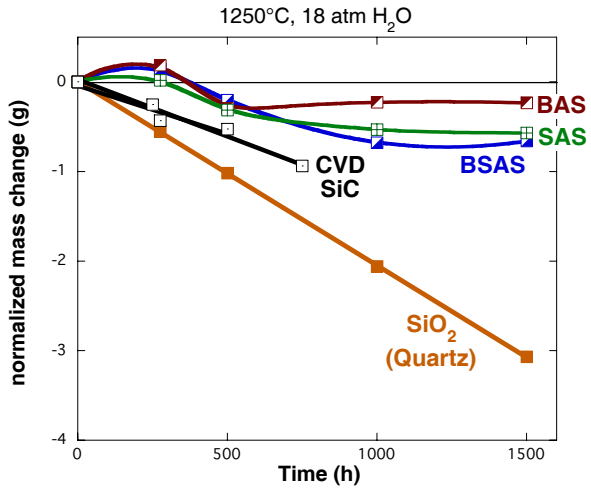

Figure 2. Gravimetric results for exposure of all bulk specimens to 18 atm of H_2O at 1250°C.

It is important to note that the utility of using higher H_2O pressures to compensate for low gas-flow velocities is critically dependent on the details of the oxidation reaction that produces the volatile species. Referring to Equation (3), the ability to use higher p_{H2O} to screen the volatilization resistance of candidate materials in systems using low values of n depends critically on z, the number of moles of H_2O needed to form one mole of volatile product. A lower z value than used for the present experimental calculations (z=2) would make it more difficult to achieve easily measurable volatile fluxes by increasing the water-

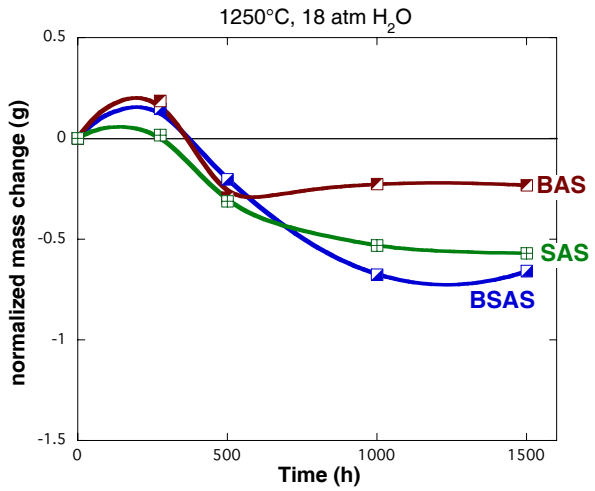

Figure 3. Gravimetric results for exposure of bulk specimens to 18 atm of H_2O at 1250°C (subset of data shown in Figure 2).

vapor pressure over a reasonable range. As an example, while there is about an order of magnitude increase in the volatile flux when p_{H2O} is increased from 1.5 to 20 atm at v = 6 X 10^{-4} m/s and 1200°C for z=1, this enhancement is about 10X less than for z=2.[11] Thus, it is important to understand the nature of the predominant volatility reaction to determine if substantially increasing p_{H2O} will yield the desired outcome and to effectively compare relative Js for different EBC compositions.

In considering the gravimetric data of Figure 2, note that, while the SiC and SiO_2 specimens exhibited mass losses at all exposure times, all of the alumino-silicates initially showed some mass gain. Figure 3 replots the BAS, SAS, and BSAS data from Figure 2 on an expanded ordinate axis to more clearly observe the gravimetric behavior of these compositions as a function of time. (The curves are intended solely to suggest trends; they are fitted to the data by a smoothing function and do not represent any specific mechanistic interpretation.) Attempts at a definitive explanation of this gravimetric behavior with time await completion of the microstructural characterization and chemical analysis of each composition at the various exposures times out to 1500 h. However, it is interesting to speculate that the delay in the onset of mass loss (volatilization) would be consistent with phase separation of a SiO_2-rich constituent, which has been observed after 328 h of exposure of these alumino-silicates under the same conditions [11] as well as in the present case after 500 h (see Figure 4). The dark phase appearing in the micrograph of Figure 4 is enriched in silica compared to the starting phases in the BAS: EPMA yielded a composition of 5.5Ba-5.4Al-24.4Si-64.4O at.%. for this Si-enriched, Al-depleted phase while the matrix phase retained its as-processed composition. Presumably, based on what was observed gravimetrically (Figure 3), localized enrichment of SiO_2 by this phase separation, which appeared to be greatest for BAS, would precede significant volatilization since recession of the alumino-silicates will occur due to preferential reaction of silica from the oxide. Furthermore, if the phase separation was sluggish relative to the rate of silica volatilization, the rate of mass loss would then decline with time and this may explain the initial higher mass loss rates of the alumino-silicates observed between 500 and 1000 h. Again, a mechanistic understanding of the oxidation processes with time in these materials depends on the completion of further microstructural analyses following additional experiments.

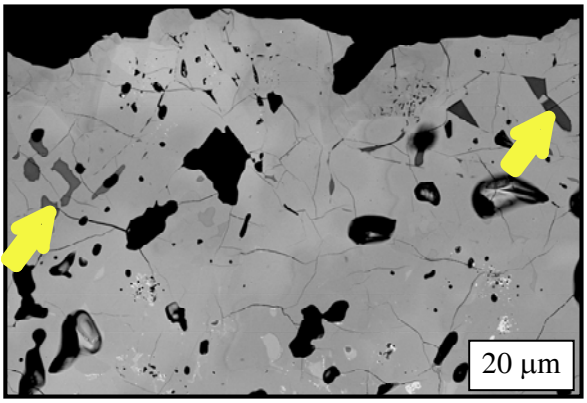

Figure 4. Surface of BAS coupon after 500 h exposure at 1250°C at 18 atm of H_2O. Dark second phase (as indicated by arrows) is enriched in silica and was not present in starting material.

Conclusions

A high-temperature furnace with a water-vapor pressure of 18 atm was used to examine whether very high-gas pressures can compensate for the low-gas velocities so as to conduct first-stage screening of EBC compositions for volatility resistance. Bulk EBC compositions and standards of SiO_2 and CVD SiC were exposed at 1250°C in 90% H_2O-10% air at a total system pressure of 20 atm. The alumino-silicate EBCs

are known to be significantly more volatilization resistant in water-bearing environments than Si-based materials that form SiO_2 under these conditions and thus provided an adequate spread in susceptibility compared to quartz and CVD SiC to evaluate the proposed approach. The gravimetric results showed clear differentiation in volatilization resistance: all three alumino-silicates exhibited similar kinetic behavior and had significantly lower rates of mass losses than the SiO_2 and SiC. As such, these findings provided the experimental proof-of-principle for using simple high-pressure, low-gas-velocity exposures for qualitative evaluation of volatilization resistance among different candidate materials being developed for EBC applications. Additional experimental work, including extensive microstructural and microchemical analyses, will be conducted during FY06 and will be required to fully elucidate the degradation/volatilization mechanisms for candidate oxide-based EBC compositions.

References

1. N.S. Jacobson, "Corrosion of Silicon-Based Ceramics in Combustion Environments," *J. Am. Ceram. Soc.,* **76**[1] (1993).
2. E.J. Opila and R.E. Hann, "Paralinear Oxidation of CVD SiC in Water Vapor," *J. Am. Ceram. Soc.,* **80**[1] (1997).
3. E.J. Opila, "Variation of the Oxidation Rate of Silicon Carbide with Water-Vapor Pressure," *J. Amer. Ceram. Soc,*. **82**[3] (1999).
4. E.J. Opila, J.L. Smialek, R.C. Robinson, D.S. Fox, and N.S. Jacobson, "SiC Recession Caused by SiO_2 Scale Volatility Under Combustion Conditions," *J. Am. Ceram. Soc.,* **82**[7] (1999).
5. R.C. Robinso and J.L. Smialek, "SiC Recession Caused by SiO_2 Scale Volatility Under Combustion Conditions: I, Experimental Results and Empirical Model," *J. Am. Ceram. Soc.,* **82**[7] (1999).
6. K.L. More, P.F. Tortorelli, M.K. Ferber, and J.R. Keiser, "Observations of Accelerated SiC Recession by Oxidation at High Water-Vapor Pressures," *J. Am. Ceram. Soc.,* **83**[1] (2000).
7. P.F. Tortorelli and K.L. More, "Effects of High H_2O Pressure on Oxidation of Silicon Carbide at 1200°C," *J. Am. Ceram. Soc.,* 86[8] (2003).
8. H.E. Eaton, G.D. Linsey, K.L. More, J.B. Kimmel, J.R. Price, and N. Miriyala, "EBC Protection of SiC/SiC Composites in a Gas Turbine," ASME Paper #2000-GT-631.
9. K.L. More, P.F. Tortorelli, L.R. Walker, J.B. Kimmel, N. Miriyala, H.E. Eaton, E.Y. Sun, and G.D. Linsey, "Evaluating EBCs on Ceramic Matrix Composites After Engine and Laboratory Exposures," ASME Paper #GT-2002-30630.
10. K.L. More, P.F. Tortorelli, amd L.R. Walker, "Verification of an EBC's Protective Capability by First Stage Evaluation in a High-Temperature, High-Pressure Furnace," ASME Paper #GT-2003-38923.
11. K.L. More, P.F. Tortorelli, T. Bhatia, and G.D. Linsey, "Evaluating the Stability of BSAS-Based EBCs in High Water-Vapor Pressure Environments," ASME Paper #GT2004-53863.

Awards/Patents

None

Publications/Presentations

1. P.F. Tortorelli and K.L. More, "The Use of Very High Water-Vapor Pressures to Evaluate Candidate Compositions for EBCs," ASME Paper #GT2005-69064. Presented at TurboExpo 2005, June 2005, Reno, NV.
2. K.L. More and P.F. Tortorelli, "Current Status of EBC Exposures in ORNL's Keiser Rigs," presentation at the ORNL/DOE EBC Workshop, November 2004, Nashville.
3. K.L. More and P.F. Tortorelli, "Evaluation of EBC Volatility at High Water-Vapor Pressures," presentation at the 29th Annual Cocoa Beach Conference and Exposition on Advanced Ceramics and Composites, January 2005, Cocoa Beach, FL.
4. P.F. Tortorelli, K.L. More, and L.R. Walker, "Evaluation of Damage in EBCs by Image Analysis," presentation at Microscopy of Oxidation 6, April 2005, Birmingham, UK.
5. K.L. More, P.F. Tortorelli, and L.R. Walker, "High Temperature Stability and Damage in EBCs Exposed at High Water-Vapor Pressures," presentation at the 107th Annual Meeting of The American Ceramic Society, April 2005, Baltimore, MD.
6. K.L. More, "Evaluating the Stability of Candidate EBCs in High Water-Vapor Pressure

Environments," Invited talk at PACRIM 2005, September 2005, Maui.

Acronyms

EBC – environmental barrier coating
ORNL – Oak Ridge National Laboratory
DOE – Department of Energy
BSAS – barium strontium alumino-silicate
BAS – barium alumino-silicate
SAS – strontium alumino-silicate
CVD – chemical vapor deposition
SEM – scanning electron microscopy
EPMA – electron probe microanalyzer

2.2.9 Environmental Protection Systems for Ceramics in Microturbines and Industrial Gas Turbine Applications—Part B: Slurry Coatings

Beth L. Armstrong
Metals and Ceramics Division
Oak Ridge National Laboratory
Oak Ridge, TN 37831-6063
(865) 241-5862; (865) 574-6918 (fax); e-mail: armstrongbl@ornl.gov

DOE Technology Development Manager: Debbie Haught
(202) 586-2211; (202) 586-7114 (fax); e-mail: debbie.haught@ee.doe.gov
ORNL Technical Advsior: Dave Stinton
(865) 574-5069; fax: (865) 576-4963; e-mail: stintond@ornl.gov

Objectives
- Develop a low-cost, slurry-based process to apply protective coatings for silicon-based ceramic materials for use in
  microturbine and/or industrial gas turbine applications.
- Coordinate efforts with other relevant projects to identify the ideal coating material for steam and high-velocity re-sistance.

Approach
- Study and implement mechanisms of colloidal chemistry for coating systems in aqueous environments.
- Evaluate the protective capacity of coated substrates in test environments.
- Work with industrial collaborators to evaluate the feasibility of the approach and candidate materials.

Accomplishments
- Demonstrated dip coating as a viable approach for a variety of material systems, including mullite, doped aluminosilicates, and rare earth doped silicates.
- Established strong collaborations with several industrial parties to ensure needs for environmental barrier coatings (EBCs) are being addressed.

Future Direction
- Continue with industrial parties to optimize and implement coating theory and technology.
- Evaluate potential of additional candidate materials as monoliths and coatings systems

Introduction

Monolithic silicon nitride ceramics and silicon carbide-silicon carbide ceramic matrix composites are currently the ceramic materials being used in combustion engine environments and are under consideration as hot-section structural materials for microturbines as well as other advanced combustion systems. Under oxidizing conditions, these materials typically form a surface oxidation (silicate) layer. In a combustion environment, this silicate layer can undergo rapid degradation due to effects of high temperature, high pressure, and the presence of water vapor. This degradation can severely limit the useful life of the ceramic in this environment. Thus, the development of an environmental protection system for the ceramic has become an essential goal for enabling the long-term utilization of these materials in advanced combustion engine applications. Similar to thermal barrier coatings for nickel-based super alloys that utilize a specialized oxide surface layer and a metallic bond coat, successful environmental protection systems for ceramics and ceramic composites will likely utilize multiple layers and complex combinations of materials. Most recent efforts have focused on the selection and deposition of the oxide surface layer, and due to numerous factors, the majority of the candidates have been from the alumino-silicate family of oxide ceramics. Stable rare-earth silicate deposits have been found on component surfaces after recent engine and rig tests, indicating there may be other stable oxide compositions that have not been fully investigated.

Approach

Thin coatings of selected compositions were deposited on silicon nitride and silicon carbide test coupons using two approaches: an aqueous based slurry process and a reactive precursor technique. If feasible, the coated specimens were exposed to simulated high-pressure combustion environments, and the materials that demonstrated good potential were investigated further.

Slurry Coatings

Efforts have focused on the development of a slurry based processing method to deposit thin dense coatings of selected compositions on silicon carbide and various silicon nitride substrates. Thin coatings of mullite and BSAS were deposited on test coupons using an aqueous based colloidal approach. The specimens were then exposed to simulated water vapor, combustion environments to determine their viability.

Reactive Coatings

The development of surface coatings that form in-situ to produce more surface layers that either slow the growth of the silica layer or prevent it entirely is another approach being developed. Diffusion processes for surface treatment of silicon-based ceramics will be explored to produce "volatility barrier coatings" that will enhance the performance and life of environmental protection systems. Previous efforts evaluated metallic coatings applied to silicon nitride substrates and heat-treated to create an alumina coating. In FY 2003 the feasibility of this approach was validated. In FY 2004 work was completed, and the paper, "Feasibility Assessment of Self-Grading Metallic EBCs/TBCs to Protect Si-Based Bond Coat Alloys for Ceramics," was published in FY 2005 fully describing this effort. No further discussion will follow in this report.

Results

Slurry Coatings Development

Last year, shear-thinning mullite (MULCR®, Baikowski International Corporation, Charlotte, NC) and celsian phase, barium-strontium aluminosilicate (BSAS, H.C. Starck GmbH, Germany) suspensions were developed to form thin, uniform coatings on silicon carbide substrates that were densified by subsequent heat treatment. In FY2005, work continued on the optimization of mullite and BSAS slurry coatings. A single layer system consisting of mullite, a two-layer mullite system, and a two layer system consisting of mullite and BSAS as the bottom and top coat, respectively, was utilized to protect SiC and SiC-SiC composite substrates. These systems were identified since the protective nature of these coating materials as-deposited by plasma spray and CVD processes has been established in high temperature steam environments, and thus, can be used for baseline comparison.[1]

In FY2004, general rheology and dip conditions were adopted using these materials that will be applicable to future candidate materials. Several colloidal processing strategies were also taken to demonstrate the flexibility of the process. The general procedure was to first disperse the ceramic particles, i.e., adequately break-up agglomerates during 24 h ball milling to obtain a uniform mixture, and then induce shear-thinning flow behavior by chemical addition. The strategies were as follows: (1) pH adjustment (pH 10) to promote

powder dispersion by electrostatics,[2] followed by rheology modifier (Additive A) addition, (2) dispersant addition to promote powder dispersion by electrosteric forces,[3,4] followed by rheology modifier (Additive B) addition, and (3) dispersant addition to promote powder dispersion by electrosteric forces, followed by rheology modifier (Additive C) addition. The dispersant was a cationic polyelectrolyte, (polyethylenimine or PEI, 10,000 g/mole, Polysciences, Warrington, PA). Additive A (200,000 g/mole) and Additive C (400,000 g/mole) are water-soluble, long-chain polymers that induce shear-thinning flow behavior due to the entanglement of the polymeric chains in solution. Additive B, on the other hand, induces shear-thinning flow behavior by flocculating the ceramic particles, i.e., anions bridge the adsorbed, cationic PEI layers on adjacent particles. Shear-thinning flow behavior was induced to form slurries suitable for the dip-coating process, as outlined by the annual report for FY2004. Latex addition was also necessary to ensure uniform, crack-free drying of the coatings.[5] Anionic latex (Rhoplex, HA8, Rohm and Haas, Philadelphia, PA) was used for the pH-adjusted slurries while cationic latex (Trudot 2608, Meadwestvaco, Stamford, CT) was used for the cationic polyelectrolyte-dispersed slurries. In this way, the latex and the ceramic particle surfaces exhibited compatible charge. Substrates of varying composition, including silicon carbide (Hexaloy, Carborundum Co., Niagara Falls, NY), SiC-SiC composites (United Technologies Research Center, Harford, CT), silicon nitride (SN282, Kyocera, Japan), and silicon nitride (NT154, Saint-Gobain, Wooster, MA) were studied. The substrates were dipped into the suspensions by hand and shaken vigorously to remove any excess material. The coatings were dried under ambient conditions and sintered under varying conditions.

Single Layer (Mullite) System

A single layer of mullite was deposited on SiC, SN282 Si_3N_4, and NT154 Si_3N_4 substrates by inserting them into 25 vol% mullite suspension containing 4 vol% Rhoplex HA8 latex and 10 mg Additive A/mL solution, drying in ambient conditions, and sintering at 1400°C for 2 h. SEM micrographs of the cross sections are shown in Fig. 1.

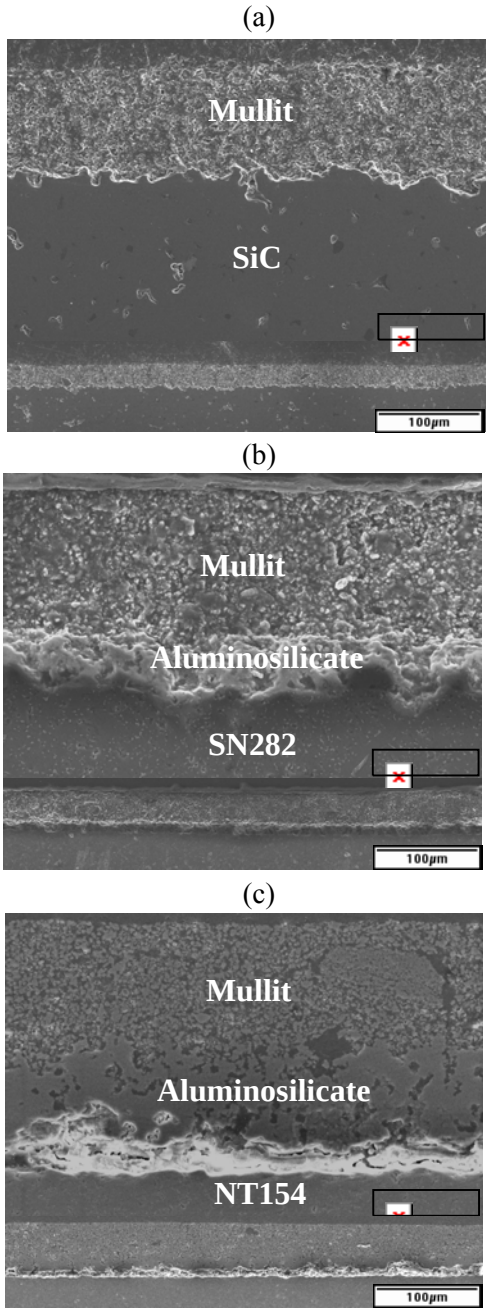

Figure 1. A single layer of mullite was deposited on (a) SiC, (b) SN282, and (c) NT154 substrates by inserting them into 25 vol% mullite suspension containing 4 vol% Rhoplex HA8 latex and 10 mg Additive A/mL solution, drying in ambient conditions, and sintering at 1400°C for 2 h.

Relatively uniform coatings were observed on all of the substrates with some thinning near the corners. Reaction between the coating material and the substrate occurred for all systems, but it was most obvious for the two silicon nitride systems. An aluminosilicate layer, with a gradient in the Al_2O_3:SiO_2 ratio emerged

at the interface. A good bond was observed between the mullite layer and the SiC and SN282 substrates; however, degradation of the mullite-NT154 interface was observed. It is unclear if the poor bonding is a result of processing or simply an artifact of SEM sample preparation. The mullite coatings on SiC and SN282 substrates had similar density, but the density of the coating on NT154 was significantly lower. EDS analysis does not reveal any obvious chemical differences between the mullite layers to explain this discrepancy. The thickness is greater for the mullite layer on NT154, i.e., 43 µm as opposed to 23 µm and 30 µ for the layers on SiC and SN282, respectively. The greater thickness is not surprising since the sintered density is low, i.e., less consolidation occurs during sintering.

Two-layer (Mullite-Mullite) System

In order to carry out exposure testing of mullite coatings on SiC test bars, a two-layer system was developed to ensure that there was coverage at the corners and edges. The first mullite layer was deposited by dipping the substrate into 25 vol% mullite suspension (pH 10) containing 4 vol% Rhoplex HA8 latex and 10 mg Additive A/mL solution. The coated test bars were dried at ambient conditions and heat treated at 1400°C for 2 h to promote densification. The second mullite layer was then deposited by repeating the process described above. The coatings were uniform and had no obvious knit line to distinguish between the first and second layer (see Fig. 2). The combined thickness of the two mullite layers was ~ 100 µm.

The coated test bars were exposed to steam at 1200°C for 500 h. SEM micrographs of the polished cross-sections before and after exposure to high temperature steam are shown in Fig. 2. Before exposure testing, an approximately 6 µm aluminosilicate reaction layer was noted at the mullite-SiC interface. This reaction layer improves the adherence of the coating to the substrate. However, after exposure testing, a silica layer of equivalent thickness was observed at the interface. Apparently, O_2 was able to diffuse through the mullite coating and react with the aluminosilicate layer. The mullite coating was not dense enough to fully protect the substrate in high temperature water vapor. Thus, additional measures to improve the density of mullite coatings are necessary.

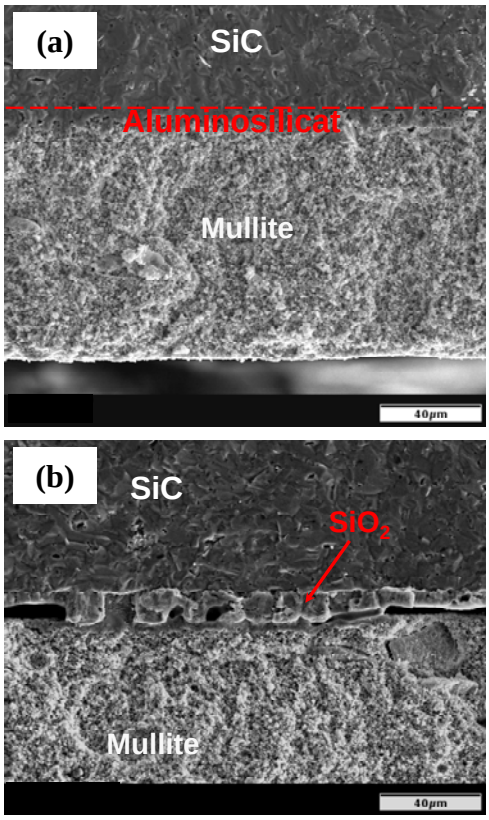

Figure 2. Two mullite layers on SiC deposited from 25 vol% mullite suspension (pH 10) containing 4 vol% Rhoplex HA8 latex and 10 mg Additive A/mL solution. The layers were applied, dried in ambient conditions, and sintered separately at 1400°C for 2 h. Images (a) and (b) show the polished cross section of a test bar before and after exposure to steam at 1200°C for 500 h.

Four point bend testing was carried out to measure the flexural strength of uncoated SiC test bars before exposure, mullite-coated SiC test bars before exposure, and mullite-coated SiC test bars after exposure to steam at 1200°C for 500 h. The results in Fig. 3 indicate little variation in the flexural strength between uncoated and coated SiC test bars. The SEM micrographs in Fig. 4 indicate that failure of the pre-exposed mullite-coated SiC test bars originate from defects in the SiC—not from the coating. Furthermore, exposure to high temperature steam did not result in significant strength degradation despite the formation of silica at the interface.

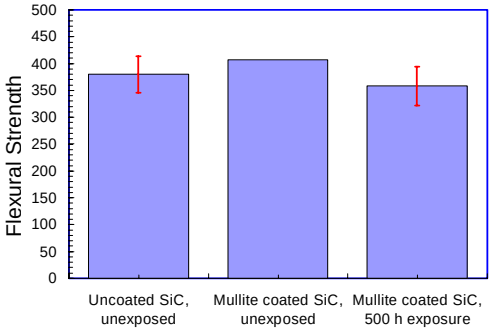

Figure 3. Four point bend flexural strength of SiC test bars before exposure, mullite-coated SiC test bars before exposure, and mullite-coated SiC test bars after exposure to steam at 1200°C for 500 h

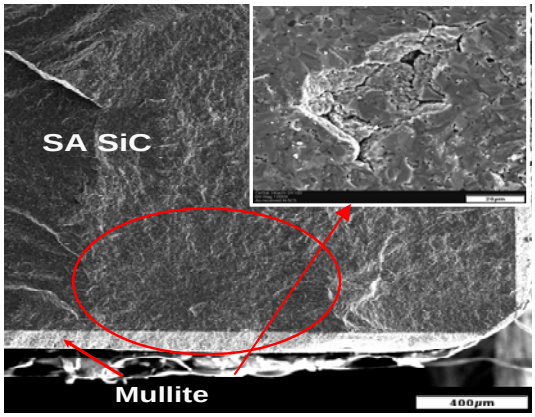

Figure 4. The fracture surface of a mullite-coated SiC test bar after four-point bend testing. Note, the specimen was not exposed to high temperature steam.

Two-Layer (Mullite-BSAS) System

In FY2005, the dip-coating process was also applied to a conventional, two-layer EBC with a mullite bottom layer and a BSAS top coat. The coating system was applied to monolithic SiC and SiC-SiC ceramic matrix composites. Monolithic SiC test bars were inserted into 32 vol% mullite suspension containing 0.25 mg PEI/m^2 mullite powder, 4 vol% Trudot 2608 latex, and 15 mg Additive C/mL solution. SiC-SiC composite substrates, however, were inserted into 32 vol% mullite suspension containing 0.25 mg PEI/m^2 mullite powder, 4 vol% Trudot 2608 latex, and approximately 0.02 *M* Addtive B. The mullite layers were dried in ambient conditions and sintered at 1350°C for 5 h. Next, the BSAS layer was formed by dip-coating the monolithic SiC and SiC-SiC composites into 32 vol% BSAS suspension containing 0.5 mg PEI/m^2 BSAS powder and 4 vol% Trudot 2608 latex. The BSAS layer was dried in ambient conditions and sintered at 1300°C for 5 h.

Cross sections of an as-sintered, mullite-BSAS coated monolith and SiC/SiC composite are shown in Fig. 5. The layers were uniform, and approximately 65-80 μm in thickness for mullite and 85-100 μm in thickness for BSAS. The coatings appear to be adherent, with a good interface between the substrate and the mullite layer, as well as between the mullite and BSAS layer. The use of Addtive B or C as rheological modifiers did not have marked impact on the quality of the coatings after sintering. This demonstrates the flexibility of colloidal processing techniques—that the rheology necessary to form uniform dip-coatings can be achieved by varying strategies.

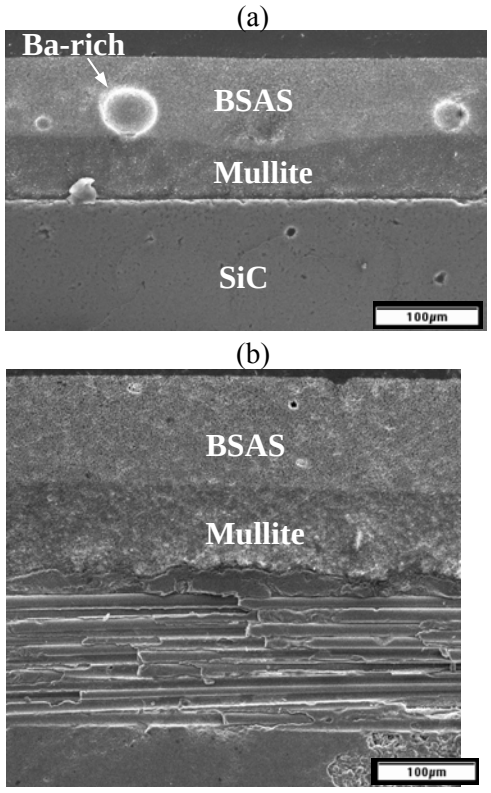

Figure 5. Mullite-BSAS coatings on (a) monolithic SiC and (b) a SiC-SiC composite. The mullite layer was deposited from 32 vol% mullite suspension containing 0.25 mg PEI/m^2 mullite powder, 4 vol% Trudot 2608 latex, and (a) 15 mg Additive C/mL solution or (b) 0.02 *M* Additive B. The BSAS layer was deposited from 32 vol% BSAS suspension containing 0.5 mg PEI/m^2 mullite powder and 4 vol% Trudot 2608 latex. The layers were applied, dried in ambient conditions, and sintered separately at 1350°C for 5 h for mullite and 1300°C for 5h for BSAS.

The coated SiC-SiC composites were exposed to steam at 1315°C for 500 h. Fig. 6 shows that a SiO_2 scale of ~ 10 μm thickness formed at the interface between the SN282 and mullite layer. The thickness of this scale was comparable to that observed at the mullite-SiC interface of plasma-sprayed EBC's, which is an

encouraging result given the fact that significant porosity is present in the mullite and BSAS layers. The coating separated at the SiO_2/mullite interface, although it is not clear if this occurred as a result of steam exposure or metallographic preparation. Mullite and BSAS mixing occurred at the interface between the bottom and top coat. Furthermore, the density of the BSAS layer increased near the mullite/BSAS interface, although some larger pores were also observed within the dense region. These pores correspond to the size and shape of a barium-rich secondary phase that was observed in the unexposed coatings (see Fig. 5a). Because this secondary phase is not always observed in as-processed BSAS layers, it is proposed that this stems from chemical inhomogeneity of the starting powder or from processing conditions. Determination of the source of this porosity observed in Fig. 6 will be investigated.

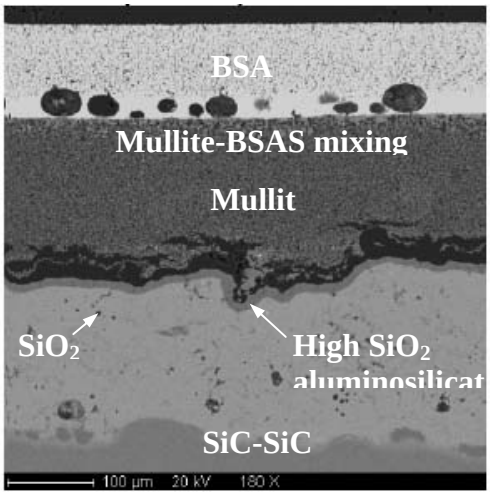

Figure 6. Mullite/BSAS coated SiC-SiC composite after exposure to steam at 1315°C for 500 h

Conclusions

Undoped and doped-aluminosilicate coatings were formed on SiC and Si_3N_4-based substrates by a low-cost, dip coating method that utilizes ceramic slurries of tailored (shear-thinning) rheological behavior. The coatings are dried in ambient conditions and heat-treated to promote densification. These coatings have been exposed to high temperature steam environments to determine if they are protective. Results indicate that slurry coatings that are not completely dense are as protective as plasma-sprayed EBC's. Furthermore, the uniform, relatively defect free coatings imparted by the slurry (dip) coating technique does not result in a significant strength debit to the overall system.

References

1. Lee, K., D. Fox, J. Eldridge, D. Zhu, R. Robinson, N. Bansal, and R. Miller, 2003, "Upper Temperature Limit of Environmental Barrier Coatings Based on Mullite and BSAS," J. Am. Ceram. Soc., **86** [8], pp. 1299-1306.
2. Hunter, R.J., 1995, *Foundations of Colloid Science*, Clarendon, Oxford, U. K.
3. Cesarano III, J. and I.A. Aksay, "Processing of Highly Concentrated Aqueous □-Alumina Suspensions Stabilized with Polyelectrolyte," *J. Am. Ceram. Soc.*, **71** [12] (1988).
4. Cesarano III, J., I.A. Aksay, and A. Bleier, "Stability of Aqueous □-Al_2O_3 Suspensions with Poly(methacrylic acid) Polyelectrolyte," *J. Am. Ceram. Soc.*, **71** [4] 250-55 (1988).
5. C. J. Martinez, J. A. Lewis, "Rheological, Structural, and Stress Evolution of Aqueous
6. Al_2O_3:Latex Tape-Cast Layers," *J. Am. Ceram. Soc.*, **85** [10] 2409-16 (2002).

FY2005 Publications/Presentations

1. Glen H. Kirby, Kevin M. Cooley, and Beth L. Armstrong, "Tailored Rheological Behavior of Mullite and BSAS Suspensions Using a Cationic Polyelectrolyte," published in the Proceedings of GT2005 ASME Turbo Expo 2005: Power for Land, Sea, and Air.
2. Glen Kirby, Kevin Cooley, HT Lin, and Beth Armstrong, "Deposition of Environmental Protection Systems from Colloidal Suspension," presented at the ITGI ASME Turbo Expo, Power for Land, Sea, and Air on June 6, 2006 in Reno, NV.
3. Brady MP, Armstrong BL, Lin HT, Lance MJ, More KL, Walker LR, Huang F, Weaver ML "Feasibility Assessment of Self-Grading Metallic EBCs/TBCs to Protect Si-Based Bond Coat Alloys for Ceramics," SCRIPTA MATERIALIA 52 (5): 393-397 MAR 2005

2.2.10 Reliability Analysis of Microturbine Components

Stephen F. Duffy and Eric H. Baker
Connecticut Reserve Technologies, LLC
Stow, Ohio 44224
(330) 678-7328, e-mail: sduffy@crtechnologies.com, baker@crtechnologies.com

DOE Technology Development Manager: Debbie Haught
(202) 586-2211; (202) 586-7114 (fax); e-mail: debbie.haught@ee.doe.gov
ORNL Technical Advisor: Matt Ferber
(865) 576-0818; fax (865) 574-6098; e-mail: ferbermk@ornl.gov

---

Objective

- Connecticut Reserve Technologies (CRT) will translate theoretical reliability concepts into design algorithms and analytical tools for participants in the DER program. This includes incorporating modeling techniques for component design, and parameter estimation techniques for data analysis, into software that is easily implemented.

Approach

- Continue to update software modules for the CARES algorithm. This software enables the design engineer to model components fabricated from ceramic materials with commercially available finite element analysis (FEA) software. CARES post processes results from FEA software and compute component reliability using Weibull analysis techniques. CARES is made available to participants in the DER program via an internet web site.

- Continue to update the WeibPar software program. WeibPar allows material vendors and test engineers to extract Weibull distribution parameters from time independent (fast fracture) specimen data and time dependent (dynamic fatigue) data. An export function allows WeibPar users to create a material parameter file for subsequent use in a CARES analysis.

Accomplishments

- CRT updated the ANSCARES module so that CARES is compatible with ANSYS version 9.0 (commercial finite element analysis software).

- CRT has upgraded the WeibPar program such that material specific life parameters (N and B associated with subcritical crack growth models) are computed. Prior to this only time independent parameters were computed.

- The web pages, www.CeramicReliability.com, have been created and posted. The pages contain ceramic reliability background theory, support, downloads, and contact information.

Future Directions

- Complete modifications to the CARES modules and the WeibPar algorithm that are underway in CRT's current contract, which spans government fiscal years. These include upgrades for ANSYS version 10 and 11, suppression of user-selected elements in the determination of P_f, A_{eff}, V_{eff}, etc., and adding cyclic fatigue calculations for repetition of single load step finite element analyses.
- Continue updating and adding to the www.CeramicReliability.com website.
- Provide software support to interface ORNL's Integrated Reliability Analysis Software (IRASoft) with CARES and WeibPar.

Introduction

Conceptually, distributed power generators in the form of microturbines provide more fuel-flexible systems near the point of energy consumption. Localized distributed generation will avoid transmission and distribution power losses. Barriers to distributed energy resources are being addressed by the Distributed Energy Resources (DER) Program that is supported by the Department of Energy (DoE). Advanced structural ceramics, such as silicon nitride, are required to enable microturbines to operate at temperatures that translate into fuel savings and emissions reductions.

Ceramics exhibit significant scatter in tensile strength, thus probabilistic design approaches must be utilized. Two software algorithms have been developed as design aids for the engineer designing components fabricated from ceramics, i.e., the CARES program (originally developed at NASA GRC) and CRT's WeibPar program.

The strength of silicon nitrides is limited by the presence of flaws that result from processing. Various surfaces of a component may see different treatments, e.g., as processed surfaces in comparison to polished surfaces. Accounting for the different surface treatments and the statistical strength distributions associated with each treated surface will lead to more accurate predictions of expected component life, expressed as component reliability as a function of time. WeibPar and CARES are critical to performing this type of analysis.

Approach

Efforts common to upgrading both CARES and WeibPar have been undertaken. New licensing key technology will allow CRT to provide executable versions of the software programs as FTP downloads. Programs can be freely downloaded and run in a demonstration mode. When a user decides to license the software, they simply run the licensing program and email a client information text file to CRT. Upon validation that the customer is a DER industrial partner, CRT creates and emails a license key back to the customer to "unlock" the full capability of the codes. With a valid license key a customer may download upgrades to the codes as they become available.

Component Analysis

ANSCARES, the CARES interface to the ANSYS finite element program, has been upgraded for ANSYS version 9.0. This interface program reads ANSYS results files and writes the nodal and element stress information to the newly formatted, multiple load step, CARES binary neutral file. The CARES program subsequently reads from this neutral file in order to perform component reliability calculations. Previous versions of ANSCARES created an individual neutral file for each load step then combined them into a single neutral file. The binary neutral file is more efficient than the original text based neutral file since it is created directly, and in general, reading and writing to binary files is more efficient both in CPU time and in total storage space. Additionally, the limits on the number of elements and number of nodes have each been increased to one million. Finally, the user may select a range of materials and a range of load steps to place in the neutral file. Finite element models often contain materials and/or load steps that are not to be analyzed in CARES.

Relative to the CARES main module, in addition to the upgrade to read the new binary neutral file, the risk of rupture subroutine has been updated. The RRI file has been reformatted and the ANSYS macro has been updated. Other minor updates have also been performed.

Parameter Estimation

In the following two sections the theory supporting the determination of time dependent reliability analysis is presented. These sections serve as an overview of some of the parameter estimation techniques incorporated into WeibPar. These concepts are typical of the design and analysis approaches that are being continuously incorporated into both WeibPar and CARES.

In addition to the theoretical concepts implemented, several practical techniques associated with data analysis have also been implemented. When analyzing a censored data set within WeibPar each data point can now be identified by a string of characters rather than the numerals 0, 1, etc. Any designation beginning with the letter 'V' will be analyzed as a volume flaw (e.g., volume, v, vol, vol1, vol2, vol3, etc). Likewise any designation beginning with the letter 'S' will be analyzed as a surface flaw. Designations beginning with anything else will be analyzed as an unknown flaw.

Finally, the component reliability module has been updated to run with the most recent version of CARES. The dialog screen was reorganized based on

user comments to make it more user friendly. The export results and export graph functions have been updated. The user may now export dynamic fatigue graphs and pooled Weibull graphs to JPEG, Bitmap, Windows Metafile, and Enhanced Windows Metafile formats. The user may also export the results of dynamic fatigue estimation and pooled Weibull estimation to either the WPR text file or the CMP file. The WPR file contains plotting information for use in other commercial graphics packages. The CMP file is a CARES Material Parameter file for direct use in CARES.

Tensile Dynamic Fatigue Data

The approach for computing the time dependent strength parameters *B* and *N* from failure data is presented in this section for a specific specimen geometry, i.e., a uniaxial test specimen. Hence the stress state is uniform throughout the specimen, and is not spatially dependent. This is not the case for arbitrary specimens, which will be described in the following section. Begin by expressing the uniaxial formulation of the probability of failure as

$$P_f = 1 - \exp\left[-\left(\frac{1}{\sigma_{0V}}\right)^{m_V} \int_V \left[\sigma_{Ieq,0}(x,y,z,t_f)\right]^{m_V} dV \right] \quad \textbf{(1)}$$
$$= 1 - \exp\left[-\left(\frac{\tilde{\sigma}(t_f)}{\sigma_{0V}}\right)^{m_V} \int_V dV \right]$$

for flaw distributions distributed through the volume of all test specimens (a similar expression exists for surface flaw distributions). Here $\tilde{\sigma}$ is referred to the inert strength in the ceramics literature (e.g., Appendix in ASTM C 1368). Under the assumption that

$$\left(\frac{\hat{\sigma}}{\tilde{\sigma}}\right)^{N-2} << 1 \quad \textbf{(2)}$$

where $\hat{\sigma}$ is the stress at failure. For monotonically increasing stress tests (dynamic fatigue) one can demonstrate

$$\tilde{\sigma}(t_f) = \left[\frac{(\hat{\sigma})^N t_f}{(N+1)B}\right]^{\frac{1}{N-2}} = \left[\frac{(\hat{\sigma})^{N+1}}{(N+1)B\dot{\hat{\sigma}}}\right]^{\frac{1}{N-2}} \quad \textbf{(3)}$$

under the assumption indicated in equation 2 Thus the stress at failure $\hat{\sigma}$ can be expressed as

$$(\hat{\sigma})^{N+1} = (N+1)B(\tilde{\sigma})^{N-2}\dot{\hat{\sigma}} \quad \textbf{(4)}$$

Now let

$$(D)^{N+1} = (N+1)B(\tilde{\sigma})^{N-2} \quad \textbf{(5)}$$

then

$$(\hat{\sigma})^{N+1} = (D)^{N+1}\dot{\hat{\sigma}} \quad \textbf{(6)}$$

Taking the natural log of both sides of equation 6 yields

$$\ln(\hat{\sigma}) = \ln(D) + \left(\frac{1}{N+1}\right)\ln(\dot{\hat{\sigma}}) \quad \textbf{(7)}$$

Thus plotting the log of the stress at failure $\hat{\sigma}$ against the log of the applied stress rate $\dot{\hat{\sigma}}$ should yield a straight line with a slope of *[1/(N+1)]*. Typically, linear regression techniques are used to determine the parameters *N* and *D*. Once these parameters are determined from the time dependent failure data this information would be combined with the Weibull distribution parameter estimates and the parameter *B* would be computed from the expressions developed below.

Substitution of equation 3 into equation 1 yields

$$P_f = 1 - \exp\left[-\left(\frac{1}{\sigma_{0V}}\right)^{m_V} \left[\frac{(\hat{\sigma})^{N+1}}{(N+1)B\dot{\hat{\sigma}}}\right]^{\frac{m_V}{N-2}} \int_V dV \right]$$
$$= 1 - \exp\left[-\left(\frac{1}{\sigma_{0V}}\right)^{m_V} \left[\frac{(\hat{\sigma})^{N+1}}{(N+1)B\dot{\hat{\sigma}}}\right]^{\frac{m_V}{N-2}} V_{gage} \right]$$

(8)

Solving this expression for $\hat{\sigma}$ yields

$$(\hat{\sigma})^{N+1} = \left\{\left(\frac{1}{V_{gage}}\right)\ln\left[\frac{1}{1-P_f}\right]\right\}^{\frac{N-2}{m_V}} (\sigma_{0V})^{N-2}(N+1)B\dot{\hat{\sigma}}$$

(9)

Comparing equation 4 and 9 leads to

$$(D)^{N+1} = \left\{\left(\frac{1}{V_{gage}}\right)\ln\left[\frac{1}{1-P_f}\right]\right\}^{\frac{N-2}{m_V}} (\sigma_{0V})^{N-2}(N+1)B$$

(10)

and solving for B from this last expression yields

$$B = \frac{(D)^{N+1}}{\left\{\left(\frac{1}{V_{gage}}\right)\ln\left[\frac{1}{1-P_f}\right]\right\}^{\frac{N-2}{m_V}}(\sigma_{0V})^{N-2}(N+1)} \quad \textbf{(11)}$$

In order to compute the parameter B from equation 11 a probability of failure must be utilized. The simplest approach would be to take

$$P_f = .50 \quad \textbf{(12)}$$

since linear regression methods are used. Also note that the parameter N will be independent of the specimen geometry used to generate time to failure data, whereas the parameter D is strongly dependent on the specimen geometry. This is similar to the fast fracture Weibull parameters, i.e., m is not dependent on the specimen geometry where σ_θ is. Noting that D is specimen dependent, keep in mind that the development above was presented for creep in a uniaxial test specimen. The next section develops an expression for B for generic test specimens.

Dynamic Fatigue Data, Arbitrary Specimen Geometry

The approach for computing the time dependent strength parameters B and N from failure data for an arbitrary specimen geometry is presented in this section. Here the stress state and stressing rate are assumed to vary spatially throughout the specimen. Begin by expressing the probability of failure as

$$P_f = 1 - \exp\left[-\left(\frac{1}{\sigma_{0V}}\right)^{m_V}\int_V \left[\sigma_{leq,0}(x,y,z,t_f)\right]^{m_V} dV\right]$$
$$= 1 - \exp\left\{-\left(\frac{1}{\sigma_{0V}}\right)^{m_V}\int_V \left[\tilde{\sigma}(t_f)\right]^{m_V} dV\right\}$$

(13)

This uniaxial stress formulation will be expanded to include multiaxial stress states momentarily. The uniaxial formulation here is strictly for convenience. Noting that

$$\hat{\sigma} = \hat{\sigma}(x,y,z) \quad \textbf{(14)}$$

and the stressing rate are spatially dependent, but

$$t_f = \frac{\hat{\sigma}}{\dot{\hat{\sigma}}} \quad \textbf{(15)}$$

is constant throughout the specimen geometry, i.e., t_f is not spatially dependent. Inserting the results from equations 3 and 15 into equation 13 yields

$$P_f = 1 - \exp\left\{-\left(\frac{1}{\sigma_{0V}}\right)^{m_V}\left[\frac{1}{(N+1)B}\right]^{\frac{m_V}{N-2}}\int_V\left[\frac{(\hat{\sigma})^{N+1}}{\dot{\hat{\sigma}}}\right]^{\frac{m_V}{N-2}} dV\right\}$$
$$= 1 - \exp\left[-\left(\frac{1}{\sigma_{0V}}\right)^{m_V}\left[\frac{t_f}{(N+1)B}\right]^{\frac{m_V}{N-2}}\int_V(\hat{\sigma})^{\frac{Nm_V}{N-2}} dV\right]$$

(16)

If we identify

$$m_1 = \frac{m_V}{N-2} \quad \textbf{(17)}$$

and

$$m_2 = \frac{N\,m_V}{N-2} \quad \textbf{(18)}$$

then

$$P_f = 1 - \exp\left[-\left(\frac{1}{\sigma_{0V}}\right)^{m_V}\left[\frac{t_f}{(N+1)B}\right]^{m_1}\int_V(\hat{\sigma})^{m_2} dV\right]$$

(19)

Next, identify $\sigma_{\max}$ as the maximum stress in the arbitrary component associated with the failure stress distribution $\hat{\sigma} = \hat{\sigma}(x,y,z)$, then

$$P_f = 1 - \exp\left[-\left(\frac{1}{\sigma_{0V}}\right)^{m_V}\left[\frac{t_f}{(N+1)B}\right]^{m_1}(\sigma_{\max})^{m_2}\int_V\left(\frac{\hat{\sigma}}{\sigma_{\max}}\right)^{m_2} dV\right]$$

(20)

The integral appearing in equation 20 can be identified as an effective volume, i.e.,

$$kV_T = \int_V\left(\frac{\sigma}{\sigma_{\max}}\right)^{m_2} dV \quad \textbf{(21)}$$

Here the subscript T emphasizes that this effective volume is a "temporal" effective volume. The modulus m_2 is not the fast fracture Weibull modulus as it was in the previous report. This modulus is a function of the fast fracture modulus and the power law exponent, as indicated in equation 18.

Now equation 20 can be written as

$$P_f = 1 - \exp\left[-\left(\frac{1}{\sigma_{0V}}\right)^{m_V}\left[\frac{t_f}{(N+1)B}\right]^{m_1}(\sigma_{\max})^{m_2}kV_T\right]$$

(22)

and with

$$t_f = \frac{\hat{\sigma}(x,y,z)}{\dot{\hat{\sigma}}(x,y,z)} = \frac{\hat{\sigma}_{\max}}{\dot{\hat{\sigma}}_{\max}} \qquad \textbf{(23)}$$

then

$$P_f = 1 - \exp\left\{-\left(\frac{1}{\sigma_{0V}}\right)^{m_V}\left[\frac{1}{(N+1)B}\right]^{m_1}\left[\frac{(\hat{\sigma}_{\max})^{N+1}}{\dot{\hat{\sigma}}_{\max}}\right]^{m_1} kV_T\right\}$$

(24)

From equation 6, one can deduce that

$$(D)^{N+1} = \frac{(\hat{\sigma}_{\max})^{N+1}}{\dot{\hat{\sigma}}_{\max}} \qquad \textbf{(25)}$$

which further simplifies equation 24, i.e.,

$$P_f = 1 - \exp\left\{-\left(\frac{1}{\sigma_{0V}}\right)^{m_V}\left[\frac{(D)^{N+1}}{(N+1)B}\right]^{m_1} kV_T\right\}$$

(26)

Noting that this derivation has focused on strength limiting flaws distributed through the volume, at this point the notation B_V, N_V and D_V is adopted. This infers that these time dependent parameters are associated with a volume flaw population. Hence this last expression can be solved for the parameter B_V such that

$$B_V = \frac{(D_V)^{N_V+1}}{\left\{\left(\frac{1}{kV_T}\right)\ln\left[\frac{1}{1-P_f}\right]\right\}^{\frac{N_V-2}{m_V}}(\sigma_{0V})^{N_V-2}(N_V+1)}$$

(27)

A similar derivation for strength limiting flaws distributed along the surface of test specimens would lead to the following expression

$$B_A = \frac{(D_A)^{N_A+1}}{\left\{\left(\frac{1}{kA_T}\right)\ln\left[\frac{1}{1-P_f}\right]\right\}^{\frac{N_A-2}{m_V}}(\sigma_{0V})^{N_A-2}(N_A+1)}$$

(28)

where kA_T is the "temporal" effective area for the specimen being analyzed.

Given a dynamic fatigue (monotonically increasing load) data set, WeibPar now calculates the dynamic fatigue parameter B, and provides an equivalent static fatigue material specific parameter for use in CARES. This allows the user to evaluate subcritical crack growth parameters using one type of load application, and apply this information to a component that is subject to another type of load application using what is commonly referred to as g-factors in the literature. Additional load application formats will be added next quarter.

Conclusion

Predicting brittle material or ceramic reliability of components simulated in finite element analysis is an important tool to the design engineer. The design engineer needs an ability to optimize the design of a component before the component is tested and manufactured. This process saves on development time and resources. Two software programs, WeibPar and CARES, assist the design engineer in this process of optimization. WeibPar extracts certain material parameters from test specimen failure data needed for a reliability analysis. CARES utilizes the material parameters along with a finite element stress analysis to predict a failure rate or a lifetime of the ceramic component.

Under this contract the both these program have been updated to work with the latest versions of commercially available finite element software. In addition, new technologies have been added to the programs for greater applications and flexibility.

2.2.11a Graphite-based Thermal Management System Components for Microturbine Heat Recovery Systems

Edgar Lara-Curzio
Metals and Ceramics Division
Oak Ridge National Laboratory
Oak Ridge, TN 37831-6069
(865) 574-1749, E-mail: laracurzioe@ornl.gov

DOE Technology Development Manager: Debbie Haught
(202) 586-2211; (202) 586-7114 (fax); e-mail: debbie.haught@ee.doe.gov

Objective
- To design, fabricate and evaluate graphite fiber-based heat recovery systems for microturbines.
- Through modeling and experimental work, determine the architecture of woven fiber structures that maximize heat transfer while optimizing pressure drop and costs.

Approach
- Utilize high-thermal conductivity graphite fibers to develop lightweight, compact thermal management systems (heat exchangers) with low density, high surface area, high permeability, high thermal effectiveness and high damage tolerance.
- Utilize commercially available graphite fibers and textile manufacturing processes to fabricate thermal management system components based on woven graphite-fiber structures.
- Combine experimental and modeling work to optimize the design of compact, lightweight thermal management system components.
- Evaluate the thermal and hydraulic performance of a prototype heat exchanger and compare results with those obtained with commercial products.

Accomplishments
- In collaboration with 3-Tex Inc. (Cary, NC) a first generation of woven structures with controlled pore structure and distribution, permeability and thermal properties was obtained using graphite fibers with intermediate elastic modulus (350 GPa) and thermal conductivity (250 W/mK). Subsequently a second-generation of woven structures incorporating fluid-carrying metallic tubing was also obtained.
- The permeability of woven graphite fiber structures (with and without metallic tubing) was determined as a function of fiber architecture and number of metallic tubing.
- Using a test rig that was designed and built in FY04, the heat transfer characteristics, permeability, and pressure drop of woven fiber structures was determined.
- Modeling efforts have been undertaken to aid the design, development and optimization of woven graphite fiber structures for the manufacture of thermal management components.
- The modeling and experimental results have led to work on a preliminary design of a prototype heat exchanger.

Future Directions
- With the aid of modeling tools, woven fiber structures will be designed and fabricated using graphite fibers with high thermal conductivity placed along directions in which heat transfer needs to be maximized. Graphite fiber of lower thermal conductivity will be used in secondary directions. While their contribution to the thermal performance of the structure will be minimal, they will be used to provide structural integrity. The resulting hybrid woven structures will be optimized for thermal and hydraulic performance and cost.
- Predictive numerical models that account for the effect of fiber architecture on permeability and heat transfer performance of woven fiber structures will be completed.
- Prototype versions of thermal management system components will be designed and fabricated for testing and evaluation.
- Cleaning, filtration and maintenance requirements of woven graphite fiber structures will be investigated. Industrial collaborations will continue to be broadened.

Introduction

Every year somewhere between 45 GWh and 90 GWh of power are lost — enough to power between 45 million and 90 million households— because of low efficiency (only about 33%) realized by traditional power generation. However, by recovering waste heat, combined heat and power (CHP) systems bring energy efficiencies to upwards of 80%. CHP systems recycle waste heat to generate steam, to dry humid air and/or to produce hot or chilled water for use in space heating, domestic water heating, or air conditioning.

Most heat recovery systems for microturbines use exhaust gas–to-water heat exchangers. Because microturbine efficiency and the effectiveness of heat recovery heat exchangers are very sensitive to pressure drops it is necessary that the design of the latter be focused on maximizing heat transfer while minimizing pressure drop.

The objective of this project is to improve the efficiency of heat recovery systems for microturbines, which currently use aluminum fin heat exchangers. Work will be focused on the design, fabrication and evaluation of graphite fiber-based heat exchangers that will be evaluated using a 30kW Capstone microturbine and a Microgen Unifin heat recovery unit. In collaboration with researchers at the University of Western Ontario, the thermal efficiency and hydraulic characteristics of the exhaust gas–to-water heat exchanger will be modeled to identify the fiber architecture of woven structures that maximizes heat transfer while minimizing pressure drop. Funding from a DOE-funded project to develop lightweight heat exchangers for fuel cell powered vehicles was leveraged to accomplish the objectives of this project.

Approach

The objectives of this project will be achieved through a combination of modeling and experimental work. Woven fiber structures will be designed and fabricated using various grades of graphite fibers and established textile techniques. Graphite fibers with high thermal conductivity will be placed in the structure along directions in which heat transfer needs to be maximized. Graphite fibers with lower thermal conductivity, or other types of fibers (e.g.- glass fibers), will be placed in the structure along directions in which heat transfer is not critical but where the fibers contribute to the structural integrity of the woven structure. The combination of fibers with different thermal properties will yield hybrid woven structures with optimized thermal performance and cost. In collaboration with weaving manufacturers, cost projections will be obtained for the large-scale manufacture of thermal management components. The geometrical features of the woven structure (e.g.- weaving pattern) and their scale (e.g.- spacing between fill and warp bundles) will be determined by a combination of experimental and modeling work in order to optimize performance and cost.

These design activities will be conducted in coordination with industrial collaborators.

Results

In collaboration with 3-Tex, Inc. (Cary, NC) a first-generation of woven graphite fiber structures were fabricated utilizing graphite fibers with an elastic modulus of 50 Msi and a thermal conductivity of 250 W/mK. Woven structures with different fiber architectures and pore structure were obtained (Figure 1).

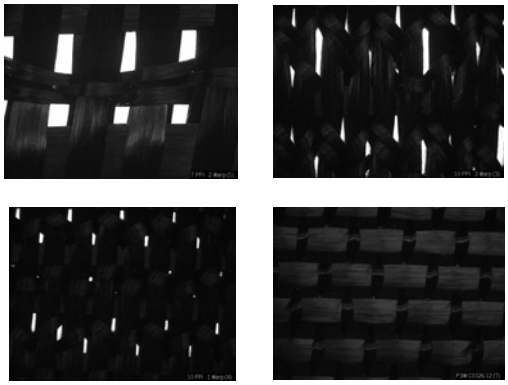

Figure 1. Woven Graphite Fiber Structures

A second-generation of woven structures was fabricated utilizing the same fibers, but with fluid-carrying metallic tubing incorporated in the structure. Figure 2 shows these woven graphite fiber structures.

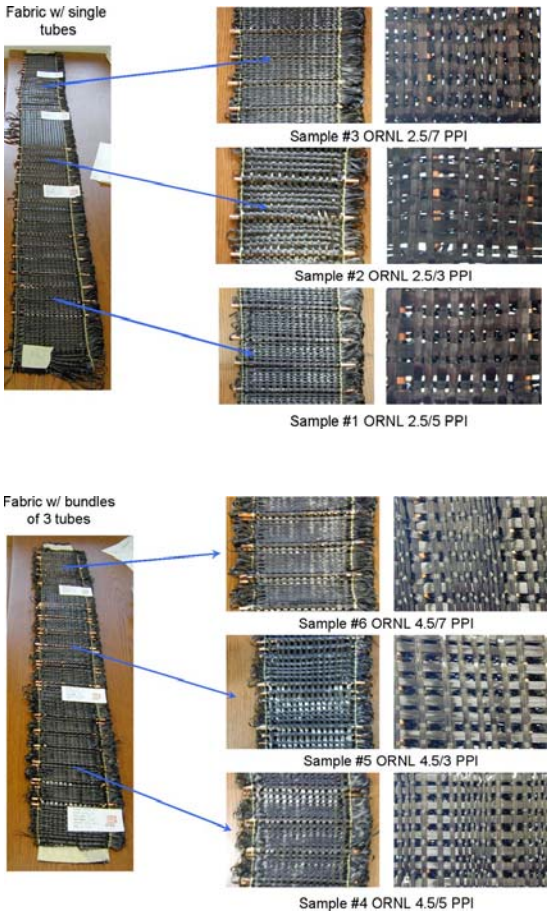

Figure 2. Woven Graphite Fiber Structures with Metallic Tubing Incorporated into the Stucture

In collaboration with the *Textile and Nonwovens Development Center* (TANDEC) at the University of Tennessee-Knoxville, air permeability measurements were made on generation 1 and 2 of graphite fiber woven structures. A schematic of the test apparatus and a plot of permeability as a function of porosity are shown in Figure .

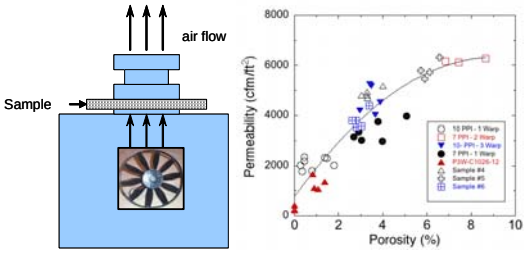

Figure 3. Permeability Test Apparatus and Results

It was found that the permeability of generation 1 and 2 of woven graphite fiber structures ranged from 225 to 6250 cfm/ft^2 and that permeability increased with porosity.

A test rig (shown in Figure) was designed and constructed to evaluate the heat transfer characteristics, permeability, and pressure drop associated with woven graphite fiber structures.

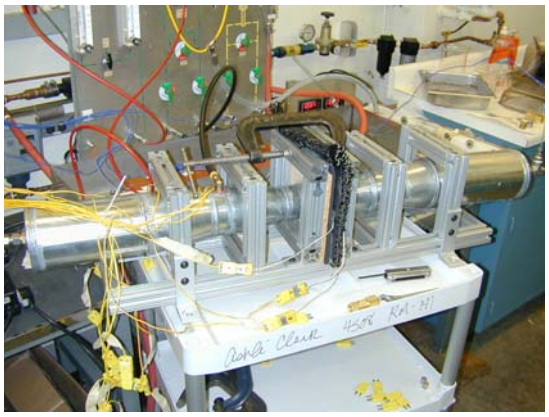

Figure 4. ORNL Heat Transfer and Pressure Drop Test Rig

Initial results of pressure drop vs. flow rate are shown in Figure for woven graphite fiber structures with single tubes and different fiber architectures. Initial results of pressure drop vs. flow rate for woven graphite fiber structures with triple tubes and different fiber architectures are shown in Figure . These results indicate that, as expected, pressure drop increases with increasing fabric density.

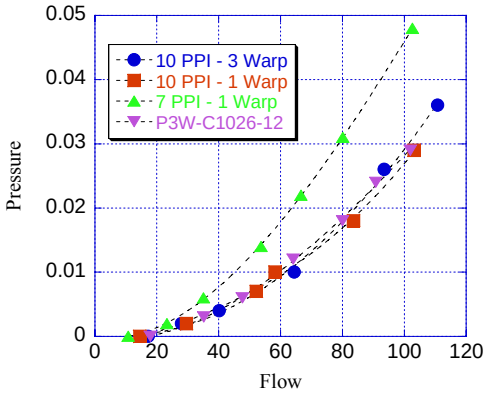

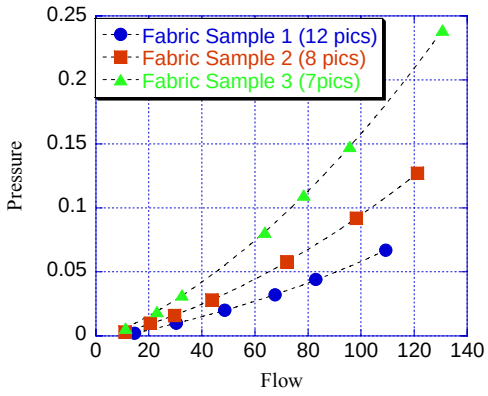

Figure 5. Pressure Drop vs. Flow for First- Generation and Second-Generation Woven Graphite Preforms (single tube configuration)

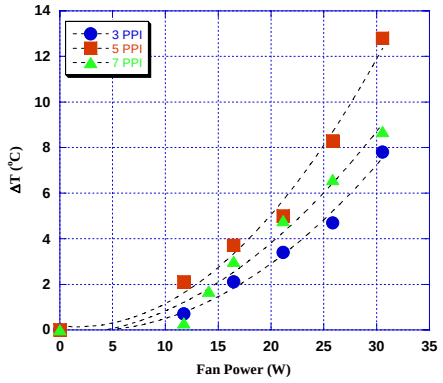

Figure 6. Pressure Drop vs. Flow for Second-Generation Woven Graphite Preforms (triple tube configuration)

It is recognized that the largest thermal resistance in these structures exists at the interface between of the fibers and the fluid-carrying tubing. To minimize the magnitude of this thermal resistance, conductive epoxies were used to bond the copper tubing to the woven structure. It was found that conductive epoxies can increase heat transfer at these interfaces by as much as 25%.

To further evaluate the performance of generation 2 woven graphite fiber structures, the test set-up shown in Figure 4 was modified to flow hot water through the copper tubing using a water recirculating system and to flow air through the woven structure using a variable-speed fan or an air blower. The change in water temperature and the pressure drop across the woven structure were recorded as a function of the initial water temperature, the power supplied to the variable speed fan and whether or not conductive epoxy was used to bond the metallic tubing to the woven fibers.

Figure 7. Retrofitted Test Rig with Blower Assembly

Figure presents a picture of the retrofitted instrumented test facility. Figure 8 is a plot of the change in water temperature (T_{inlet} - T_{outlet}) as a function of the electric power used to operate the blower while 9is a plot of the pressure drop across the fabric as a function of electric power used to operate the blower.

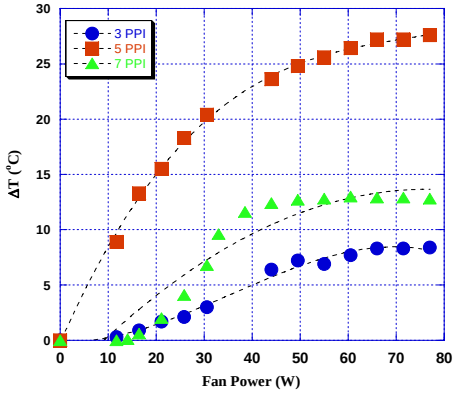

Figure 8. Water Temperature Drop as a Function of Fan Power.

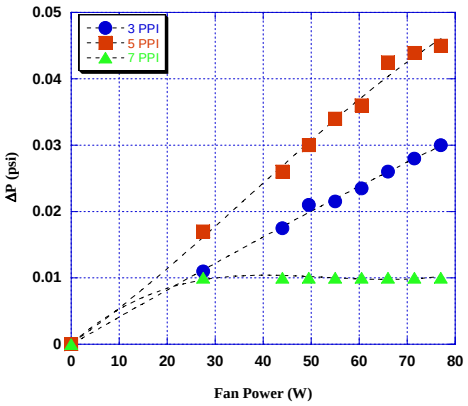

Figure 9. Pressure Drop as a Function of Fan Power.

Modeling of the woven fabric structure has continued. Two major findings have come out of this work. The first is that only the fibers oriented perpendicular to the metallic tubing actively transfer heat. Therefore, subsequent weavings will consist of high thermal conductivity graphite fibers in this direction and low grade glass fibers in the other two directions. This will allow for strength of the fabric while still maintaining high heat transfer. Higher grade graphite fibers, than those previously used, have been identified and purchased. Additionally, this will greatly reduce the cost of the woven fabric. The second finding relates to the spacing between the metal tubes. This distance is currently being optimized through the modeling effort. Modeling efforts have also been undertaken to aid in the design of a prototype heat exchanger.

The modeling and experimental results have led to work on a preliminary design of a prototype heat exchanger. The current concept involves stacking layers of composite fabric (high thermal conductivity graphite fibers and low grade glass fibers) containing single tubes as shown in Figure 5. The individual layers would then be connected using headers on the front and back of the unit.

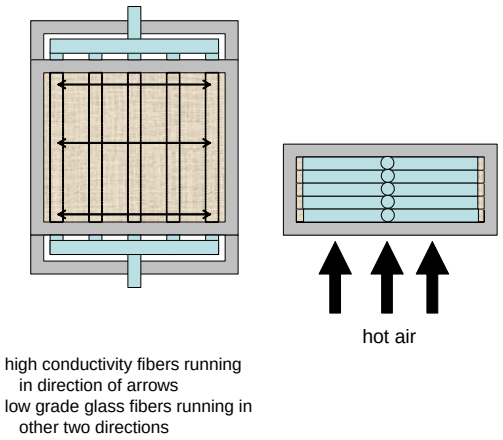

Figure 5. Concept for Preliminary Design of Prototype Heat Exchanger

Summary

Thermal management components are being developed using woven graphite fiber structures. In collaboration with 3-Tex, Inc., woven graphite fiber structures incorporating copper tubing were fabricated using graphite fibers with intermediate elastic modulus and thermal conductivity. The thermal and hydraulic performance of these woven structures was determined and correlated to their fiber architecture using a test rig designed and constructed at ORNL. The ability of these structures to remove heat from water flowing through the copper tubing was demonstrated and the results were correlated to the power required to operate a variable speed fan used to blow air through the woven structure.

It was found that the heat transfer between copper tubing and the fibers could be increased by 25% when using thermally conductive epoxies and future work will be focused on developing hybrid structures incorporating different grades of graphite fibers that are aligned in order to optimize heat transfer and cost.

Special Recognitions & Awards/Patents Issued

One UT-Battelle, LLC invention disclosure submitted for thermal management components based on woven graphite fiber structures. June 2005.

2.2.11b Characterization of Porous Carbon Foam as Material for Compact Recuperators

Anthony G. Straatman, Qijun Yu, andBrian Thompson
University of Western Ontario
London, Ontario, Canada N6A 5B9
(519) 661-2111; Fax: (519) 661-3020

DOE Technology Development Manager: Debbie Haught
(202) 586-2211; fax: (202) 586-7114; e-mail: Debbie.Haught@ee.doe.gov
ORNL Technical Advisor: David P. Stinton
(865) 574-4556; fax: (865) 241-0411; e-mail: stintondp@ornl.gov

Objectives
- Establish laws for fluid pressure drop and convective heat transfer in porous carbon foam.
- Determine the foam structure or morphology that results in optimum heat transfer for various thermal management applications.

Approach
- Measure the heat transfer performance and fluid pressure drop across porous carbon foam heat sinks using a small-scale laboratory test apparatus.
- Study fundamental mechanisms of heat transfer in carbon foam and develop an engineering model that allows comparison of conventional and carbon foam heat exchangers.

Accomplishments
- Produced foams with a variety of pore structures; measured the heat transfer and pressure drop obtained by passing water through the foam samples
- Established consistent set of scaling parameters for representing the heat transfer from porous carbon foam and other porous metals
- Developed an engineering model for use in the development of electronic heat exchanges.

Future Direction
- Develop computational tools for optimization of the internal structure of porous carbon foam.
- Characterize the different bonding techniques and their influence on overall performance of foam-based heat exchangers.

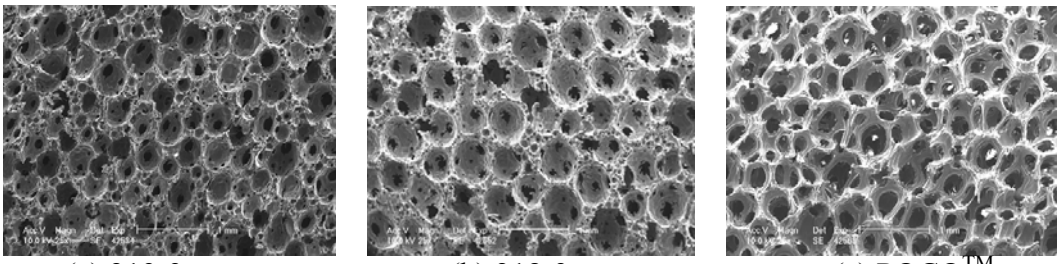

(a) 219-3 (b) 218-3 (c) POCO^{TM}

Figure 1: Scanning Electron Microscope images of the porous carbon foam specimens tested.

Table 1: Summary of properties for the carbon foam specimens tested.

Specimen	**Porosity** [%]	**Average Void Dia.** [μm]	***β**** [m^2/m^3]	k_{eff} [W/m K]
219-3	86	350	6850	72
218-3	88	400	5640	61
POCO^{TM}	82	500	5240	120

* As obtained from the unit-cube geometry model [7]

Abstract

Experiments are presented to quantify the convective heat transfer and the hydrodynamic loss that is obtained by forcing water through blocks of porous carbon foam heated from one side. The experiments were conducted in a small-scale water tunnel instrumented to measure the pressure drop and the temperature rise of the water passing through the blocks and the base temperature and heat flux into the foam block. In comparison to similar porosity aluminum foam, the present results indicate that the pressure drop across the porous carbon foam is higher due to the large hydrodynamic loss associated with the cell windows connecting the pores, but the heat transfer performance suggests that there may be a significant advantage to using PCF over aluminum foam for extended surface convection elements in recuperators and electronic cooling devices.

Introduction

Cast or foamed materials like porous carbon foam typically have an open, interconnected void structure which enables fluid exposure to internal surface area and thus the potential for significant convective heat transfer. Thus, such materials have the potential for wide application in energy exchange and heat recovery. Porous carbon foam (hereafter referred to as PCF) is produced by a process of foaming, carbonization and subsequent graphitization of a carbon-based precursor material. PCF has a high effective conductivity (40-160 [W/m K]) [1] due to the high material conductivity of the graphitized carbon material (800-1900 [W/m K]). In comparison, similar porosity aluminum foams have effective conductivities of 2-26 [W/m K], resulting from material conductivities of 140-237 W/m K (for various aluminum alloys) [2]. The high conductivity of the graphitized solid enables PCF to readily entrain heat into the solid structure of the foam to be swept away by passing fluid. Another significant advantage of PCF over aluminum or other metal foams is the high internal surface area that results from the foaming process. The internal surface area, which can be as high as 5,000-10,000 m^2/m^3, serves to reduce the convective resistance thereby fostering energy exchange at the pore level. It is this combination of high material conductivity and high internal surface area that makes PCF attractive as a heat transfer material for both single and multiphase applications.

While data is available quantifying the convective heat transfer in open cell metal foams (see, for example Calmidi and Mahajan [3], Boomsma and Poulikakos [4] and Boomsma et al. [5]), there is relatively little information available on the fundamental characterization of porous carbon foam. Gallego and Klett [6] provided some of the first data on the pressure drop and heat transfer for PCF. Their study provides estimates of the influence of configuration on the heat transfer and pressure drop, but not enough detail was provided to assess the influence of porosity, pore diameter and Reynolds number. Yu [7] proposed a sphere-centered unit-cube geometry model to characterize the internal structure of PCF. The unit-cube model provides expressions for the internal and external surface area, and the effective (or stagnant) conductivity as a function of the porosity and the void diameter. Straatman et al. [8] recently considered the convective enhancement obtained by bonding a layer of PCF to a metal substrate and subjecting the layer to parallel airflow. Convective enhancements of 30% - 10% over that obtained from the flat plate alone were observed over the range of Reynolds numbers 150,000 – 500,000. Furthermore, the highest enhancements were observed for relatively thin (3 mm) layers of foam owing to the small depth of penetration of the cooling air.

The purpose of the present work is to further explore the heat transfer and pressure drop obtained when passing fluid through the internal structure of PCF. The motivation for this body of work is to develop expressions describing the pressure drop and pore-level heat transfer such that PCF can be considered in design applications such as recuperators and electronic heat sinks. Experiments are described that establish the flow and convective heat transfer obtained by forcing water through PCF specimens of different porosity and pore diameter. Results are presented to show the hydrodynamic and thermal performance of the PCF specimens, and a recommendation is made concerning the appropriate length scale and area used in the formation of the dimensionless heat transfer coefficient.

Carbon Foam Specimens

Three different PCF specimens have been considered in the present work. The geometric properties and effective thermal conductivities of the specimens are summarized in Table 1. Scanning Electron Microscope (SEM) images of the foam specimens are given in Fig. 1. On the basis of the large pore diameter and high effective conductivity, the tabulated data indicates that the POCO^{TM} foam has the best combination of properties for convective heat transfer. Conversely, the 218-3 foam appears to have the poorest combination of geometric and thermal properties. The images in Fig. 1 indicate that there are also significant differences between the foams in terms of the size of the cell windows connecting the pores. The cell windows provide the interconnectivity between the voids and thus afford access to the internal surface area of the foam. From the point of view of heat transfer, it is best to have small cell windows to maximize the internal surface area available for convection. However, from the point of view of flow into the foam, small cell windows will lead to much higher pressure drops due to the hydrodynamic loss associated with rapid contraction/expansion through the cell windows. Thus, the most *open* foam will undoubtedly yield the lowest pressure, however it may not necessary yield the highest convective heat transfer because of the lower internal surface area. Something the SEM images do not show, because of the high magnification, is the small porosity gradient that can occur in the foaming process. The gradient is due to gravity and is typically only in the foaming (vertical) direction, however the images in Fig. 1 clearly show lateral non-uniformity, particularly in the 219-3 foam. For the present experiments, test specimens were machined such that the (gravity) gradient was aligned with the vertical coordinate of the channel. Samples of foam were cut such that the nominal plan dimensions were 50 x 50 mm and the nominal thickness was 6mm, to minimize gradient effects. Approximately 0.2mm was added to each nominal dimension so that the foam specimens could be pressed into the test section to avoid fluid bypass.

The Experiments

Experiments have been conducted in a small-scale test rig to measure the heat transfer and pressure drop across obtained by passing water through specimens of PCF. The test setup, shown in Fig. 2, consists of a channel with a water inlet and outlet, a heating

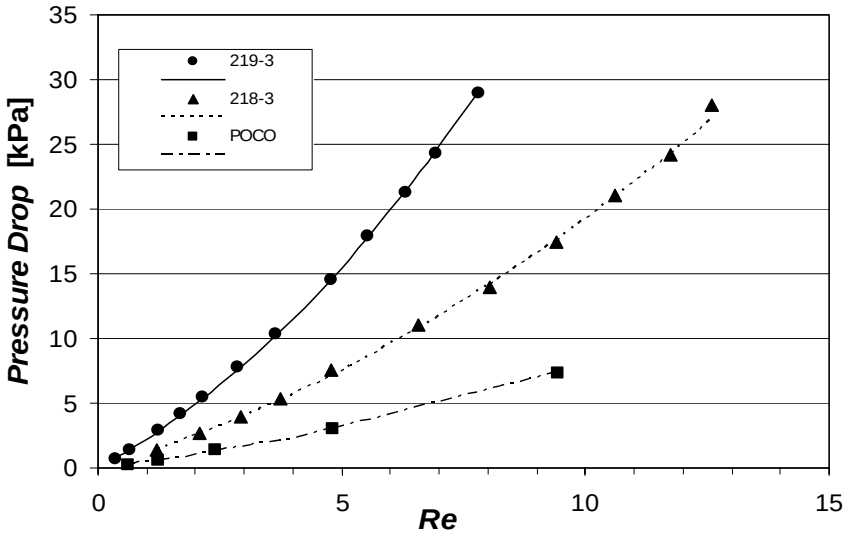

Figure 3: Plot showing the pressure drop as a function of Reynolds number for the 3 foam specimens considered. The symbols are measured data and the curves are generated from Eq.1 with the values of permeability and form drag summarized in Table 2.

element, and instrumentation to measure the flow rate, the heat input, the fluid pressure drop and temperature across the foam specimen (from position 1 to 2), and the base temperature of the heating element. The flow channel was 50mm wide by 6mm high. Foam specimens, described in the previous section, were pressed into the test section of the channel. As shown in Fig. 2, the upper 50 x 50 mm surface of the foam was pressed against the heating element and the lower surface was pressed against a plexiglass wall, which was insulated to avoid heat loss. As such, the foam specimens represent 50 x 50 mm cross-section extended surfaces heated from one side.

The specimens were subjected to a range of water flow rates and power densities to quantify variations of pressure drop and thermal effectiveness on the foam structure (characterized by porosity, ε, and void diameter, D_p) and the flow Reynolds number, defined as $Re = \rho v D_{ep}/\mu$, where ρ is the density of the fluid, v is the channel bulk velocity, D_{ep} is the equivalent particle diameter of the foam and μ is the dynamic viscosity of the fluid. The equivalent particle diameter is the solid particle diameter that preserves the interior surface area of a single spherical void and is obtained using the method described in Yu [7].

For each foam specimen, tests were initially run without heating to establish the pressure drop as a function of flow for ambient (cold) conditions. The pressures were monitored very carefully to ensure that the reported results were for steady-state conditions. The tests were then repeated for several power densities to establish the heat transfer under different flow conditions.

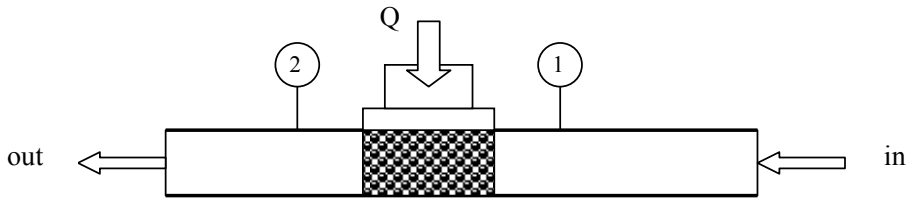

Figure 2: Schematic of experimental setup showing the position and orientation of the carbon foam, the fluid inlet and outlet, and the heat input.

Results and Discussion

The pressure data is used to obtain permeability and form drag coefficients so that the classical Darcy-Forchheimer law for porous media can be used to describe pressure losses:

$$\frac{\Delta P}{L} = \frac{\mu}{K} v + \frac{c_f}{\sqrt{K}} \rho v^2 \qquad (1)$$

Here, ΔP is the pressure drop across the foam specimen, L is the length of the specimen along the flow direction (50 mm in the present work), v is the filter (bulk) velocity, and K and c_f are the permeability and Forchheimer (form drag) coefficient. The permeability and form drag coefficients are evaluated simultaneously by considering the whole Re range at the tested conditions. Results for the pressure drop as a function of Re are shown in Fig. 3 for the three foam specimens considered. Figure 3 shows measured pressure drops in symbolic form and curves generated using Eq. 1 (converted to the Re scale) with the permeability and form drag coefficients established and shown in Table 2. It is clear from Fig. 3 and Table 2 that the permeability and thus the pressure drop is very different for the three specimens tested, with the 219-3 foam having the highest fluid pressure drop and POCO^{TM} having the lowest. As suggested in section 2.0, the pressure drop is strongly affected by the pore diameter and perhaps more importantly, the size of the cell windows connecting the pores, due to the hydrodynamic loss associated with the sudden contraction/expansion. While the results show the expected trend, it is difficult based on the present result to assess the impact of pore diameter and cell window size separately.The results for pressure drop can be compared in terms of permeability to similar results obtained for aluminum foams. Boomsma and Poulikakos [4] evaluated the permeability of 6101 aluminum alloy foams with and without compression. The uncompressed foam had porosities in the range 92-93% and internal surface areas of 820-2700 m^2/m^3, while the compressed foams had

Table 2: Summary of properties for the carbon foam specimens tested.

Specimen	Permeability, K [m^2]	Forchheimer Coefficient, c_f
219-3	2.37×10^{-10}	0.8802
218-3	4.19×10^{-10}	0.5023
POCO^{TM}	6.23×10^{-10}	0.5878

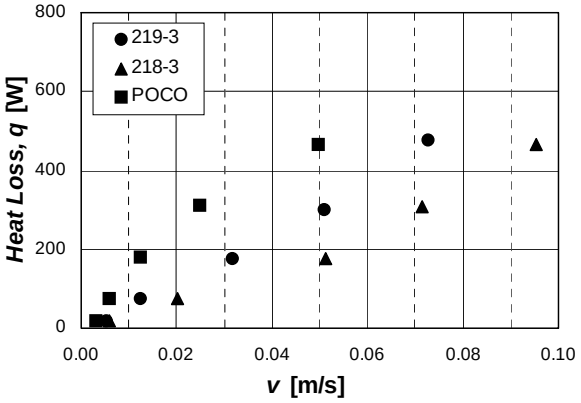

Figure 4: Plot showing the heat loss as a function of the filter velocity v for the foam specimens tested.

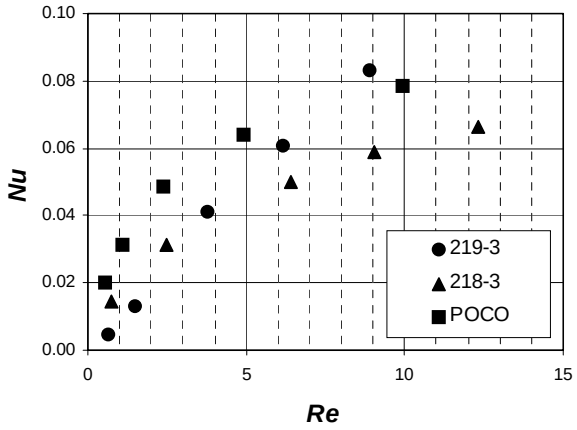

Figure 5: Plot showing the Nusselt number as a function of Re (based on D_{ep} and A_{eff}) for the three foams considered.

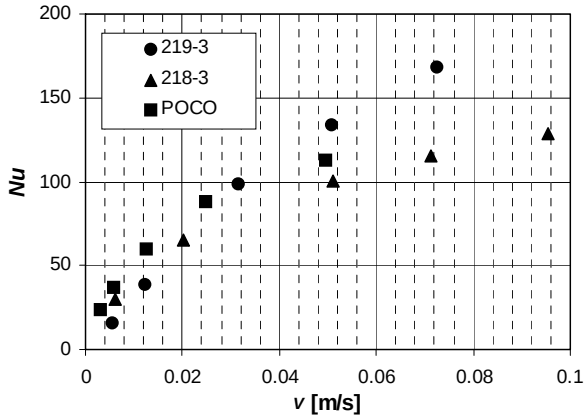

Figure 6: Plot showing the Nusselt number (based on D_{hyd} and A_b) as a function of the filter velocity v.

porosities in the range 66-88% and internal areas 2 to 4 times higher than those noted above. In comparison to the POCO^{TM} foam, which has the lowest pressure drop among the foams tested herein, a similar porosity 6101 compressed aluminum foam has a permeability approximately 3 times higher, indicating that it is much easier to pass a fluid through the aluminum foam. This is largely due to the difference between the internal structures of the aluminum and PCF foams. The aluminum foam is comprised of thin fused strands and large open cell windows, but relatively little internal surface area. The PCF is comprised of spherical

voids and small(er) cell windows, but a larger amount of internal surface area. Since the low permeability of the current PCF is due to the large hydraulic loss associated with the cell windows that link the spherical voids, it is of interest to modify the foaming process for PCF to provide larger and smoother cell windows to increase the permeability of the foam.The heat transfer measured in the present experiments for the PCF specimens is plotted in Fig. 4 as a function of the filter velocity. The plot indicates that POCO^{TM} foam dissipates the most heat followed by 219-3 and 218-3. This figure is important because it gives the actual energy dissipated by equivalent-sized foam specimens of different geometric and thermal properties. This figure does not, however, provide universal information about the foam specimens that can be used in design applications. The required information can be generated from the data shown in Fig. 4, but care must be taken to ensure that the scaled data reflects the correct physics

The heat transfer data is used to form the Nusselt number, which is obtained by:

$$Nu = \frac{h_{sf} D}{k_{fa}} = \frac{D}{k_{fa} A} \frac{q_{avg.}}{\Delta T} \qquad (2)$$

where h_{sf} is the heat transfer coefficient at the pore level, D is a length scale; $q_{avg.}$ is the average heat transfer obtained from the power applied to the heater (and from an energy balance on the fluid); k_{fa} is the thermal conductivity of the fluid evaluated at the average fluid temperature; A is an area; and ΔT is the mean temperature difference between the heater base and the fluid. As suggested, the length and area scales can be based on different variables and the virtues of those mentioned will be discussed in terms of the presented results. In the present treatment, the length scale D is based on either the equivalent particle diameter of the foam, D_{ep}, or the hydraulic diameter of the channel. The hydraulic diameter is obtained as $D_{hyd} = 4A_{chan}/P$, where A_{chan} is the cross-sectional area of the channel and P is the wetted perimeter. The area in Eq. 2 is either the effective heat transfer surface area or the heated base area of the foam sample. The effective surface area is obtained as: $A_{eff} = \eta A_f + A_b$, where η is the equivalent micro-fin efficiency of the foam obtained using the Taylor model [9], A_f is the interior wall surface area of the foam specimen obtained from $A_f = \beta V$, where β is the area factor (Yu, [7]) and V is the volume of the specimen, and A_b is the bare surface area of the heater that is not covered by the porous foam. The heated based area of the foam is simply A_b = 50 x 50 = 2500 mm^2 for the present case.

The thermal performance of the foam specimens is shown in terms of the Nusselt number in Figs. 5 and 6. In Fig. 5 the data is presented using D_{ep} and A_{eff} as the scales in the Reynolds and Nusselt numbers, whereas Fig. 6 shows the Nusselt number based on D_{hyd} and A_b as a function of the filter (bulk) velocity (as used in Boomsma et al [5]). The figures make evident the fact that the chosen scales produce a different picture in terms of the thermal performance of the foam specimens. Fig. 5 shows POCO^{TM} to be the superior foam followed by 219-3 and 218-3, while Fig. 6 shows all three foams to be similar for low velocities with 219-3 emerging as the superior foam at higher velocities. By comparison of Figs. 5 and 6 to Fig. 4, the more accurate representation of the thermal performance of the foams is given in Fig. 5. As described above, the length scale and area used in Fig. 5 include geometric properties of the foam; furthermore, by inclusion of the equivalent micro-fin efficiency in A_{eff}, the effective conductivity of the foam is also accounted for. The real differences between the foams can only be reconciled by considering all these parameters. The 219-3 and 218-3 foams have a similar effective conductivity, but 219-3 has significantly more internal surface area and thus a better capacity to remove energy that is conducted in. POCO^{TM} foam has a substantially higher effective conductivity than 219-3 and thus a higher micro-fin efficiency. In this case the thermal performance of POCO^{TM} is considerably higher despite its smaller internal surface area. On the basis of the present measurements, and considering both the hydrodynamic and thermal characteristics, the POCO^{TM} foam is considered to perform best.

Comparisons to the measured performance of 6010 aluminum foam [5] can be made by considering the data in Fig. 6. The comparisons, which are not shown

explicitly in this paper, indicate that POCO™ foam is slightly better than compressed aluminum in terms of thermal performance. However, since the data in [5] is presented in terms of the scales used in Fig. 6, it is important to consider how proper scaling will influence the comparison. The heat transfer measurements in Boomsma et al [5] were conducted on 2 mm-thick compressed aluminum foam specimens (of 40 x 40 mm cross-section). Thus, the fin efficiency was likely quite high over the full range of *Re* considered. However, because of the low effective conductivity of aluminum, the fin efficiency would drop considerably with increased thickness and thus, the heat transfer effectiveness of the thicker specimen would be poor. Since the effective conductivity of PCF is 5-20 times higher than that for aluminum foam, the heat transfer effectiveness would remain high for much thicker extended surfaces. Thus, if similar thickness specimens were considered, the heat transfer performance of PCF would be many times higher than that of the aluminum. This is perhaps one of the most important merits of PCF and forms the motivation for pursuing PCF as a convective enhancement material in energy exchange and electronics applications.

Conclusions

Measurements of the pressure drop and heat transfer obtained by forcing water through blocks of porous carbon foam are reported. The pressure drop is seen to be a function of the pore diameter and porosity, but also strongly affected by the size of the cell windows connecting the spherical pores. This is due to the large hydrodynamic loss associated with the fluid contracting/expanding through the windows. The heat transfer was seen to be a function of the effective conductivity and the internal surface area, as might be expected. A comparison of two different sets of scaling parameters showed the importance of including geometric and thermal parameters in the formation of the Nusselt number. Of the specimens tested, the POCO™ foam offers the best combination of hydrodynamic and thermal performance. The present results suggest that there may be a significant advantage for using PCF as an extended surface convective enhancement material in energy exchange and electronic cooling applications.

Acknowledgments

This work has been sponsored by the DE Materials Program, DOE Office of Distributed Energy, under contract DE-AC05-00OR22725 with UT-Battelle, LLC, and by the Natural Science and Engineering Research Council of Canada (NSERC).

References

1. Klett, W.J., Hardy, R., Romine, E., Walls, C., Burchell, T., 2000, "High-thermal conductivity, mesophase-pitch-derived carbon foam: effect of precursor on structure and properties," *Carbon*, 38, pp. 953-973.
2. Paek, W.J., Kang, H.B., Kim Y.S. and Hyum, M.J., 2000, "Effective Thermal Conductivity and Permeability of Aluminum Foam Materials," *Int. J. of Thermophysics*, 21(2), 453-464.
3. Calmidi, V. V. and Mahajan, R. L., 2000, "Forced Convection in High Conductivity Metal Foams," *ASME J. Heat Transfer*, 122, pp. 557-565.
4. Boomsma, K., Poulikakos, D., 2002, "The Effects of Compression and Pore Size Variations on the Liquid Flow Characteristics in Metal Foams," *ASME J. Fluids Engineering*, 124, pp. 263-272.
5. Boomsma, K., Poulikakos, D., Zwick, F., 2003, "Metal Foams as Compact High Performance Heat Exchangers," *Mechanics of Materials*, 35, pp. 1161-1176.
6. Gallego, C.N. and Klett, W.J., 2003, "Carbon foams for thermal management," *Carbon*, 41, pp.1461-1466.
7. Yu, Q., Thompson, B. E., Straatman, A. G., "A unit-cube based model for heat transfer and pressure drop in porous carbon foam," Submitted for publication to *ASME J. Heat Transfer*, 2004.
8. Straatman, A. G., Gallego, N. C., Thompson, B. E., Hangan, H., "Thermal Characterization of Porous Carbon Foam – Convection in Parallel Flow," Submitted for publication to *J. Heat and Mass Transfer*, 2004.
9. G.I. Taylor, 1971, "A model for the boundary condition of a porous material. Part 1," *J. Fluid Mechanics*, 1971, 49, pp. 319-326.

2.2.13a Polymer Derived EBCs for Monolithic Silicon Nitride

Rishi Raj and B. Sudhir
University of Colorado
Boulder, CO – 80302
(303)492-1029, E-mail: Rishi.Raj@Colorado.EDU

DOE Technology Development Manager: Debbie Haught
(202) 586-2211; fax: (202) 586-7114; e-mail: debbie.haught@ee.doe.gov
ORNL Technical Advisor: Karren More
(865) 574-7788; fax: (865) 576-5413; e-mail: morekl1@ornl.gov

Objective

- Develop a cost effective and efficient hydrothermal testing apparatus for laboratory scale evaluation of candidate EBC materials.
- Develop an adherent and compliant polymer-derived ceramic (PDC) EBC coating.
- Optimize the PDC coating composition and structure.

Approach

- Process and hydrothermally test porous PDC composites.
- Determine the microstructure of candidate bond coat materials from mechanical and microstructural studies on processed and tested specimens.

Accomplishments

- A cost-effective laboratory scale testing apparatus was fabricated whose performance is comparable to some of the high-pressure burner rigs.
- Preliminary characterization studies revealed that porous composites of hafnia with (polymer-derived) SiCNO/SiO_2 at the interface retain their strength even after prolonged hydrothermal exposure at 1300°C for 200 hr.
- The results continue to confirm that porous PDC composites exhibit “self-healing” behavior.
- Preliminary coating studies verified that porous PDCs act as good bond coats between silicon nitride substrate and a hafnia top coat and survive up to 1300°C.

Future Direction

- Optimize the composition and architecture of the porous bond coat.
- Improve the coatings in order to survive higher temperatures and longer durations.

Introduction

SiC/Si_3N_4 components undergo unacceptable material loss during gas turbine operation due to the presence of streaming water vapor in the turbine environment. Hence, the need for Environmental Barrier Coatings (EBCs) in order to realize the potential of these high temperature structural materials is well established from past studies. Top coats of transition metal oxides, such as zirconia and hafnia, are known to resist recession. However, these oxides bond poorly to silicon-nitride, and a large difference in the thermal expansion between them and silicon-nitride based ceramics can produce spalling. The design and materials selection for the bond coat, is therefore, a key barrier in the design of successful EBCs. Earlier studies have shown that polymer-derived, oxide-nonoxide silicon carboxynitride (SiCNO) ceramic can act as a key constituent in the design of the bond coat. These early studies also revealed that the porous composites can exhibit "self-healing" behavior. During the current year the project's aim was to determine the composite microstructure that would result in the ideal bond coat. In addition, design and fabrication of an efficient laboratory scale hydrothermal testing apparatus was also accomplished.

Approach

A hydrothermal testing apparatus was designed in which water was injected directly into the hot-zone of the furnace. The large thermal expansion involved in the conversion of water to steam gave high steam velocities even with low water flow rates (a water flow rate of 2 ml/min gives a steam linear velocity of 35 cm/sec. In comparison, other laboratory scale testing units operate at a maximum of 10 cm/sec steam velocity. This apparatus was used to test silicon nitride (AS800) coupons to evaluate its performance.

Polymer-derived composites with two microstructures were prepared: (a) Particulate composites of 50 vol% hafnia (or zirconia) - 50 vol% SiCNO were prepared by mixing the respective powders, followed by cold compaction and sintering to obtain a porous disc, and (b) a hafnia-5 vol% SiCNO composite in which the polymer precursor is mixed with the hafnia powder and then pyrolyzed at 1000°C in nitrogen. This resulted in SiCNO being distributed at the hafnia grain boundaries (this is designated as the 'interface' composite). The samples were hydrothermally tested and characterized by weight change, XRD, BET, electron microscopy and three-point bending tests.

Results

I. Hydrothermal testing on Si_3N_4:

Si_3N_4 (AS800) bend bars obtained from Honeywell, Inc. were tested at 1300°C at steam velocities in the range of 1 to 35 cm/sec. Figure 1 shows the data obtained in the present study along with some of the results reported in the literature. As seen in the figure, the results from the present study are in good agreement with literature values. Please note that in Figure 1, the data from the literature (other than those in the turbulent regime) have been normalized to our experimental conditions ($P(H_2O) = P(total) = 1$ atm.). The data indicate that there are three regimes: a "pseudo-threshold" velocity below which weight loss rate is appreciably lower than predicted, followed by a regime in which the weight-loss rate is governed by the laminar flow of steam over the Si_3N_4 surface and finally at higher velocities steam flow becomes turbulent.

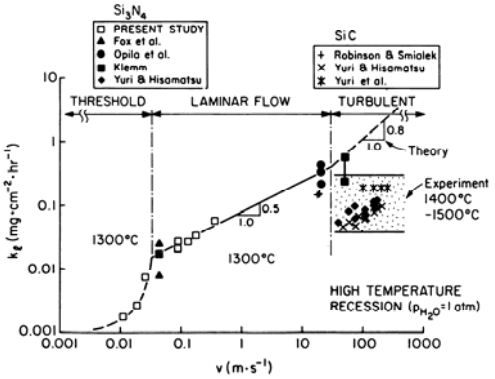

Figure 1: Weight-loss rate vs steam velocity for Si_3N_4 and SiC on a double log scale.

A significant feature of the apparatus is that the obtained weight-loss rates are comparable to those

obtained in some of the High-Pressure Burner Rigs (HPBR) (Figure 2).

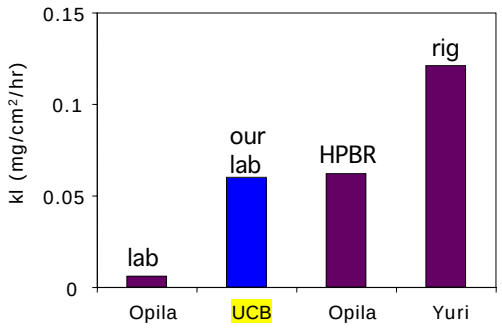

Figure 2: Comparative plot shows that the weight-loss rates obtained in our apparatus are comparable to those obtained in some HPBRs

II. Results on hydrothermally tested Hafnia-(polymer-derived) SiCNO composites:
Figure 3 shows microstructures of the particulate and 'interface' composites: Figure 3(a) is the SEM microstructure of the particulate composite shows the fracture surface of the sample that was hydrothermally tested at 1300°C for 100 hours. Figure 3(b) is the TEM microstructure of the 'interface' composite tested at 1300°C for 200 hours at a steam velocity of 35 cm/sec.

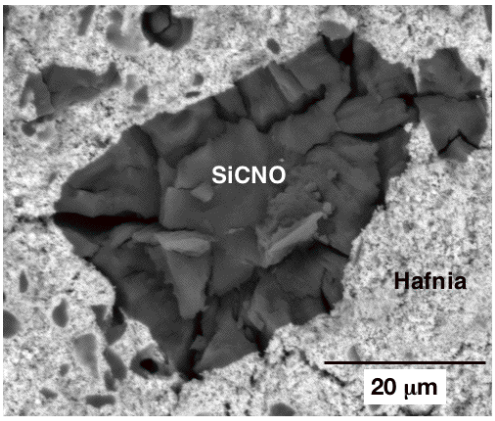

Figure 3(a): SEM micrograph of the fracture surface of tested hafnia-50 vol% SiCNO particulate composite.

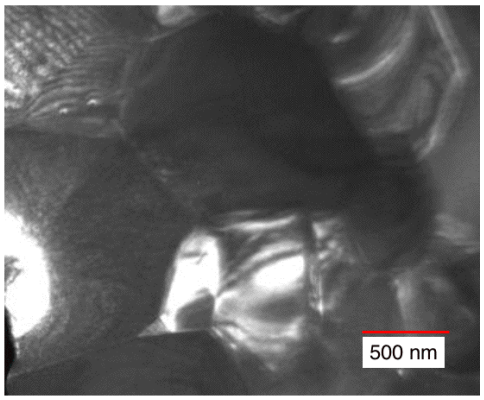

Figure 3(b): TEM (dark-field) micrograph of the hafnia-5 vol% SiCNO 'interface' composite. The SiCNO (silica) is distributed at the hafnia grain boundaries and is about 5 nm thick.

As seen in the figure, the SiCNO (silica) particles show extensive cracking, which is related to volume changes occurring due to the oxidation of the SiCNO particles to silica. Such cracking was not observed on the fracture surfaces of the 'interface' composites.

Figure 4 shows the evolution in the flexure strength on the hydrothermally tested particulate and 'interface' composites as determined from three-point bending tests.

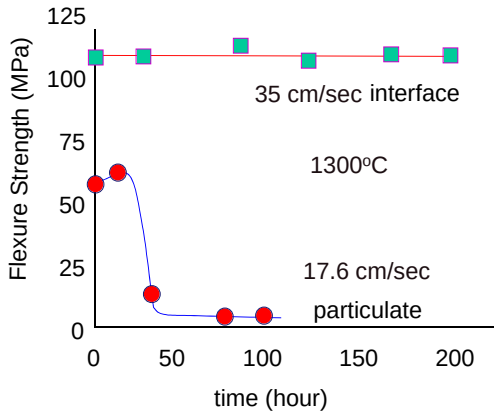

Figure 4: Evolution in flexure strength of the composites as a function of testing time.

As seen in Figure 4, at 1300°C, the interface composites retain their strength even after 200 hour of hydrothermal testing at 35 cm/sec. In comparison, the strength of the particulate composites decreases significantly after nearly 30 hours of testing even at a steam velocity of 17.6 cm/sec. This degradation in strength is related to the oxidation induced micro-cracking of the SiCNO particles. Thus, the 'interface' composites are more suitable for EBCs from the standpoint of corrosion resistance.

Conclusion

A cost effective hydrothermal testing apparatus has been developed in which high steam velocities are obtained by directly injecting steam into the hot zone of the furnace. Studies on Si_3N_4 using this novel apparatus have shown that the resulting weight-loss rates are comparable to those reported in some of the high pressure burner rigs. Studies on particulate and 'interface' composites (50 vol% hafnia-50 vol% SiCNO or hafnia-5 vol% SiCNO, respectively) have shown that the 'interface' composites retain their strength even after hydrothermal testing at 1300°C for 200 hours. In contrast, the particulate composites show a significant drop in strength after only ~ 30 hours of testing. This decrease in strength is related to the cracking of the SiCNO particles during oxidation to form silica.

Publications/Presentations

1. B. Sudhir and R. Raj, "Effect of Steam Velocity on the Hydrothermal Oxidation/Volatilization of Silicon Nitride." (Accepted) *J. Am. Ceram. Soc.*
2. B. Sudhir, R. Raj, K. L. More and A. Saha, "Hydrothermal Oxidation Behavior of a Zirconia – SiCN Particulate Composite." 29th International Conference on Advanced Ceramics and Composites, January 23-28, 2005. Cocoa Beach, Florida, USA.

2.3.1 Advanced Materials for Reciprocating Engine Components

P.J. Maziasz, N.D. Evans, and J.P. Shingledecker
Metals and Ceramics Division
Oak Ridge National Laboratory
P.O. Box 2008, MS-6115
Oak Ridge, TN 37831-6115
(865) 574-5082; fax: (865) 754-7659; e-mail: maziaszpj@ornl.gov

DOE Technology Development Manager: Debbie Haught
(202) 586-2211; fax: (202) 586-7114; e-mail: debbie.haught@ee.doe.gov
ORNL Technical Advisor: Karren More
(865) 574-7788; fax: (865) 576-5413; e-mail: morekl1@ornl.gov

---

Objectives

- Determine the temperature and performance limitations for reciprocating engine exhaust valves and identify alloy/processing/coating options for improved valve durability.
- Provide testing and support in evaluation of CF8C-Plus cast stainless steel as a performance upgrade option compared to Ni-resist cast iron for exhaust components in reciprocating engines.

Approach

- Analyze and compare fresh, engine-tested and failed exhaust valves made from current Ni-based superalloys to establish performance and temperature limitations.
- Develop partnership with valve supplier TRW to identify and test alternative alloys, processing changes, and coatings for exhaust valves with improved performance and reliability.
- Work with exhaust component supplier Stainless Foundry and Engineering to make and test new exhaust components of cast CF8C-Plus stainless steel.

Accomplishments

- Identified microstructural changes causing properties degradation of exhaust valves of Pyromet 31V and showed evidence for moisture enhanced oxidation on valve surfaces.
- Established collaborative program with TRW to explore coatings, alloy selection, and processing changes to enhance performance and reliability of exhaust valves.
- Creep-rupture testing showed that CF8C-Plus cast steel was much stronger than Ni-resist cast iron; first casting trial of CF8C-plus steel exhaust components was successful.

Future Directions

- Test and characterize new TRW commercial alloy/coating combinations to evaluate the improvements in temperature capability expected for exhaust valves.
- Provide testing and characterization support to enable engine-testing of new cast CF8C-Plus steel exhaust components, and explore making other exhaust components (manifolds, turbocharger casings) made from this steel.

Introduction

Achieving higher efficiency and lower emissions in advanced natural-gas reciprocating engine systems requires increased pressures and temperatures. Component materials face the paradox of increased life and reliability, while still withstanding higher temperatures, which tends to reduce both, all with the constraint of reasonable costs. In FY2005, this project evolved into a new stand-alone effort on high temperature components, including both exhaust valves and other hot-gas path structural components, from the combined in-cylinder program last year. Further, this program evolved from an ORNL/Waukesha collaborative program into a broader, expanded program, which now includes collaborations with the commercial component/materials suppliers for target exhaust valves or exhaust system components. After concluding an initial problem-definition stage last year, FY2005 efforts were directed toward providing solutions to enable exhaust valves and other components to have increased performance, temperature capability, and reliability.

Approach

Exhaust Valves

This new initiative began with analyzing and comparing standard fresh and engine-tested (but unfailed) exhaust valves of Pyromet 31V Ni-based superalloy, exposed to very high temperatures (above 1400°F) for times ranging from 2000 to 22,000 h. It then expanded to include valves that failed after only 3000 h of service in the field. This project has consistently identified the microstructural evidence for near-surface oxidation and bulk alloy aging effects associated with observed properties degradation. During this year, aging studies of standard and potential upgrade valve alloys began in order to calibrate and match the complex microstructural changes occurring in actual valves with a set of aged specimens having a well-defined time/temperature history. Finally, at the encouragement of Waukesha Engine- Dresser (WED), ORNL and TRW defined and began a collaboration to determine how to make exhaust valves with different designs, processing, and alloys for increased temperature capability and reliable performance. The end goal of this new collaboration is producing prototypes of such valves for engine-testing and valves that can also be scaled up for commercial production.

Structural Exhaust Components

Similar to the exhaust valve portion of this project, Waukesha expressed concern about increasing exhaust temperatures over a year ago. The current alloys for structural exhaust components (manifolds, bridges and turbocharger casings) included SiMo cast iron and Ni-resist cast austenitic iron. ORNL and Caterpillar, Inc. had recently developed a new CF8C-Plus cast stainless steel for such applications, so Waukesha also encouraged a collaborative project with their exhaust component supplier, Stainless Foundry & Engineering (SF&E). This year, SF&E cast blocks for high temperature mechanical properties specimens (tensile and creep-rupture) of both Ni-resist cast-iron and the new CF8C-Plus cast stainless steel. SF&E also made component casting trials with the new CF8C-Plus steel. Materials testing and component evaluations are in progress and will continue next year.

Technical Process

Exhaust Valves

Fresh exhaust valves of Pyromet 31V Ni-based superalloy (Ni-22.5Cr-15Fe-2Mo-2.25Ti-1.25Al-C), given the standard heat-treatments for strengthening, have been characterized. The standard heat treatments produce fine precipitation of Cr-rich $M_{23}C_6$ along the grain boundaries, and a dense dispersions of finer $Ni_3(Al,Ti)$ γ' particles (about 48 nm dia.) within the grains (see Fig. 1a). Aging during service produces significant changes in the microstructure after about 2000-3000 h, and then approach terminal microstructures that appear to depend mainly on temperature after as long as 22,000 h.

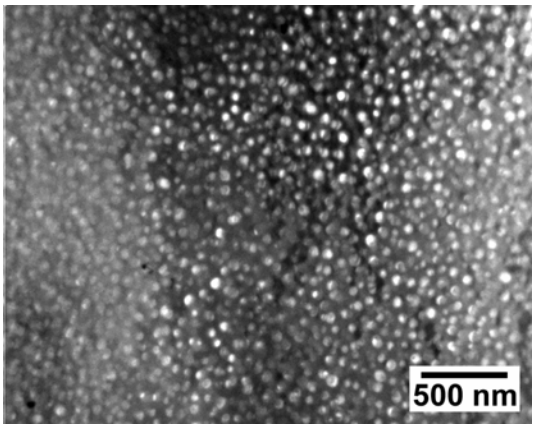

(a)

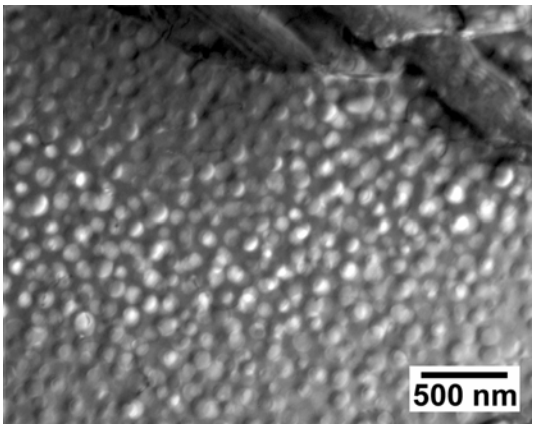

(b)

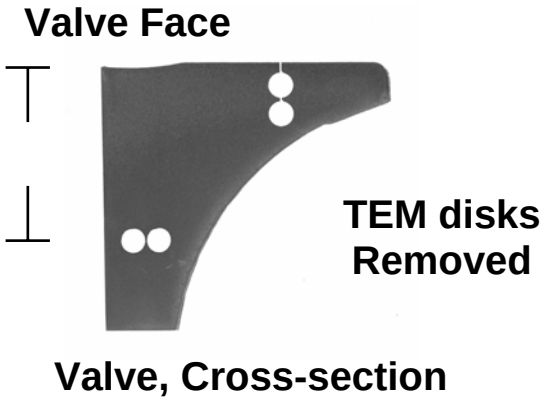

(c)

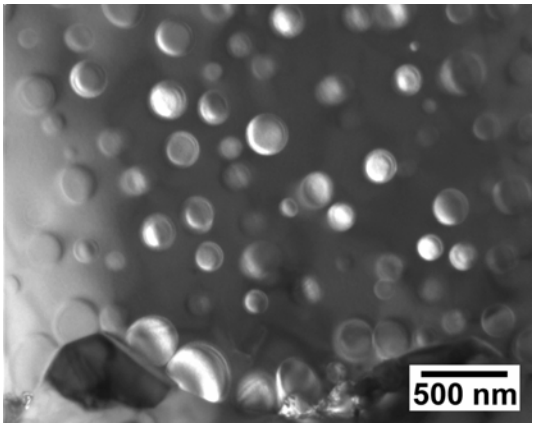

(d)

Figure 1 – TEM dark-field imaging of $Ni_3(Al,Ti)$ γ' precipitation in specimens taken from exhaust valves made of Pyromet 31V with the standard heat-treatments. (a) γ' precipitation in a fresh, as-heat-treated valve (uniform throughout), and (b) and (d) after engine service at temperatures >1400°F for 22,000 h (microstructure varies with valve location, which have different temperatures). (c) Diagram showing the locations of TEM discs cut from the engine-exposed valve, with (b) coming from just under the valve face and (d) coming from the stem just above the tulip region.

Exposure to engine service produces more and coarser Cr-rich $M_{23}C_6$ carbide precipitation along the grain boundaries of the exhaust valve, and coarse needle/lath particles of α-Cr phase within the grains.[1] Inside the grains, aging causes some coarsening of the initially fine dispersion of $(Ni,Ti)_3Al$ γ' precipitation near the valve face (Fig. 1b and 1c), and far more coarsening/dissolution of γ' in the stem region above the tulip, where the valve temperatures are highest.[2] For comparisons in the same valve location, there seems to be only minor changes in γ' distribution between 2,400 h and 22,000 h.

Analysis of oxidation near the surface of the stem region at or near maximum temperature also reveals significant oxidation after about 3,000 h (Fig. 2). Further, the nature of the oxides, with non-protective mixed Ni- and Fe-rich outer oxides on top of a Cr-rich oxide layer suggest the effects of moisture-enhanced oxidation, similar to that seen in gas-turbine and microturbine exhaust environments.

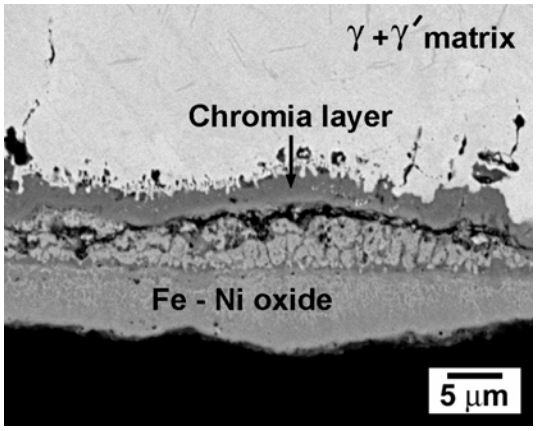

Figure 2 – Back-scattered SEM imaging of the surface oxides in the stem region of an exhaust valve after engine service of about 3,000 h. The outer layer is a mixed Fe- and Ni-rich oxide scale above the original surface, with complex oxides and Cr-rich oxide layer underneath. The dark features in the metal beneath the oxide scales are small particles of Ti- and Al-rich internal oxides.

Information on the effects of aging and surface oxidation are being used to define changes and degradation during engine-service exposure, and to provide a baseline for efforts to improve the aging-resistance of such exhaust valves.

In the last part of FY2005, a new collaborative project began between ORNL and TRW, valve supplier for WED, because both organizations were investigating similar Pyromet 31V exhaust valves. This new project is currently in the definition and objectives phase, but it will clearly address changing valve design and alloy processing, as well as considering alternate alloys to

provide exhaust valves with more temperature capability and reliability relative to standard valves. The initial phases will involve lab-scale testing and microstrutural studies, but the end goal is producing prototype valves with upgraded performance, which can then be engine-tested by Waukesha. This effort will continue and expand in FY2006.

Structural Exhaust Components

In FY2003, ORNL and Caterpillar developed a new cast austenitic stainless steel, CF8C-Plus, which has the potential for use as exhaust component applications in advanced heavy-duty diesel engines. Typical exhaust manifolds and turbocharger housings are made from SiMo cast iron, which has poor strength above 550-600°C, and can be susceptible to thermal fatigue cracking during severe cycling after prolonged use. Some applications use Ni-resist cast iron for better heat-resistance. Standard CF8C steel (Fe-19Cr-9Ni-0.7Nb-0.07C), which has good castability and sufficient strength up to about 600-625°C, is not strong enough at higher temperatures. CF8C-Plus steel was developed to be stronger and much more resistant to fatigue and thermal fatigue, so that it could be used in severe thermal cycling conditions found in exhaust manifolds and turbocharger casing for heavy-duty truck diesel engines.

In FY2005, ORNL began a collaboration with SF&E to make pieces for test specimens and trial exhaust components of the new CF8C-Plus cast steel for Waukesha. SF&E is the parts supplier to Waukesha for exhaust components currently made of Ni-resist austenitic cast iron, whose physical properties are otherwise similar to CF8C-Plus cast austenitic stainless steel. Kiel blocks were cast of both Ni-resist and CF8C-Plus to make specimens for tensile and creep-testing, and testing was done at ORNL in air at 750-850°C. A plot of creep-rupture stress versus Larson-Miller Parameter (LMP) is shown in Figure 3. This plot clearly shows that the new CF8C-Plus cast stainless steel is many times stronger than Ni-resist cast iron, and far stronger than SiMo cast iron.[3] This very large difference in high temperature creep strength then led to an effort by SF&E to produce prototype exhaust components using the CF8C-Plus cast stainless steel.

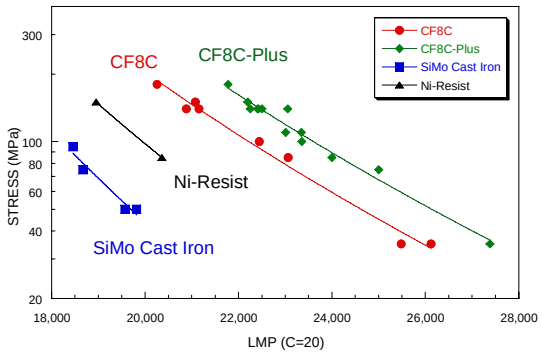

Figure 3 – Larson Miller parameter (LMP) plot of creep rupture stress for high SiMo and Ni-resist cast irons and standard CF8C and the new CF8C-Plus cast stainless steels tested in air at various temperatures in the range of 550 – 850°C. The LMP is calculated using creep temperature and creep rupture life to create a master curve for each alloy.

Figure 4 – A CF8C-Plus cast stainless steel exhaust component for a Waukesha natural gas reciprocating engine made by Stainless Foundry & Engineering. This component is the bridging structure between the exhaust manifolds and the turbocharger.

SF&E successfully cast good, defect-free components of CF8C-Plus cast stainless steel on the first trials. They found that CF8C-Plus had good castability due to the Mn addition relative to standard CF8C steel, and the new CF8C-Plus parts are currently being compared dimensionally to similar Ni-resist cast iron parts, and machined to final dimensions. If these parts are accepted by Waukesha, they may be ready for engine-testing trials to compare their performance directly to Ni-resist components in FY2006.

Conclusion

The initial characterization phase of exhaust valves made from standard Pyromet 31V alloy is complete. These valves showed changes in the microstructure in the hottest parts that indicate significant coarsening/dissolution of γ', but also suggest that such changes occur rapidly after short times, and then produce terminal microstructures that remain fairly

stable at 3000 – 22,000 h. Changes in bulk microstructure and surface oxidation suggest that actual valve temperatures are higher than the 1400°F design temperatures. Comparison of valves with aged specimens of Pyromet 31V are underway to better establish the valve temperatures.

ORNL and TRW began and are defining a collaborative program to explore alternate processing and alternate alloys with more stable microstructures for upgraded performance relative to standard Pyromet 31V. Together with valve design changes, the ultimate goal of this project is to provide exhaust valves with more temperature capability and reliability for engine-testing.

ORNL and SF&E have begun a collaborative program with Waukesha to identify and test exhaust component alloys with more temperature capability and creep strength than standard Ni-resist cast iron. The new CF8C-Plus cast stainless steel shows much more oxidation and creep-rupture strength than Ni-resist cast iron at 750-850oC. The first casting trial to make exhaust components with CF8C-Plus were successful, and machining and assessment of the suitability of those components for engine-testing for direct comparison of performance with Ni-resist is currently underway, and will continue in FY2006.

References

1. N.D. Evans, P.J. Maziasz, and J.J. Truhan, "Phase Transformations During Service Aging of Nickel Based Superalloy Pyromet 31V," to be published in Proc. Solid-Solid Phase Transformations in Inorganic Materials 2005 (held 29 May – 3 June, 2005, Phoenix, AZ), TMS, Warrendale, PA (2005).
2. S.K. Schaefer, J.M. Larson, L.F. Jenkins, and Y. Wang, "Evolution of Heavy Duty Engine Valves – Materials and Design," in Conf. Proc. Valvetrain System Design and Materials, ASM-International, Materials Park, OH (1997) pp. 129-139.
3. J.P. Shingledecker, P.J. Maziasz, N.D. Evans, and M.J. Pollard, "Alloy Additions for Improved Creep-Rupture Properties of a Cast Austenitic Stainless Alloy," in Conf. Proc. Creep Deformation and Fracture, Design, and Life Extension, TMS, Warrendale, PA (2005), pp. 129-138.

FY2005 Awards/Patents

None

FY 2005 Publications/Presentations

1. J.P. Shingledecker, P.J. Maziasz, N.D. Evans, and M.J. Pollard, "Creep Behavior of a New Cast Austenitic Alloy," in Proc. ECCC Conference on Creep and Fracture in High Temperature Components – Design and Life Assessment Issues, Eds. I.A. Shibli, S.R. Holdsworth, and G. Merckling, DEStech Publishing, Inc., Lancaster, PA (2005) pp. 99-109.
2. N.D. Evans, P.J. Maziasz, and J.J. Truhan, "Phase Transformations During Service Aging of Nickel Based Superalloy Pyromet 31V," to be published in Proc. Solid-Solid Phase Transformations in Inorganic Materials 2005 (held 29 May – 3 June, 2005, Phoenix, AZ), TMS, Warrendale, PA (2005).
3. J.P. Shingledecker, P.J. Maziasz, N.D. Evans, and M.J. Pollard, "Alloy Additions for Improved Creep-Rupture Properties of a Cast Austenitic Stainless Alloy," in Conf. Proc. Creep Deformation and Fracture, Design, and Life Extension, TMS, Warrendale, PA (2005), pp. 129-138.
4. P.J. Maziasz, "Update on ORNL/CAT CRADA on CF8C-Plus Cast Stainless Steel: Progress and Commercial Scale-Up in 2004/2005," invited talk, DOE FreedomCAR and Vehicular Technologies Review, March 2, 2005, Oak Ridge, TN.
5. J.P. Shingledecker, "Development, Properties and Application of CF8C-Plus," invited talk at MetalTek International, Inc., June 27, 2005, Waukesha, WI.
6. N.D. Evans, "Phase Transformations During Service Aging of Nickel Based Superalloy Pyromet 31V," presentation at TMS Conference on Solid-Solid Phase Transformations in Inorganic Materials 2005, May 29 – June 3, 2005, Phoenix, AZ.
7. J.P. Shingledecker, Creep Behavior of a New Cast Austenitic Alloy – CF8C-Plus," Invited Plenary Talk at ECCC Creep Conference, September 12-14, 2005, London, UK.
8. P.J. Maziasz, "Alloy Additions for Improved Creep-Rupture Properties of a Cast Austenitic Stainless Steel – CF8C-Plus with Cu, W," presentation at the Symposium on Creep Deformation and Fracture, Design, and Life Extension, MS&T'05, September 25-28, 2005, Pittsburgh, PA.

Acronyms

WED – Waukesha Engine - Dresser

SF&E – Stainless Foundry & Engineering

ORNL – Oak Ridge National Laboratory

LMP – Larson-Miller Parameter

TEM – transmission electron microscopy

SEM – scanning electron microscopy

2.3.2 Characterization and Development of Spark Plug Materials and Components

H. T. Lin,[*] R.K. Richards,[**] and M. P. Brady[*]
[*]*Metals and Ceramics Division*
[**]*Engineering Science & Technology Division*
Oak Ridge National Laboratory, Oak Ridge, TN 37831-6068
Phone: (865) 576-8857; Fax: (865) 574-6098; E-mail: linh@ornl.gov

DOE Technology Program Manager: Debbie Haught
Phone: (202) 586-2211; Fax: (202) 586-7114; E-mail: Debbie.haughtee.doe.gov
ORNL Technical Advisors: David Stinton and Tim Theiss
Phone: (865) 574-4556; Fax: (865) 241-0411; E-mail: stintondp@ornl.gov
Phone: (865) 946-1348; Fax: (865) 946-1248; E-mail: theisstj@ornl.gov

---

Objective

- Provide insight into wear mechanisms of spark plug electrodes as a function of field exposure time and engine conditions.
- Increase the wear resistance of spark plug electrode materials for advanced natural gas reciprocating engines to extend spark plug lifetime to at least 1 year while attaining engine emission and efficiency goals.

Approach

- Characterize engine tested spark plugs to identify key erosion mechanisms and limitations of existing materials.
- Develop and optimize new electrode materials for improved erosion resistance based on results from the characterization effort.

Accomplishments

- Optical spectroscopic and metallurgical analysis of spark plugs tested over a range of time, ignition system, and engine exposure conditions led to the identification of electrode oxidation and cracking mechanisms that control spark plug wear in natural gas engines.
- Incorporation of spectroscopic observations into a model of wear/erosion for aiding in the design of new materials.
- In collaboration with Federal Mogul (Champion®), multiple sets of natural gas engine spark plugs incorporating ORNL developmental electrode alloys designed to isolate key materials properties to provide a basis for improved spark plug lifetimes were manufactured for engine test evaluation.
- Design and procurement of advanced spark plug test chamber with high temperature/high pressure capability.

Future Directions

- Engine testing of spark plugs utilizing ORNL developmental electrode alloys.
- Evaluation of spark plugs in high temperature/high pressure test chamber under simulated NG environments.
- Optimization of developmental electrode alloys based on test chamber results and post-engine test spectroscopic and metallurgical characterization

Introduction

Natural gas (NG) reciprocating engine manufacturers have identified ignition systems as one of the key technologies to achieve cost/performance/emission characteristic goals for lean and stoichiometric engines. Spark plug erosion and subsequent failure have been identified as a major issue in long-term durability of natural gas ignition system. Current spark plug lifetimes are on the order of only ~2-6 months, which results in loss of performance and necessitates frequent, costly downtime maintenance for the plug replacement. Desired spark plug lifetimes for NG engine end users are on the order of at least 1 year. It has been recognized that as cylinder pressures, compression ratios, and ignition voltages are increased, and conditions further move towards leaner burning combustion, spark plug reliability and lifetime performance will become even more critical and could limit further advances in engine development. The goal of this effort is to identify the mechanisms of electrode wear and to design new electrode materials to improve the lifetime and reliability of NG spark plugs to meet the 1-year lifetime goal.

Approach

Microstructural and spectroscopic analysis of end-of life spark plugs from field-operated NG engines led to the identification of electrode wear phenomena driven by oxidation and cracking of the electrode material during engine operation. These findings were unexpected, as wear of spark plug electrodes is typically associated with loss of material due to sputtering, melting, ablation, and particle erosion phenomena during sparking. In FY 2005, optical spectroscopic and metallurgical investigations of field-tested NG reciprocating engine spark plugs were systematically pursued over a range of time, ignition system, and engine exposure conditions to determine the relative importance of the oxidation/cracking to electrode wear. Oxidation tests of conventional electrode materials were also carried out in conjunction with Federal Mogul and correlated with phenomena observed in field tested spark plugs. These studies have provided a basis to design new spark plug electrodes alloys for improved lifetimes. To pursue this, ORNL and Federal Mogul are teaming to manufacture and engine test conventional J-type spark plugs utilizing new electrode alloys.

Results

End of life spark plugs with ~6 months of field service in a NG engine showed extensive intergranular cracking and loss of material in the Pt-4W ground electrode insert tip and oxidation/cracking at the Ni-base ground electrode/Pt-4W interface (Fig. 1). This phenomena would significantly degrade the ignitability and performance of spark plugs, and is likely a key life-limiting step.

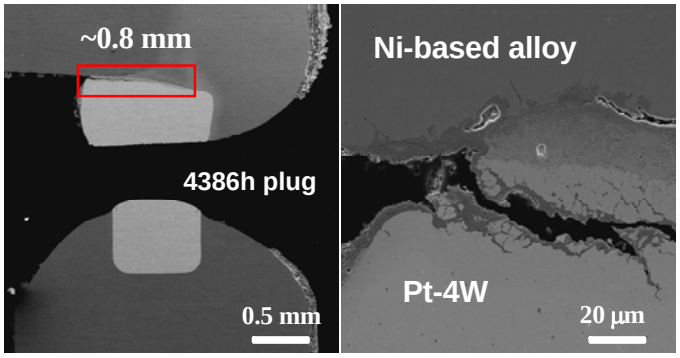

Figure 1 SEM microphotographs show crack initiation and oxidation were observed at Pt-alloy tip insert and Ni-based electrode interface after only a few days of engine operation

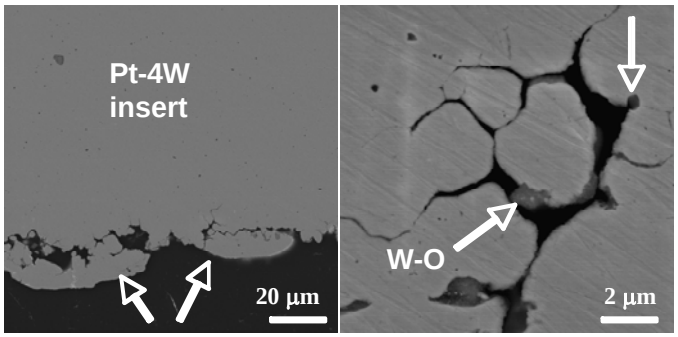

Figure 2 SEM microphotographs show substantial intergranular cracks were also observed in the Pt-W alloy electrode inserts after only a few days of field service. This cracking was found to result from internal oxidation of W additions made to the Pt

In collaboration with GTI, a series of spark plugs were run in a Cummins natural gas engine and removed after short-time intervals to gain insight into the onset of the degradation phenomena observed in end-of-life plugs. Analysis of spark plugs tested for 108 and 188 h showed oxidation/crack initiation at the Ni alloy ground electrode/Pt-4W insert interface, and intergranular cracking in both of the Pt-4W ground electrode and Ir

center electrode inserts (Fig. 2), similar to those observed in the end-of-life plugs. The extent of cracking/oxidation was less than that observed in the end-of-life spark plugs, and suggests that these degradation processes occur throughout the life of the plug.

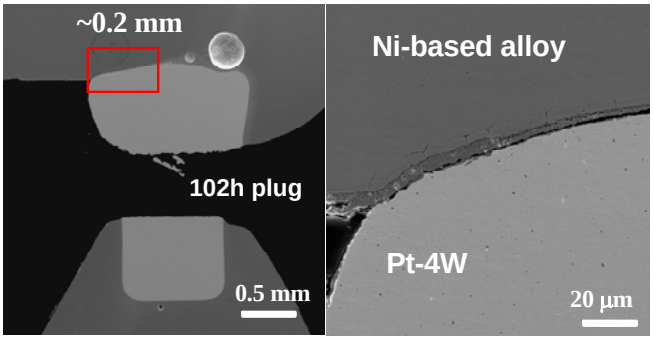

Figure 3 SEM microphotographs show extensive crack growth and oxidation at P*t-alloy tip insert and Ni-based electrode interface after 6-month lifetime.

Spectroscopic examination of the sparks produced from the 108 and 188 h plugs indicated a high level of calcium, which was also observed in end-of-life field-tested plugs. Metallurgical analysis of the oxides formed on Pt-4W and Ir electrode surfaces in engine tested plugs reveals Ni-Pt-O and Ni-Ir-O oxides, respectively, modified by elements including Ca, Zn, P, and S. Other elements from the Ni electrode alloys, particularly Cr, Mn, and Si have also been detected. The source of the Ca, Zn, P, and S is likely the lubricant used for NG engines. Although the electrode wear appears to result primarily from the intergranular attack of the Pt-4W electrode insert tips and the oxidation/cracking at the Ni alloy electrode/Pt-4W interface, introduction of Ca (known as glass modifiers) could significantly decrease the softening temperature and viscosity of the oxide phases, possibly further accelerating the wear of the electrode.

In collaboration with Federal Mogul, laboratory gasoline engine tests and simple oxidation exposures were conducted on a range of currently used, commercially produced Ni alloy electrodes and Pt alloy inserts. Despite the different engine and ignition conditions, the laboratory engine tested spark plugs all showed similar degradation phenomena to the field tested NG spark plugs, i.e., intergranular attack of the Pt insert alloys and cracking at the Ni alloy electrode/Pt alloy interface. These results indicate that fundamental materials related issues play a significant role in defining spark plug electrode durability.

Air oxidation tests indicated that the currently used Ni alloy electrodes were generally found to be susceptible to internal attack, due to inadequate levels of protective scale-forming elements. Intergranular attack in the Pt alloy inserts was linked to additions made to reduce breakdown voltage and/or improve manufacturability. In particular, cracking was associated with internal oxidation of W additions at Pt grain boundaries in Pt-4W alloys, and subsequent volatilization of W-oxides. The presence of W-oxide in the regions on intergranular attack in Pt-4W insert alloys was confirmed in the 108 h NG tested spark plug (Fig. 3).

Figure 4 Photo shows the conventional J-type natural gas engine spark plugs incorporating ORNL developmental alloys.

The observed cracking/oxidation wear mechanisms establish a basis to develop new electrode alloy materials to extend spark plug lifetimes. To pursue this, ORNL and Federal Mogul are teaming to manufacture and NG engine test the conventional J-type spark plugs utilizing new electrode alloys. Three sets of spark plugs are planned for the initial series of evaluations. The 1st set will use developmental alloys with improved oxidation resistance in the engine environments and will be tested without precious metal inserts to establish baseline behavior. The 2nd set of plugs will utilize a control, standard Pt-alloy precious metal insert with oxidation-resistant developmental electrode alloys selected for greater thermophysical compatibility with the Pt alloy to mitigate cracking at the electrode alloy/Pt insert interface. The 3rd set will utilize developmental high-melting point alloys of high corrosion resistance in place

of Pt alloys for the electrode insert tip to evaluate the potential to prevent the material loss by intergranular cracking observed for the Pt alloys. In FY05, the first set of plugs were manufactured and included sixty-five spark plugs, incorporating 5 ORNL developmental alloys, 3 control Champion® alloys, and replicates were manufactured (Fig. 4). Engine testing and post-test spectroscopic and microstructural characterization of the developmental spark plugs will be pursued in FY 2006.

Spectroscopy

Using a pressurized test chamber, sets of plugs were analyzed for impurities using spectroscopic line emissions. A comparison between a new and used plug is illustrated in Fig. 5. The spectral data is used to identify line radiation from components in the arc such as the working gas (i.e., an air mixture of nitrogen and oxygen) and material being removed from the spark plug tip. For new plugs large quantities of nickel are observed due to sputtering. For used plugs large quantities of calcium and reduced quantities of nickel are observed. No spectral lines from the electrode insert alloys can be found, and this includes iridium, platinum, and tungsten. The absence of these materials in the spectrum would indicate that they are not eroding in a standard way such as sputtering or evaporation.

Fig. 6 summarizes the spectroscopic analysis of the time history of the used spark plug sets. Results show that the impurities reach an equilibrium value after a very short time in the engine.

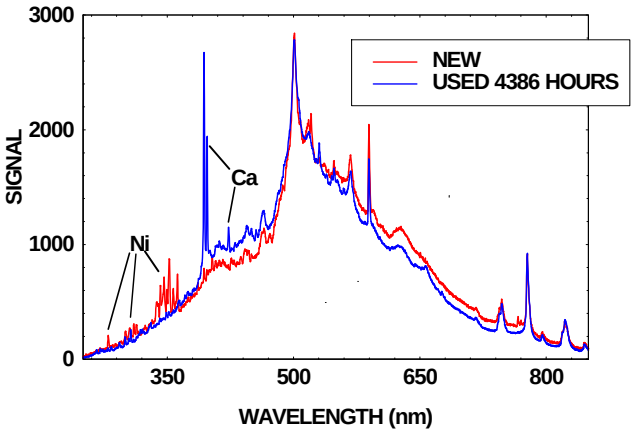

Figure 5. Spectroscopic data showing a comparison between a new and used spark plug. Spectral lines from nitrogen, oxygen, calcium, nickel and iron can be identified. Noticeably missing are lines from the electrode tip inserts; iridium, platinum and tungsten.

Conclusions

Extensive optical spectroscopic and metallurgical investigation of field-tested NG reciprocating engine spark plugs indicated the presence of several unexpected failure modes of the spark plug electrodes, which somewhat defies conventional wisdom regarding spark plug degradation. Key degradation modes were intergranular cracking of the Pt alloy inserts, and extensive oxidation and cracking at the Ni alloy/Pt alloy insert interface. The Ni alloy electrodes were generally found to be susceptible to internal attack, due to inadequate levels of protective scale-forming elements. Intergranular attack in the Pt alloy inserts was linked to additions made to improve manufacturability and reduce breakdown voltage. The results are being used to design new alloys for spark plug electrodes for improved lifetimes in collaboration with Federal-Mogul.

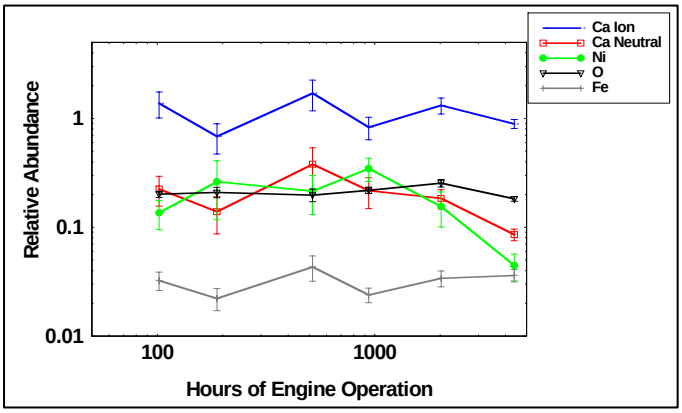

Figure 6 Summary of the spectroscopic analysis of the spark plug sets with different hours of use. Note that the values remain relatively constant after a short time in the engine.

FY 2005 Honors/Awards/Patents

1. M. P. Brady named to Advisory Board of the new journal *Trends in Corrosion Research.*
2. M.P. Brady and H.T Lin, "Erosion Resistant Materials for Spark Plug Electrodes", submitted to United State Patent Office Feb. 2005.

FY2005 Publications/Presentations

Publications:

1. H. T. Lin, M. P. Brady, R. K. Richards, and D. M.

Layton "Characterization of Erosion and Failure Processes of Spark Plugs After Field Service in Natural Gas Engines," Wear Vol. 259/7-12 pp. 1063-1067 (2005).

2. R. K. Richards, D. M. Layton, H. T. Lin, and M. P. Brady, "Characterization of Erosion Mechanisms for Natural Gas Engine Spark Plugs," ICEF2004-875 published at Proceedings of Internal Combustion Engine Division of ASME 2004 Fall Technical Conference, October 24-27, 2004, Long Beach, CA

Presentations:

1. R. K. Richards, D. M. Layton, H. T. Lin, and M. P. Brady, "Characterization of Erosion Mechanisms for Natural Gas Engine Spark Plugs," presented at the Internal Combustion Engine Division of ASME 2004 Fall Technical Conference, October 24-27, 2004, Long Beach, CA.
2. R. K. Richards, H.T Lin, M.P. Brady, "Identification of Spark Plug Erosion Mechanisms", presented at the 2nd Annual Advanced Stationary Reciprocating Engines Conference- Moving Forward in Low Emissions and High Efficiency Technologies, March 15 – 16, 2005, South Coast Air Quality Management District Headquarters Diamond Bar, California
3. H. T. Lin, M. P. Brady, R. K. Richards, and D. M. Layton "Characterization of Erosion and Failure Processes of Spark Plugs After Field Service in Natural Gas Engines," presented at the 15th International Conference on Wear of Materials, April 24-28, San Diego, CA.
4. L R Walker, H T Lin, I Levina,* M. Brady, J. Lykowski,* "SEM and EPMA Analysis of Spark Plug Electrode Erosion", presented at Microscopy & Microanalysis 2005, July 31-August 4, 2005, Honolulu, Hawaii. * Federal Mogul (Champion®)

2.3.3 Optimization of In-Cylinder Materials for Reciprocating Natural Gas Engines

J. J. Truhan and K. L. More
Metals and Ceramics Division
Oak Ridge National Laboratory, Oak Ridge, TN 37831-6063
Phone: (865) 574-1057, E-mail: truhanjjjr@ornl.gov

DOE Technology Development Manager: Debbie Haught
(202) 586-2211; (202) 586-7114 (fax); e-mail: debbie.haught@ee.doe.gov
ORNL Technical Advisor: Karren L. More
(865) 574-7788; (865) 576-5413 (fax); e-mailmorekl1@ornl.gov

Objectives
- Identify materials issues and approaches in natural gas-fired reciprocating engines to achieve lower friction and wear to improve mechanical efficiency and durability.
- Treat the power cylinder as a system to achieve better performance. This includes the lubricant in addition to the materials of construction
- Better identify the engine operating environment for more effective materials recommendations
- Better match advanced materials with advanced lubricants to optimize in-cylinder performance.

Approach
In collaboration with Waukesha Engine - Dresser (WED), a two-step approach is being taken:
- Characterize the engine and identify new materials, surface treatments and lubrication formulations that improve engine performance and durability.
- Develop a strategy to prevent or minimize deposit formation on engine components (valves, guides, seats). The initial phase is to develop a test method to determine precursors to deposit formation and to investigate the use of self-lubricated materials.

Accomplishments
- Completed characterization of deposit formation on intake valves taken from field engines. Results indicated higher than expected operating temperatures leading to metal attack.
- Developed a test method by which the amount of decomposition products known as sludge in the lubricating oil can be quantified. Sludge formation is a precursor to eventual oil deposit formation on valves and rings.

Future Directions
- Conduct additional engine tests with WED to determine the effect of oil condition on deposit formation. Oil condition will be controlled by the oil additive package and level of on-engine filtration
- Conducts tests of "self-lubricated" valve guides to minimize lubricant migration.
- Coordinate with NTRC/GTI project to develop oil additive packages friendly to the exhaust catalyst by testing the tribological behavior of new candidate formulations.
- Extend the examination of in-cylinder materials to consider advanced ring and liner materials compatible with advanced lubricants.

Introduction

In order to achieve optimum performance of natural gas reciprocating engines in terms of efficiency and durability at comparable or lower cost, it will require the integration of research on materials and processes development, lubricant formulation, surface characterization and extensive rig and engine testing. The approach of this effort is to define the operating environment, identify desired materials properties, select materials and/or processes to meet these requirements and to characterize the compatibility of materials with common lubricants in the new and used condition by use of advanced surface analytical techniques. This includes impact of lubrication on components, such as deposit formation or exhaust catalyst poisoning.

Approach

The issue of oil deposits was of immediate concern for WED, thus, two general approaches were taken to address the problem. First was a thorough characterization as to the nature and effect that deposits had on performance, specifically intake valves. The second was a plan to avoid the formation of deposits in the first place. This included the specification of suitable lubricants and on-engine filtration to control the lubricant chemistry. To this end, it was necessary to develop a method by which the organic precursors to oil deposits could be quantified in the oil. Minimizing the migration of lubricants through the use of self lubricating materials such as carbon or graphite foams for bearing surfaces is also being investigated.

Results

Intake valves from natural gas-fired reciprocating engines displaying "torching" were examined to determine their failure mechanism. The principal features of the "torched" valves include a relatively thick black deposit on the tulip area of the valve extending to the sealing surface, partial loss of those deposits in various locations, and localized metal loss, oxidation and/or surface cracking in the spalled regions (Figure 1). Electron probe microanalysis, scanning electron microscopy, and optical microscopy were employed to characterize the deposit formation and metal loss mechanisms. The initial cause of the torching was likely due to the localized spallation of a loosely adherent (Ca,Zn) phosphate oil deposit adjacent to the valve/seat seal which created a channel of hot, high velocity combustion gases. Within the torched area, significant metal oxidation and metal recession due to erosion/corrosion was observed on the valve sealing face, creating a relatively wide gap where a valve/seat seal should be (Figure 2). In areas where torching was not evident on the valve sealing surface, no appreciable metal recession (but limited metal oxidation) was observed.

Figure 1. Overall view of a torched intake valve (7000 h engine test) showing the partial spallation of a heavy oil deposit.

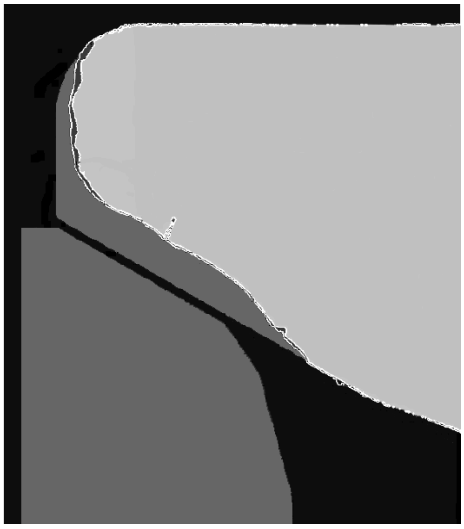

Figure 2. Cross section of a torched valve (7000 h) showing about 1 mm metal recession due to erosion, oil deposits, metal oxidation and surface cracking. The degree of recession is shown by the original (dark gray) profile.

Temperature measurements were carried out using fluorescence thermography directed at several locations on an intake valve in an operating engine.

This technique employs a temperature-sensitive phosphor coating on a valve in the region of interest. A fiber optic probe records the duration of fluorescence produced by activation of the phosphor with a high power light emitting diode. The duration of the emission is then related to the temperature.

Fluorescence thermography readings for engines running from idle to 110% of rated conditions recorded temperatures ranging from approximately 260 to 350^{o} C. These temperatures are high enough to oxidize the lubricant base stock, leaving behind the inorganic additive ash as deposits. These measurements were taken prior to any oil deposition and subsequent torching. If improper sealing of the valves allow hot combustion gases past the seal, substantially higher surface temperatures can result.

Deposit formation can result if precursor decomposition products are not removed through filtration and are allowed to build up in the oil. These precursors, colloquially referred to as sludge, are not detected in conventional oil analysis. A method by which the concentration of sludge can be determined would assist the engine operator in choosing more effective lubricants and filtration products and setting the optimum service intervals to avoid deposit formation in the first place.

A method was developed in FY05 which adapted a standard soot concentration measurement using thermogravimetric analysis (TGA) for diesel engine oil [1]. By monitoring the first derivative of the TGA curve, it was observed that a transition existed from the light volatiles to the medium to heavy volatiles at about 550^{o} C. The remaining weight, in percent, is linear with respect to engine running time as seen if Figure 3. The weight remaining for a new oil (t=0) corresponds to the ash content of the additive package. The amount of sludge in the oil is determined by subtracting this initial weight from the total weight remaining. As would be expected, the increasing amount of sludge in the oil has the effect of increasing the viscosity. Figure 4 illustrates this strong correlation. Although not shown here, the sludge concentration can be linked to the enhanced oxidation and nitration levels in the oil as measured in conventional oil analysis.

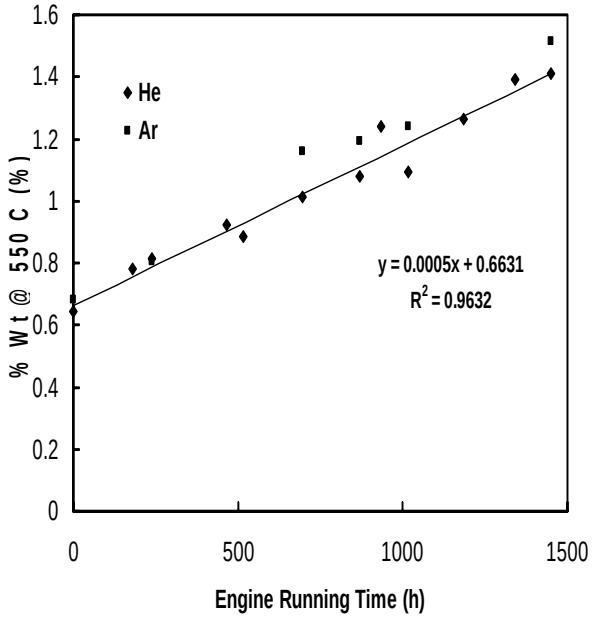

Figure 3. The relationship between the concentration of sludge and engine running time.

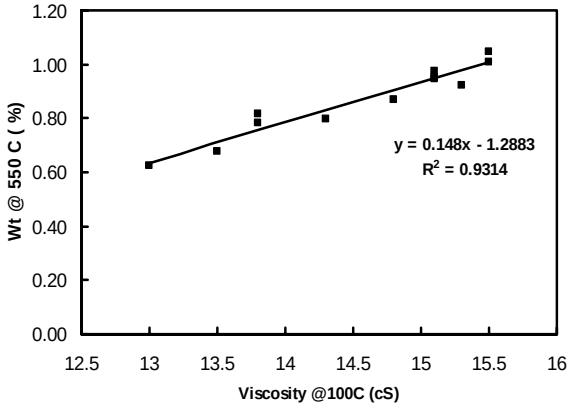

Figure 4. The correlation between the sludge concentration and oil viscosity

Conclusions

- Temperature measurements indicated higher than expected operating temperatures leading to accelerated thermal aging, metal oxidation and metal recession.
- Materials with higher temperature capabilities will be required in these engines.
- Higher operating temperatures also accelerated lubricant degradation including oxidation and nitration.
- Oil deposits found on the valve sealing surfaces were a loosely adherent coating of oxides and

phosphates of Ca and Zn which originated from the oil additive package.

- Lubricant decomposition products can act as precursors to in-cylinder deposits, however they may be removed by the filtration system.
- A test has been developed to quantify the concentration of the lubricant decomposition products allowing for an early warning of lubricant failure.

References

1. ASTM Method D5967-04 Annex 4

Awards/Patents

None

Publications/Presentations

1. "The Erosion-Corrosion of Intake Valve Sealing Surfaces due to the Formation of Lubricating Oil Deposits," J. J. Truhan, K. L. More, and R. Rangarajan, Proceedings of the World Tribology Congress III, Paper No. WTC2005-64227, Washington D.C., Sept, 2005.

2. Program update to WED, June 28, 2005

Acronyms

WED- Waukesha Engine - Dresser
TGA- Thermogravimetric analysis

2.4.1 Ancillary Services Offered by DE Systems

John Kueck , Tom Rizy, Burak Ozpineci, Leon Tolbert
Engineering Science and Technology Division
Oak Ridge National Laboratory
Oak Ridge, TN 37932-6070
(865) 574-5178, email; kueckjd@ornl.gov
(865) 574-5203, email: rizydt@ornl.gov

Debbie Haught, DOE Program Manager
(202) 586-2211, email: debbie.haught@ee.doe.gov

Objectives

- Evaluate the economic and engineering feasibility of supplying reactive power locally from distributed energy resources (DE) to regulate local voltage and control power factor to improve the efficiency and reliability of the utility distribution system.
- Determine if reactive power can be supplied from local DE sources with independent voltage control so that an expensive hierarchical control and communications system is not required.
- Address the key barriers to the local supply of reactive power so that it may be supplied without requiring the local utility to either modify the existing distribution system or perform engineering analysis of the circuit.
- Evaluate the incremental costs and potential benefits of distributed energy as a source of reactive power in the electric transmission & distribution power grid. Evaluate economically viable ancillary services from DER.

Approach

- Establish a reactive power laboratory with both generator and inverter-based DE technologies to test individual and multiple reactive power producing DE.
- Use the ORNL campus distribution system to demonstrate that several reactive power producing DE devices can operate in close electrical proximity to regulate voltage or net power factor without extensive communications and control.
- Use a mathematical programming platform (Matlab/Simulink) and real-time controller (dSpace software and controller) to implement various control algorithms and strategies for feedback control.
- Use commercial power system analysis software (SKM and ETAP) to model the performance of the DE in controlling voltage and net power factor and evaluate local control methods.
- Demonstrate that DE inverter designs with local control can be developed and packaged to economically supply adequate reactive power levels to satisfy utility and user needs.
- Conduct an economic assessment of distributed energy as a source of reactive power. Identify potential market value based on available information and conduct a limited number of case studies using specific utility information. The approach has focused on the incremental cost of incorporating reactive power into distributed energy versus the additional ancillary benefit of having this capability such as supporting distribution voltage or regulating local power factor dynamically.

Accomplishments

- A unique and first-of-its kind R&D laboratory for evaluating reactive power from DE has been established at the Oak Ridge National Laboratory. The Reactive Power Laboratory is capable of testing both rotating-based (generators, motors) and static-based (inverters) reactive power producing DE.
- A 300kVar Synchronous Condenser (250hp synchronous motor unloaded and overexcited) is operational at the laboratory for evaluating the local control of rotating-based DE with an actual distribution system. The synchronous condenser interfaces with a 2.4kV distribution circuit of the ORNL distribution system through a 480V/1000A power panel. The operation of the synchronous condenser met a milestone of injecting reactive power into the distribution system in May 2005. The synchronous condenser regulates

the line voltage and net power factor of the local circuit by varying its reactive power output. ***AOP Milestone 4.2.14.***

- A test of the synchronous condenser was performed during the summer with the device providing a maximum of 311kVar of reactive power. The operation of the synchronous condenser was monitored locally with instrumentation at the laboratory and with a distribution system wide monitoring system ("PowerNet"). The local monitoring captured local voltages, currents and power while the PowerNet captured voltages, currents and power at the substation and circuit level.
- A commercial power system analysis software and steady state model of the ORNL distribution system utilizing input data from the tests was used to model the voltage and current changes on the distribution system. The model results at the device location agree well with the actual data taken during the testing although the feeder and substation data have poor agreement.
- The capability of testing 3-phase inverters for producing reactive power from DE has been established at the Reactive Power Laboratory. The laboratory has the capability to test 75, 150 and 300A inverters off the grid using resistive and reactive load banks and to test them interfaced with the ORNL distribution system through a 480V/600A distribution panel that interfaces with a second 2.4kV circuit fed from the 3000 substation at ORNL.
- A Matlab/Simulink Software Platform and dSpace Real-Time Control Hardware and Software provide a versatile programming environment for developing and testing various control algorithms and schemes for the reactive power producing DE in the Reactive Power Laboratory. AOP Milestone 2.4.1.A report has been completed that assesses the viability of using Distributed Energy systems to provide different ancillary services. Ancillary services may create additional value streams for DE systems to improve the economical viability of installing these systems. A market for unbundled services would promote further installation of DG where costs could not be justified purely on real power generation. Power electronics offer significant potential to facilitate the use of DG in this application. ***AOP Milestone 2.4.1b.***
- A report entitled "Power Electronics for Distributed Energy Systems and Transmission & Distribution Applications" is complete. This report evaluates the R&D needs for DE systems and T&D applications including materials development, integration of multiple DE devices and provides recommendations for Power Electronics research and development activities. ***AOP Milestone 2.4.2***.
- The phase I report[2] on the potential economic viability of incorporating reactive power into distributed energy was completed and its results were presented to the industry partners and team at the Reactive Power Project Meeting on September 29th at ORNL in Oak Ridge. The next phase of the report will be to incorporate feedback from the industry partners. ***AOP Milestone 5.1***.

Future Direction

- Develop automated feedback control schemes for both the synchronous condenser and inverters for varying reactive power output based on local voltage
- Determine how to better model the voltage, current and power changes due to reactive power producing DE at the circuit and substation levels. These include expanding the model capabilities to cover unbalanced loading, voltage sensitive loads, and real-time loading changes.
- Develop a cost goal for the local supply of reactive power from DE so that inverter and synchronous generator/condenser based DE can be evaluated to determine at what cost level it would be competitive with conventional reactive power compensation, such as feeder-level shunt capacitor based regulation.
- Operate multiple DE in parallel to evaluate interaction with multiple devices, prove control concept and develop engineering guidelines for DE application in providing voltage regulation and net power factor regulation.
- Move the concept of reactive power producing DE from the laboratory to the field environment by working with our partners, such as Southern California Edison's and their distribution circuit of the future, to implement the concept to a much larger extent (provide all of the local reactive power) on a utility distribution system.

[2] Evaluation of Distributed Generation as a Source of Reactive Power Supply, prepared for Oak Ridge National Laboratory by Energetics, Inc., draft report, June 17, 2005.

Abstract
The Reactive Power Laboratory is a new and unique first-of-its kind R&D facility for testing reactive power producing distributed energy resources (DE). Reactive power doesn't perform work like real power, but it is necessary for energizing inductive and capacitive loads and for supporting voltage and preventing voltage collapse. Reactive power occurs when reactive loads (capacitors or inductors) are present and voltage and current are out of phase. When reactive power is present, current either lags (when reactive power is being consumed) or leads (when reactive power is being produced) the voltage. Real (or active) power, which does work, is only present when voltage and current are in phase. However, when voltage and current are out of phase, greater overall power capacity (due to the vector sum of real and reactive power) is needed to get the same level of real power and do the same level of work. The laboratory is exploring the use of both rotating (generators, motors) and static-based (inverters) Distributed Energy (DE) technologies for producing reactive power for supporting voltage and correcting power factor both locally and on the campus distribution system.

The goal of the laboratory is to work with the power industry, manufacturers, and universities in developing local control for producing reactive power from reciprocating engines, microturbines and fuel cells using synchronous generators and inverters. The first part of the laboratory is fully operational with the installation, operation and testing of a 300kVar synchronous condenser (250hp synchronous motor operated unloaded and overexcited). The second part of the laboratory is the inverter testing area which currently is capable of testing an inverter off the grid using resistive and reactive load banks or interfacing with the ORNL distribution system via a 480V/600A distribution panel to a 750kVA transformer connected to a circuit from the 3000 substation. Three different ratings of three-phase programmable inverters (75, 150 and 300A) will be configured and tested.

Tests of the 300kVar synchronous condenser (SC) were conducted on May 24th and July 1st. These results provide some preliminary information on the startup, operational and response characteristics of the SC and its ability to support local and substation voltages. Also, the test data was used as input to the model analysis. The model analysis provides an evaluation of commercial power system software performance in modeling the benefits of reactive power production for distribution systems. The testing and modeling results are important for developing a feedback control system for the SC.

Introduction
Alternating Current (AC) is supplied in a 60Hz waveform. Reactive power is produced when the current waveform is out of phase with the voltage waveform due to inductive or capacitive loads. Current lags voltage with an inductive load, and leads voltage with a capacitive load. Only the component of current in phase with voltage produces real power which does work. Current is in phase with voltage for a resistive load, like an incandescent light bulb. Reactive Power is necessary for producing the electric and magnetic fields in capacitors and inductors.

The additional current flow associated with reactive power can cause increased losses, excessive voltage sags, and increased power capacity requirements. Transmission system operators have to ensure that reactive reserves are available to handle system contingencies such as the loss of a generator or transmission line because increased current flows after the occurrence of these types of contingencies can produce greatly increased reactive power absorption in transmission lines. Some transmission system operators are now considering new rules for distribution systems which require a minimum allowable power factor. These minimum power factors could reduce the amount of reactive reserves that the system operator would have to provide. Distributed Energy Resources (DE) could be ideally suited for providing reactive reserves in the distribution system.

DE, includes such resources as microturbines, reciprocating engine generators, and fuel cells. DE is often installed at or near electrical loads for local power and to take advantage of CHP or cooling, heating and power benefits that come from waste heat recovery of DE by thermally-activated technologies. With the right control scheme and algorithms, DE could be controlled to supply local reactive power and to regulate local voltage. Some DE devices contain synchronous generators, which can be directly connected to the local power system, and some, such as fuel cells or microturbines, must be interfaced to the local power system through an inverter because they produce DC or

high-frequency AC that must be converted to 60Hz AC. Similar to a synchronous generator, the inverter can also be designed and controlled to "inject" reactive power locally and regulate voltage. Thus, a DE with a synchronous condenser or inverter could supply reactive reserves.

The Oak Ridge National Laboratory (ORNL) has established the Reactive Power Laboratory which is a new and unique first-of-its kind laboratory for studying reactive power supplied from DE. ORNL is unique in that it owns and operates its own electric distribution utility for the laboratory campus, and can configure the distribution system to provide optimum opportunities for testing of reactive power injection effects from the laboratory. The ORNL distribution system is directly fed by the TVA 161kV backbone transmission system. The reactive power laboratory and project is also unique in that the tests are designed by representatives from the electric utility industry and DE manufacturers to address the actual challenges faced by DE and utilities currently and in the future.

The testing to date at the Reactive Power Laboratory has focused on four aspects: 1) characterization of the synchronous condenser; 2) development of the instrumentation scheme for measuring the necessary voltage, current and power readings at the synchronous condenser and on the distribution system; 3) development of algorithms for analyzing data measurements from the various test runs; and 4) validation of a steady-state model for the synchronous condenser via the use of a commercial software package to study its effects on the ORNL 13.8/2.4kV distribution network.

The Reactive Power Project has the overall goal of developing methods of incorporating distributed energy (DE) that can produce reactive power locally and for injecting into the distribution system. The objective for this new type of DE is to be able to provide voltage regulation and dynamic reactive power reserves without the use of extensive communication and control systems.

Reactive Power Laboratory

The "Reactive Power" Laboratory has been established for studying reactive power supplied from both rotating and static-based DE. The electrical design and layout of the Reactive Power Laboratory is shown in Figures 1 and 2. Figure 1 shows the laboratory's interface with the ORNL distribution system while figure 2 shows the layout at the laboratory itself. The laboratory is located at the north end of the Oak Ridge National Laboratory campus at building 3114. The test areas of the laboratory are in the building while the transformers and load banks are just to the east of the building. The laboratory equipment interfaces to the ORNL distribution system through two different distribution circuits (#4 and #2 fed from ORNL's 13.8/2.4kV Distribution Substation 3000). The rotating-based DE of the laboratory, which current includes a 300kVar synchronous condenser (250hp synchronous motor unloaded and overexcited) is fed from circuit #4. The static-based DE of the laboratory, which current includes a 75A 3-phase inverter is fed from circuit #2. The synchronous condenser portion of the laboratory is fully operational and testing began in May 2005. The inverter-portion of the Laboratory is nearly operational with the goal of injecting reactive power from an inverter in early FY06. The first run of the 75A rated inverter in the off-grid operation occurred on September 28th.

The laboratory includes the following equipment:

- 250hp synchronous motor for use as a synchronous condenser
- 75A, 150A, and 300A programmable inverters
- Two 750kVA 2.4kV/480V pad-mount transformers for interfacing to circuits #4 and circuit #2 of the ORNL 13.8/2.4kV distribution network at the 3000 Substation
- 480V/900A three-phase electrical panel configuration for the 250HP synchronous condenser interface (via a 540A motor starter) to the ORNL 2.4kV distribution circuit #4
- 480V/600A three-phase electrical panel configuration for the inverter interface to ORNL 2.4kV distribution circuit #2
- 2 Dranetz/BMI PowerGuide 4400 Meters; one located at the motor/starter and the second at the electrical panel.
- 1 Yokogawa WT3000 Digital Power Meter
- Danfysik Ultrastab 866 Current Transducer System
- Matlab/Simulink and Real-Time Workshop software
- dSpace real-time control hardware and software
- 150kW dc power supply for the programmable inverters
- 6.6kW dc power supply for excitation of the synchronous condenser
- 500kW resistive load with remote control375kVAr inductive load with remote control

- 75HP Induction Motor for dynamic characterization of the synchronous motor

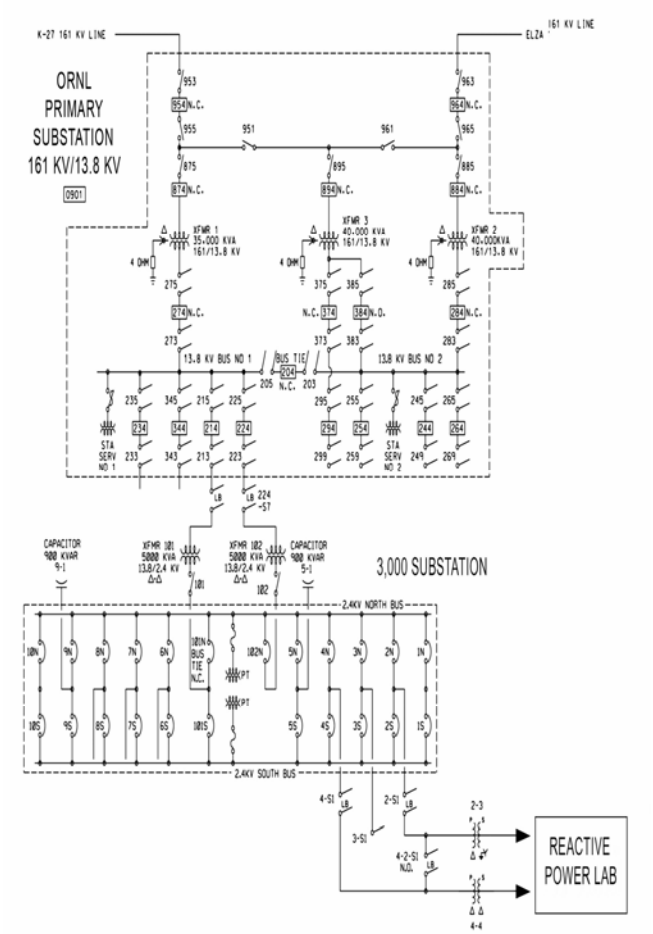

Figure 6. Reactive Power Laboratory Interface with the ORNL Distribution System.

Important capabilities of the laboratory include:

Testing Areas: The laboratory provides testing capability of rotating (generator or motor) and static (inverter) based DE. Also, the laboratory has the capability to test vendor provided reactive power producing DE, such as a microturbine or reciprocating engine.

Distribution Interface: The laboratory interfaces at two different electrical locations on the ORNL distribution system. This provides the capability to test single or multiple reactive power producing DE and also their interaction.

Substation: The reactive power compensation at the substation can be relaxed to provide a more severe testing scenario for the reactive power laboratory. Shunt capacitor banks at the substation provide power factor correction for the ORNL distribution system. The reactive power compensation can be relaxed by switching out some of these capacitor banks. Presently, the substation has 900kVar of reactive power compensation in capacitor banks in units of 150kVar.

Distribution and Power System: The laboratory interfaces with the TVA grid through the ORNL distribution system. The TVA feeders provide power at 161kV and it is stepped down to 13.8kV at ORNL's primary substation (X-10 substation). The secondary substations, such as the 3000 substations which provides the electrical interface for the laboratory, steps it down further to 2.4kV. Our ownership of the distribution system allows the capability to vary loading and reconfigure the distribution feeder circuits for testing different operating scenarios for the Reactive Power Laboratory.

Figure 7. Reactive Power Laboratory Layout

Tests Results at Laboratory
Some initial results of testing the synchronous condenser (SC) at the Reactive Power Laboratory include:

- The SC injected 311kVAr of reactive power at 370A of line current during the test conducted on July 1st, 2005 and shows great potential for use as a source of reactive power for voltage support. The line voltage during the test was regulated on average from 478V to 491V. Additional tests with new circuit configurations (more load, large dynamic motors and higher path impedance with an increased circuit length to the substation) and adjustments in SC location relative to other loads on the circuit are needed to better demonstrate its positive effects on the voltage support of a distribution system with higher path impedances and additional loads.
- The synchronization time of the SC can be minimized by immediately setting the DC field voltage and current such that the SC is operating at unity power factor immediately after the SC is started. Failure to do so may cause the SC to unnecessarily produce high currents and draw large amounts of reactive power before it begins to supply reactive power to the network. This situation becomes extremely important in cases where there is an immediate demand for reactive power such as the prevention of voltage collapse and the SC is not synchronized. Normally, the line current of the SC decreases as excitation is applied after startup and excitation current is between 3.5 to 4.5A. We found that one out of every five times when the SC is started and not immediately set to unity power factor (by applying 85 to 90V of excitation) that the SC doesn't synchronize until the minimal excitation level (about 4A) is reached. As a result the current instead of being around 200A after it is started can be closer to 400A.
- The excitation and losses of the SC (percentage of real power needed to spin the SC divided by the KVA capacity of the device) especially at lower than a 15% output level are significant making a strong case for an inverter-based reactive power producing DE. We found that the losses settle out to about 4% once the SC is operated at 50% and higher output.
- When considering the use of multiple SC units, the potential for circulating currents must be examined. It will be necessary to develop a voltage droop characteristic to ensure appropriate distribution of reactive power from each unit.
- Initial comparisons have shown that the simulation model based on the SKM commercial power system analysis software is fairly accurate except for the modeling of substation voltages and currents which can be affected by overall changes on the distribution system. For real-time power analysis, a much better estimation of the load distribution must be made. Furthermore, with a better estimation, future scenarios may be simulated before the actual tests are done to have an overall understanding of the system's behavior.

Economic Evaluation of DE as a Reactive Power Supply
An initial economic evaluation has been performed that considers the value of incorporating reactive power as an additional ancillary service for distributed energy. The effort compares conventional devices that can provide reactive power against distributed energy systems. Determination of reactive power payments was made through information gathering from various ISOs, and RTOs including PJM, NYISO, CAISO, ISO-NE, MISO, and ERCOT. However, a refinement of the approach considers incremental cost of incorporating reactive power producing capability with distributed energy.

The initial phase focuses on the cost effectiveness of rotating-based DE. The approach considers oversizing a generator for rotating-based DE to supply reactive power from these devices. By oversizing the power converter, a DE can provide the same level of real power as needed while at the same time has the ability to provide reactive power to correct power factor or regulate voltage. For comparison, the study effort has started to pull together generic capabilities and costs of conventional devices that can provide reactive power both at the transmission system level (typically 69kV and above) and distribution system level (typically below 69kV to 4kV) and end user voltage (480V and 240V). In order to achieve market acceptance, reactive power producing DE will need to compete with these technologies in terms of costs and benefits.

In terms of capability, DE can provide reactive power dynamically which adds a new and unique capability for responding to motor starts, pulse loads and other fast load events. Also, DE can relieve distribution capacity, reduce conductor losses and maintain tighter operating voltages by correcting power factor and regulating voltage locally at the loads. Although, capacitors can be

used along the feeder circuit or at the end-user load to perform this type of function, they can't perform at the same dynamic, variability or resolution capability. The difficulty is putting a proper value on these reactive power compensation capabilities. The cost per kVar ($/kVar) which is the incremental cost of supplying 1 kVar of reactive power is the capital cost metric for comparing the various devices. Basically for transmission level conventional devices, this cost ranges from approximately $40 to $100/kVar while for distribution level devices, this cost ranges from approximately $5 to $30/kVar. The cost benefit (revenue from reactive power payments minus the capital and maintenance costs) of reactive power producing DE must beat this metric to be considered as cost effective. Although currently reactive power producing DE cannot beat capacitor banks on a capital cost basis, they may in the future be able to compete based on their value of improving power system operations in return for reactive power payments for power factor correction or local voltage regulation. Much of this depends on reducing the cost of power conversion hardware for DE and a developing reactive power supply market from local devices.

The results of the initial phase of this effort were presented at the Reactive Power Project Meeting on September 29th generating very useful feedback from our industry team members. For example, there was feedback on how reactive power producing DE can compare both economically and functionally with shunt capacitor banks. Shunt capacitor banks, which are typically used for compensating reactive power consumption of loads on distribution systems, are very commonly used because they are very cost effective in terms of capital costs. However, capacitor banks can require extensive maintenance especially due to their exposure to lightning at the top of utility poles. Also, it can be problematic finding failed capacitor banks and their maintenance can be expensive requiring crews and bucket trucks. Another shortcoming of capacitor banks is the fact that they usually are only one size at a location (typically sized as 300, 600, 900 or 1200kVAr) and thus don't have variable range as do reactive power producing DE and can not respond to dynamic loads.

The second phase of this effort is refinement of the initial report and incorporates comments from our industry team members that were solicited in September. The report needs to better define the market value of reactive power for the several case studies that have been selected. This next phase of the effort is also looking at the economics and technical requirements for oversizing an inverter for static-based DE. In addition, a new potential device for supplying reactive power is that of adjustable speed drives. They are quite numerous and one manufacturer has indicated that they can provide an adjustable speed drive capable of varying power factor correction; both leading and lagging power factor. The case studies are looking at a diversity of applications and industries such as a power distributor versus a power generation and transmission provider.

A future phase which isn't currently funded would be to gather more extensive and detailed information on the value of conventional reactive power supplying devices as well as their capital and maintenance costs. Capacitor banks cannot provide reactive power dynamically or respond in milliseconds to reactive power load shifts due to motors or other fast responding loads. Furthermore, additional case studies need to be performed to assess the variables affecting the potential value of dynamic reactive power from distributed energy. Also, system studies need to be conducted to determine how a significant penetration of reactive power producing DEs (such as 40% or greater of the reactive power needs of a distribution system) that are strategically placed could benefit overall power

grid reliability. The potential exists for reactive power producing DE to provide higher overall reliability and make the transmission system less vulnerable to voltage collapse. A value needs to be determined for this overall system benefit. Another part of this effort needs to consider how to reduce the cost of inverter technology to reduce the cost of inverter-based DE devices.

References

1. Reactive Power Laboratory: Synchronous Condenser Testing & Modeling Results, Interim Report, Oak Ridge National Laboratory, ORNL/TM-2005/174, August 22, 2005.

2. J. D. Kueck, B. J. Kirby, L. M. Tolbert, D. T. Rizy, "Voltage Regulation: Tapping Distributed Energy Resources," Public Utilities Fortnightly, vol. 142, no. 9, September 2004, pp. 47-51, http://www.pur.com/puftocs/sep04.cfm.

2.4.3 Development of Electrodes for NO_x and Ammonia Sensors

Timothy R. Armstrong (Primary Contact), Fred C. Montgomery, and David L. West
Oak Ridge National Laboratory
1 Bethel Valley Rd.
Oak Ridge, TN 37831-6064
Phone: (865) 574-7996; Fax: (865) 241-0112; E-mail: armstrongt@ornl.gov

DOE Technology Development Manager: Debbie Haught
Phone: (202) 586-2211; Fax: (202) 586-7114; E-mail: Debbie.Haught@ee.doe.gov
ORNL Technical Advisors: David Stinton and Tim Theiss
Phone: (865) 574-4556; Fax: (865) 241-0411; E-mail: stintondp@ornl.gov
Phone: (865) 946-1348; Fax: (865) 946-1248; E-mail: theisstj@ornl.gov

Objectives
- Develop NO_x sensors for remediation and monitoring of natural gas fired reciprocating engines.
- The sensors should have an operating temperature of 500–700 ^oC, and be able to measure NO_x concentrations from ~10–1500 ppm at oxygen levels from 5 to 20 vol%.
- Since "NO_x" refers to mixtures of NO and NO_2, it will be required to have sensors selective for either NO or NO_2, or able to measure "total NO_x" ([NO] + [NO_2]).

Approach
- Prototype sensing elements are fabricated by screen printing electrode layers onto oxygen-ion conducting (typically yttria stabilized zirconia (YSZ)) substrates.
- Elements are operated either in a "non-Nernstian" mode (where the output is a voltage) or under DC electrical bias.
- Characterize sensor in bench setting and in NG engine exhaust for NO_x sensor response, sensitivity to varying [O_2], and recovery/response kinetics.
- Develop breadboard based sensor for exhaust gas sensing

Accomplishments
- Sensing elements displaying near "total NO_x' behavior and stable in simulated long-term service have been developed.
- Sensing elements are capable of repeatedly detecting [NO_x] in the range of ~10 ppm and can operate at temperatures as high as 750 ^oC with ± 1ppm sensitivity.
- Novel techniques for applying electrical stimulus have been developed to combat drift of the sensor background output.

Future Direction
- The stability and performance of these sensing elements in real exhaust streams will be evaluated to quantify and correct for drift.
- The cross-sensitivity to other species (e.g., CO) that may be present in real exhaust streams needs to be characterized.
- Both the sensing mechanism and the cause(s) for sensor drift need to be clarified.

Introduction

Natural gas engines operated under lean (or dilute) combustion offer efficiency and maintenance advantages; however, to meet NO_x emissions targets and comply with the more stringent environmental regulations, NO_x reduction in a lean or oxygen-rich exhaust is required. To meet this challenge, NO_x remediation techniques such as the lean NO_x trap (LNT) and selective catalytic reduction (SCR) are currently being explored. The implementation of either of these techniques would be greatly simplified if a compact, robust, and low-cost NO_x sensor for *in-situ* [NO_x] monitoring of engine exhausts could be developed. This sensor could be used to monitor trap conditions in the case of the LNT and control reagent injection in the case of SCR.

The objective of this research is the development of a NO_x sensor for *in-situ* monitoring of natural gas engine exhaust. Ideally, such a sensor would operate at temperatures near 600 ^oC, measure [NO_x] in the range 10–500 ppm, be insensitive to varying [O_2] and [H_2O], and be insensitive to other oxidizible or reducible species (e.g., CO) that may be present in the exhaust. Also important for this application is the fact that "NO_x" is a mixture of NO and NO_2. NO is the dominant equilibrium form at temperatures above 600 ^oC,[1] but equilibrium conditions cannot be assumed to prevail in the exhaust.

Approach

The approach selected is to build a sensing platform on yttria-stabilized zirconia (YSZ). YSZ, an oxygen-ion conducting material, is currently widely used in [O_2] sensors for gasoline engines. This approach is not original, as two NO_x sensors based on YSZ are near commercialization and have been proven by the engine manufacturers association to not be adequate to measure NOx less than 50 ppm. In addition, both are relatively complex with multi-cavity constructions. This construction is required because in the first design [2] preliminary O_2 removal from the sampled exhaust is required before the NO_x is measured amperometrically, and in the second design[3] the sampled exhaust passes over a conversion electrode in order to convert the NO_x into NO_2 before measurement in the sensing cavity.

The lion's share of work to date has focused on the sensing *element* portion of the sensor. This is the portion of the sensor that responds to the presence of NO_x. The reason for adopting this approach is that the working characteristics of the sensing element will dictate many aspects of sensor design (operating temperature, need for catalytic overlayers, etc.).

In order to fabricate sensing elements electrodes are screen-printed and fired onto YSZ substrates (Fig. 6). These elements are then tested for NO_x response using a furnace to simulate elevated temperature service and a commercial gas mixing unit to deliver blends of N_2, O_2, NO_x (either NO or NO_2), and other species as required.

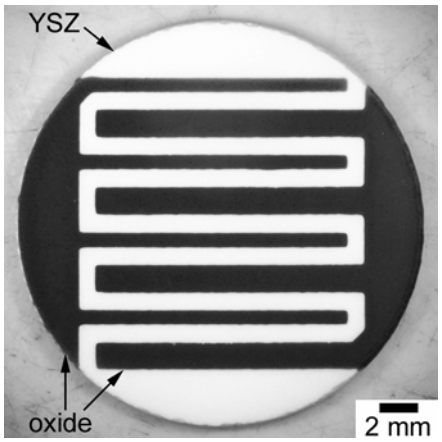

Figure 1: prototype sensing element.

Results

Much of the work on this project has been devoted to all-oxide "total NO_x" sensing elements. These sensing elements, a sample of which is depicted in Fig. 1, consist of compositionally identical oxide electrodes on a YSZ substrate. These sensing elements are attractive because the use of a single electrode material will reduce production cost and more importantly, their "total NO_x" (similar response to NO and NO_2) sensing behavior would enable measurement of [NO_x], regardless of the [NO]:[NO_2] ratio in the exhaust gas. This obviates the necessity to perform any NO_x conversion of the type described in ref. [3].

Several electrode compositions have been evaluated in order to develop a composition with large NO_x response magnitudes. The best of these, when operated at 600 ^oC and 7 vol% O_2, had responses to 77 ppm NO and NO_2 of -37%[3] and -40% respectively. However, long term (>200 hr.) lab scale testing of this composition revealed that it was unstable in exhaust conditions, and thus the

[3] This is the change in measured voltage when NO_x is present.

development of new compositions, stable in exhaust conditions, has been carried out.

The NO_x sensing performance of two promising new compositions is shown in Fig. 7. It can be seen that the NO_x responses are similar in magnitude over the concentration range 20–190 ppm, and efforts are ongoing to narrow the response between [NO] and [NO_2].

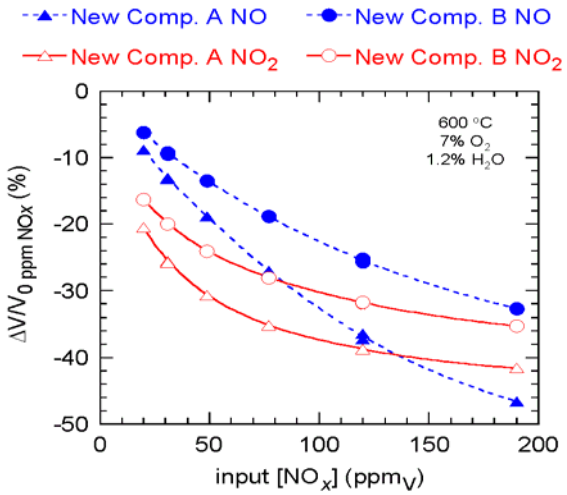

Figure 2: NO_x responses of two new electrode compositions.

Figure 8 shows x-ray diffraction patterns from extensively tested sensing elements made with old electrode composition and the new composition. The new composition is clearly more stable as shown by

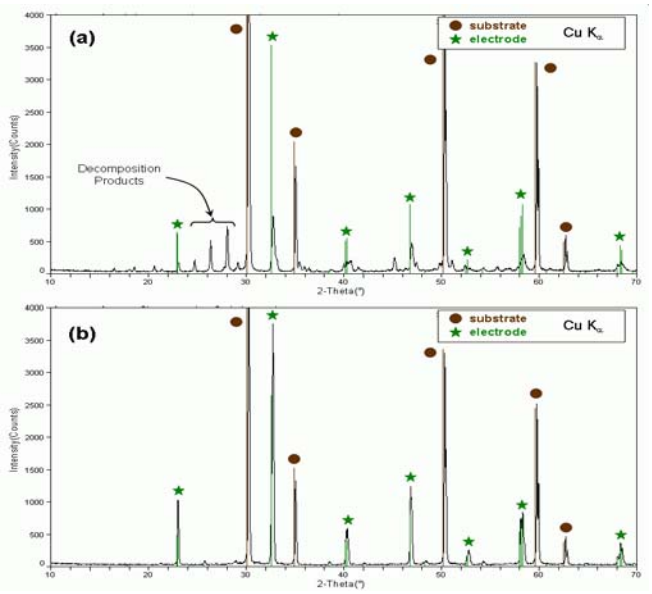

Figure 3: X-ray diffraction patterns of used elements made with original (a) and new (b) compositions.

The data in Fig. 2 was collected at 600 °C. It may be desirable to operate the sensing element at higher temperatures, both in order to improve the response/recovery time and prevent condensation on the sensing element. The higher temperature NO sensing performance of these sensing elements is illustrated in Fig. 9, which shows sensing element performance at 750 °C. Two aspects of the sensing performance in Fig. 4 differ from that observed in Fig. 2. First, the magnitude of the changes due to NO are much smaller. Second, the dependence of the response on [NO] is linear. Note also that the response decreases with increasing [O_2]. This means that operation at these temperatures will most likely require lowering of the [O_2] in the sampled exhaust (by means of a pumping cell).

These sensing elements are electrochemical in nature, and electrochemical sensing elements are prone to drift. Drift is frequently observed because electrochemical sensors usually rely on charge transfer at interfaces, and these interfaces will age with use of the sensor.

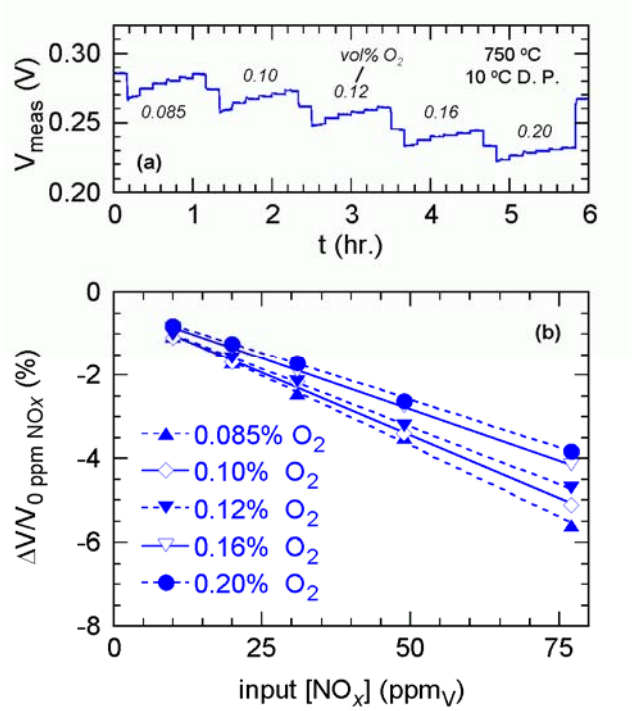

Figure 4: Sensing performance at 750 °C. In (a) [NO] is stepped through the sequence 0, 77, 49. 31, 20, 10, 0 ppm at the indicated [O_2]. Computed changes in voltage are shown in (b).

Sample drift behavior observed with these sensing elements is illustrated in Fig. 10. Shown there are the element responses to identical programmed changes in [NO] and [O_2] after 0, 10, and 70 hours of continuous operation. The background resistance of the element is monotonically increasing, but the responses to the gas concentration changes are repeatable.

In order to combat this drift, we have been investigating alternate methods of applying an electrical stimulus to the sensing element. One such example is shown in Fig. 6.

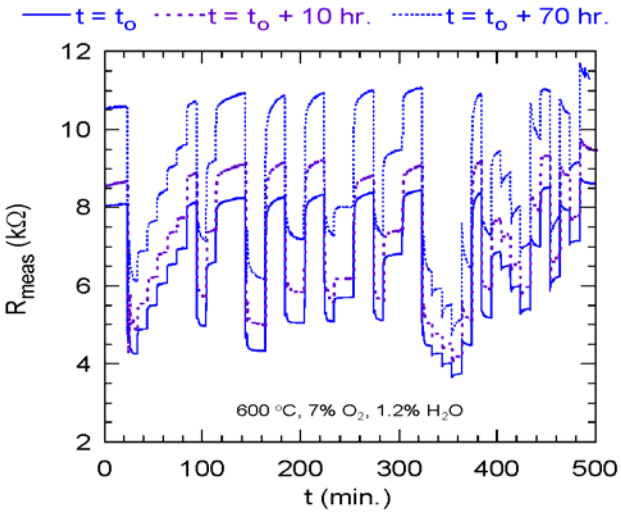

Figure 5: Response to identical changes in [NO] and [O_2] after 0, 10, and 70 hr. of continuous operation.

The electrical stimulus was alternated between positive and negative values (only the negative values are shown in Fig. 6. During every third negative excursion, the [NO] concentration was varied systematically as indicated in Fig. 6. Operated in this manner, the sensing element is capable of repeatedly detecting [NO] changes on the order of 10 ppm over more than 10 hours of continuous operation. These are thought to be the demands that monitoring of a lean NO_x trap would place on a NO_x sensor.

Conclusions

Sensing elements capable of "total NO_x' sensing behavior are under development. During the course of this project the following accomplishments have been achieved:

- Sensing elements displaying near "total NO_x' behavior and stable in simulated long-term service have been developed.
- NO sensing elements have been demonstrated.
- Sensing elements are capable of repeatedly detecting [NO_x] in the range of ~10 ppm and can operate at temperatures as high as 750 °C with ± 1ppm sensitivity.
- Sensing elements stable for more than 1000 hrs in oxygen and steam containing environments have been developed.

The challenges ahead are fourfold: (1) the stability and sensitivity of these elements must be examined in real exhaust streams, (2) the cross-sensitivity to other species that may be present in the exhaust must be characterized, (3) techniques for combating drift must be introduced and optimized, and (4) the sensing mechanism of these elements needs to be elucidated.

This last item is important as ease of fabrication and cost may dictate changes in materials or geometry during the incorporation of these elements into sensors suitable for natural gas engines. Understanding of the sensing mechanism will be critical in predicting how such changes might affect the sensor performance.

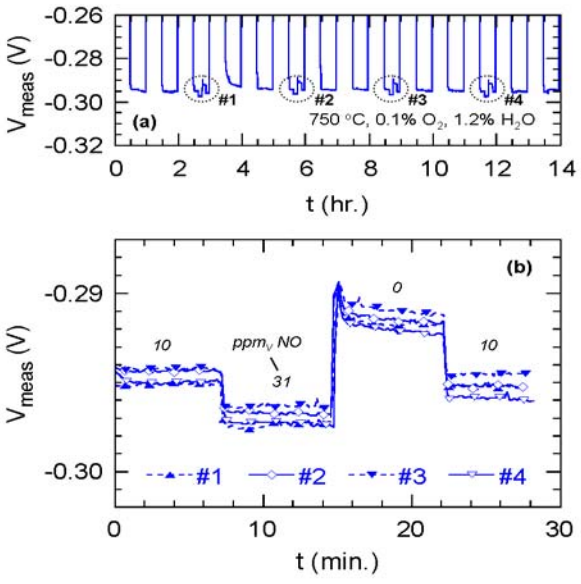

Figure 6: Element performance with alternating application of positive and negative electrical stimulus.

References

1. K. B. J. Schnelle and C. A. Brown, "NO_x control," in *Air pollution control technology handbook*, CRC Press, 2001, pp. 241-255.
2. N. Kato, H. Kurachi, and Y. Hamada, "Thick film ZrO_2 sensor for the measurement of low NO_x concentration," SAE Technical Paper 980170, 1998.
3. A. Kunimoto, M. Hasei, Y. Yan, Y. Gao, T. Ono, and Y. Nakanouchi, "New total-NOx sensor based on mixed potential for automobiles," SAE Technical Paper 1999-01-1280, 1999.

Patents

F. C. Montgomery, D. L. West, T. R. Armstrong, and L. C. Maxey, "NO_x Sensing Devices Having Conductive Oxide Electrodes" *ORNL Docket 1348C*.

Publications/Presentations

1. D. L. West, F. C. Montgomery, and T. R. Armstrong, "'Total NO_x' sensing elements with compositionally identical oxide electrodes," accepted by *Journal of the Electrochemical Society*, Sep. 2005.
2. D. L. West, F. C. Montgomery, and T. R. Armstrong, "NO-selective NO_x sensing elements for combustion exhausts," accepted by *Sensors and Actuators B*, Feb. 2005.
1. D. L. West,* F. C. Montgomery, and T. R. Armstrong, "All-oxide "total NO_x" sensing elements," *207th Meeting of the Electrochemical Society*, 2005.
2. D. L. West, F. C. Montgomery, and T. R. Armstrong, "DC electrical-biased, all-oxide NO_x sensing elements for use at 873 K," *29th International Cocoa Beach Conference on Advanced Ceramics and Composites*, 2005.
3. D. L. West, F. C. Montgomery, and T. R. Armstrong, "High-T NO_x sensing elements using conductive oxides and Pt," *Proceedings of ICEF: Engines for Mobile, Marine, Rail, Power Generation and Stationary Applications*, 2004.

3.1b – TAT Lab and Performance Evaluations

Abdi Zaltash
Engineering, Science and Technology Division
Oak Ridge National Laboratory
(865)-574-4571; email: zaltasha@ornl.gov

DOE Technology Development Manager: Ron Fiskum
202-586-9154; email: ronald.fiskum@hq.doe.gov

Objective
Oak Ridge National Laboratory (ORNL) investigates emerging technologies, identifies R&D opportunities and, in consultation with the Department of Energy (DOE) Program Manager, selects the technologies to be developed and conducts supporting in-house research.

Advanced designs for thermally activated technologies (TATs) will entail extensive research, development, manufacturing cost analysis, field-testing, and performance verification. Performance evaluation of advanced TAT designs can enhance existing applications such as heating, cooling, refrigeration, humidity control, and direct fuel-fired activities, as well as potential new applications. The objective is to develop "next generation" TAT equipments with better designs and materials that will lower the cost and improve the performance of heating, cooling, refrigeration, ventilation, and humidity control technologies.

Approach
Novel TATs are needed for using thermal energy and waste heat. Laboratory tests and prototype evaluations will be required to prove the feasibility of new ideas and to develop "next generation" TAT units with improved performance and lower cost. These tests are conducted at the Thermally Activated Heat Pump (TAHP) Environmental Chambers according to the applicable standards [1-5].

Accomplishments:
Evaluation of a novel industry confidential prototype gas-fired heat pump (split system with outdoor and indoor sections) with R22 (base-line refrigerant) and R407C (interim alternate refrigerant) at the Thermally Activated Heat Pump (TAHP) Environmental Chambers. This evaluation resulted in an integrated package gas-fired heat pump (rooftop unit) with internal heat recovery from the radiator/the exhaust for better overall efficiency. Report on performance test results of R22 and R407C will be completed by the industry partners. Significance of ORNL work: (1) private industry partner did not have access to a suitable psychrometric chamber for the evaluation of performance and emissions, (2) evaluation of quality and quantity of waste heat streams which are available for the internal heat recovery for improving efficiency, and (3) ORNL has years of experience working with the chemical industry in developing and testing alternative refrigerants, thus was able to recommend alternative refrigerants (R407C), modify the prototype at ORNL, and evaluate the modified prototype.

Evaluation of absorption chillers and "heating only" absorption unit at the TAHP Environmental Chambers at various ambient conditions. These set-ups consist of a prototype outdoor unit coupled to a standard off-the-shelf indoor fan coil. Significance of ORNL work: (1) private industry partner did not have access to a suitable psychrometric chamber for the evaluation of performance and emissions of these units over a wide range of outdoor and indoor conditions (with temperature and humidity control) and (2) independent evaluation of these units with their respective indoor units to verify the ease of installation, reliability and durability of these units and their sub-components.

Future Direction:
ORNL will continue to provide technical support to the private industry partners to develop the "next generation" heat pumps and chillers with better designs and materials that will lower the cost and improve the performance.

Introduction

Thermally activated technologies (TATs) can be directly fired or operated using waste heat in combined heat and power applications. TATs have a long history and have seen generations of service both in direct-fired systems (where fossil fuels are used directly) to produce chilled water for air conditioning or in refrigeration and dehumidification as well as in equipment using steam or hot water to provide these services. Further advances in efficiency, size, and cost will result in greater use of TATs and in progress toward national energy and environmental goals. This is particularly true in the development of TATs that are powered by recovered waste heat.

TATs represent a diverse portfolio of equipment that uses heat for heating, cooling, humidity control, thermal storage, or shaft/electrical power. TATs are the essential building blocks for integrated energy systems (IES) that can help maximize energy savings and economic return. Thermally activated systems also offer customers reduced seasonal peak electric demand and enable future electric and gas grids to operate with more level loads.

DOE's TAT development activities in recent years have focused primarily on absorption technology and desiccant technology. Desiccant equipment has been successfully applied for many years in industrial applications or where humidity control is critical. New desiccant technology is being adapted to meet the emerging comfort and indoor environmental quality needs of commercial and institutional buildings. It is expected that, in the next 1-3 years, U.S. industries will begin commercialization of a natural gas-fired small commercial absorption chiller and residential heat pump now under development as part of this program. DOE and ORNL are cooperating in a national partnership to support final product development and commercialization.

Commercial Thermally Activated Heat Pump R&D

In Japan, many hundreds of thousands of small natural gas-driven heat pumps have been sold (typically 50,000 to 80,000 annually). Although very reliable and energy efficient, the Japanese products are not suited for normal U.S. commercial applications (Japanese equipment is split-system zoned refrigerant equipment that is not suitable for typical U.S. high temperature applications). This activity is to start with the basic technology used in the best Japanese gas-driven heat pumps (the engine) and develop gas-engine driven heat pumps suitable for U.S. drop-in commercial rooftop applications (by far the single largest product segment). Initial evaluations include:

- baseline (emissions, efficiency, and fuel consumption)
- development of several heat transfer components for U.S. applications (exhaust heat exchanger, engine coolant exchanger, and micro-channel outdoor coil)
- vibration and noise (minimize in design)
- engine intake and exhaust system (including catalyst)
- controls (fuel/engine management and complete heat pump system controls)
- parasitic load reduction (starting system and transformer)
- development of single packaged rooftop configurations.

TAT Ammonia-Water Absorption (Heat Pump, Air-Conditioning and Refrigeration) Equipment

Historically, the natural gas-fired ammonia-water absorption technology for individual chillers and heat pumps for energy savings was a primary emphasis of the TAT program. Advanced technology ammonia-water absorption equipment (for residential and small commercial applications - typically less than 15 RT) has been developed in the laboratory with DOE and gas industry support. The gas industry has formed a new company to bring this advanced ammonia-water absorption heat pump and air-conditioner technology to market in 2005 – 2008. This technology is moving out of the laboratory into pre-commercial prototype development and field-testing. Additionally, this ammonia-water absorption technology is able to provide below-freezing refrigeration temperatures using high temperature heat recovered from power generation equipment (for example from a microturbine).

Potential benefits:

- These heat pump systems offer 40% to 50% higher heating efficiency than the best existing furnaces or boilers for heating small buildings in the winter.
- Adaptation to IES applications using recovered heat promise residential and small to medium size commercial systems at the highest possible energy efficiency levels.

For the residential and light commercial space conditioning market, the technology is based on the ammonia-water absorption cycle with generator-

absorber recuperative heat exchange. Performance levels (1.4 heating COP and 0.7 cooling COP) favor a primary market in the northern half of the country due to its exceptional heating efficiency.
This study will focus on the performance and emissions of these units in a controlled environment according to the applicable standards [1-5] and work with the industry partners to develop "next generation" TATs with better designs and materials that will lower the cost and improve the performance.

Results

Commercial Thermally Activated Heat Pump R&D

Performance and emissions evaluation of a 10-ton gas-driven heat unit (split unit) were conducted in the ORNL TAHP Environmental Chambers. The air-cooled outdoor unit was installed in the larger room (outdoor chamber with 15 ft by 18 ft footprint) with the air-handler unit (AHU) in the smaller room (indoor chamber with 15 ft by 12 ft footprint). Refrigerant lines connected the AHU to the outdoor unit. Initial evaluations were conducted with R22 as the baseline refrigerant followed by the interim replacement refrigerant R407C. This refrigerant was selected by the industry partner based on ORNL recommendation.

These absorption units were operated over a wide range of ambient conditions including the operating conditions for standard rating and performance tests [1]. Table 1 shows these operating conditions. It should be noted that the evaluations were conducted at high and low speed of the engine. In addition, the quality and quantity of all the available waste heat streams were investigated for potential internal heat recovery and improved performance in the future designs particularly in the packaged unit.

Figures 1-5 compare the performance of R22 with the interim replacement refrigerant R407C. Results show that R407C provides comparable performance at temperatures below 110ºF. It should be noted that the engine could not maintain the high speed of 2,310 rpm with R407C at higher ambient temperatures (≥110ºF) due to the higher discharge pressure of this refrigerant. In these cases, the fuel flow was adjusted to maintain this speed.

Test	INDOOR UNIT Air Entering			OUTDOOR UNIT Air Entering		
	DB (°F)	DP (°F)	WB (°F)	DB (°F)	DP (°F)	WB (°F)
COOLING TESTS						
Standard Rating Conditions "A" Cooling Steady State*	80	60.2	67	95	66.5	75**
"B" Cooling Steady State*	80	60.2	67	82	55	65**
"C" Cooling Steady State Dry Coil*	80	36.8	57***	82	55	65**
Low Temperature Operation Cooling*	67	49.8	57	67	49.8	57**
Maximum Operating Cooling Conditions*	80	60.2	67	115	55	75**
High Ambient Temperature	80	60.2	67	110	58.2	75**
"D" Cooling Cyclic Dry Coil*	80	36.8	57***	82	55	65**
Higher Ambient Temperature	80	60.2	67	120	51.3	75**
Highest Ambient Temperature	80	60.2	67	125	47.1	75**
HEATING TESTS						
Standard Rating Conditions High Temperature Heating Steady State*	70	53.5	60 (max)	47	38.7	43
High Temperature Heating Cyclic*	70	53.5	60 (max)	47	38.7	43
High Temperature Heating Steady State*	70	53.5	60 (max)	62	52.7	56.5
Low Temperature Heating Steady State*	70	53.5	60 (max)	17	9.4	15
Maximum Operating Conditions*	80			75	59.5	65

* Operating Conditions for Standard Rating and Performance Tests [1].
** Wet bulb temperature (WB) condition is not required
*** Wet bulb sufficiently low that no condensate forms on evaporator
Note: DB is the dry-bulb temperature and DP is the dew-point temperature.

Table 1. Operating conditions for evaluation of commercial thermally activated heat pump

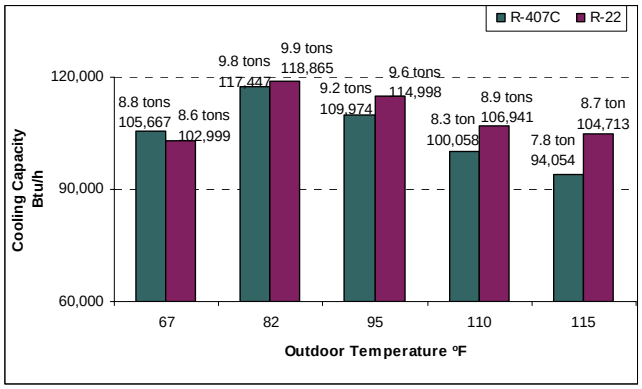

Figure 1. Comparison of cooling capacities between R22 and R407C at high speed

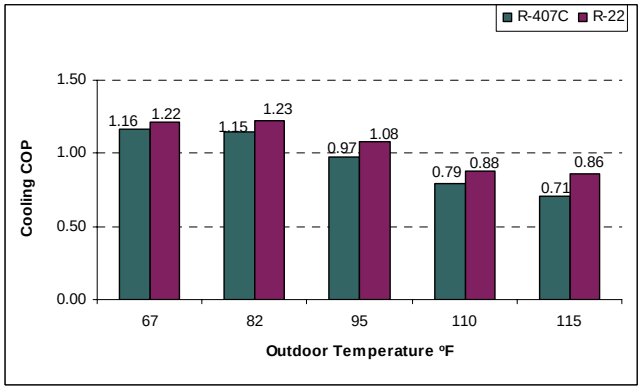

Figure 2. Comparison of cooling Coefficient of Performance (COP) between R22 and R407C at high speed

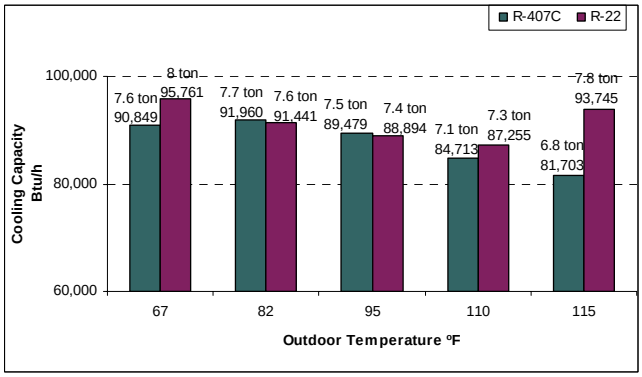

Figure 3. Comparison of cooling capacities between R22 and R407C at low speed

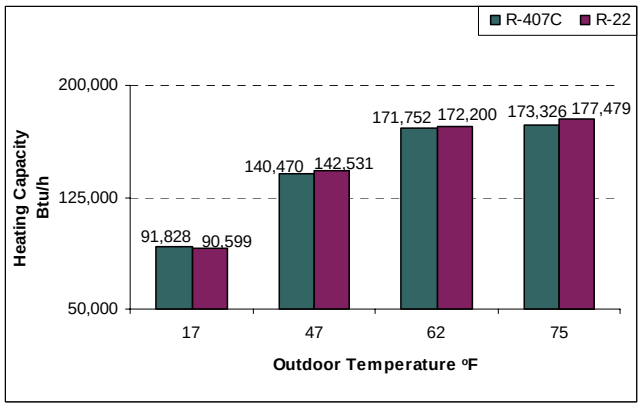

Figure 4. Comparison of heating capacities between R22 and R407C at high speed

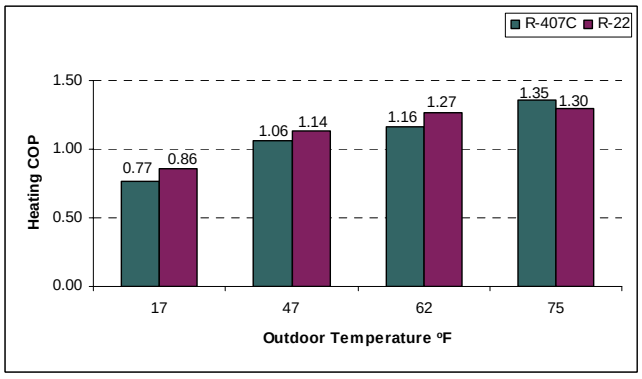

Figure 5. Comparison of heating Coefficient of Performance (COP) between R22 and R407C at high speed

TAT Ammonia-Water Absorption (Heat Pump, Air-Conditioning and Refrigeration) Equipment

Performance and emissions evaluation of two pre-commercial 5-ton chillers (Beta #3 and #13) and one "heating only" absorption prototype unit were conducted in the ORNL TAHP Environmental Chambers. The air-cooled absorption unit (outdoor unit) was installed in the larger room (outdoor chamber) with the AHU in the smaller room (indoor chamber). Water loop connected the AHU to the absorption unit (Figure 6).

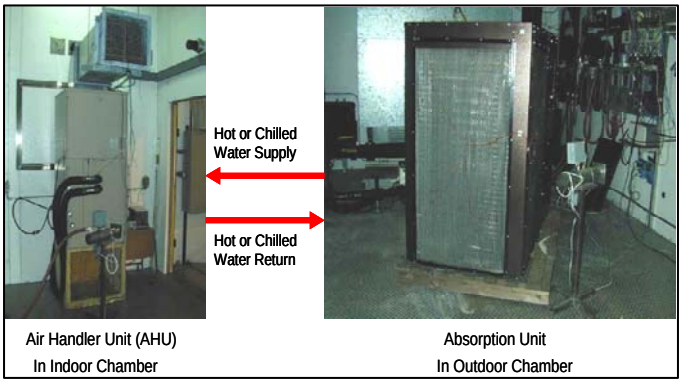

Figure 6. Set-up used for performance evaluation of absorption units

These absorption units were operated over a wide range of ambient conditions including the operating conditions for standard rating and performance tests (Table 2). Figures 7 and 8 show the capacity and COP of the absorption chiller units Beta #3 and #13. Performance data shows the close agreement between these two chiller units. The capacity of these chillers was found to be approximately 56,500 Btu/h with COP of 0.66 at the standard rating of 95°F outdoor condition which is within the accuracy of the instrumentation to the desired performance levels for both capacity and COP (60,000 Btu/h or 5-tons and cooling COP of 0.7). In addition, this unit was operated at ARI "C" cooling condition - steady state, dry coil [1]. At this condition, the unit was using its modulating burner capability to optimize its performance by maintaining the chilled water temperature around 45°F. The COP and capacity were found to be 0.72 and 48,000 Btu/h respectively.

At the ARI low temperature cooling condition of 67°F outdoor/67°F indoor, the capacity was found to be approximately 39,000 Btu/h with a COP of 0.81 at low firing rate. Figure 9 shows the emissions from pre-commercial absorption chiller unit (Beta #3). The CO concentration was found to be 8 ppm with NO_x concentration of less than 13 ppm at the measured oxygen content.

Table 2. Operating conditions used for evaluation of absorption chillers Beta units

Test	INDOOR UNIT Air Entering			OUTDOOR UNIT Air Entering		
	DB (°F)	DP (°F)	WB (°F)	DB (°F)	DP (°F)	WB (°F)
Standard Rating Conditions "A" Cooling Steady State*	80	60.2	67	95	66.5	75**
"B" Cooling Steady State*	80	60.2	67	82	55	65**
"C" Cooling Steady State Dry Coil*	80	36.8	57***	82	55	65**
Low Temperature Operation Cooling*	67	49.8	57	67	49.8	57**
Maximum Operating Conditions*	80	60.2	67	115	55	75**
High Ambient Temperature	80	60.2	67	105	61.2	75**

* Operating Conditions for Standard Rating and Performance Tests [1].
** Wet bulb (WB) temperature condition is not required
*** Wet bulb sufficiently low that no condensate forms on evaporator.
Note: DB is the dry-bulb temperature and DP is the dew-point temperature.

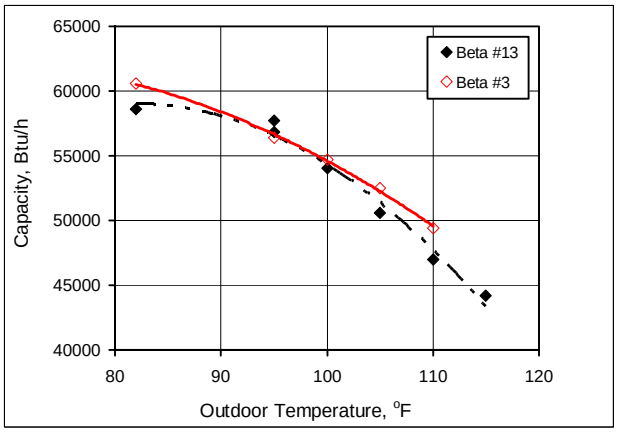

Figure 7. Capacity of absorption chiller Beta units #3 and #13

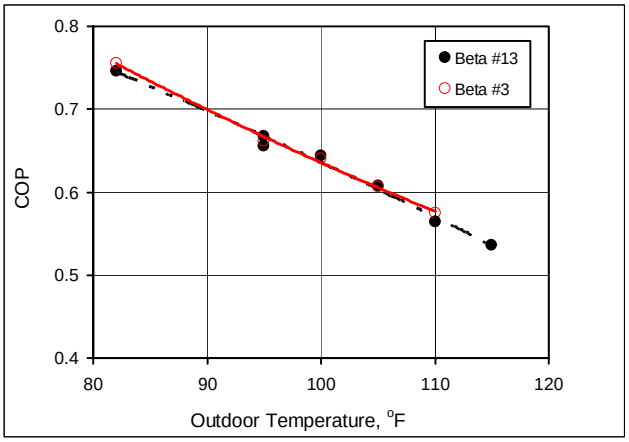

Figure 8. Coefficient of Performance (COP) of absorption chiller Beta units #3 and #13

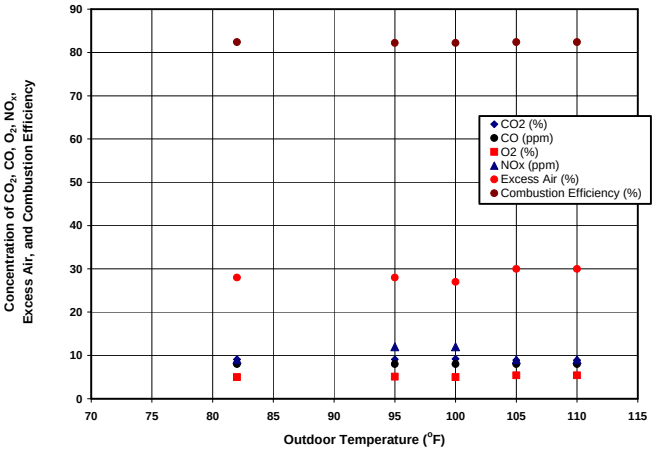

Figure 9. Flue gas composition and combustion efficiency of absorption chiller Beta unit #3

The "heating only" absorption unit was operated over a wide range of heating conditions. Due to the small size of the coil inside the AHU (designed for 5 ton of cooling or 60,000 Btu/h) and lower air flow rate (designed for 5 ton of cooling with approximately 2,000 scfm), the ARI standard rating [1] and performance tests for heating could not be performed. However, tests were conducted for 95°F and 100°F hot water return temperature to emulate a properly-sized AHU. The heating capacity and COP of the "heating only" unit are shown in Figures 10 and 11. The capacity of this unit was found to be approximately 123,000 Btu/h with COP of 1.37 at 47°F outdoor condition and 95°F hot water return temperature. This performance is within the accuracy of the instrumentation to the performance levels reported by the industry partner (Figures 10-11) and the desired heating COP of 1.4. At the low temperature heating condition of 17°F outdoor, the capacity was found to be approximately 107,320 Btu/h with COP of 1.12 (excluding defrost cycle). With the inclusion of the defrost cycle the COP decreased to 1.08 with capacity of 103,382 Btu/h. Figure 12 shows the power consumption of this unit at various ambient conditions. The average power used by this unit was found to be approximately 900 W.

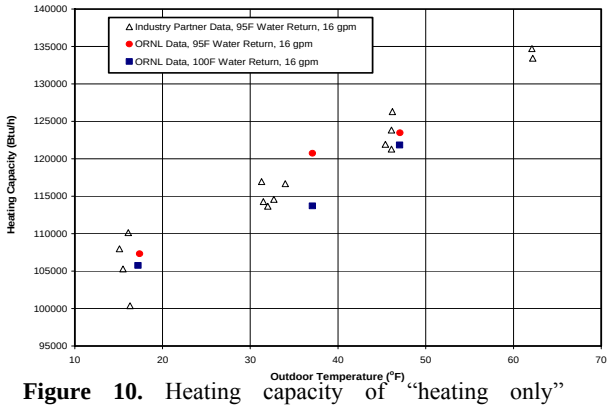

Figure 10. Heating capacity of "heating only" absorption unit

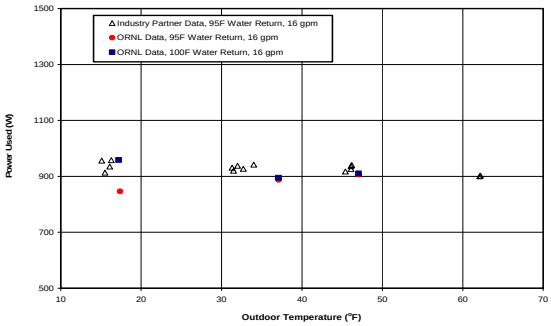

Figure 11. Coefficient of Performance (COP) of "heating only" absorption unit

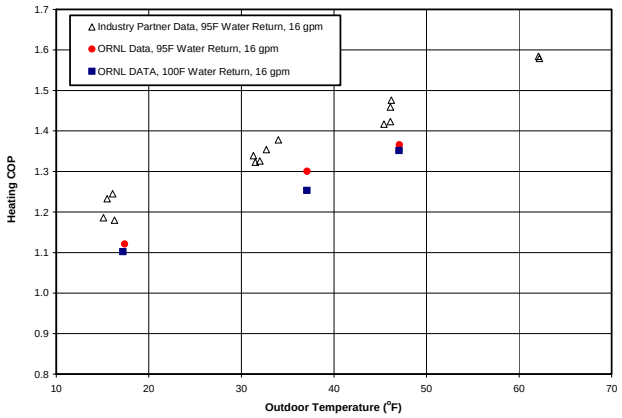

Figure 12. Power consumption of "heating only" absorption unit

Figure 13 shows the emissions of the "heating only" unit at various ambient conditions. The CO concentration was found to be less than 13 ppm with NO_x concentration of less than 10 ppm at the measured oxygen content.

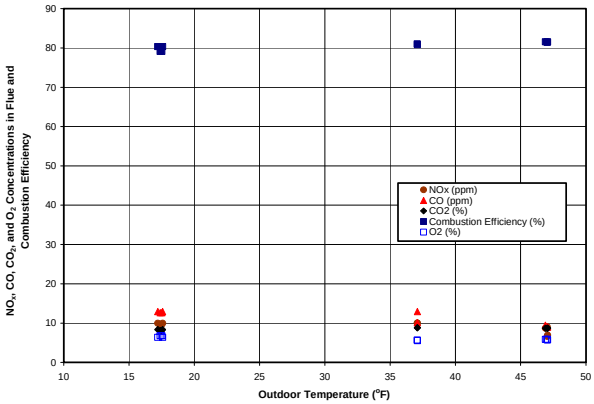

Figure 13. Flue gas composition and combustion efficiency of heating only absorption unit

Conclusions and Recommendations

Commercial Thermally Activated Heat Pump R&D

This heat pump unit operated well at various ambient conditions with R22 (the baseline refrigerant) and R407C (the interim replacement refrigerant). This evaluation resulted in an integrated package gas-fired heat pump (rooftop unit) with R407C and internal heat recovery from the radiator/the exhaust for better overall efficiency. The performance of this package unit will be evaluated in the TAHP Environmental Chambers.

TAT Ammonia-Water Absorption (Heat Pump, Air-Conditioning and Refrigeration) Equipment

Generally, these units operated well over a wide range of ambient conditions with minimal degradation due to several control strategies used such as variable speed condenser fan, modulating burner, and active refrigerant flow control (TXV). During these tests, the controller

maintained the chilled water supply temperature around 45°F by modulating the gas burner. This same type of scheme was used to maintain the hot water supply temperature between 117 to 120°F. In addition, the defrost cycle in the "heating only" unit seem to work adequately however the duration of this cycle will need to be optimized. The main problem encountered was with the liquid level in the generator which resulted in several unexpected shut-downs of these units. This is a solution inventory problem which could be easily resolved by the industry partners.

References

1. ANSI/ARI 210/240-94 Standard, "Unitary Air-Conditioning and Air-Source Heat Pump Equipment", 1998.
2. ANSI/ASHRAE Standard 40-2002, "Methods of Testing for Rating Heat-Operated Unitary Air-Conditioning and Heat Pump Equipment", 2002.
3. ANSI Z21.40.4a-1998 and CGA 2.94a-M98 Standard, "Performance Testing and Rating of Gas-Fired, Air-Conditioning and Heat Pump Appliances", 1998.
4. ANSI/ASHRAE Standard 37-2005, "Methods of Testing for Rating Electrically Driven Unitary Air-Conditioning and Heat Pump Equipment", 2005.
5. ANSI/ARI Standard 560, "Absorption Water Chiling and Water Heating Packages", 2000.

3.3b Integrated Active Desiccant Heat Pump Development Collaboration

Jim Sand, Andrei Petrov, and Abdi Zaltash
Engineering Science & Technology Division
Oak Ridge National Laboratory
Oak Ridge, TN 37831-6070
(865) 574-5819, E-mail: sandjr@ornl.gov

DOE Technology Development Manager: Patricia Hoffman
(202) 586-6074, (202) 586-7114 (Fax), E-mail: Patricia.Hoffman@hq.doe.gov

Objective

- In collaboration with SEMCO, develop and test an operational heat pump mode for the SEMCO, *Revolution*™ hybrid rooftop air conditioning/dehumidification product. Establish the *Revolution*™ as a direct replacement for the conventional rooftop unit by developing its ability to function as a heat pump for cold weather heating.

- Characterize and establish the performance capabilities of the SEMCO *Revolution*™ product when waste heat from a distributed generation source is used for desiccant regeneration. Establish the utility of this hybrid desiccant rooftop product in an integrated CHP energy system.

Approach

- Build a SEMCO *Revolution*™ unit with the added refrigerant circuitry, thermal expansion valving, and 4-way reversing valve which allow it to function as a vapor-compression heat pump.

- Incorporate a heat exchanger in the desiccant regeneration air path of a SEMCO *Revolution*™ that will allow desiccant regeneration with a liquid waste heat source.

- Install and test this augmented integrated desiccant system in Oak Ridge National Laboratory's CHP Integration Laboratory, Building 3114, at varying ambient conditions.

Accomplishments

- Preliminary modeled heat pump performance simulations of the SEMCO *Revolution*™ integrated active desiccant rooftop (IADR) using the ORNL heat pump model which led to several hardware modifications.

- Development of a heat pump control algorithm that could be programmed into the *Revolution*™*'s* programmable controller module.

- Extensive laboratory testing and system performance monitoring that resulted in system hardware modifications and selection of a heat pump defrost algorithm.

- Incorporation of a heat pump operational mode into SEMCO's standard line of *Revolution*™ IADR products.

- Initiation of a field demonstration R&D project in which the SEMCO *Revolution*™ is used as the waste heat utilization technology in an islanded, distributed generation, integrated energy CHP system at Pepperell High School in Lindale, Georgia.

Future Direction

- Demonstration/Field Verification installations of heat pump augmented systems in more extreme climates where heat pump satisfies all of the heating

- Further development and research on the possibility of using the desiccant wheel thermal regeneration system as a supplemental heat source and as a product convenience feature during heat pump defrost

.

Introduction

As described in **ORNL/SUB-01-4000010402** entitled "Desiccant Based Combined Systems: Integrated Active Desiccant Rooftop Hybrid System Development and Testing" the IADR product was developed to independently control both temperature and humidity delivered to an occupied space, during the cooling season, while accommodating up to 100% outdoor air. The system has the unique advantage of being able to process any percentage of outdoor air and adjusting to the load requirements of the space by varying the sensible heat ratio (SHR). The need for improved cooling season humidity control (dehumidification), especially when high outdoor air volumes are required, is essential for facilities located in hot and humid climates designed to meet the ventilation requirements set by ASHRAE 62 and the energy efficiency requirements set by ASHRAE 90.1.

During the heating season, the IADR system will often be required to act as a heating unit as well. This is especially true if the system is installed as a dedicated outdoor air system (DOAS) where it operates with all outdoor air. Traditionally this heating is accomplished through the use if either an indirect gas fired heat exchanger or electric resistance heat. Each method presents a performance disadvantage, especially when high outdoor air volumes are required.

Indirect gas fired options typically do not offer the modulation necessary to accommodate large outdoor air percentages. This presents two potential problems. One is the introduction of very warm air during moderate outdoor air conditions. Since minimum run times are required to protect the life of the heat exchanger, this can result in a wide fluctuation in space temperature. The other is that during the heating season design days, undesirably cold air can be "dumped" to the space when the heater is cycled off but the supply fan continues to run as required to deliver the necessary ventilation air. The use of electric resistance heat has the obvious disadvantage of extreme operating costs due to its very low operating efficiency. At traditional energy costs, a BTU of electric resistance heat will cost approximately 2.2 times the cost of the indirect fired gas approach assuming an 80% efficient heat exchanger. Unless a high end electric heating control method is employed (i.e. SCR) to modulate the heating output, the electric resistance heating approach can result in the same dumping of cold air associated with the indirect gas approach.

Another important market driven factor is that since hot and humid climates have, by definition, relatively mild heating seasons, electrical utilities have been extremely successful convincing their customers to design around all electric facilities (i.e. use electric resistance heat) in exchange for favorable electric rates. Although the heating season is short, the heating cost per BTU is extremely high with this heating method so annual energy costs can be significant. This is supported by the research findings resulting from a DOE sponsored demonstration sites (discussed later). A major pharmacy located in south Florida and using electric resistance heat paid the same amount for electricity in February as it did in August.

To address the need for heating by the IADR and to accomplish a stated development objective of high operating energy efficiency, the necessary parts were combined with novel control capabilities to integrate a heat pump cycle into the refrigeration portion of the hybrid system. This option offers an excellent fit to the hot and humid climates most likely to employ the IADR since they inherently have moderate heating seasons, allowing the enhanced heat pump performance capable with this system to satisfy the entire heating season needs.

IADR Design for Dehumidification Benefits the Heat Pump Integration

Since the IADR hybrid system includes an advanced vapor compression cooling section, only a few additional parts are required to complete the infrastructure for an effective air cooled heat pump system. A simplified heat pump piping schematic is provided as Figure 1 to show the major components required for heat pump operation.

To accommodate 100% outdoor air operation in the dehumidification/cooling mode, the cooling side components (coils, compressors, etc.) designed into the IADR have a much greater capacity per cubic foot per minute (cfm) of airflow processed than traditional packaged equipment. Traditional packaged systems are designed for approximately 400 cfm/ton of cooling output while the IADR is designed for approximately 175 cfm/ton. This design approach results in the size of the evaporator coil, condenser coil, condenser airflow and compressor capacity being large relative to the

airflow delivered. This design approach is highly beneficial for heat pump operation.

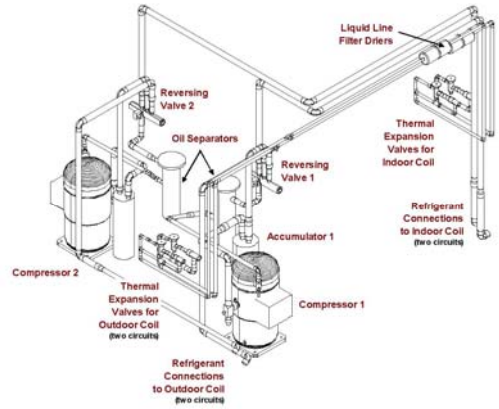

Figure 1: A schematic showing the major components required by the heat pump cycle integrated into the IADR hybrid system (outdoor and indoor coils are not shown)

Compressor Capacity

In addition to the high ratio of compressor tons to airflow processed, a high heating output results from the fact that all of the energy output experienced when in the heat pump mode is translated into temperature increase. During the cooling mode, a portion of the energy produced is allocated to condensing moisture (latent load). This latent portion is significant (say 50%) if all outdoor air is being processed. This is not the case in the heat pump mode.

Another factor enhancing performance in the heat pump mode is the compressor heat. This heat degrades cooling capacity but increases the heat output provided during the heat pump mode.

Outdoor Coil and Airflow Capacity

During the heat pump operation the outdoor air coil becomes the "cooling coil" while the indoor coil becomes the "heating coil". Since the heating performance is directly impacted by the difference between the refrigerant temperature and the ambient air temperature, and since the ambient air temperature can be quite low during the heating season, it is advantageous to keep this temperature difference to a minimum. This is accomplished by maximizing the outdoor coil surface area and operating with the highest possible outdoor airflow. High outdoor coil area and low temperature differentials are also important to minimize the likelihood and duration of frost formation on the outdoor coil. When the outdoor ambient humidity content is above the dew point of the outdoor coil surface, and if this surface temperature is below freezing, frost can slowly accumulate on the coil surface. This frost is removed by reversing the refrigeration flow and temporarily reverting back to cooling so that the outdoor air coil heats up and melts the frost. Since cold air leaves the indoor coil when heating is actually needed, it is advantageous to minimize both the frequency and duration of this defrost cycle.

Installation Sites Used to Obtain Performance Verification

Three separate IADR systems were investigated at different locations to benchmark the heating performance resulting from the integration of a heat pump option. The first system installed to condition the ORNL CHP laboratory located in Oak Ridge Tennessee provided an excellent opportunity to observe heating performance at high outdoor air percentages and in a relatively cold environment.

The second site selected was an existing pharmacy located in St. Petersburg Florida to provide data from a hot and humid climate during continuous actual operating conditions. The third system was installed within the SEMCO test laboratory located in Columbia, Missouri allowing a wide range of tests to be completed since airflows and indoor coil entering conditions could be modulated as desired. Basic details are provided for two of these installations.

Oak Ridge National Laboratory's CHP Test Lab

An IADR system having a nominal cooling capacity of 12.5 tons was installed to condition the CHP Laboratory at ORNL located in Oak Ridge Tennessee. The system was operated to provide approximately 3,200 cfm of supply airflow which comprised of between 50 and 100% outdoor air depending upon the pressurization needs of the facility. A small fume hood exhausted approximately 1,000 cfm and the building envelope was not well sealed. This new system was installed during July of 2004 and it has been operated to handle the outdoor air sensible and latent cooling loads, all of the space latent load and most of the space sensible load. An existing split system and hot water space heaters supplement the capacity of the IADR when needed. The 99% heating design condition for this location is 19ºF according to the 2001 ASHRAE Fundamentals.

Traditionally, heat pumps would not be successfully applied to facilities with this limate, especially of high outdoor air percentages were required.

Figure 2: Photos of the IADR installed at the ORNL CHP laboratory.

SEMCO Inc.'s Research and Development Test Laboratory

An IADR system having a nominal cooling capacity of 12.5 tons was installed to help condition the SEMCO R&D Air Test Laboratory located in Columbia Missouri. The system is operated to provide approximately 3,000 cfm of supply airflow which is comprised of approximately 50% outdoor air.

This system has been operating since November of 2004 and it has provided an excellent opportunity to test a variety of operating conditions for the heat pump capability of the IADR system. The 99% heating design condition for Columbia Missouri is 5°F according to the 2001 ASHRAE Fundamentals. This provided the most extreme heating season operating conditions of the sites investigated. As shown by Figure 3, the IADR system located within the SEMCO test laboratory differed from the systems installed at the other two sites in that the system was built as a "split system" with the main system being located indoors but the condensing section being located outdoors.

Figure 3: Photos of the IADR system installed within (main unit) and outside (condensing portion) of the SEMCO R&D Test Lab in Columbia Missouri

The extreme outdoor air temperatures and consistent cold conditions that existed for this system due it location offered the most effective site for optimizing the defrost control algorithms and methods. The application of air side heat pump technology used to condition a high percentage of outdoor air, as was the case for this test site is highly unusual and provided an excellent challenge to the performance capabilities of the IADR heat pump integration.

Performance Documented for the IADR Heat Pump Option

The sites discussed in the previous section were all operated over at least one heating season allowing data to be collected and archived. Over 45 state points were continuously monitored for each of the systems investigated. The onboard DDC control system also served as the data acquisition system to archive this data.

In addition to the state points monitored by way of digital or analog inputs to the controller, an additional 40 pieces of information relative to the various frequency inverters employed were monitored by way of modbus communications. The data provided by the monitoring and testing of these systems were analyzed to optimize operational and control functions and to provide the performance data as summarized in the following sections.

Initial Modeling with the ORNL Heat Pump Performance Model

ORNL has considerable expertise with regard to heat pump modeling. Oak Ridge has developed the ORNL HPDM Simulation model which has become an industry standard used by many of the large heat pump packaged unit manufacturers for product development and optimization.

As part of this development program, ORNL was provided the design parameters used for all aspects of the IADR heat pump design. More than 70 input parameters are required for this analysis. This modeling provided various performance parameters of interest including projected heating and cooling capacity, power consumption, COP values, supply temperatures, suction temperatures, discharge temperatures and sub cooling values.

Two of the more interesting pieces of modeling data provided by the analysis are the projected heating capacity and supply air temperature. Figure 4 shows a summary of the modeled heating capacity output anticipated as a function of outdoor ambient temperature. Shown in yellow is the average of actual

data measured as part of the testing completed at ORNL. Excellent agreement was obtained proving the effectiveness of the ORNL HPDM Simulation model. The results of this testing were very favorable to the IADR since a high amount of heating output was available even at the very low ambient temperatures experienced at the Oak Ridge Tennessee test location.

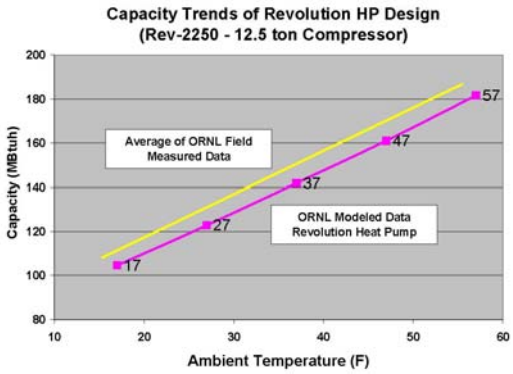

Figure 4: Actual test data showing heating capacity output as a function of ambient temperature compared with that projected for the IADR heat pump option using the ORNL HPDM Simulation model. Based upon 3,600 cfm of supply airflow and a full recirculation mode (no outdoor air).

Figure 5 shows the projected supply air temperature leaving the IADR system with heat
pump integration when operated as a 100% outdoor air system. The supply air temperature is shown as a function of the outdoor temperature and is based upon a *Revolution* 2250 system operated at its 2250 cfm nominal airflow.

These results are based upon the ORNL HPDM model and also agree well with actual test data.This data is interesting in that typical heat pump units are not used for systems located in cool climates or those involving high outdoor air percentages. The fact that the IADR system is capable of preheating outdoor as cold as 20oF to approximately 65°F demonstrates how this system differs from conventional systems and opens up opportunities to users to benefit from the elevated energy efficiency associated with this technology in the heating mode.

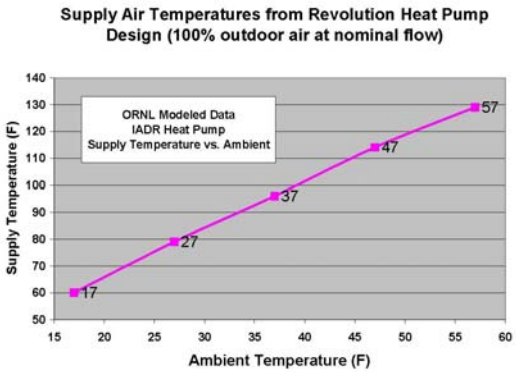

Figure 5: Projected supply air temperature delivered by IADR heat pump option when operated as a 100%outdoor air system based upon the ORNL HPDM Simulation model. The Revolution 2250 unit serves as the basis of the analysis and is operated at the nominal 2250 cfm airflow.

Heating Data Collected at Pilot Installation Sites

A very large amount of data was collected to map the performance of the heat pump integration into the IADR system. The sites described previously were all fitted with full instrumentation that was continuously monitored and archived. To provide a sampling of the data collected, Figure 6, have been prepared to summarize data collect at the Oak Ridge National Laboratory site covering a time period from November 2004 though March of 2005.

This data shows a wide variety of outdoor air percentages, outdoor temperatures, compressor modulation and delivered heating capacity. The electrical energy consumption was monitored for each component within the system and the heating output was measured by equating the supply airflow and the associated temperature increase. Good agreement was found between the modeled results and those measured. For example, the 10:45 data point collected on 11/26 shows approximately 2400 cfm of outdoor air being heated from 38 degrees to 87 degrees, resulting in a heating capacity output of 124,500 btu/hour. The compressor was operating at approximately 80%. The ORNL modeling predicts an output of 142,000 btus/hour at 100% compressor capacity.

Revolution Heat Pump Performance Analysis at ORNL CHP Lab

Time	OA Temp	Airflow (cfm)	Entering Coil Temp	Leaving Coil Temp	Heating BTUs Delivered	Compressor HZ	Compressor % Full Capacity	Total KW Input[3]	BTUs Delivered per KW Input	Energy Cost[4] per million btus
100% Outdoor air 11/26/2004										
9:30 AM	47	2411	49.8	92.4	110925	35	58%	7.2	15323	$4.57
10:15 PM	40	2400	40.9	83.2	109642	41.4	69%	7.9	13905	$5.03
10:35 PM	38.7	2402	39.1	86	121666	46.9	78%	8.8	13771	$5.08
10:45 PM	38.5	2389	38.5	86.8	124620	48	80%	9.3	13386	$5.23
0% Outdoor air 11/27/2004										
8:46 AM	41	2407	70.6	99.3	74607	25.6	43%	6.5	11478	$6.10
40% Outdoor air										
9:42 AM	46	2399	68.8	99.5	79541	24.6	41%	6.7	11872	$5.90
60% Outdoor air 11/28/2004										
7:30 AM	43.1	2411	59.2	93.8	90094	29	48%	6.8	13249	$5.28
100% Outdoor air with flow increased by 12.5 % to 2700 cfm 11/28/2004										
8:13 AM	44	2697	49.9	83.9	99034	29.6	49%	6.2	15867	$4.41
8:25:00 AM [1]	44	2700	47.8	82.7	101768	32.9	55%	6.5	15707	$4.46
8:30:00 AM [1]	44.3	2706	47.1	85.1	111054	35.3	59%	6.8	16395	$4.27
8:40:00 AM [1]	44.4	2721	46.8	86.5	116666	36.9	62%	7.1	16528	$4.24
8:58:00 AM [2]	45.1	2680	46.9	88	118960	37.7	63%	7.1	16696	$4.19
50% Outdoor air with flow back to 2400 cfm and 75 deg set point 12/3/2004										
9:05 PM	36.8	2408	61.8	91.6	77499	27.5	46%	6.7	11571	$6.05
9:41 PM	36.1	2406	61.8	87.1	65742	22	37%	5.8	11363	$6.16
10:22 PM	35	2400	52.5	94.8	109642	50	83%	10.3	10686	$6.55
11:52 PM	34	2400	53.4	90.6	96422	36	60%	7.6	12687	$5.52
30% Outdoor air, 2400 cfm and 75 deg set point 12/5/2004										
8:40 AM	36	2413	71.2	98.1	70102	24	40%	5.6	12518	$5.59
50% Outdoor air, 2400 cfm and 75 deg set point 12/5/2004										
9:06 AM	38.3	2395	64	90.6	68804	24.2	40%	5.5	12510	$5.60
9:06 AM	38.4	2402	63.2	91.6	73674	25.87	43%	6.05	12178	$5.75
50% Outdoor air, 2400 cfm and 75 deg set point 12/12/2004										
8:30 AM	39.8	2385	62.8	91.9	74956	23.9	40%	6.2	12090	$5.79
50% Outdoor air, 2400 cfm and 75 deg set point 12/14/2004										
8:20 AM	30.7	2444	57.9	100	111124	53	88%	11.1	10011	$6.99
10% Outdoor air, 2400 cfm and 75 deg set point 12/20/2004										
8:28 AM	19.9	2415	61	102.4	107979	50	83%	10.73	10063	$6.96
8:41 AM	22	2413	61.5	102.7	107369	49.3	82%	10.43	10294	$6.80
10% Outdoor air, 2400 cfm and 75 deg set point 12/20/2004										
8:53 AM	38.2	2413	71.5	105.5	88605	29.3	49%	7.4	11974	$5.85
Note: Fan KW increases due to flow increase and impacts the btu/kw values										
50% Outdoor air, 3000 cfm and 75 deg set point 1/30/2005										
11:33 AM	40.7	2999	64.2	82.9	60568	19.9	33%	4.8	12618	$5.55
30% Outdoor air, 3000 cfm and 75 deg set point 2/10/2005										
4:45 PM	36.1	3073	60.2	85.7	84630	28.5	48%	6.6 5.2	12823 16275	$5.46
6:05 PM	35	3021	60	85.3	82546	29.7	50%	6.4 5.1	12898 16185	$5.43
0% Outdoor air, 3000 cfm and 75 deg set point (space temp closed damper) 2/11/2005										
8:00 PM	28	3030	63.8	89.9	85410	40.2	67%	8.3 6.9	10290 12378	$6.80
8:23 PM	29.8	3020	64.4	91.1	87085	36	60%	8.3 6.9	10492 12621	$6.67
50% Outdoor air, 3000 cfm and 75 deg set point 2/11/2005										
12:50 PM	43	2955	63.3	81	56488	19.9	33%	5.2	10863	$6.44
50% Outdoor air, 3000 cfm and 75 deg set point 2/13/2005										
7:30 AM	41.9	3019	62.8	82.5	64232	19.9	33%	5.5	11679	$5.99
70% Outdoor air, 3000 cfm and 75 deg set point 2/13/2005										
7:45 AM	42	3031	55.5	77.2	71035	23.9	40%	4.96	14321	$4.89
7:51 AM	42	3029	54.3	78.8	80147	25.9	43%	5.77	13890	$5.04
7:57 AM	42	3027	53.8	79.7	84671	26.3	44%	5.98	14159	$4.94
80% Outdoor air, 3000 cfm and 75 deg set point 2/13/2005										
8:35 AM	42.9	3002	50.8	77.1	85269	26.3	44%	5.88	14501	$4.83
8:45 AM	43	3002	51	76.5	82675	25.6	43%	5.58	14816	$4.72
100% Outdoor air, 3000 cfm and 75 deg set point 2/13/2005										
9:35 AM	43	3006	45.4	79.9	112004	36.7	61%	7.2	15556	$4.50
9:45 AM	43	2997	45.2	83.1	122673	41	68%	7.6	16141	$4.34
9:55 AM	43	3005	45	85.6	131763	44.3	74%	8.9	14805	$4.73
50% Outdoor air, 3000 cfm and 75 deg set point 2/13/2005										
7:45 AM	38.4	3018	61.7	86.5	80834	28.4	47%	6.3	12831	$5.46
50% Outdoor air, 3000 cfm and 75 deg set point 3/2/2005										
7:47 AM	27.4	3005	56.7	91.6	113264	49.6	83%	10	11326	$6.18
8:01 AM	28.1	3002	58	92.8	112827	48.3	81%	9.7	11632	$6.02
8:21 AM	28.4	3007	58.7	92.9	111067	47.8	80%	8.62	12885	$5.43
70% Outdoor air, 3000 cfm and 75 deg set point 3/2/2005										
9:02 AM	30.9	3005	47.3	89.1	135658	60	100%	11.2	12112	$5.78
9:14 AM	31.1	3007	47.4	89.3	136073	60	100%	11.2	12149	$5.76
20% Outdoor air, 3000 cfm and 75 deg set point 3/2/2005										
9:52 AM	37.1	3005	71.9	91.8	64583	22.6	38%	5.5	11742	$5.96
40% Outdoor air, 3000 cfm and 75 deg set point 3/2/2005										
10:52 AM	38	3005	67	87	64908	22.6	38%	5.9	11001	$6.36
								Average	14515	$5.52

1. Raised space set point to 78 deg to increase compressor HZ output and to eliminate compressor cycling
2. Steady state condition, no cycling - good data point
3. The KW shown corrects for 5% inverter inefficiency
4. The cost of operation is based on an electrical cost of $.07/KWH

Figure 6: Heat pump operation field test data from the ORNL CHP lab installation site

Contrasting Indirect Gas Heating and the IADR Heat Pump

Two distinct advantages are offered by the heat pump option, compared to indirect gas fired heating (which the IADR also can provide). Both were documented as part of this research. The first advantage is the stability of the delivered air temperature from the system. Figure 7 shows the stability of the supply air leaving the IADR when in heat pump mode versus the temperature fluctuation associated with a common gas fired furnace. This figure shows the indirect gas fired heater operating with minimal outdoor air and thereby under the best possible conditions for temperature stability. Had a higher outdoor air percentage been involved, two stages if heat would have been required and the temperature being delivered would have fluctuated far more. The stability of the delivered temperature associated with the heat pump is independent of the outdoor air percentage due to the exceptional control capabilities offered by the variable speed compressor.

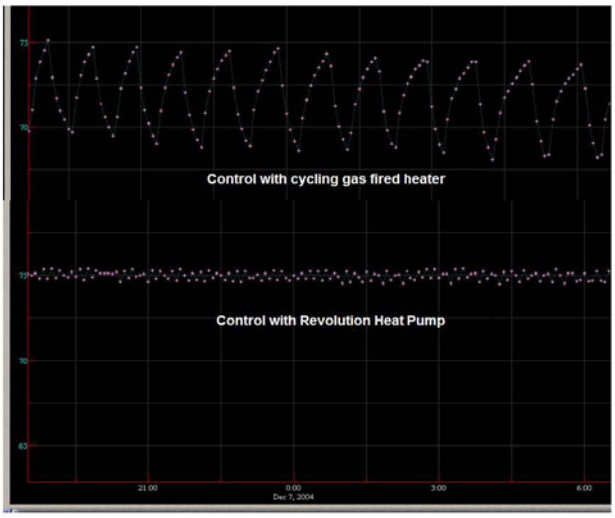

Figure 7: Field data showing the improved stability of the supply air temperature associated with the heat pump approach as compared to a typical indirect gas fired heater.

The second advantage is one of lower cost of operation. This is particularly true at the moment where natural gas prices are at record levels and the higher cost of primary energy has not yet been fully reflected in electric rates. As shown by figure 6, the average cost for creating 1,000,000 btus of heating output using the IADR heat pump option as between $5.50 and $6.00 at the Oak Ridge site assuming and electrical cost of $.07/KWH. Indirect fired gas, assuming a 78% efficient heat exchanger and gas costing $8/million BTU results in a delivered cost of approximately $10.2/million BTU.

Hot and humid climates have, by definition, relatively moderate cooling seasons. As a result, they are excellent candidates for the use of this heat pump integration since the heating loads can be easily accommodated while offering the end user the opportunity for significant energy savings. It is very common for buildings constructed in hot and humid climates to be heated with electric resistance heat. Using the heat pump approach reduces the cost of heating from what would be $20.5/million BTU to $6/million BTU, a 71% reduction. As shown by the Pharmacy example discussed previously, using the electric resistance heating option will result in very high heating costs despite the moderate heating climate.

Managing the Defrost Cycle

One of the main barriers to heat pump use, especially where high outdoor air percentages are required is the need for defrost cycles. When operating in the heating mode, the heat pump essentially "flips" the normal cooling cycle so that the outdoor coil acts as the evaporator and the indoor coil becomes the condenser. As the outdoor coil cools the outdoor air, the coil surface temperature frequently drops below 32° F.. If the outdoor dew point is above the coil surface temperature, moisture in the outdoor will be condensed and frost will begin to form. As the frost builds, airflow across the coil will slowly decrease while the frost begins to degrade the transfer characteristics of the coil. The net result is less heating capacity being available and the need for the compressor to work harder to meet the desired condition. Therefore, this frost formation must be carefully managed and removed before a significant degradation in performance occurs (see Figure 8).

The elimination of this frost formation is easily done. By switching back to "cooling mode" through the activation of a "reversing valve" the outdoor coil once again becomes the condensing coil, heats up and quickly melts the frost that has formed. The problem during defrost occurs at the indoor coil. When in defrost mode, the indoor coil cools the supply air to very low temperatures which is problematic, especially if outdoor air is being delivered by the system. As a result, most heat pump systems currently rely on inefficient electric resistance heat to operated during the defrost cycle to isolate the occupied space from the cold air leaving the coil.

Figure 8: Photo of outdoor coil of the IADR installed at the ORNL site just before the defrost mode is initiated

The IADR incorporates the capability of using the gas fired regeneration burner and the variable speed active desiccant wheel to provide an effective indirect gas fired heating source. A novel approach was devised to anticipate the need for a defrost cycle then bring on the indirect fired gas heat for a short duration to maintain an acceptable supply air temperature. In this way, the defrost control algorithm optimized as part of this research was used to isolate the space from the cold air leaving the indoor coil during the defrost mode.

Figure 9 shows how this control methodology functioned. In this figure the temperature leaving the indoor coil, the supply temperature to the space and the temperature entering the regeneration site of the active desiccant wheel are shown. The increase in the temperature entering the desiccant wheel reflects the burner being initiated. When the burner and regeneration fan are not energized, the temperature shown reflects the internal system temperature since dampers are closed. Outdoor air is used for regeneration of the desiccant wheel. This figure shows how the leaving temperature from the coil becomes extremely cold during a typical defrost cycle (approximately 34°d F) and how the initiation of the gas burner isolates this from the space air supplied at 68° F not 34.

This graphic also shows the typical duration of a well designed defrost cycle. As shown, the defrost cycle only involved a 10 minute time frame. One optimization that was incorporated as a result of this data was to better anticipate the defrost cycle. In doing so the gas burner would be initiated several minutes earlier so that the supply air temperature would remain even more stable.

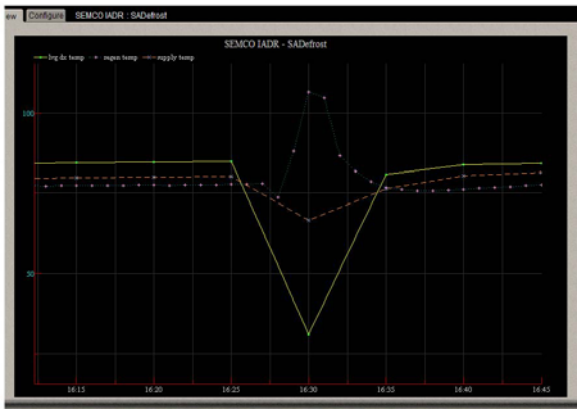

Figure 9: Data showing a typical defrost cycle and how the gas fired heating capability is used to provide a consistent supply air temperature despite the extremely cold air leaving the indoor coil.

A second optimization that was incorporated into future systems was an increase in the regeneration heater capacity so that it was sufficient to provide a consistent supply air temperature even during extreme days. This is discussed further by the technical article prepared for presentation at the 2005 ASME International Mechanical Engineering Congress and Exhibition being held in Orlando entitled "Performance Analysis of Integrated Rooftop with Heat Pump During the Heating Mode", see the reference section.

Optimizing Performance with Advanced DDC Control Algorithms

It would not be possible to operate the heat pump cycle integrated into the IADR system without proven, advanced control algorithms. These control algorithms far exceed the capacity of standard, prepackaged control systems. As a result, a significant portion of the research involved determined the best way to control the heat pump cycle, how to manage the defrost cycle and which control state points are needed.

Parameters that were evaluated as part of the defrost algorithm include outdoor air ambient temperature, outdoor dew point, pressure loss across the outdoor coil, outdoor air coil suction temperature, outdoor air coil suction pressure, minimum defrost time and minimum time between defrost cycles. By monitoring these parameters carefully and having the unique control flexibility offered by the variable speed compressor, an effective defrost cycle was optimized to provide the maximum heating output with the minimum amount of time operated in the defrost mode.

This feature is critical to objective of using the IADR as a high outdoor air percentage unit (often at 100% outdoor air) in both moderate and hot and humid climates. Also, by minimizing the amount of time in the defrost cycle, the significant decrease in cost of operation over even gas fired systems is recognized which quickly justifies the added cost associated with advanced controls.

Conclusions and Recommended Future Work

These research/demonstration installations involving the integrated vapor compression – active desiccant hybrid system (IADR) with heat pump integration were successful. All original objectives were met, the measured performance matched or exceeded the modeled expectations and all end users are very satisfied with the results. Attractive heating costs relative to either gas or electric resistance heating were documented as a result of high system operating efficiency.

Owners applying this technology could expect to reduce the cost associated with heating by approximately 40% and 71% compared to indirect gas and electric resistance heating respectively.

This design approach will be duplicated and implemented as part of a much larger, newly constructed high school located in Georgia and scheduled to be completed in 2006. This project will apply numerous IADR systems which include the heat pump option. These IARD systems will be applied as both dedicated outdoor air systems and complete VAV systems. This opportunity will allow the performance of the IADR and the integrated heat pump cycle to be further optimized since all systems will be equipped with instrumentation and data trending. Four of the systems will also be combined with on-site power generation to form an effective CHP site, using the heat of rejection from the engine to regenerate the active desiccant wheels. This heat will also be used for space heating with the heat pump being used for back-up heat as needed.

Further work that would be highly advantageous would be additional demonstration sites located in extreme climates where the heat pump option would satisfy the vast majority of the heating hours with the integral indirect gas capability handling the more infrequent extreme conditions.

References

1. Fischer, J., and J. Sand, **ORNL/SUB/01/4000010402**, Desiccant-Based Combined Systems: Integrated Active Desiccant Rooftop Hybrid System Development and Testing, August 2004.
2. ANSI/ARI, 2000, "Commercial and Industrial Unitary Air-Conditioning and Heat Pump Equipment," Standard 340/360, Air Conditioning & Refrigeration Institute, Arlington, VA
3. ASHRAE, 2001, "Ventilation for Acceptable Indoor Air Quality," Standard 62-2001, American Society of Heating, Refrigerating, and Air-Conditioning Engineers, Atlanta, GA.
4. ACEE, 2004, "Consensus Agreement on Air Conditioner Efficiency Standards Reached: Will Avoid Need for Twenty-Five Power Plants,: American Council for Energy Efficient Economy, Washington, DC.
5. Copeland Application Engineering Bulletin, 2001, "Application Guidelines for ZR90K3 to ZR19M3 and ZR250KC to ZR300KC Copeland Scroll Compressors," AE 4-1316, Emerson, St. Louis, Missouri.
6. Petrov, A.., et al, "Performance Analysis of Integrated Active Desiccant Rooftop Air-Conditioning System Operating in the Heating Mode," IMECE 2005-79238, ASME, Orlando, Nov. 5-11, 2005 (in press).

3.4b Industry Partnerships – Field Verification Installations of New Product Developments

Jim Sand and Ed Vineyard
Engineering Science & Technology Division
Oak Ridge National Laboratory
Oak Ridge, TN 37831-6070
(865) 574-5819, E-mail: sandjr@ornl.gov

DOE Technology Development Manager: Patricia Hoffman
(202) 586-6074, (202) 586-7114 (Fax)
E-mail: Patricia.Hoffman@hq.doe.gov

Objective

- The objective of this work is to demonstrate and document the energy saving and improved performance features of the integrated, active-desiccant HVAC system products developed as a result of DOE sponsored research through installation and monitoring of field units in several demanding field applications not adequately served by current, conventional air conditioning systems.

- Characterize and establish the performance capabilities of the SEMCO *Revolution*™ product and the Trane Co CDQ™ desiccant air conditioning systems in field trial, performance verification sites.

Approach

- Demonstrate and characterize the performance capabilities, IAQ benefits and relative energy consumption performance of the SEMCO *Revolution*™ integrated active desiccant units (IADRs) in several high profile, national account installations where shortcomings of a conventional AC installation were seen. Installations in a nationally recognized movie theater, school, resort hotel, and big box retail store are sought.

- Installation and monitoring of four to six Trane Co. *CDQ*™ field units in several demanding field applications not adequately served by current, conventional air conditioning systems.

Accomplishments

- Successful SEMCO retrofit installation and side-by-side comparison with conventional rooftop systems demonstrated at a CineMark movie theater in Plano, Texas.

- Successful retrofit installation of a SEMCO IADR system on a elementary school that had IAQ problems and poor humidity control in Cobb County Georgia, resulting in correction and solution of previous IAQ, mold, mildew, and humidity problems.

- Extensive laboratory testing and system performance monitoring that resulted in system hardware modifications and selection of a heat pump defrost algorithm.

- Three filed installation of the Trane CDQ™ desiccant assisted air conditioning systems in a document achieving building in Florida and two hospital operating suites with demanding humidity control requirements.

Future Direction

- Integration of these active desiccant products with distributed electric regeneration systems to produce a Integrated Energy system CHP product.

- Further development and research on the possibility of using the desiccant wheel thermal regeneration system as a supplemental heat source and as a product convenience feature for cold weather heating.

Introduction

The U. S. Department of Energy (DOE) through programs administered by its national laboratories is committed to providing building heating, ventilating, and air conditioning industry consumers with an array of clean, reliable, and affordable Thermally Activated Technologies (TATs) that will increase the efficiency and productivity of energy use, improve the security of energy resources, and enhance the quality of indoor environments. In combination with distributed power generation equipment, integreated TATs provide not only electricity but also heating and cooling resources (i.e., combined heat and power [CHP]), which dramatically improves overall energy efficiency and fuel utilization. As DOE's goal is to achieve 70% useful energy utilization from the input fuel energy, ORNL is interested in projects that show the efficiency and environmental benefits of desiccant TAT and the opportunites for integration with electricity production and useful thermal application. These activities are intended to encourage technical coordination between Federal research and private companies through cost-shared R&D proposals. This work also fosters the goal of education and outreach to key stakeholders through collaborative work with national accounts who are identified as industry leaders in application and end-use of efficient and effective new technologies.

Desiccant HVAC systems permit increased fresh air ventilation and active humidity control in modern commercial and institutional buildings. The commercially packaged rooftop units used to air condition most commercial buildings in the United States only dehumidify when the unit runs to remove heat. Under part-load conditions which constitute most of the cooling season, the sensible heat load is low resulting in short operating and cycle times for this equipment which reduces its dehumidification effectiveness. Combined-desiccant HVAC systems like those being developed through ORNL's collaborative work with industry are effective and efficient solutions for controlling indoor humidity and allowing adequate fresh air ventilation rates to insure acceptable indoor air quality. Field demonstration of packaged TAT rooftop systems with sensible-heat-ratio (SHR) performance ratios down to 0.25 with a maximum 25% cost adder in current market applications is one of the specific goals called for in DOE's Thermally Activated Technologies Roadmap.

Based upon a comprehensive initial marketing investigation and subsequent interest (expressed as willing pilot site participants) by numerous major national account companies, the integrated, active desiccant – high efficiency D.X. packaged rooftop system hybrid (IADR) system has been determined to fill a large market driven need. As a result of market feedback and a product introduction that took place in early 2004, additional field pilot testing and product performance verification is being aggressively pursued.

CineMark Theater Installation

The TinselTown CineMark theater in Plano, Texas brings some new, innovative features to the movie theater going public. "We learn how to improve things every time we build
a new theatre," said Randy Hester, Vice President of Marketing Communications for CineMark USA, inc. This new complex features stadium-style seating in every auditorium, offering a sixteen-inch height difference between each row, allowing greater visibility and enhanced, unobstructed sight lines to the screen. Cinemark currently operates 18 locations with stadium seating across the country.

The Tinseltown theatre in Plano also boasts twenty wall-to-wall screens, high-back lounger rocking chair seats with extra padding and cupholder armrests, as well as a forty-five inch clearance between rows for extra leg room, offering significantly more comfort for the patron.

Three separate concession areas featuring soft drinks, bottled water, popular candy, freshly popped popcorn, all-beef hot dogs, nachos, and dill pickles make getting movie treats as easy as ever. Four box offices with a total of eight computerized ticketing stations will help speed up service time and will also allow same-day and up to four-day advance ticket sales. Convenience, service and comfort for the movie patron are Cinemark's top priorities when building a new facility.

Seven Auditoriums on the each side of the theater complex were instrumented and one wing will be retrofitted with two SEMCO integrated preconditioning systems and the other wing served as a control. A sketch shown in Figure 1 depicts the general installation of the systems on this theater.

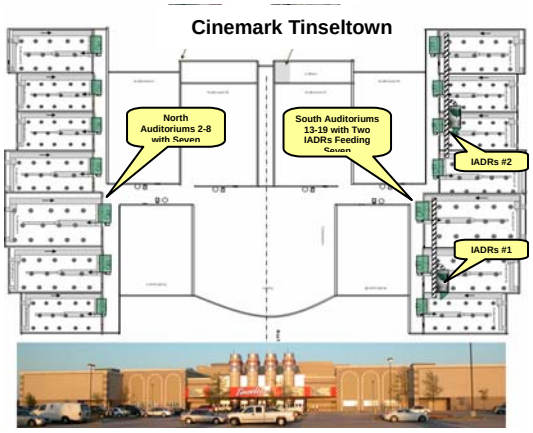

Figure 1: CineMark Tinseltown theater showing side-by-side installation of SEMCO IADR units and conventional rooftop units for field trial test.

The most obvious impact of this retrofit installation was active control of humidity which is synonymous with comfort. The absolute humidity level (dew point) impacts perspiration evaporation rate, which helps regulate the body's energy balance, skin moisture levels, and thermal sensation. As the dew point decreases, the rate of evaporation from the skin's surface increases as does the associated energy loss. This causes the skin temperature to drop, the body to feel cooler and the desire for a warmer space temperature to achieve comfort.

Theaters are a classical problem for rooftop air conditioning and humidity control. The auditoriums have no windows (with no solar gain), peak use is in the evening and night when humidity is more of a problem than heat, and people are densely populated requiring increased ventilation with a high latent and low sensible load. CineMark recognized these problems in the operation of this theater and agreed to participate in this field trial of the new SEMCO technology.

Extensive monitoring data from these theaters indicate that the SEMCO, desiccant system conditioned wing controls humidity below 60% RH in the south wing of the theater as opposed to 2961 occupied hours of greater than 60% RH in the conventionally conditioned wing. Operating costs for the SEMCO system in this application were 12% less than that for conventional rooftops capable of the same degree of humidity control. The extensive experimental data from this site was also used to develop a computer model simulation of these desiccant systems in similar applications.

Cobb County Elementary School

Students and teachers in one section of a Georgia elementary school are breathing clean, low-humidity air in their classrooms, thanks to an innovative natural gas-fired hybrid cooling and dehumidification system developed by SEMCO.

The 25-ton Integrated Active Desiccant Rooftop (IADR) system, also known as the SEMCO Revolution™ system, was installed as a retrofit at Timber Ridge Elementary School in Marietta, Georgia, outside Atlanta. It replaced one of the larger air-handling units in an area of the school experiencing serious indoor air quality problems. This 10,000-sq.-ft. area includes eight classrooms, four teacher rooms, four hallways, two restrooms, and several storage areas. All were previously cooled by a 30-ton conventional packaged variable air volume (VAV) system, Figure 2.

Figure 2: Old rooftop unit replaced with a SEMCO IADR on Timber Ridge School

For years, Timber Ridge staff complained about humidity, mold and other indoor air quality problems. To try and solve the humidity problem, the outdoor air louvers in the original HVAC units were sealed, and commercial dehumidifiers were brought in to combat mold growth on carpets and ceiling tiles. The problems continued. The Cobb County school district decided to install a new cooling and dehumidification system to serve the area of the school where humidity problems were severest. They obtained funding from the Oak Ridge National Laboratory in Oak Ridge, Tennessee, and the U.S. Department of Energy to field-test the IADR system. Researchers from the Georgia Tech Research Institute (GTRI) and Georgia State University studied the air quality inside the school both before and after the installation.

Each of the 19 zones in the study area were fitted with a variable volume/variable temperature (VVT) box. Each

box contains a DDC box controller and airflow monitor that communicates with both the space thermostat and the main control logic board installed inside the IADR system mounted on the roof. Return air enters the IADR system by way of a ceiling plenum on each floor of the two story school facility.

The system at Timber Ridge controls space humidity without the costly over-cooling followed by reheat required by conventional VAV systems. During cool, humid days, the IADR system is able to control moisture without the use of cooling. By contrast, humidity remained a problem in other areas of the school. Other benefits of the new cooling system include the ability to utilize relatively inexpensive gas for winter heating, and to operate in an energy-efficient "unoccupied mode" that still controls humidity when school is not in session. This mode protects against microbial problems at a low operating cost.

After a full year of operation, school officials pronounce the IADR system a success. "It's working great," says Gene Trull, Maintenance Supervisor for HVAC and Energy Manager for the Cobb County Public Schools. "We have experienced excellent IAQ and comfort conditions at all times. Most importantly, the teachers are very happy with the new system." Trull says the new technology "enables schools to provide a cost-effective way to meet the ventilation code requirements, control space humidity, and minimize operating costs."

Data resulting from the GTRI investigation confirmed a significant improvement in IAQ, humidity control and occupant comfort, according to their report. The investigators found the hybrid system was able to maintain both the space temperature and humidity as desired while delivering the outdoor air ventilation rate required by ASHRAE Standard 62. The level of improvement in indoor air quality and the overall Revolution system energy efficiency were measured and found to be very high.

Among the study findings were the following:

- Greatly improved IAQ
- Elimination of IAQ complaints in this section of the school
- Cost savings from removal of commercial dehumidifiers.
- Increased comfort that allowed occupants to raise thermostat settings by an average 2.4 degrees, to significantly reduce operating costs.
- Significant energy savings associated with the integrated total energy recovery module, the high efficient variable speed DX cooling section and novel active desiccant dehumidification approach.

A conventional system without energy recovery would need 50 tons of cooling capacity to supply the 47°F air required to reach desired humidity levels. Using total energy recovery, such a system would require 40 tons of cooling capacity. With the IADR, only 25 cooling tons are needed.

According to a cost analysis completed for the school district by the design engineer of record, "the IADR system was less expensive to install than other, less efficient options, most of them unable to deliver the required ventilation while maintaining the desired space humidity levels." See Table 1 below.

Summary of Results from Installed Cost Comparison

System Approach	Cost Per 10,000 sqft	Cost/Sqft	Operating Cost/Sqft	Humidity Control
Rooftop only (no recovery)	$121,140	$12.1	Very High	Poor
Rooftop and ERV	$170,590	$16.6	Fair	Fair
WS Heat Pump and DOAS	$142,655	$15.1	Very High	Best
WS Heat Pump and ERV	$130,055	$13.0	Fair	Fair
Revolution and VAV	$100,950	$10.2	Lowest	Best

Assumptions:
1) Cost of Revolution unit with FV provides the baseline analysis cost based on actual data from the Timber Ridge pilot site
2) Baseline case (Timber Ridge) is 10,000 square feet involving 19 zones, 8 classrooms, 2 hallways, 2 rest rooms, 4 teacher work rooms and 2 storage rooms
3) All other system cost estimates are base on 2002 Means data, reviewed by two separate mechanical consultants

Table 1: Relative cost of alternative school air conditioning systems

The study found the cost of a conventional rooftop cooling system, using 2002 prices, ranged from $16.60 per sq. ft. for a unit with energy recovery, to $12.10 per sq ft without energy recovery, while the Revolution and VAV cost $10.20 per sq ft.

Trane CDQ™ Sites

UCF Storage Facility The University of Central Florida (UCF) located in Orlando, FL operates an extension campus in Cocoa Florida, Figure 3. The Florida Solar Energy Center (FSEC), is a research institute of UCF and is co-located with the extension campus in Cocoa, FL. The high humidity of the Cocoa costal area makes storage of documents and equipment

problematic without humidity control. This desiccant/air-conditioning system was installed on May 27, 2005 to provide the air conditioning and humidity control of a pre-manufactured building used for FSEC equipment and document storage.

Figure 3: University of Central Florida document achieve being served by Trane CDQ™ desiccant system

The combined desiccant/AC system is a Precedent Model manufactured by Trane Co. rated at 3 tons, with a CDQ™ (Cool, Dry, Quiet) desiccant wheel curb attachment for enhanced humidity control. The CDQ™ combined desiccant/AC application has eliminated the need to use reheat for humidity control of the space. The Trane CDQ™ unit was installed to replace a Bryant 5 ton split system with a 3360 Watt reheat coil used for AC and humidity control of the space. For the 2005 Summer cooling season, both units are monitored for performance and energy use. The facility has been operated on one system (with the other off and isolated) for two week intervals, then the alternative system is used for two weeks. In this way, comparison data on the operation of the two systems has been obtained. A snapshot of the web-based, real time monitoring capability of this site is shown in Figure 4.

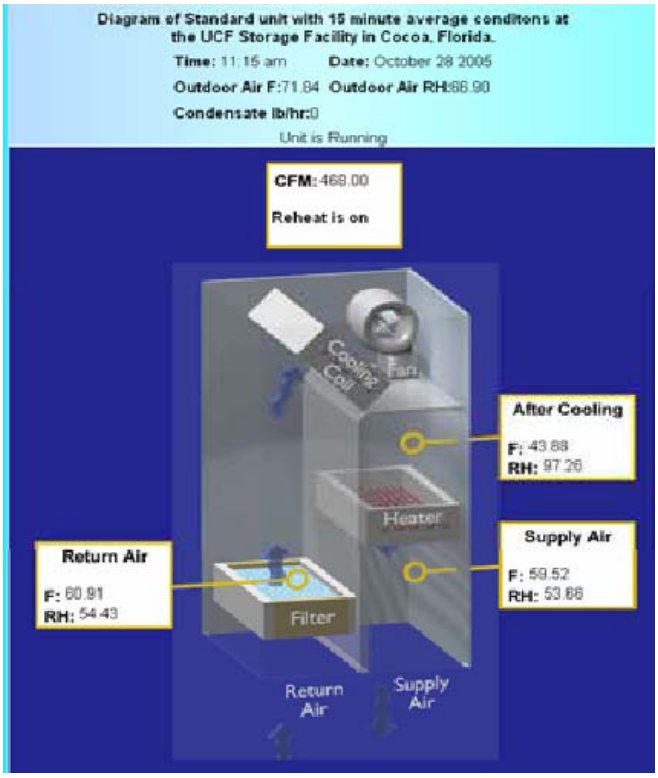

Figure 4: Snapshot of the continuous, real time, web-based monitoring graphic for the University of Central Florida Trane CDQ™ field installation site

Franklin Memorial Hospital

Franklin Memorial Hospital (FMH) in Farmington, Maine, is a 70-bed nonprofit community general hospital that for over seventy-five years has provided high-quality, cost-effective, patient-centered health care to west central Maine. Franklin Memorial Hospital is fully qualified and accredited to handle a broad range of medical, surgical, pediatric, obstetric, and gynecological procedures. The hospital also has specialized strengths in cardiology, ophthalmology, orthopedics, otolaryngology, rheumatology, internal medicine, urology, emergency care, and occupational health. FMH also includes the Western Maine Center for Heart Health, the Family Birthing Unit, and the Breast Care Center where services are available to all women, regardless of their ability to pay.

Nationally acclaimed as a healthcare leader and one of the best hospitals in New England, FMH was the 2003 Winner of the Carolyn Boone Lewis Living the Vision Award by the American Hospital Association (AHA), the1998 Runner Up for AHA's Foster G. McGaw Prize for excellence in community service, and was 1996

Runner Up for the AMA's NOVA Award for collaborative programs focused on community health. For more information on Franklin Memorial Hospital, go to its web site at http://www.fchn.org/fmh.

FMH is noted for innovation. This was Maine's first hospital to offer prenatal nurse home visits to all first-time parents, the first to perform laparoscopic gall-bladder surgery, and the first in the state to declare itself smoke-free. It was among the first in the state of Maine to offer heart healthy dining in its Healthy Heart Cafe. Recently, national attention has focused on the "Contract for Care," one of the Hospital's innovative programs to serve economically disadvantaged residents. The selection of the Trane CDQ™ Combined Desiccant/AC System to provide controlled temperature and humidity to its newly installed operating room addition and renovation is another example of Franklin Memorial Hospital's use of the latest technology to provide optimal service to its staff and patients.

The combined desiccant/AC system is a Custom Climate Changer™ Air Handling System manufactured by Trane Co. The air handling system is a complete packaged turn key unit. Unit cooling is produced by a Trane Intellipak™ air cooled scroll liquid chiller. A Trane CDQ™ (Cool, Dry, Quiet) desiccant wheel is used for enhanced humidity control. The unit can operate as a stand alone unit and operate off a back up generator if needed. When available the unit will also utilize central plant chilled water with a second cooling coil to precool the air. The system was designed by Harriman Associates of Auburn, ME. This unit treats return and outside air with approximately 30% of the total air flow from outside air. The air handling system serves the Hospital's Operating Rooms Suite, which contains four operating rooms used for various surgical procedures. A schematic representation of this desiccant system installation which is posted on the internet as a real time, continuous display of current operating conditions at this site is shown in Figure 5. The CDQ™ was designed to maintain the operating rooms at 62F, 50%RH by delivering 50F air at 40F dew point on design day. The unit can provide air drier and colder if necessary. It is expected this will save energy by reducing the amount of cooling needed, improving the cooling efficiency, and reducing the need for reheat to control humidity in the space.

Figure 5: Graphic Schematic of the Franklin Memorial Hospital CDQ™ desiccant installation continuously available on the internet

St. Vincent's Hospital

Saint Vincent's Hospital, located in Birmingham Alabama, serves the five county area surrounding Birmingham. This 338 bed acute care hospital is a member of Ascension Health, the nation's largest not-for-profit health system. St. Vincent's is a past winner of the Alabama Quality Award for Healthcare and has been named a McKesson Clinical Leader. Service areas include: Women's and Children's Services, Oncology, Cardiology, Orthopedics, Neurology and Surgical Services. St. Vincent's consistently ranks among the top 15 percent in inpatient satisfaction in the nation's largest patient satisfaction database, and has earned numerous awards for its community involvement and commitment to caring for the poor and vulnerable. Additional information about St. Vincent's is available at www.stv.org. Designated as Ascension Health's flagship digital hospital, St. Vincent's has been recognized nationally for its technology initiatives and has been named one of the country's 100 Most Wired Hospitals. St. Vincent's desiccant system is another example of its taking advantage of the latest technology for the benefit of its patients and staff. The combined desiccant/AC system is a M-Series Climate Changer Model manufactured by Trane Co., with a CDQ™ (Cool, Dry,

Quiet) desiccant wheel included for enhanced humidity control. The central chilled water plant utilizes a Trane CenTraVac™ (a water cooled centrifugal water chiller) to deliver 45 F chilled water to this air handler as well as other cooling equipment in the hospital. This system is shown schematically in Figure 6 which is a screen capture picture of the web-based continuous real time monitoring system employed by Trane at this site.

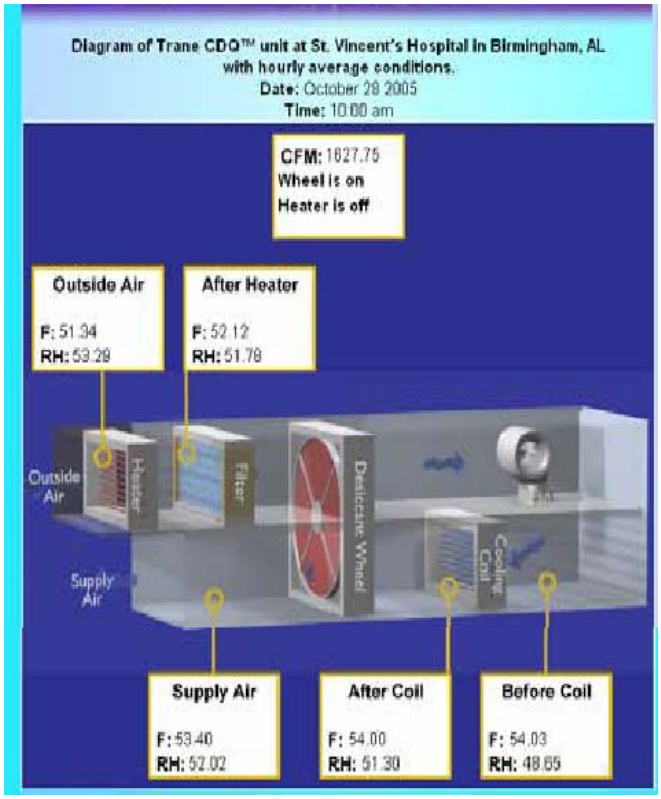

Figure 6: Screen picture of St. Vincent's Hospital CDQ™ desiccant web-based,continuous monitoring system

The system was designed by Whitaker & Rawson, Inc. and installed by Hardy Corporation of Birmingham. This unit operates on 100% outside air and feeds into the Hospital's Operating Rooms Suite. It is expected that the CDQ™ combined desiccant/AC application will prevent the need for auxiliary dehumidification equipment and prevent the need to lower the central plant chilled water temperature while still meeting dehumidification and outside air requirements. The 45F chilled water will be used to dehumidify the outside air down to a 42F dew point to keep the operating room at 62F and 50%RH at design day conditions. It is expected this will save energy by reducing the amount of cooling needed, improving the cooling efficiency, and reducing the need for reheat to control humidity in the space.

Conclusions

Highly visible and accessible field installations of newly developed desiccant products and systems like those described in this report help promote the awareness and industry acceptance of desiccant-based systems in the broad-based HVAC markets.

3.6c Zeotropic Working Fluids for Organic Rankine Cycle Efficiency Improvement

Solomon Labinov and Jim Sand
Engineering Science & Technology Division
Oak Ridge National Laboratory
Oak Ridge, TN 37831-6070
(865) 576-4908, E-mail: labinovsd@ornl.gov

DOE Technology Development Manager: Patricia Hoffman
(202) 586-6074, (202) 586-7114 (Fax), E-mail: Patricia.Hoffman@hq.doe.gov

Objective

- Analytically assess how much improvement is possible by using mixed, zeotropic working fluids for an organic Rankine thermal energy conversion cycle as compared with a pure, single-component, working fluid.
- Determine the most effective independent variables available for improving the efficiency of an Organic Rankine Cycle (ORC) being operated with a zeotropic, mixed working fluid.

Approach

- Conduct an internet and literature search on existing organic Rankine cycle applications and efficiencies.
- Develop a fundamental thermodynamic algorithm for calculating thermally activated Rankine cycle efficiencies from the physical properties of the working fluid.
- Tabulate and assess practical thermally activated Rankine cycle improvements made possible with mixed, zeotropic working fluids compared with pure, single-component working fluids.

Accomplishments

- A maximum thermal conversion efficiency was established for pure, single-component working fluids in an ORC assuming reasonable heat source and thermal sink conditions and practical heat exchanger, compressor and expansion turbine conditions.
- A calculation algorithm was developed for estimating the thermal conversion efficiency of ORC using practical assumptions and the thermophysical properties of the working fluids.
- It was determined that at least a 5-10% improvement in the overall thermal conversion efficiency of an ORC could be realized through the use of mixed, zeotropic working fluids.
- Operating conditions, working fluid compounds, and working fluid combinations and compositions to achieve optimal ORC efficiency were categorized.

Future Direction

- Bench-top laboratory experiments with breadboarded engine system
- Preliminary design and testing of heat exchanger components needed for a working model of this thermal conversion engine
- Assessment of the commercial/manufacturing feasibility of mixed zoetrope ORC engines

Introduction

Organic Rankine Cycles (ORCs) offer the potential for conversion of high or low quality thermal energy into useful mechanical or electrical energy and, thereby, improve the efficiency of integrated energy systems where the waste heat from some distributed electrical generation source must be gainfully applied for a useful building function. One problem with currently proposed and used ORCs is that their thermal conversion efficiency is very low for lower quality thermal sources like those available from internal combustion (IC) engine generator water jacket sources. Using zeotropic (non-azeotropic) blends of compounds for the working fluid in an ORC presents several opportunities for efficiency improvement.

Zeotropic working fluids in ORC applications can improve the efficiency by:

- The non-isothermal phase change of zeotropic working fluids (temperature glides) affords more efficient heat transfer with the temperature profiles of sensible heat transfer fluids used as the thermal sources and sinks for ORC thermal conversion equipment.

- The larger temperature glide (non-isothermal) temperature profile associated with the vaporization and condensation phase change of the zeotropic working fluid in an ORC give the overall cycle the ability to more effectively recuperate heat from the low pressure (condensation) side of the Rankine cycle to the high pressure (vaporization) side of the cycle.

- Automated, internal composition adjustments of a zeotropic working fluid blend in a ORC are possible through fractionation which would give the cycle the ability to work efficiently with a wide range of waste heat temperature quality levels. Working fluids with higher concentrations of higher boiling components could more efficiently deal with higher temperature waste heat streams, whereas zeotropic blends with high concentrations of lower boiling components would be needed to work well with cooler waste heat sources.

The advantages of the Organic Rankine Cycle over the water (steam) Rankine Cycle in case of low grade heat conversion to electricity are considered and analyzed. It has been shown that ORC efficiency directly depends on cycle parameters and the thermophysical properties of the organic working fluid. It has been established that mixtures of pure organic fluids with different thermophysical properties can be employed in the ORC to improve overall cycle efficiency. Practically acceptable limits of temperature and pressure have been found for the ORC.

Data on critical parameters and normal boiling temperatures of organic substances is presented. On the basis of this data, an initial evaluation has been made to determine which of these substances could be employed as efficient ORC working fluids. They are: n-butane, n-pentane, n-hexane, n-decane, benzene, Genetron® 245fa, siloxanes and mixtures of these pure substances. The efficiency and specific power of the ORC employing these substances and some of their mixtures have been determined. The Lee-Kessler-Plöcker equation of state has been applied jointly with the Labinov-Sand method of binary interaction coefficient determination to calculate thermophysical properties of ORC working fluids [1].

The ORC employs organic compounds (halocarbons, for example) in capacity of a working fluid instead of water in a thermally driven, turbine power conversion cycle where the working fluid is alternately heated and evaporated or cooled and condensed. So the name "organic cycle" refers to the chemical composition of working fluids which includes the element carbon or carbon chemically combined with hydrogen. ORCs began to be studied and applied as energy conversion engines in the middle of the last century to utilize low grade heat. The sources of low grade heat where ORCs were used include: geothermal waters, solar energy from liquid and vapor collectors, industrial waste heat, biomass combustion, etc. The important feature of these heat sources is the low temperature of a heating media - from 70 to 350° C, which means that the working fluid cannot be heated above 330º C (600 K). Below this temperature, the Brayton cycle gas-turbine is unable to operate practically because the turbine does not produce enough power to drive the compressor required for the cycle.

The water/steam Rankine Cycle is used to generate electricity in many utility power stations. Superheated steam is generated in a boiler, and then expanded in a steam turbine. The turbine drives a generator to convert the mechanical work into electricity. The remaining steam is then condensed and recycled as feedwater back to the boiler. A disadvantage of water/steam working

fluid mixture is that superheated steam has to be used prior to turbine expansion, otherwise the moisture content after expansion resulting in liquid water formation, which would erode the turbine blades . Organic substances, that can be used below a temperature of 400^{o} C, do not need to be superheated. For many organic compounds superheating does result in a higher efficiency of the cycle .

ORCs can be applied for low temperature waste heat recovery (industry), efficiency improvement in power stations, and recovery of geothermal and solar heat. Small scale ORCs have been used commercially or as pilot plants in the last two decades. It is estimated that about 30 commercial ORC plants were built before 1984 with an output of 100 kW. Several organic compounds have been used in ORCs (e.g. CFCs, halocarbons, iso-pentane or ammonia) to match the temperature of the available waste heat source. The efficiency of ORC is estimated to be between 10 and 30%, depending on operating temperature levels. For many sites no suitable use is available for low temperature/low quality waste heat, hence upgrading by the use of a heat pump (or heat transformer) or the ORC is a good candidate for energy recovery. However, the maximum temperature of ambient cooled heat pumps is still limited, making the ORC a good technology for heat recovery for base load applications in the range of 150º to 200^{o} C, if no other use for the waste heat is available on site. To minimize costs and energy losses, it is necessary to locate the ORC near the heat source, and to have a large amount of available waste heat at stationary conditions. In a Rankine power generation cycle there is also a need to condense the working vapor after expansion and cooling. in ORCs. Therefore, a cooling medium has to be available on site. In a Rankine power generation cycle there is also a need to condense the working vapor. Therefore, a cooling medium, usually ambient air or a cooling tower should be available on site.

Currently ORCs still have high capital costs, and, therefore, other applications of waste heat utilization will generally be more economically attractive. The planned ORC at Hydro Agri in the Netherlands (fertilizer production) has not yet been implemented due to the appeal and convenience of other less capital intensive applications for the waste heat. The ORC would have been installed to generate electricity from a waste heat stream of 190^{o}C (cooling to 150^{o} C) with isopentane as the working medium, an installed capacity of 2.6MWe was estimated which would have resulted in a savings of about 83 TJ annually[2].

At present time, there are several dozen low power energy plants (0.5 - 5 MWe) based on the ORC [2-8]. A typical example of such a plant is the 1 MWe power plant operating in the City of Altheim (Austria) and using geothermal water as the source of heat [9]. Despite the fact that three new areas of ORC application have emerged -- in the capacity of a bottoming cycle for a molten carbonate fuel cell power plant, CHP system, or distributed power source -- ORC power plants have not been widely adopted. [10-14] Several, unresolved problems account for this. They are: the selection of an optimal working fluid, the complete hermetic sealing of the working fluid circuit, and the poor heat exchange process in the heater, recuperator and cooler used for the cycle. The problem related to selection of a working fluid is the most important and difficult to solve. Because of this, the first part of this Project is devoted to analyzing and evaluating the basic aspects of optimal working fluid selection.

Thermophysical properties of selected organic working fluids

The selection of a working fluid for the ORC depends largely on how well the thermophysical properties of a fluid correspond to the conditions of its operation in the cycle. The ORC is a closed cycle where heat supply in a main heater, heat transfer in a recuperator and heat removal in a cooler are carried out with the help of a surface heat exchanger. To provide for practically acceptable dimensions of these units, the log mean temperature difference (LMTD) has to be within the limits of 10-30 K. According to the ORC operational conditions, the temperature of heating agent must be within the range of 70 -350^{0} C, and the temperature of cooling agent (ambient air or water) equals 25 ^{0} C. So, the maximum temperature of working fluid in the ORC cannot exceed 600 K, and the minimum temperature cannot be lower than 310 K.

Using the data in Table 1 to see how themophysical properties of working fluids (hydrocarbon alkanes) correspond to the operational conditions of ORC [15].

Table 1. Critical parameters and heat of evaporation for hydrocarbon alkanes

Substance	Critical pressure Pc , atm	Critical temperature Tc, K	Normal Boiling Temperature (NBP) Tb, K	Heat of vaporization at NBP Qv, kJ/kg
Water	225.15	647.4	373.15	2250
Methane	46.95	190.55	111.68	511
Ethane	49.76	305.43	184.52	490
n-Propane	43.33	369.82	231	425
n-Butane	38.71	425.16	272.65	385
n-Pentane	34.35	469.65	309.22	357
n-Hexane	30.72	507.35	341.89	335
n-Heptane	27.90	540.15	371.57	317
n-Octane	25.35	568.76	398.815	302
n-Nonane	23.33	594.56	423.948	288
n-Decane	21.45	617.5	447.22	277

As indicated in Table 1, all substances having a molecular weight below that of n-pentane exhibit a normal boiling point temperature below 310 K. To employ these substances as working fluids in an ORC, it is necessary to have the pressure of condensation (the cycle minimum pressure) above 1 atm with ambient heat rejection. To satisfy this condition, the pressure before the turbine must be increased to provide sufficiently useful output power during turbine expansion. So, substances with molecular weights less than n-pentane can be only employed in the ORC which operates in the area of high pressure. High pressure energy plants usually have a low ratio of power density to equipment weight, high cost, and circuit sealing problems.

Substances with molecular weight higher than that of n-pentane have normal boiling temperatures above that usually required for most ORC applications, what means that the pressure of condensation (the cycle minimum pressure) would have to be less than 1 atm to achieve a reasonable power output from turbine expansion. Plants which operate under lower pressure have problem of ambient air leaking into the system and a resulting fire and explosion hazard with hydrocarbon working fluids.

Only one substance in the hydrocarbon alkane series shown in Table 1, n-pentane, has a boiling temperature within the limits established for the ORC. A similar regularity is seen in each homologous series of organic compounds, that is, each series has only one substance with boiling temperature within the established limits. Such substances in corresponding series are: n-pentyne (313 K), cyclopentane (319 K), ethyl alcohol (311 K), etc.

The data in Table 1 also allows evaluation of the influence of critical parameters on selecting substances as working fluids. The critical pressure of all members of the hydrocarbon alkane series shown is 5-10 times lower than that for water. But especially important is the fact that the heat of evaporation for all members of alkane homologous series at pressures under 1 atm is 4 - 8 time less than that of water. Therefore, heat required to change the phase state of common normal alkanes is much lower than that for water, which allows a reduction in the dimensions of the evaporator and a corresponding increase in the cycle efficiency.

For all organic substances, the next important feature related to the value for the latent heat of vaporization is the shape of the two-phase region on a temperature/entropy (T-S) plot. Diagrams showing these two-phase areas for alkanes and water are illustrated in Figure 1. From these figures, one can see that the two-phase state area for alkanes is much narrower than that for water, and the critical point is shifted in the direction of increased entropy. As a result of this configuration, the adiabatic process of isentropic expansion (S = const), which is started at any point on the saturated vapor line, terminates in an area indicating a vapor state for the alkane compounds. So, the process of working fluid expansion in the turbine for these substances does not lead to a mixed liquid/vapor phase after turbine expansion. In the case of water, the process of adiabatic expansion started at any point along the saturated vapor line ends up in a two-phase area at any final value of low pressure. To avoid this, the water Rankine cycle (steam cycle) turbine expansion step is usually initiated with highly superheated vapor. For the ORC, there is no need to superheat the vapor of working fluid.

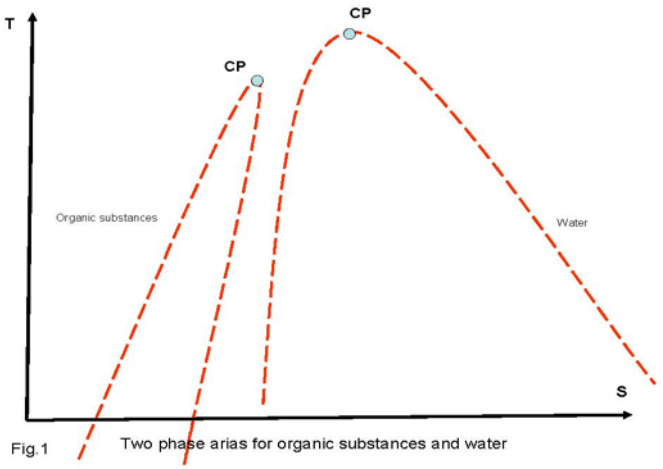

Fig.1 Two phase arias for organic substances and water

These conclusions made specifically for alkanes in Table 1 are true for any homologous series of hydrocarbons.

Organic Rankine cycle thermodynamic analysis

The typical ORCs for pure substances and mixtures are illustrated in Figure 2. As these diagrams show, all ORCs are able to recouperate heat internally in the cycle from the area of low-pressure working fluid to the area of the high-pressure working fluid prior to turbine expansion. However, pure substances cycles and cycles employing mixtures have different opportunities of heat recouperation. In the pure substance cycles, heat is transferred only from the low pressure vapor phase,heat transfer from the two-phase area of condensation being impossible because the isobar of condensation is parallel to S-axis. In the ORCs employing mixtures, heat can be transferred from both the low pressure vapor phase and two-phase condensation area because the condensation isobar is not isothermal and forms an angle with S-axis. In all cases, the heat transferred from the low-pressure working fluid is used to heat the liquid after compression and to provide for vaporization.

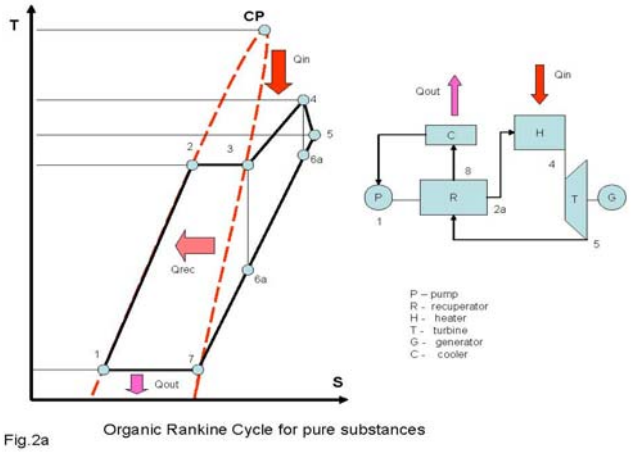

Fig.2a Organic Rankine Cycle for pure substances

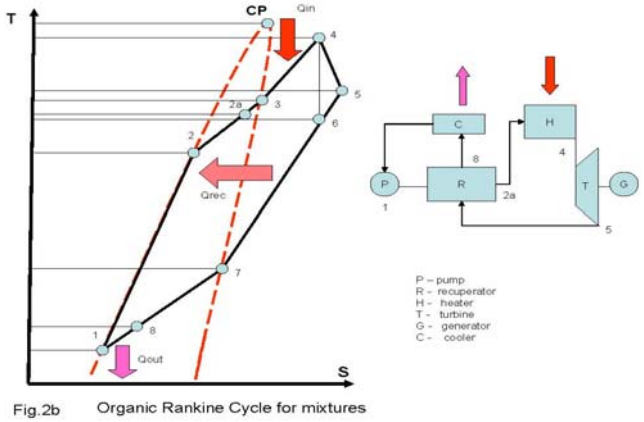

Fig.2b Organic Rankine Cycle for mixtures

ORC basic parameters, efficiency, and specific power depend on how the processes of expansion in the turbine and heat transfer in the recuperator are organized. To analyze these processes, the following basic thermodynamic equations have been used.

Power density,

$$\left(\frac{dH}{dP}\right)_S = \frac{R \cdot T}{\mu \cdot P} \qquad \textbf{(1)}$$

where: H is enthalpy,
P is pressure,
R is universal gas constant,
T is temperature,
μ is molecular weight,
S is entropy,

or, using finite differences and average values,

$$\left(\frac{\Delta H}{\Delta P}\right)_S = \frac{R \cdot T_{av}}{\mu \cdot P_{av}} \qquad \textbf{(2)}$$

Equation 2 shows that the enthalpy change available from an adiabatic turbine expansion process like that involved in an ORC is directly proportional to the working fluid temperature before expansion, T_{av} , and inversely proportional to the working fluid molecular weight, μ, and pressure after expansion, P_{av} . So, to produce maximum power density an ORC working fluid with the smallest molecular weight should be chosen with a maximum temperature before the turbine as well as a minimum pressure after the turbine (condensation pressure).

Efficiency

The ORC efficiency depends on the degree of regeneration. The heat transfer in the ORC is carried out by surface heat exchangers. The surface area , and, finally, the size, weight and cost of a heat exchanger ,with prescribed heat flow, depends on total heat transfer coefficient

$$k = \frac{\alpha 1 \cdot \alpha 2}{\alpha 1 + \alpha 2} \qquad \textbf{(3)}$$

where: α1 is the coefficient of heat transfer from A wall to a heated substance,. α2 is the coefficient of heat transfer from a heating substance to a wall.

The range of $\alpha 1$ and $\alpha 2$ numerical values are in Figure 3(16). From this figure, one can see that the heat transfer coefficient of a gas is several orders of magnitude less than that of a liquid or two-phase medium. The heated substances in the ORC recuperator are liquid and two-phase fluid streams which have larger heat transfer coefficients. The heating substances in the ORC are: either a gas (pure substance) or a gas and two-phase substance (mixture). The total heat transfer coefficient is always lower than the lowest heat transfer coefficient ($\alpha 1$, $\alpha 2$). Thus, for pure substances, the values of k are low (about 100-200 W/m^2 °K). For mixtures in the recuperator, heat exchange takes place between two-phase mediums , the value of k is about 10^3- 10^4 W/m^2 °K .

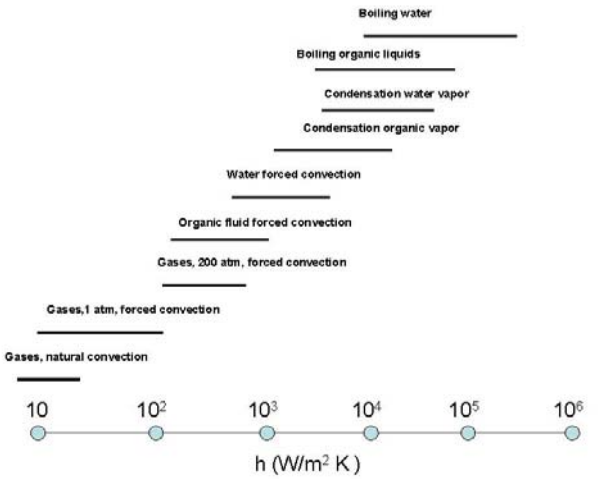

Heat exchanger coefficients for different substances

Fig. 3

When working fluids with larger molecular weights are employed, the pressure after the turbine are decreased to sub-atmospheric values (0.1- 0.01 atm), in order to reach high values of output power. When these sub-atmospheric pressures are used, the heat transfer coefficient which is dependent decreases abruptly on the low pressure side of the recuperator, and its size becomes practically unacceptable.

The considerations given above allow analysis and calculation of the working parameters of ORCs with different working fluids. In order to select the optimal working fluid, the calculations have been carried out for pure substances and mixtures as working fluids. Assumptions used for all the calculations are a turbine efficiency of 0.87, a recuperator efficiency of 0.7, and a cooling heat sink temperature of 290 K. The results for these cycle simulations are given in Tables 2 - 5.

Table 2. Parameters of ORCs with pure organic substances

Parameter	n-Decane	n-Decane	n-Heptane	n-Heptane	n-Pentane	n-Butane	Benzene	Siloxane MM
Tmax , K	600	600	600	600	600	600	550	510
Pmax,atm	10	10	10	10	10	45.6	41.5	17.8
Tmin , K	447	374	371	310	310	310	310	310
Pmin,atm	1	0.1	1	0.1	1	3.6	0.2	0.1
W,kJ/kg	56	120	88	180	125	195	212	107
EF	0.09	0.143	0.1	0.18	0.122	0.152	0.25	0.171
EFrec	0.132	0.217	0.165	0.267	0.195	0.289	0.283	0.274
EF_{CARNOT}	0.258	0.377	0.381	0.483	0.483	0.483	0.436	0.39
EFRC	0.349	0.379	0.262	0.372	0.252	0.314	0.573	0.438
EFRCrec	0.511	0.575	0.433	0.552	0.4	0.598	0.649	0.7

Table 3. Parameters of ORCs with organic subtances mixtures

Parameter	Decane 0.4 Heptane 0.6 (mol e %)	Decane 0.4 Heptane 0.6 (mole %)	Heptane 0.5 Propane 0.5 (mole %)	iso-Butane 0.56 iso-Pentane 0.44 (mole %)
Tmax , K	600	600	600	450
Pmax, atm	10	10	10	34
Tmin , K	389	318	300	310
Pmin , atm	1	0.1	1	5.7
W , kJ/kg	73	147	124.5	-
EF	0.09	0.151	0.121	0.157
EFrec	0.249	0.214	0.315	-
EF_{CARNOT}	0.358	0.47	0.5	0.31
EFRC	0.251	0.321	0.242	-
EFRCrec	0.695	0.455	0.63	0.5

Table 4. Parameters of ORCs with pure Halocarbons

Parameter	Genetron® 245fa (12)	HCFC-123	CFC-11
Tmax , K	425	425	425
Pmax , atm	32.13	19.6	19.7
Tmin , K	310	310	310
Pmin , atm	1.32	0.42	0.61
EF	0.162	0.146	0.137
EF_{CARNOT}	0.27	0.27	0.27
EFRC	0.6	0.54	0.51

Table 5. Parameters of ORCs with siloxane mixtures(17,18)

Parameter	Fluid 1	Fluid 2	Fluid 3	Fluid 4	Fluid 1	Fluid 1	Fluid 5	Fluid 5
Tmax, K	530	525	530	520	520	520	540	540
Pmax,atm	12.9	12.4	11.2	4.5	14.1	14.1	11.0	11.0
Tmin, K	300	300	300	300	310	325	300	325
Pmin,atm	0.04	0.03	0.02	0.01	0.07	0.16	0.03	0.11
W, kJ/kg	118	112	112	86	105	88	107	83
EF	0.168	0.167	0.168	0.135	0.162	0.145	0.153	0.128
EFrec	0.3	0.297	0.3	0.269	0.28	0.249	0.298	0.257
EF_{CARNOT}	0.434	0.428	0.434	0.423	0.403	0.398	0.444	0.398
EFRC	0.387	0.391	0.387	0.319	0.401	0.364	0.345	0.321
EFRCrec	0.691	0.693	0.691	0.634	0.7	0.625	0.671	0.635

The designations in Tables 1-5 are:

	W	is output power density,
	EF	is efficiency without recuperation,
	EFrec	is efficiency with recuperation,
	EF_{CARNOT}	is Carnot cycle efficiency,
	EFRC	is EF/EF_{CARNOT},
	EFRCrec	is $Efrec/EF_{CARNOT}$,
	Fluid 1	is MM(0.7)/MDM(0.3), (mole %)
	Fluid 2	is MM(0.5)/MDM(0.5), (mole %)
	Fluid 3	is MM(0.3)/MDM(0.7), (mole %)
	Fluid 4	is MM(0.3)/MD_2M(0.7), (mole %)
	Fluid 5	is MM(0.5)/MDM(0.25)/MD_2M(0.25), (mole %)
where:	MM	is $C_6H_{18}OSi_2$,
	MDM	is $C_8H_{24}O_2Si_3$,
	MD_2M	is $C_{10}H_{30}O_3Si_4$.

In Figures 4-6, the dependencies of calculated values of EFrec, Qrec, and Qrec/W on ORC recuperation rate for pure alkanes and their mixtures are shown. The results in Figures 4-6 and Tables 2-5confirm the theoretical analysis of ORC parameters presented earlier and allow quantitative recommendations for working fluid selection.

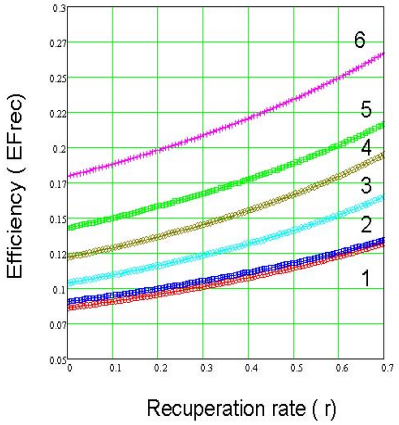

Efficiency versus recuperation rate for pure substances

1.Decane Pmax -10 atm, Pmin-1 atm, Tmax-600 K
2.Decane Pmax -15 atm, Pmin-1 atm, Tmax-600 K
3.Heptane Pmax -10 atm, Pmin-1 atm, Tmax-600 K
4.Pentane Pmax -10 atm, Pmin-1 atm, Tmax-600 K
5.Decane Pmax -10 atm, Pmin-0.1 atm, Tmax-600 K
6.Heptane Pmax -10 atm, Pmin-0.1 atm, Tmax-600 K

Fig 4a

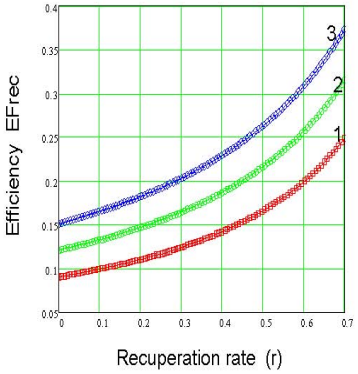

Efficiency versus recuperation rate for mixtures

1. Heptane 0.6/Decane 0.4 Pmax-10 atm, Pmin- 1 atm, T max 600 K
2. Heptane 0.6/Decane 0.4 Pmax-10 atm, Pmin- 0.1 atm, T max 600 K
3. Heptane 0.5/Pentane o.5 Pmax-10 atm, Pmin- 1 atm, T max 600 K

Fig. 4b

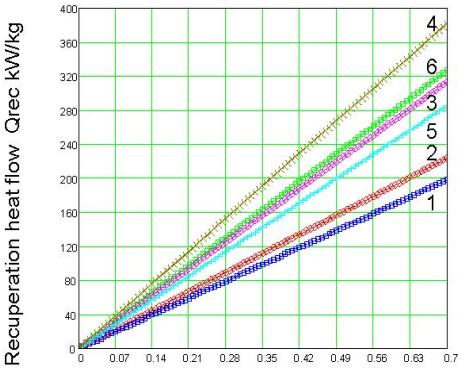

ORC recuperation heat flow for pure substances

1.Decane Pmax -10 atm, Pmin-1 atm, Tmax-600 K
2.Decane Pmax -15 atm, Pmin-1 atm, Tmax-600 K
3.Heptane Pmax -10 atm, Pmin-1 atm, Tmax-600 K
4.Pentane Pmax -10 atm, Pmin-1 atm, Tmax-600 K
5.Decane Pmax -10 atm, Pmin-0.1 atm, Tmax-600 K
6.Heptane Pmax -10 atm, Pmin-0.1 atm, Tmax-600 K

Fig. 5a

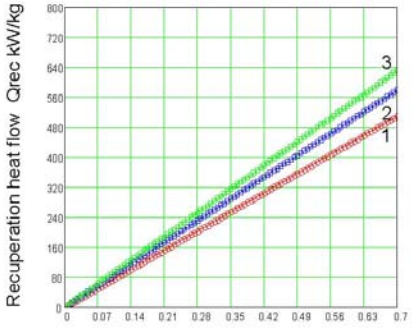

ORC recuperation heat flow versus recuperation rate for mixture

1.Heptane 0.6/Decane 0.4 Pmax-10 atm, Pmin- 1 atm, T max 600 K
2.Heptane 0.6/Decane 0.4 Pmax-10 atm, Pmin- 0.1 atm, T max 600 K
3.Heptane 0.5/Pentane 0.5 Pmax-10 atm, Pmin- 1 atm, T max 600 K

Fig. 5b

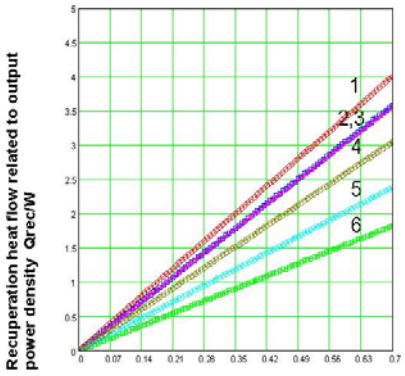

Recuperation heat flow related to output power density

1.Decane Pmax -10 atm, Pmin-1 atm, Tmax-600 K
2.Decane Pmax -15 atm, Pmin-1 atm, Tmax-600 K
3.Heptane Pmax -10 atm, Pmin-1 atm, Tmax-600 K
4.Pentane Pmax -10 atm, Pmin-1 atm, Tmax-600 K
5.Decane Pmax -10 atm, Pmin-0.1 atm, Tmax-600 K
6.Heptane Pmax -10 atm, Pmin-0.1 atm, Tmax-600 K

Fig. 6a

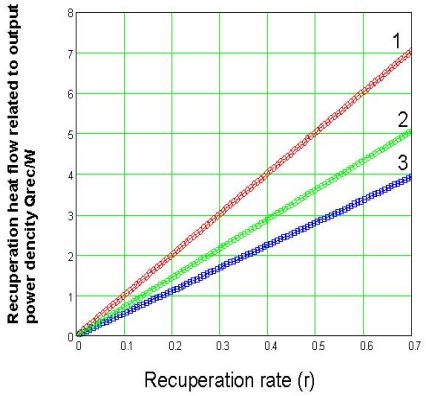

Recuperation heat flow related to output power density

1.Heptane 0.6/Decane 0.4 Pmax-10 atm, Pmin- 1 atm, T max 600 K
2.Heptane 0.6/Decane 0.4 Pmax-10 atm, Pmin- 0.1 atm, T max 600 K
3.Heptane 0.5/Pentane o.5 Pmax-10 atm, Pmin- 1 atm, T max 600 K

Fig. 6b

Conclusions

- To achieve the maximum value of output power density from an ORC operating with a pure working fluid, the following substances can be recommended: Genetron® 245fa, n-pentane, n-btane, benzene and Siloxane MM.
- To receive the highest efficiency with a mixed fluid ORC, mixtures of siloxane are recommended as well as the mixtures n-decane and n-heptane.
- Pure organic working fluids can be successfully employed in an ORC to convert low grade heat with a temperature below 600 K to electricity or shaft power with an efficiency limited to less than 30%.
- The use of mixtures as working fluids allows an increase of the ORC efficiency by 5-10% in comparison with pure substances because of the expansion of heat regeneration zone in the cycle.
- The energy or power available from thermal recuperation is 4 to 7 times greater than that available from turbine expansion, and it is approximately 1.5-2 times greater than that possible with a gas-turbine, Brayton cycle.
- Because an essential part of heat in the ORC recuperator is transferred from the liquid which is condensing to the liquid which is boiling, the total heat transfer coefficient can be 10-20 times greater than that for the Brayton cycle. With this, the ORC recuperator dimensions would be 3-5 times smaller than those of a Brayton cycle recuperator.
- The recuperator, prime heater, and cooler are the key units of ORC. In order to achieve acceptable thermal efficiencies with an ORC, it is necessary to improve and augment the heat exchange efficiency in these components.

References

1. S.D. Labinov, J. R. Sand. An Analytical Method of Predicting Lee-Kesler-Plöcker Equation of State Binary Interaction Coefficients. International Journal of Thermophysics, Vol. 16, No.6, November 1995.
2. http://europa.eu.int/comm/energy_transport/atlas/htmlu/orcrtdc.html
3. Angelino, G., Colonna di Paliano, P., "Multicomponent Working fluids for Organic Rankine Cycle (ORCs)", Energy - The International Journal, Vol. 23 (6), 1998, 449-463.
4. Gaia, M., K.Sheidegger, Bini, R., Bertuzzi, P., "Small Scale Biomass Powered CHP Plants featuring Thermal Oil Boiler and Organic Rankine Cycle Turbogenerators", Proceedings of the1st World Conference on Biomass for Energy and Industry, 5-9 June 2000, Sevilla , Spain.
5. Braun, R.J., Gaggioli, R.A., Dunbar, W.R., "Improvements of a Molten Carbonate Fuel Cell Power Plant via Exergy Analysis", Journal of EnergyResources Technology, 1999, Vol.121(12), 277-285.
6. Lobachyov, K.V., Richter, H.J., "Addition of Highly Efficient Bottoming Cycles for the Nth-Generation Molten Carbonate Fuel Cell Power Plant", Journal of Energy Resources Technology, 1997, Vol.119 (6), 103-108.

7. Cycle Tempo - A program for thermodynamic modeling and optimization of energy conversion systems - Department of Process and Energy Technology, Faculty of Mechanical Engineering and Marine Technology, Delft University of Technology, © 1998-1999.
8. HTFS ACOL 6.1 - AEA Technology Engineering Software, © 1992-1999.
9. http://www.geothermie.de/gte/gte36-37//altheim_gaia.htm
10. http://www.honeywell.com/
11. http://www.honeywell.com/sites/sm/chemicals/genetron/organicrank.htm
12. http://www.turboden.it/orc.asp
13. http://www.icr2003.org/abstracts/ICR0508.pdf
14. http://www.turboden.it/orc.asp
15. R. C. Reid&J. M. Prausnits. The properties of gases and liquids. McGraw Hill Book Company, 1977.
16. Adrian Bejan. Thernal Design and Optimization. John Wiley&Sons, Inc., 1996.
17. http://www.cycle-tempo.nl/ScientificArticles/2000Colonna_b.pdf
18. http://www.ocp.tudelft.nl/et/Publications/2000/2000Colonna_a.pdf

3.7a Heat and Mass Transfer Based Technology

Eddie Vineyard and Steve Allison
Engineering, Science and Technology Division
Oak Ridge National Laboratory
(865) 574-0576; email: vineyardea@ornl.gov

DOE Technology Development Manager: Patricia Hoffman
(202) 586-6074, (202) 586-7114 (Fax); email: Patricia.Hoffman@hq.doe.gov

Objective

The objective of this activity is to focus on heat and mass transfer innovations that significantly reduce the volume, footprint, and weight of key thermally activated technologies, such as equipment used in absorption, desiccants, and energy recovery. This work complements ORNL projects under Integrated Energy Systems and End-Use Systems Integration. Specifically, work involves:

- Development of capabilities for testing advanced heat exchangers for thermally activated equipment,
- Measurement and analysis of the effects of maldistribution in heat exchangers, and
- Development of microchannel heat exchangers for a 5 to 10 ton refrigeration unit.

Approach

- Acquire and install heat exchanger test loops and additional instrumentation for heat and mass transfer energy flow,
- Develop methods for the rapid, noninvasive measurement of multiple temperature points throughout a heat exchanger, and
- Develop industry partnerships for the design and development of advanced heat exchangers.

Accomplishments:

- Completed the installation of two heat exchanger loops for testing heat exchangers used for waste heat recovery applications and refurbished an existing test loop for evaluating evaporator and condenser heat exchangers used in absorption and gas-fired heat pumps.
- Developed methods for measuring temperatures on heat exchanger surfaces using phosphor paint and thermal imaging cameras.
- Initiated projects with UTRC and Modine to develop improved microchannel heat exchangers for thermally activated equipment.

Future Direction:

- Initiate testing of microchannnel heat exchangers to evaluate different orientations, header designs, and flow paths,
- Develop a plan for prioritizing heat exchanger designs for various types of thermally activated equipment,
- Address hotter surfaces and wider temperature ranges with fiber optics, and
- Continue to develop partnerships with industry.

Introduction

In the field of low temperature energy recovery, represented by CHP systems, volume, footprint, and weight are important indicators of energy efficiency, technical feasibility, application flexibility and economic viability. Stand-alone heat recovery equipment is vintage technology that has been developed as an auxiliary device without consideration for the proper integration of power generation and TAT equipment. DOE's role is to partner with industry to accelerate the research and development of higher efficiency and lower cost integrated heat recovery systems based upon IES laboratory, test bed and field experience. In working to achieve that goal, ORNL is in the process of installing and upgrading test facilities for developing advanced heat exchangers through the use of advanced materials, improved flow paths, and different geometries and orientations.

In addition to installing new test facilities, ORNL is also developing advanced measurement techniques to reduce the test time and improve the accuracy of heat transfer measurements for heat exchangers. This report describes the use of thermally sensitive phosphor coatings applied to both stationary and moving heat exchanger surfaces to accomplish temperature measurement. Fluorescence of the coating excited by ultraviolet light indicates coating temperature. Temperatures ranged from 50 to 120 F and achieved a precision as good as +/- 0.5 F for the stationary surface. The technique is independent of emissivity and enables thermometry of difficult regions in a heat exchanger that are difficult to reach. A fiber optic means for producing and capturing the fluorescence is required but, unlike a thermocouple, it is not necessary that it be in intimate contact with the surface.

Advanced Heat Exchanger Test Facility

The Advanced Heat Exchanger Test Laboratory is dedicated to reducing the size, weight, and cost of heat exchangers used for thermally activated technologies. The laboratory, located in Building 5800, is equipped with state-of-the-art instrumentation for noninvasive temperature measurement which enables reduced set-up times and higher accuracies. High resolution thermal imaging cameras produce temperature scans which may be downloaded directly to an Excel file, thus shortening the time required to reduce and analyze the data.

ORNL is working with several industry partners to design advanced heat exchangers and fluids for thermally activated technology applications. The partners include, United Technologies Research Center, Modine, Southwest Gas, and DuPont. Collaborative research activities include the design of fluids for advanced cycles and improvements in heat exchanger materials and orientations.

The test loops are comprised of two wind tunnels, one a high temperature (550^{o}C), and the other a medium temperature (325^{o}C), which simulate temperature levels and air flow rates from engine-driven power generating equipment and micro turbines. A third wind tunnel, is used for low temperature applications.

Figure 1 Low temperature wind tunnel located in Building 3115

Researchers are presently working on designing micro channel heat exchangers for use in a 10 ton rooftop unit that runs on natural gas. The goal is to achieve a heat exchanger design that will reduce the profile of the unit to make it possible to be installed on a rooftop. One of the limitations is that some micro channel heat exchanger designs are prone to refrigerant maldistribution as a result of the heat exchanger orientation or header design. Maldistribution reduces the heat exchanger capacity and results in a larger unit. ORNL will investigate several designs to evaluate the maldistribution and correct any problems.

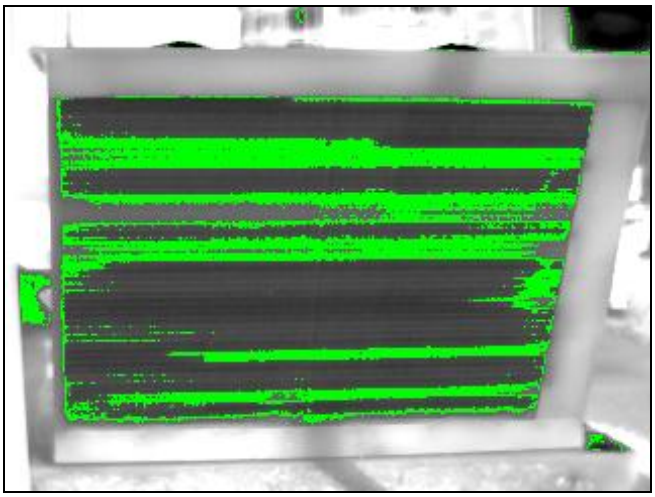

Figure 2 Flow maldistribution shown with thermal imaging camera

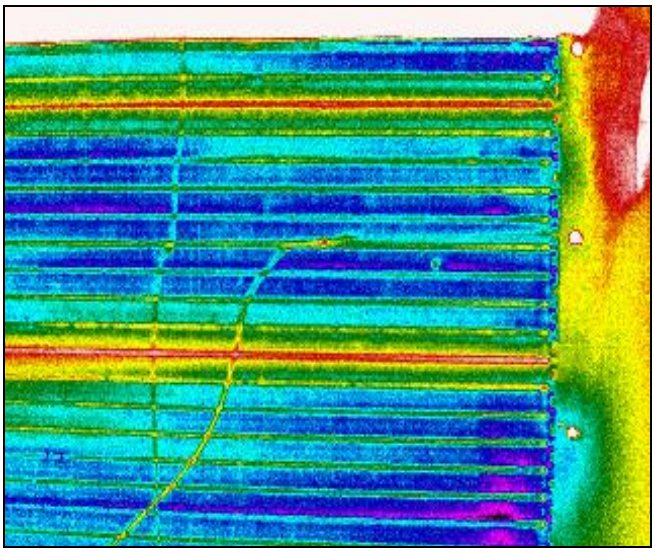

Figure 3 Temperature gradients in heat exchanger

Future research will concentrate on greater improvements using improved materials, such as graphite fiber and advanced concepts, such as rotating heat exchanger designs. In addition, more detailed experimental and analytical tools will be added to the laboratory, such as multiphysics modeling capabilities using partial differential equations and flow visualization techniques.

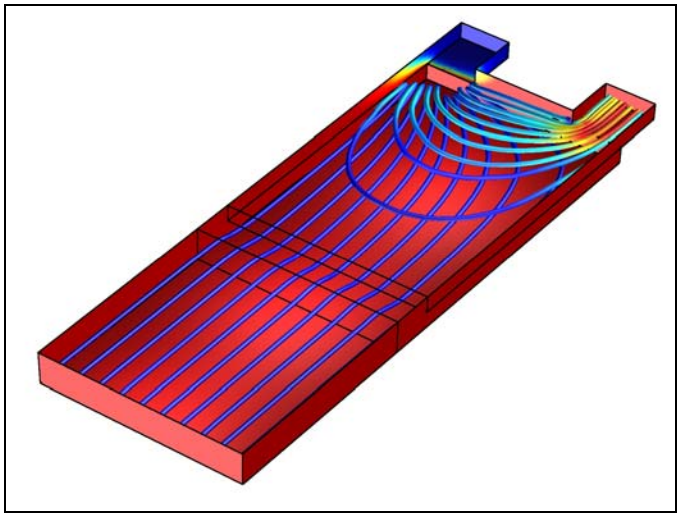

Figure 4 Micro channel heat exchanger analysis (photo courtesy of COMSOL**)**

Phosphor Thermometry Temperature Measurement

The major goal of the present effort is to exploit a new means for addressing a variety of heat exchanger temperature measurement applications. The technique is generally termed phosphor thermometry. It makes use of temperature dependent properties of thermographic phosphors (1, 2). In brief, a paint comprised of such phosphor is applied to a surface of interest. Fluorescence is generated from a remote illuminating light source, usually a pulsed ultraviolet laser. When the laser terminates, the fluorescence will persist, decreasing at a characteristic rate. The duration of this fluorescence, called the lifetime or also the decay time, is a sensitive indicator of temperature. The phosphor may also be applied to the tip of an optical fiber in order to function in a manner similar to a thermocouple.

The technique is adaptable to a variety of situations. For relatively inaccessible locations, optical fibers may be articulated to illuminate and capture the temperature indicating fluorescence. Different phosphor materials cover different temperature ranges. Generally, laboratory characterizations indicate the range from cryogenic to 1700 C may be covered by selection of the correct phosphor. Fluorescence lifetimes are usually short, ranging from nanoseconds to milliseconds. Thus, rapidly changing, or transient, temperature measurements are feasible.

A major advantage of this method over infrared methods is that the measurement does not depend on emissivity. Commercially available infrared cameras have marvelous capabilities but the results are always predicated on known and/or constant emissivity. Many

surfaces are well behaved so infrared cameras function well. However, with heat exchanger surfaces, the presence of fins, the inaccessibility of some surfaces to direct viewing, and the presence of moisture etc., complicate the measurement and make interpretation of camera data difficult. In such situations, the phosphor method can therefore replace, supplement or verify IR camera application as the conditions require.

Figure 5 illustrates the scatter in the data for constant temperature for the present setup in a laboratory environment. The results are for two analysis routines, one termed C-Code and the other AIM. Over the course of a fifteen minute data run, the scatter in temperature is seen to be about 0.1 and 0.2 C, respectively.

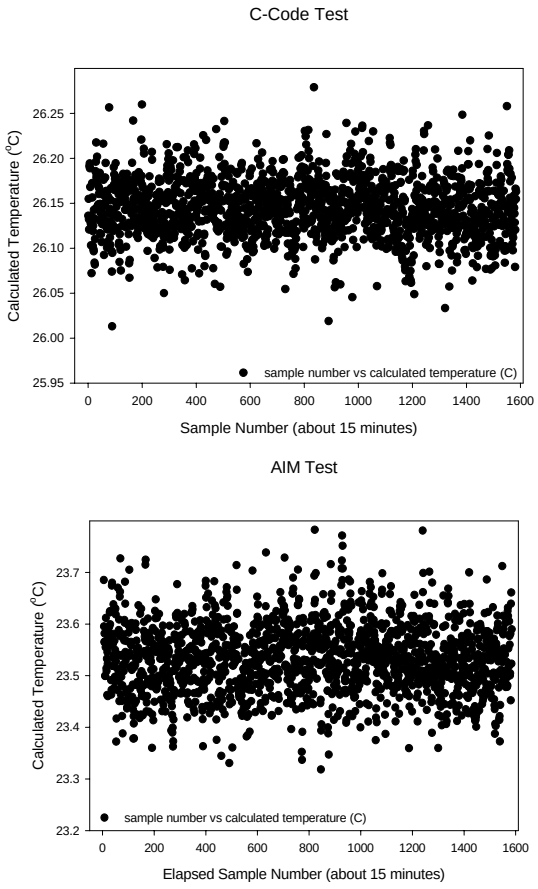

Figure 5 Lab data at constant temperature Light Source and Phosphor Downselect

The first activity towards implementing the phosphor method for a particular situation is to select the correct phosphor and light source. These are two interrelated considerations. Generally, in the lower temperature range, X_2O_2S:Eu (where X may be La, Gd, or Y) phosphors are the most sensitive to temperature. However, they usually require a nitrogen laser for adequate excitation. They can be excited to some degree with recently available light emitting diodes (LEDs). Improvements in LED technology are occurring almost monthly so this mandates vigilance. LEDs are of course much less expensive than lasers. Cr-doped materials cover a wider temperature range and are easily excited by LEDs. The drawback is that they are not as sensitive to temperature.

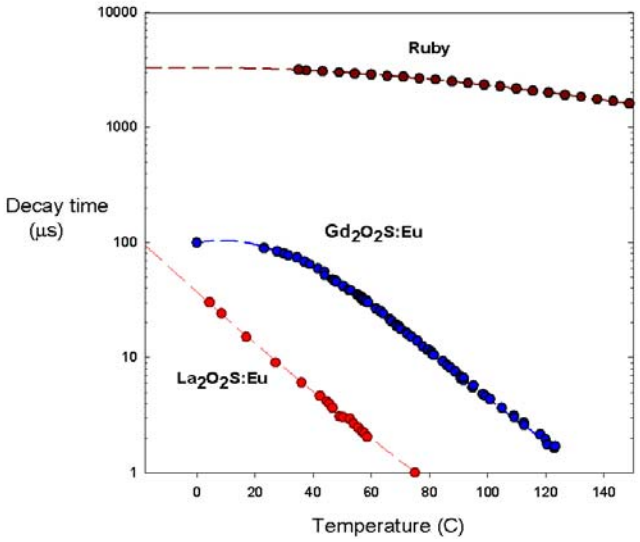

Figure 6 Decay time vs. temperature for sample phosphors

This is illustrated in Figure 6. Up to about 80 C (about 176 F) the La_2O_2S is the phosphor of choice. The effect of varying the dopant concentration of Eu from 0.1, 1, and 3% was also addressed and it was determined that a 1 % Eu concentration is the best. Ruby is Cr doped Al2O3 and it may be used up to at least 700 C. Thus, in a situation with wide temperature excursions, it may be the right choice.

For all the subsequent measurements made, the La_2O_2S:Eu sufficed. Phosphor can be applied in several ways. The method of choice for the heat exchangers is to air brush or paint a slurry of phosphor and Sperex binder. The latter is a high temperature paint used by the racing industry for painting surfaces that are subjected to high heat.

Prototype System Application

The purpose of this task was to exercise a prototype phosphor thermometry system and gain experience with the needs and characteristics of heat exchanger applications.

To measure the temperature of a heat exchanger unit, a coating of La_2O_2S:Eu was painted on the surface of the

flow tube. For this, the cooling fins had to be spread apart slightly. A nitrogen laser (337 nm) is coupled into a fiber optic cable. That cable is then coupled into the end of thin fiber probe used for excitation. A second fiber probe is placed next to the excitation probe and is run into a photomultiplier tube (PMT) with a 510 nm filter. Figure 7 shows the fiber probes inserted into the heat exchanger fins. The signal from the PMT is routed into a digital oscilloscope. Signals from the oscilloscope are then captured and processed through an interface to a virtual instrument (VI). The VI then fits the decay curve and determines the decay time (τ). The value of τ is then compared to a prepared calibration and the surface temperature is determined.

For these tests, the oscilloscope was set to 10 µs/div and 20 mV/div. The signal was averaged over 64 traces with a 50 Ω termination. The oscilloscope was triggered off of the negative going phosphor signal at -86 mV.

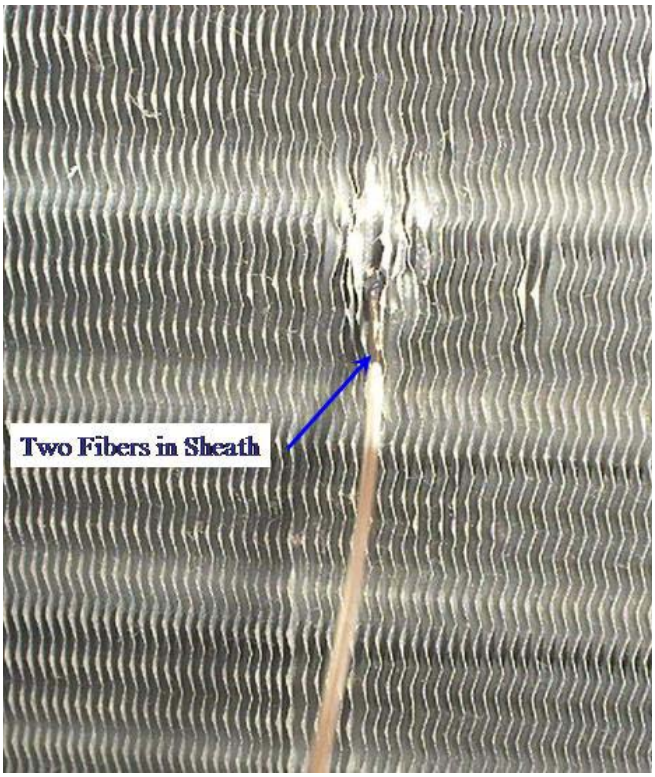

Figure 7 Fiber inserted into heat exchanger fins

Two series of tests were performed. The first series was for steady state operation. The decay signals from that test are shown in Figure 8. Over the 15 minutes of the test, there is very little difference in the signal as would be expected for steady state operation. A plot of temperature versus elapsed time is shown in Figure 9. The temperature indicated by the phosphor decay time is approximately 114 +/- 0.5 ^{o}F.

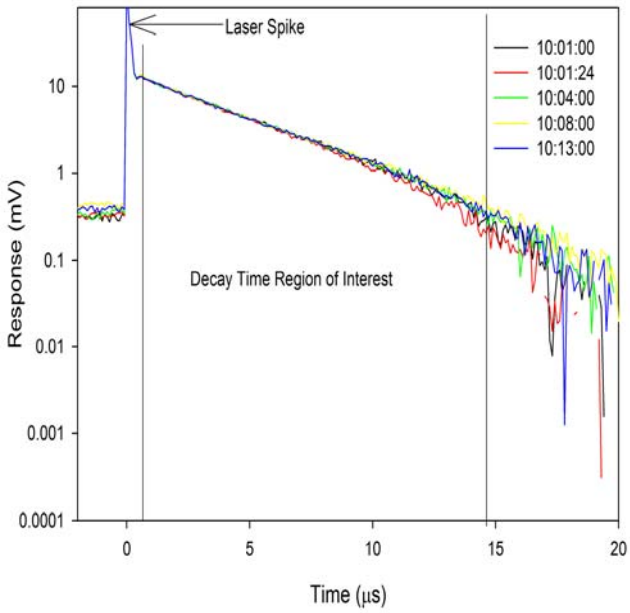

Figure 8 Decay signals for steady state operation

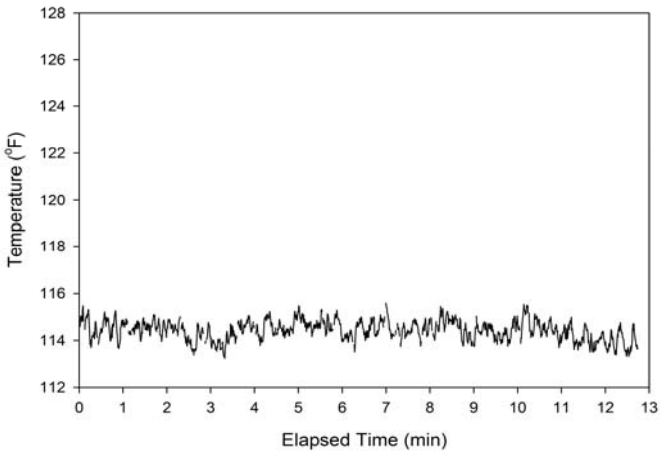

Figure 9 Temperature calculated from phosphor decay

Conclusions

Surface temperature measurements using the phosphor thermometry technique effectively track temperature on stationary surfaces with ± 0.5 F precision. A phosphor coating may be applied anywhere in an HVAC system. Such a coating may be accessed with an optical probe at a small distance from the surface so as not to perturb the measurement.

References

1. S. W. Allison and G. T. Gillies, "Remote thermometry with thermographic phosphors Instrumentation and applications." Rev. Sci. Instrum, **68** (7), 2615-2650, 1997.


EFFICIENTLY POWERING A HEALTHIER AMERICA
CHP

4.2 Distributed Energy Systems Applications Integration

C. Randy Hudson
Engineering Science and Technology Division
Oak Ridge National Laboratory
Oak Ridge, TN 37830-6070
(865) 574-0578 email: hudsoncrii@ornl.gov

DOE Technology Development Manager: Debbie Haught
(202) 586-2211 email: debbie.haught@ee.doe.gov

Objective
One of the missions of the Distributed Energy Program is to lead a national effort to integrate DE technologies at end-user sites and to document and disseminate the findings of those efforts. Strategies to accomplish that mission include:

- Investment in a diverse portfolio of RD&D projects across complementary technologies: prime movers, thermally activated technologies, and CHP systems,
- Performance of systems integration, implementation, and outreach activities aimed at addressing infrastructure, institutional, and regulatory needs, and
- The establishment of collaborative technology transfer partnerships, including cost-shared RD&D projects.

Over the last four years, a balanced portfolio of projects in selected high-opportunity market sectors has been developed to support the above mission.

Approach
Three cost-shared solicitations have been conducted in the industrial, high-tech, and institutional market sectors. In FY 2004, the institutional market sector solicitation was issued for cost-shared projects that would utilize integrated (packaged) distributed energy systems in the specific markets of healthcare, education, hospitality, and grocery/supermarkets. All accepted projects had to have a minimum vendor cost share of 50% and had to have the potential for further replication in the marketplace without federal assistance. Out of 46 vendor proposals, eight vendors were selected for award. Eight projects from that solicitation are currently active.

Accomplishments

- Largest fuel-cell installation in the U.S. became operational at a critical telecomm facility in June 2005
- Four projects started initial design efforts in FY 2005
- Five projects were under construction in FY 2005

Future Activities
In FY 2006, projects that are operational will collect operating experience data and prepare and disseminate final documentation on the overall project experience. Other projects will complete construction and commence operations in FY2006. All projects will be completed and documented by the end of FY 2007.

Introduction

A large portion of the existing distributed generation and the potential for future distributed generation installations is found in the industrial and commercial sectors. As a result, the foci of this effort are to identify and assess promising applications for integrated distributed energy (DE) systems and to conduct projects that validate and demonstrate the benefits of DE technologies in targeted sectors.

This activity is intended to encourage the expanded use of distributed energy technologies in applications where there is a suitable combination and coincidence of electrical and thermal demand. Demonstration projects, begun in FY04, are underway to encourage the utilization of integrated packaged systems in the healthcare, education, hotel, and grocery sectors. Descriptions of the active projects are provided below.

Eastern Maine Medical Center

ORNL integrated a team that includes Eastern Maine Medical Center (EMMC), in Bangor, Maine, Vanderweil Engineering, and Cianbro. The team is designing and installing a Solar Turbines gas turbine to generate 4.4 MW of electricity, 24,000 lb/hour of steam, and drive a 500 ton absorption chiller for the hospital. The new CHP system will respond to the following concerns: high energy costs, fuel use diversity, the need for additional chilled water capacity, the need to deliver services under any climatic condition, utility reliability, diverse thermal heating load profile, and emissions compliance. The turbine has been ordered with manufacturing nearing completion. Balance of plant major equipment has been ordered. The project is on schedule with an expected commissioning in the Fall of 2006.

ORNL rallied the CHP community to support Eastern Maine Medical Center in seeking approval of its Certificate of Need (CON) from the Commissioner of the State of Maine Department of Health and Human Services (DHHS), which is required for major capital expenditures. Resources within the CHP community submitted case study documentation on how hospitals have benefited from on-site CHP systems to aid in the decision process. The DHHS Commissioner approved EMMC's CON on February 4, 2005. However, Bangor Hydro filed a "Petition for Reconsideration of CON" with DHHS on March 4, 2005. The Commissioner reasserted approval of the CON on March 31, 2005, citing CHP case study information as influencing his decision. ORNL summarized findings for dissemination to the CHP community.

Butler Hospital

Butler Hospital, a 380,000-ft^2 hospital complex located in Providence, Rhode Island, installed a United Technology Corporation (UTC) PureComfort System, which packages four Capstone microturbines to generate 240 kilowatts of electricity and 110 tons of chilled water using a Carrier exhaust fired absorption chiller. Although hospitals have backup power generation for critical functions in case of blackouts, integrated systems, like the one at Butler, enable greater flexibility for system operators to provide a range of services in case of grid failure. Of particular interest is how Butler has replaced steam use with hot water using the same room-by-room terminal heaters/chillers. Butler now runs hot water through the units during the winter, and cold water through the same units in the summer. In addition, handling, storage and heating of No. 6 fuel oil is eliminated, both reducing cost and eliminating the need for an air emissions permit. The project demonstrates the cost and energy savings of this pre-engineered, packaged integrated energy system that can be easily replicated throughout the healthcare sector of the economy while acquiring data on system performance in this high-profile setting. Butler Hospital projects an annual savings of $92,000 in utility costs from the IES installation. Operation is scheduled for November 2005.

UTC PureComfort System installation at Butler Hospital

Verizon

The telecommunications industry requires reliable high-quality power and facility cooling for critical central office switch operations. To meet these needs, Verizon Communications, Inc., under a DOE/ORNL cost-shared competitive procurement, has installed the largest fuel-cell based CHP system in the United States into a 300,000 sq. ft. Central Office on Long Island in New York. The CHP system is a topping cycle with base-

load electrical power provided to the building by seven UTC PureCell 200 kW fuel cells and a dual-fuel (natural gas and diesel) engine. The fuel cell/engine combination generates up to 2.6 MW of electricity, providing essentially all the electrical needs of the large facility. Supplemental/backup power comes from the Long Island Power Authority (LIPA) grid and two standby diesel engines. Waste thermal energy from the fuel cells drives two 70-ton Thermax lithium bromide (LiBr) absorption chillers for cooling in the summer and an unfired heat recovery steam generator (HRSG) for space heating in the winter.

The fuel cells and the engine are typically paralleled to the grid, but can run in isolation should the grid become unavailable. The system became operational in June 2005. Annually, the facility is expected to produce approximately 11,100 MWh of electrical energy and 16,000 million BTU (MMBTU) of useful thermal energy. The fuel cell, engine, chiller and HRSG CHP system were designed to enhance the reliability of Verizon's telecommunications facility while providing an essentially free source of heating and cooling.

Fuel cells and absorption chillers outside Verizon central office facility

Pepperell High School

The Pepperell High School CHP/active-desiccant field demonstration, field performance verification project in Lindale, Georgia is a unique integration of islanded IC engine power generation with thermally activated, desiccant, building ventilation and humidity control. Participants collaborating in the project are DOE, ORNL, SEMCO Corporation, Deutz Corporation, CM Engineering, and Floyd County Schools. The IES concept of this project is to use the electrical and thermal power provided by a 215 kWe Deutz, packaged, IC-engine cogeneration system to operate four SEMCO Revolution™ active-desiccant/vapor compression rooftops as grid independent, dedicated, outdoor air systems supplying up to 18,000 cfm of fresh ventilation air to this new 1500 student high school. CHP/IES system installation and start up are scheduled for late winter/early spring of 2006, with school occupancy starting that fall.

This R&D work will demonstrate what should be a very cost effective, energy efficient approach to integrating three important technologies: distributed natural gas power generation combined with hybrid active desiccant air conditioning, the ideal combination potential of IC engine DG technology with desiccant dedicated outdoor air systems, and full utilization of building exhaust air for total energy recovery.

Ritz Carlton Hotel

This project will install and monitor the performance of a United Technology Corporation (UTC) PureComfort System, which packages four Capstone microturbines to generate 240 kilowatts of electricity and 110 tons of chilled water using a Carrier exhaust fired absorption chiller, at the Ritz Carlton Hotel, San Francisco, CA. The results from this project will be used to provide the traditionally risk-adverse hotel building design community with confidence that integrated CHP systems are technically and commercially viable alternatives to traditional power and HVAC products. In addition, the knowledge gained from this hotel installation will be directly invested in further integration of future PureComfort systems and will serve as a basis for the development of next generation integrated CHP systems. The startup date for the system was October 2005.


UTC PureComfort System at the Ritz Carlton Hotel

Utica College
This project will focus on an IES system at Utica College that will provide CHP and be used for the engineering curriculum. The modular packaged CHP system will include four Cummins gas-fired reciprocating engine generator sets with heat recovery. One generating set will be retrofitted with an advanced selective high temperature catalytic reduction (SCR) system. The advanced emissions control system is designed to meet proposed CA requirements, where advanced after-treatment solutions will be needed to meet emissions standards for lean-burn engines until the advanced ARES engines are commercialized. The anticipated benefit of the high temperature catalyst is reduced pressure loss and broader application to IC engines. The new technology should also offer improved system reliability due to the removal of auxiliary equipment such as dilution air systems. The performance and economics of the advanced catalyst system will be compared to the other three engines at Utica, to an identical engine located in California with a traditional SCR system, and to the same engine type equipped with an exhaust gas recirculation system installed in the Wingate hotel project (see description below). Startup is planned for November 2006.

Wingate Hotel
The emissions generated by this PowerCold natural-gas fired reciprocating engine are clean by virtue of a process that combines the ultra low emissions capabilities of a stoichiometric-catalyst package with the high efficiency and power density of a lean burn prime mover through the use of an exhaust gas recirculation design. The integrated energy system is completely designed, tested and all components and sub-systems are factory built and packaged. The Wingate Hotel in Henderson, Nevada is one of over 100 Wingate properties in the US. Via this demonstration, "in-house" energy managers will recognize the advantages of an integrated system, thus opening a channel for replication throughout the Wingate system as well as other hotel chains. Moreover, this project will provide confidence to the broader and traditionally risk-adverse hotel building design community by showing them that integrated systems are technically and commercially viable alternatives to traditional power and HVAC products. Startup is scheduled for May 2006.

Basin Electric
The goal of this project is to verify the technical and economic feasibility of capturing thermal energy from a 30 MW gas turbine driving a natural gas pipeline compressor with an Organic Rankine Cycle (ORC) machine producing 4 MW of emission-free (no fuel and virtually no emissions) electricity in the summer and 6 MW in the winter. The site selected supports an electric coop that requires power and voltage support for the grid, which includes an Indian Nation with an important hospital load. This project integrates the ORC generator assembly into an ownership structure involving a partnership between the utility, a developer, Ormat, and the pipeline. The pipeline owner sells the resource (waste heat) to the developer. The developer uses that resource to produce electricity and delivers the power to the utility. The utility then integrates that resource into the grid, firming the power supply and interconnecting the project to the consumers. The resulting overall system uses natural gas as a fuel to cogenerate mechanical power (for the compressor) and electrical power (for the grid) at a remote site. Operation is expected to start in the summer of 2006.

Industrial End-Use Activities with Project Partner Energy Solutions Center
This project addresses CHP systems and how to integrate DG equipment within manufacturing processes with the greatest opportunity to use waste heat. This program focuses on innovative packaged CHP systems for specific applications that are highly replicable and can be integrated with industrial process energy needs. The Faith Plating project in Hollywood, California, was completed in FY05. Equipment installation was completed at Higgins Brick [Chino Hills, California] and data collection was started. A new project, Arrow Linen [Brooklyn, New York], was added in FY05. All work will be completed in FY06.

Faith Plating
The goal of this project is to verify the technical and economic feasibility of a combined heat and power system at a metal plating facility. The CHP system

consists of 4 Capstone Model C-30 microturbines and a Unifin gas-to-hot-water heat exchanger. The Unifin heat exchanger converts most of the turbine exhaust heat to hot water to be used in the heated dip tanks that are used to plate the bumpers and other vehicle components. The heat exchanger generates 40-90 gallons per minute of hot water, raising the temperature of the water by 12-31 degrees. The hot water from the heat exchangers either displaces hot water from the existing boiler or electricity from the immersion heaters used on some of the dip tanks. Further, the system allows for additional recovery of exhaust heat from the heat exchanger to be used to dry a recyclable precipitate, which is a by-product of the plating operations. In addition to environmental benefits, the unique aspects of the project are: during peak periods, the electricity purchased from the grid is reduced by up to 60%, the new patented precipitate dryer [that is run off the exhaust heat] reduces the cost and time to process the precipitate over conventional dryers, and landfill disposal costs are reduced by 60% [due to the reduced weight and volume of the precipitate with the new dryer]. The results of this project are documented in a case study document that can be found on the DOE DE website.

Issuance of this case study fulfills the Joule level milestone: Complete a case study on a CHP Installation that uses heat from a microturbine to provide plate tank heating and sludge drying at an industrial facility, contributing to the PART long-term measure of developing a 70% efficient CHP Integrated System. Completed on-schedule.

Higgins Brick

The goal of this project is to verify the technical and economic feasibility of a combined heat and power system at a brick making facility. An innovative Combined Heat and Power (CHP) plant was installed at the site that uses three 80 kW Bowman microturbines to provide power and waste heat for preheating the combustion air of a large brick kiln. The twelve-month evaluation period was initiated effective May 1, 2005. A Connected Energy website allows the project team to remotely monitor and collect data on the operation of the CHP system. An instrumentation installation report has been completed for this site. Due to some anomalies in the contract between Higgins Brick and Simmax, the plant energy service provider, purchased gas is charged to Higgins Brick. In Sepetember, Higgins Brick asked Simmax to shut down the system while the plant evaluates the effect of the current high natural gas prices. A meeting has been scheduled between project partners for early-FY2006 to determine the course of action for the remainder of the year.

Initial results show that system efficiencies of 75-79% can be achieved with only two of the three microturbines in operation and that it may be possible to lower the marginal cost of electricity to a level below 6 cents/KW-hr for a natural gas fuel cost of about $7 per million Btu. Preliminary results are provided in the two graphs below. The first provides system efficiencies.

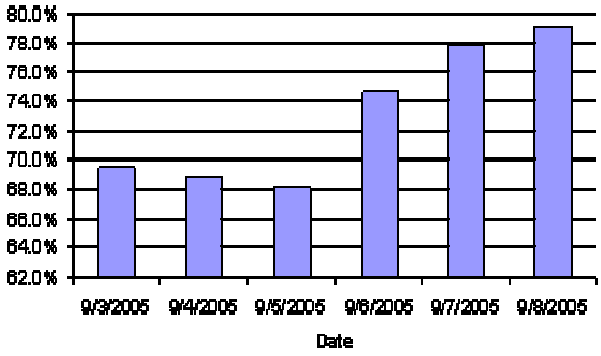

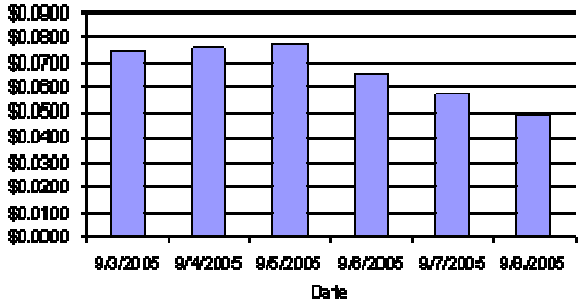

The second graph provides the marginal cost of power production. The increase in system efficiency and decrease in power production costs were achieved by operating the two turbines closer to design capacity.

The following deliverables were issued in FY2005:
Host Site Agreement for Data Collection and Evaluation of a Combined Heat and Power System
Heat Recovery Analysis Report
Plant Efficiency Analysis White Paper

Arrow Linen

A 4th project, added in FY05, evaluates a CHP system at Arrow Linen in Brooklyn, NY. The project, in coordination with KeySpan and NYSERDA will also evaluate the ASERTTI long term testing protocol. The CHP system is comprised of two 150 kW Coast Intelligen packaged systems using MAN engines. Two heat exchangers recover heat from both the jacket and the exhaust of the engines to provide process hot water for use in the laundry operation and to preheat boiler make-up water for production of 115 psig steam that is used throughout the plant.

A project kick-off meeting was held at the site on June 22. Information from this meeting will be used to complete a full site assessment and to specify the additional instrumentation required for meeting the ASERTTI protocol monitoring plan. Data acquisition for the twelve-month data evaluation period has been scheduled to begin on October 1, 2005.

The following deliverables were issued in FY2005:
Host Site Agreement for Data Collection and Evaluation of a Combined Heat and Power System
Instrumentation and Data Analysis Report

4.2.14 & 2.4 Ancillary Services Offered by DE Systems

John Kueck, Tom Rizy, Burak Ozpineci, Leon Tolbert
Engineering Science and Technology Division
Oak Ridge National Laboratory
Oak Ridge, TN 37932-6070
(865) 574-5178, email; kueckjd@ornl.gov
(865) 574-5203, email: rizydt@ornl.gov

Debbie Haught, DOE Program Manager
(202) 586-2211, email: debbie.haught@ee.doe.gov

Objectives

- Evaluate the economic and engineering feasibility of supplying reactive power locally from distributed energy resources (DE) to regulate local voltage and control power factor to improve the efficiency and reliability of the utility distribution system.
- Determine if reactive power can be supplied from local DE sources with independent voltage control so that an expensive hierarchical control and communications system is not required.
- Address the key barriers to the local supply of reactive power so that it may be supplied without requiring the local utility to either modify the existing distribution system or perform engineering analysis of the circuit.
- Evaluate the incremental costs and potential benefits of distributed energy as a source of reactive power in the electric transmission & distribution power grid. Evaluate economically viable ancillary services from DER.

Approach

- Establish a reactive power laboratory with both generator and inverter-based DE technologies to test individual and multiple reactive power producing DE.
- Use the ORNL campus distribution system to demonstrate that several reactive power producing DE devices can operate in close electrical proximity to regulate voltage or net power factor without extensive communications and control.
- Use a mathematical programming platform (Matlab/Simulink) and real-time controller (dSpace software and controller) to implement various control algorithms and strategies for feedback control.
- Use commercial power system analysis software (SKM and ETAP) to model the performance of the DE in controlling voltage and net power factor and evaluate local control methods.
- Demonstrate that DE inverter designs with local control can be developed and packaged to economically supply adequate reactive power levels to satisfy utility and user needs.
- Conduct an economic assessment of distributed energy as a source of reactive power. Identify potential market value based on available information and conduct a limited number of case studies using specific utility information. The approach has focused on the incremental cost of incorporating reactive power into distributed energy versus the additional ancillary benefit of having this capability such as supporting distribution voltage or regulating local power factor dynamically.

Future Direction

- Develop automated feedback control schemes for both the synchronous condenser and inverters for varying reactive power output based on local voltage
- Determine how to better model the voltage, current and power changes due to reactive power producing DE at the circuit and substation levels. These include expanding the model capabilities to cover unbalanced loading, voltage sensitive loads, and real-time loading changes.
- Develop a cost goal for the local supply of reactive power from DE so that inverter and synchronous generator/condenser based DE can be evaluated to determine at what cost level it would be competitive with conventional reactive power compensation, such as feeder-level shunt capacitor based regulation.
- Operate multiple DE in parallel to evaluate interaction with multiple devices, prove control concept and develop engineering guidelines for DE application in providing voltage regulation and net power factor regulation.
- Move the concept of reactive power producing DE from the laboratory to the field environment by working with our partners, such as Southern California Edison's and their distribution circuit of the future, to implement the concept to a much larger extent (provide all of the local reactive power) on a utility distribution system.

Abstract
The Reactive Power Laboratory is a new and unique first-of-its kind R&D facility for testing reactive power producing distributed energy resources (DE). Reactive power doesn't perform work like real power, but it is necessary for energizing inductive and capacitive loads and for supporting voltage and preventing voltage collapse. Reactive power occurs when reactive loads (capacitors or inductors) are present and voltage and current are out of phase. When reactive power is present, current either lags (when reactive power is being consumed) or leads (when reactive power is being produced) the voltage. Real (or active) power, which does work, is only present when voltage and current are in phase. However, when voltage and current are out of phase, greater overall power capacity (due to the vector sum of real and reactive power) is needed to get the same level of real power and do the same level of work. The laboratory is exploring the use of both rotating (generators, motors) and static-based (inverters) Distributed Energy (DE) technologies for producing reactive power for supporting voltage and correcting power factor both locally and on the campus distribution system.

The goal of the laboratory is to work with the power industry, manufacturers, and universities in developing local control for producing reactive power from reciprocating engines, microturbines and fuel cells using synchronous generators and inverters. The first part of the laboratory is fully operational with the installation, operation and testing of a 300kVar synchronous condenser (250hp synchronous motor operated unloaded and overexcited). The second part of the laboratory is the inverter testing area which currently is capable of testing an inverter off the grid using resistive and reactive load banks or interfacing with the ORNL distribution system via a 480V/600A distribution panel to a 750kVA transformer connected to a circuit from the 3000 substation. Three different ratings of three-phase programmable inverters (75, 150 and 300A) will be configured and tested.

Tests of the 300kVar synchronous condenser (SC) were conducted on May 24th and July 1st. These results provide some preliminary information on the startup, operational and response characteristics of the SC and its ability to support local and substation voltages. Also, the test data was used as input to the model analysis. The model analysis provides an evaluation of commercial power system software performance in modeling the benefits of reactive power production for distribution systems. The testing and modeling results are important for developing a feedback control system for the SC.

Introduction
Alternating Current (AC) is supplied in a 60Hz waveform. Reactive power is produced when the current waveform is out of phase with the voltage waveform due to inductive or capacitive loads. Current lags voltage with an inductive load, and leads voltage with a capacitive load. Only the component of current in phase with voltage produces real power which does work. Current is in phase with voltage for a resistive load, like an incandescent light bulb. Reactive Power is necessary for producing the electric and magnetic fields in capacitors and inductors.

The additional current flow associated with reactive power can cause increased losses, excessive voltage sags, and increased power capacity requirements. Transmission system operators have to ensure that reactive reserves are available to handle system contingencies such as the loss of a generator or transmission line because increased current flows after the occurrence of these types of contingencies can produce greatly increased reactive power absorption in transmission lines. Some transmission system operators are now considering new rules for distribution systems which require a minimum allowable power factor. These minimum power factors could reduce the amount of reactive reserves that the system operator would have to provide. Distributed Energy Resources (DE) could be ideally suited for providing reactive reserves in the distribution system.

DE, includes such resources as microturbines, reciprocating engine generators, and fuel cells. DE is often installed at or near electrical loads for local power and to take advantage of CHP or cooling, heating and power benefits that come from waste heat recovery of DE by thermally-activated technologies. With the right control scheme and algorithms, DE could be controlled to supply local reactive power and to regulate local voltage. Some DE devices contain synchronous generators, which can be directly connected to the local power system, and some, such as fuel cells or microturbines, must be interfaced to the local power system through an inverter because they produce DC or high-frequency AC that must be converted to 60Hz AC. Similar to a synchronous generator, the inverter can also be designed and controlled to "inject" reactive power locally and regulate voltage. Thus, a DE with a

synchronous condenser or inverter could supply reactive reserves.

The Oak Ridge National Laboratory (ORNL) has established the Reactive Power Laboratory which is a new and unique first-of-its kind laboratory for studying reactive power supplied from DE. ORNL is unique in that it owns and operates its own electric distribution utility for the laboratory campus, and can configure the distribution system to provide optimum opportunities for testing of reactive power injection effects from the laboratory. The ORNL distribution system is directly fed by the TVA 161kV backbone transmission system. The reactive power laboratory and project is also unique in that the tests are designed by representatives from the electric utility industry and DE manufacturers to address the actual challenges faced by DE and utilities currently and in the future.

The testing to date at the Reactive Power Laboratory has focused on four aspects: 1) characterization of the synchronous condenser; 2) development of the instrumentation scheme for measuring the necessary voltage, current and power readings at the synchronous condenser and on the distribution system; 3) development of algorithms for analyzing data measurements from the various test runs; and 4) validation of a steady-state model for the synchronous condenser via the use of a commercial software package to study its effects on the ORNL 13.8/2.4kV distribution network.

The Reactive Power Project has the overall goal of developing methods of incorporating distributed energy (DE) that can produce reactive power locally and for injecting into the distribution system. The objective for this new type of DE is to be able to provide voltage regulation and dynamic reactive power reserves without the use of extensive communication and control systems.

Reactive Power Laboratory

The "Reactive Power" Laboratory has been established for studying reactive power supplied from both rotating and static-based DE. The electrical design and layout of the Reactive Power Laboratory is shown in Figures 1 and 2. Figure 1 shows the laboratory's interface with the ORNL distribution system while figure 2 shows the layout at the laboratory itself. The laboratory is located at the north end of the Oak Ridge National Laboratory campus at building 3114. The test areas of the laboratory are in the building while the transformers and load banks are just to the east of the building. The laboratory equipment interfaces to the ORNL distribution system through two different distribution circuits (#4 and #2 fed from ORNL's 13.8/2.4kV Distribution Substation 3000). The rotating-based DE of the laboratory, which current includes a 300kVar synchronous condenser (250hp synchronous motor unloaded and overexcited) is fed from circuit #4. The static-based DE of the laboratory, which current includes a 75A 3-phase inverter is fed from circuit #2. The synchronous condenser portion of the laboratory is fully operational and testing began in May 2005. The inverter-portion of the Laboratory is nearly operational with the goal of injecting reactive power from an inverter in early FY06. The first run of the 75A rated inverter in the off-grid operation occurred on September 28th.

The laboratory includes the following equipment:

- 250hp synchronous motor for use as a synchronous condenser
- 75A, 150A, and 300A programmable inverters
- Two 750kVA 2.4kV/480V pad-mount transformers for interfacing to circuits #4 and circuit #2 of the ORNL 13.8/2.4kV distribution network at the 3000 Substation
- 480V/900A three-phase electrical panel configuration for the 250HP synchronous condenser interface (via a 540A motor starter) to the ORNL 2.4kV distribution circuit #4
- 480V/600A three-phase electrical panel configuration for the inverter interface to ORNL 2.4kV distribution circuit #2
- 2 Dranetz/BMI PowerGuide 4400 Meters; one located at the motor/starter and the second at the electrical panel.
- 1 Yokogawa WT3000 Digital Power Meter
- Danfysik Ultrastab 866 Current Transducer System
- Matlab/Simulink and Real-Time Workshop software
- dSpace real-time control hardware and software
- 150kW dc power supply for the programmable inverters
- 6.6kW dc power supply for excitation of the synchronous condenser
- 500kW resistive load with remote control375kVAr inductive load with remote control

- 75HP Induction Motor for dynamic characterization of the synchronous motor

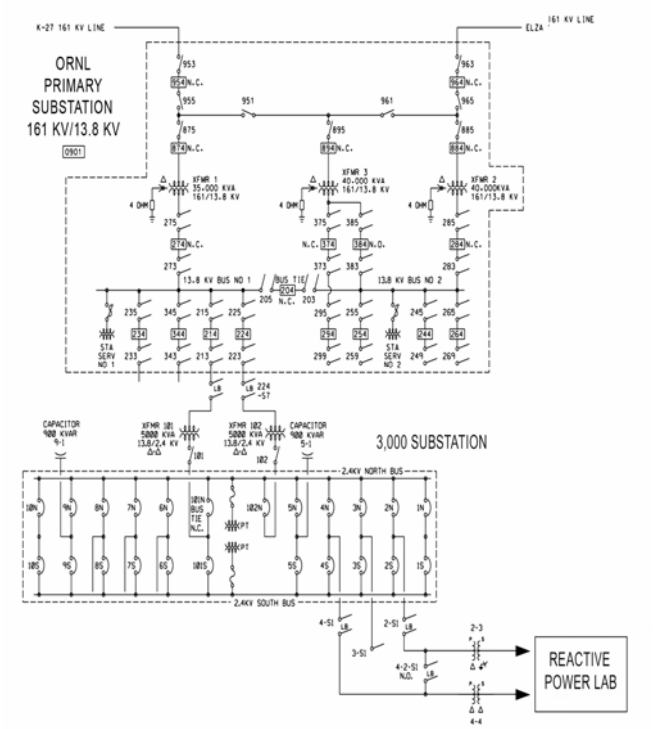

Figure 8. Reactive Power Laboratory Interface with the ORNL Distribution System.

Important capabilities of the laboratory include:

Testing Areas: The laboratory provides testing capability of rotating (generator or motor) and static (inverter) based DE. Also, the laboratory has the capability to test vendor provided reactive power producing DE, such as a microturbine or reciprocating engine.

Distribution Interface: The laboratory interfaces at two different electrical locations on the ORNL distribution system. This provides the capability to test single or multiple reactive power producing DE and also their interaction.

Substation: The reactive power compensation at the substation can be relaxed to provide a more severe testing scenario for the reactive power laboratory. Shunt capacitor banks at the substation provide power factor correction for the ORNL distribution system. The reactive power compensation can be relaxed by switching out some of these capacitor banks. Presently, the substation has 900kVar of reactive power compensation in capacitor banks in units of 150kVar.

Distribution and Power System: The laboratory interfaces with the TVA grid through the ORNL distribution system. The TVA feeders provide power at 161kV and it is stepped down to 13.8kV at ORNL's primary substation (X-10 substation). The secondary substations, such as the 3000 substations which provides the electrical interface for the laboratory, steps it down further to 2.4kV. Our ownership of the distribution system allows the capability to vary loading and reconfigure the distribution feeder circuits for testing different operating scenarios for the Reactive Power Laboratory.

Figure 9. Reactive Power Laboratory Layout

Tests Results at Laboratory

Some initial results of testing the synchronous condenser (SC) at the Reactive Power Laboratory include:

- The SC injected 311kVAr of reactive power at 370A of line current during the test conducted on July 1st, 2005 and shows great potential for use as a source of reactive power for voltage support. The line voltage during the test was regulated on average from 478V to 491V. Additional tests with new circuit configurations (more load, large dynamic motors and higher path impedance with an increased circuit length to the substation) and adjustments in SC location relative to other loads on the circuit are needed to better demonstrate its positive effects on the voltage support of a distribution system with higher path impedances and additional loads.
- The synchronization time of the SC can be minimized by immediately setting the DC field voltage and current such that the SC is operating at unity power factor immediately after the SC is started. Failure to do so may cause the SC to unnecessarily produce high currents and draw large amounts of reactive power before it begins to supply reactive power to the network. This situation becomes extremely important in cases where there is an immediate demand for reactive power such as the prevention of voltage collapse and the SC is not synchronized. Normally, the line current of the SC decreases as excitation is applied after startup and excitation current is between 3.5 to 4.5A. We found that one out of every five times when the SC is started and not immediately set to unity power factor (by applying 85 to 90V of excitation) that the SC doesn't synchronize until the minimal excitation level (about 4A) is reached. As a result the current instead of being around 200A after it is started can be closer to 400A.
- The excitation and losses of the SC (percentage of real power needed to spin the SC divided by the KVA capacity of the device) especially at lower than a 15% output level are significant making a strong case for an inverter-based reactive power producing DE. We found that the losses settle out to about 4% once the SC is operated at 50% and higher output.
- When considering the use of multiple SC units, the potential for circulating currents must be examined. It will be necessary to develop a voltage droop characteristic to ensure appropriate distribution of reactive power from each unit.
- Initial comparisons have shown that the simulation model based on the SKM commercial power system analysis software is fairly accurate except for the modeling of substation voltages and currents which can be affected by overall changes on the distribution system. For real-time power analysis, a much better estimation of the load distribution must be made. Furthermore, with a better estimation, future scenarios may be simulated before the actual tests are done to have an overall understanding of the system's behavior.

Economic Evaluation of DE as a Reactive Power Supply

An initial economic evaluation has been performed that considers the value of incorporating reactive power as an additional ancillary service for distributed energy. The effort compares conventional devices that can provide reactive power against distributed energy systems. Determination of reactive power payments was made through information gathering from various ISOs, and RTOs including PJM, NYISO, CAISO, ISO-NE, MISO, and ERCOT. However, a refinement of the approach considers incremental cost of incorporating reactive power producing capability with distributed energy.

The initial phase focuses on the cost effectiveness of rotating-based DE. The approach considers oversizing a generator for rotating-based DE to supply reactive power from these devices. By oversizing the power converter, a DE can provide the same level of real power as needed while at the same time has the ability to provide reactive power to correct power factor or regulate voltage. For comparison, the study effort has started to pull together generic capabilities and costs of conventional devices that can provide reactive power both at the transmission system level (typically 69kV and above) and distribution system level (typically below 69kV to 4kV) and end user voltage (480V and 240V). In order to achieve market acceptance, reactive power producing DE will need to compete with these technologies in terms of costs and benefits.

In terms of capability, DE can provide reactive power dynamically which adds a new and unique capability for responding to motor starts, pulse loads and other fast load events. Also, DE can relieve distribution capacity, reduce conductor losses and maintain tighter operating voltages by correcting power factor and regulating voltage locally at the loads. Although, capacitors can be used along the feeder circuit or at the end-user load to

perform this type of function, they can't perform at the same dynamic, variability or resolution capability. The difficulty is putting a proper value on these reactive power compensation capabilities. The cost per kVar ($/kVar) which is the incremental cost of supplying 1 kVar of reactive power is the capital cost metric for comparing the various devices. Basically for transmission level conventional devices, this cost ranges from approximately $40 to $100/kVar while for distribution level devices, this cost ranges from approximately $5 to $30/kVar. The cost benefit (revenue from reactive power payments minus the capital and maintenance costs) of reactive power producing DE must beat this metric to be considered as cost effective. Although currently reactive power producing DE cannot beat capacitor banks on a capital cost basis, they may in the future be able to compete based on their value of improving power system operations in return for reactive power payments for power factor correction or local voltage regulation. Much of this depends on reducing the cost of power conversion hardware for DE and a developing reactive power supply market from local devices.

The results of the initial phase of this effort were presented at the Reactive Power Project Meeting on September 29th generating very useful feedback from our industry team members. For example, there was feedback on how reactive power producing DE can compare both economically and functionally with shunt capacitor banks. Shunt capacitor banks, which are typically used for compensating reactive power consumption of loads on distribution systems, are very commonly used because they are very cost effective in terms of capital costs. However, capacitor banks can require extensive maintenance especially due to their exposure to lightning at the top of utility poles. Also, it can be problematic finding failed capacitor banks and their maintenance can be expensive requiring crews and bucket trucks. Another shortcoming of capacitor banks is the fact that they usually are only one size at a location (typically sized as 300, 600, 900 or 1200kVAr) and thus don't have variable range as do reactive power producing DE and can not respond to dynamic loads.

The second phase of this effort is refinement of the initial report and incorporates comments from our industry team members that were solicited in September. The report needs to better define the market value of reactive power for the several case studies that have been selected. This next phase of the effort is also looking at the economics and technical requirements for oversizing an inverter for static-based DE. In addition, a new potential device for supplying reactive power is that of adjustable speed drives. They are quite numerous and one manufacturer has indicated that they can provide an adjustable speed drive capable of varying power factor correction; both leading and lagging power factor. The case studies are looking at a diversity of applications and industries such as a power distributor versus a power generation and transmission provider.

A future phase which isn't currently funded would be to gather more extensive and detailed information on the value of conventional reactive power supplying devices as well as their capital and maintenance costs. Capacitor banks cannot provide reactive power dynamically or respond in milliseconds to reactive power load shifts due to motors or other fast responding loads. Furthermore, additional case studies need to be performed to assess the variables affecting the potential value of dynamic reactive power from distributed energy. Also, system studies need to be conducted to determine how a significant penetration of reactive power producing DEs (such as 40% or greater of the reactive power needs of a distribution system) that are strategically placed could benefit overall power grid reliability. The potential exists for reactive power producing DE to provide higher overall reliability and make the transmission system less vulnerable to voltage collapse. A value needs to be determined for this overall system benefit. Another part of this effort needs to consider how to reduce the cost of inverter technology to reduce the cost of inverter-based DE devices.

Accomplishments

- A unique and first-of-its kind R&D laboratory for evaluating reactive power from DE has been established at the Oak Ridge National Laboratory. The Reactive Power Laboratory is capable of testing both rotating-based (generators, motors) and static-based (inverters) reactive power producing DE.
- A 300kVar Synchronous Condenser (250hp synchronous motor unloaded and overexcited) is operational at the laboratory for evaluating the local control of rotating-based DE with an actual distribution system. The synchronous condenser interfaces with a 2.4kV distribution circuit of the ORNL distribution system through a 480V/1000A power panel. The operation of the synchronous condenser met a milestone of injecting reactive power into the distribution system in May 2005. The synchronous condenser regulates the line voltage and net power factor of the local circuit by

varying its reactive power output. ***AOP Milestone 4.2.14.***

- A test of the synchronous condenser was performed during the summer with the device providing a maximum of 311kVar of reactive power. The operation of the synchronous condenser was monitored locally with instrumentation at the laboratory and with a distribution system wide monitoring system ("PowerNet"). The local monitoring captured local voltages, currents and power while the PowerNet captured voltages, currents and power at the substation and circuit level.
- A commercial power system analysis software and steady state model of the ORNL distribution system utilizing input data from the tests was used to model the voltage and current changes on the distribution system. The model results at the device location agree well with the actual data taken during the testing although the feeder and substation data have poor agreement.
- The capability of testing 3-phase inverters for producing reactive power from DE has been established at the Reactive Power Laboratory. The laboratory has the capability to test 75, 150 and 300A inverters off the grid using resistive and reactive load banks and to test them interfaced with the ORNL distribution system through a 480V/600A distribution panel that interfaces with a second 2.4kV circuit fed from the 3000 substation at ORNL.
- A Matlab/Simulink Software Platform and dSpace Real-Time Control Hardware and Software provide a versatile programming environment for developing and testing various control algorithms and schemes for the reactive power producing DE in the Reactive Power Laboratory. AOP Milestone 2.4.1.A report has been completed that assesses the viability of using Distributed Energy systems to provide different ancillary services. Ancillary services may create additional value streams for DE systems to improve the economical viability of installing these systems. A market for unbundled services would promote further installation of DG where costs could not be justified purely on real power generation. Power electronics offer significant potential to facilitate the use of DG in this application. ***AOP Milestone 2.4.1b.***
- A report entitled "Power Electronics for Distributed Energy Systems and Transmission & Distribution Applications" is complete. This report evaluates the R&D needs for DE systems and T&D applications including materials development, integration of multiple DE devices and provides recommendations for Power Electronics research and development activities. ***AOP Milestone 2.4.2***.
- The phase I report[4] on the potential economic viability of incorporating reactive power into distributed energy was completed and its results were presented to the industry partners and team at the Reactive Power Project Meeting on September 29th at ORNL in Oak Ridge. The next phase of the report will be to incorporate feedback from the industry partners. ***AOP Milestone 5.1***.

References

3. Reactive Power Laboratory: Synchronous Condenser Testing & Modeling Results, Interim Report, Oak Ridge National Laboratory, ORNL/TM-2005/174, August 22, 2005.
4. J. D. Kueck, B. J. Kirby, L. M. Tolbert, D. T. Rizy, "Voltage Regulation: Tapping Distributed Energy Resources," Public Utilities Fortnightly, vol. 142, no. 9, September 2004, pp. 47-51, http://www.pur.com/puftocs/sep04.cfm.

[4] Evaluation of Distributed Generation as a Source of Reactive Power Supply, prepared for Oak Ridge National Laboratory by Energetics, Inc., draft report, June 17, 2005.

4.3 Cooling, Heating, and Power

Patti Garland
Engineering, Science and Technology Division
Oak Ridge National Laboratory
(202)479-0292; email: garlandpw@ornl.gov

DOE Technology Development Manager: Merrill Smith

202-586-3646; email: merrill.smith@hq.doe.gov

Objective

The objective of this activity is to promote CHP installations into the public and private sectors by focusing on the issues of CHP awareness, regulatory and institutional barriers, and CHP economic feasibility. In regards to CHP awareness, there is a tremendous need to educate citizens, business executives, and public policy makers on the merits of clean, efficient energy generation using CHP. In regards to regulatory and institutional barriers, there are CHP systems that are commercially viable today but that developers have trouble getting installed because of roadblocks in siting, permitting, and interconnecting. This work complements ORNL Projects under Integrated Energy Systems and End-Use Systems Integration.

Approach

ORNL issued a solicitation at the end of FY 2002 for CHP-related projects. The objective of the solicitation was to support activities that facilitate and encourage the use of CHP technology in the U.S. The statement of work for the solicitation was developed in response to the "Consensus Action Items from the CHP Roadmap Process" issued in June 2001, which supports the National Energy Plan. ORNL is synthesizing the data and tools developed under these contracts and is disseminating the information to the CHP application centers and stakeholders.

Accomplishments:

- In the 3 year period of this effort, over 19 reports were issued. Other products include databases, tools, calculators, presentations, workshops, case studies, and briefings.
- Held a CHP Subcontractor Coordination Review Meeting in Washington DC in April 2005. Presentations at: www.eere.energy.gov/de/chp/chp_applications/projects.html
- Continued biannual face-to-face meetings and quarterly conference calls with the RACs.
- Developed screening software for evaluating CHP potential in multi-family housing.
- ORNL developed a model that supports the US Green Building Council's initiative to ensure that appropriate LEED credit is assigned for innovative on-site cooling, heating and power (CHP) systems.
- Completed and delivered the CHP toolkit for Regional Application Centers

Future Direction:

- ORNL will continue to provide technical support to the CHP Regional Application Centers through screening, analyses, modeling, and coordination of activities.
- ORNL will continue to provide technical support to HUD.
- ORNL will continue to take an active role in getting proper credit for CHP in LEED certification.

Introduction

The National CHP Roadmap set the course for achieving 92 GW of CHP capacity in the U.S. This goal is expected to result in estimated energy savings of 2.4 quadrillion Btu per year and a reduction of 276 million tons of CO_2 per year compared to separate electricity and thermal energy generation. The National CHP Roadmap was the culmination of a wide array of industry-led activities including meetings, workshops, and public forums. The origin of these activities was a conference held in Alexandria, Virginia, on December 1, 1998, where the "CHP Challenge" was initiated by the DOE and the U.S. Environmental Protection Agency (EPA) with the goal of doubling the amount of CHP capacity in the U.S. from 46 GW to 92 GW by 2010. The purpose of the roadmapping effort was to organize all the ideas into a plan for action. Eighteen CHP workshops were held at locations across the country to convene stakeholders and discuss problems and solutions. These workshops involved almost 1000 individuals, representing equipment manufacturers, electric and gas utilities, architect and engineering firms, project developers, federal and state agencies, universities, national laboratories, and public interest groups.

The culminating event was the National CHP Roadmap Workshop held October 12-13, 2000, in Baltimore, Maryland. This workshop brought together representatives from the previous workshops to discuss progress made and to chart the next steps. As a result, the Roadmap consists of a series of specific actions for raising CHP awareness, eliminating regulatory and institutional barriers, and developing markets and technologies, all aimed at achieving the CHP Challenge goal of doubling CHP by 2010.

ORNL, in support of the National CHP Roadmap is interested in substantial improvements in the number of applications of combined CHP systems. The vision of this project is to maximize the use of affordable combined heat and power systems powered by distributed energy resources in order to make the U.S. energy system cleaner, more efficient, and more reliable. The results, successes, and experiences from the tasks in this project will be posted to the DOE DE website and distributed to the Regional CHP Application Centers and industry partners through webcasts, conferences, workshops, training, teleconferences, and face-to-face meetings.

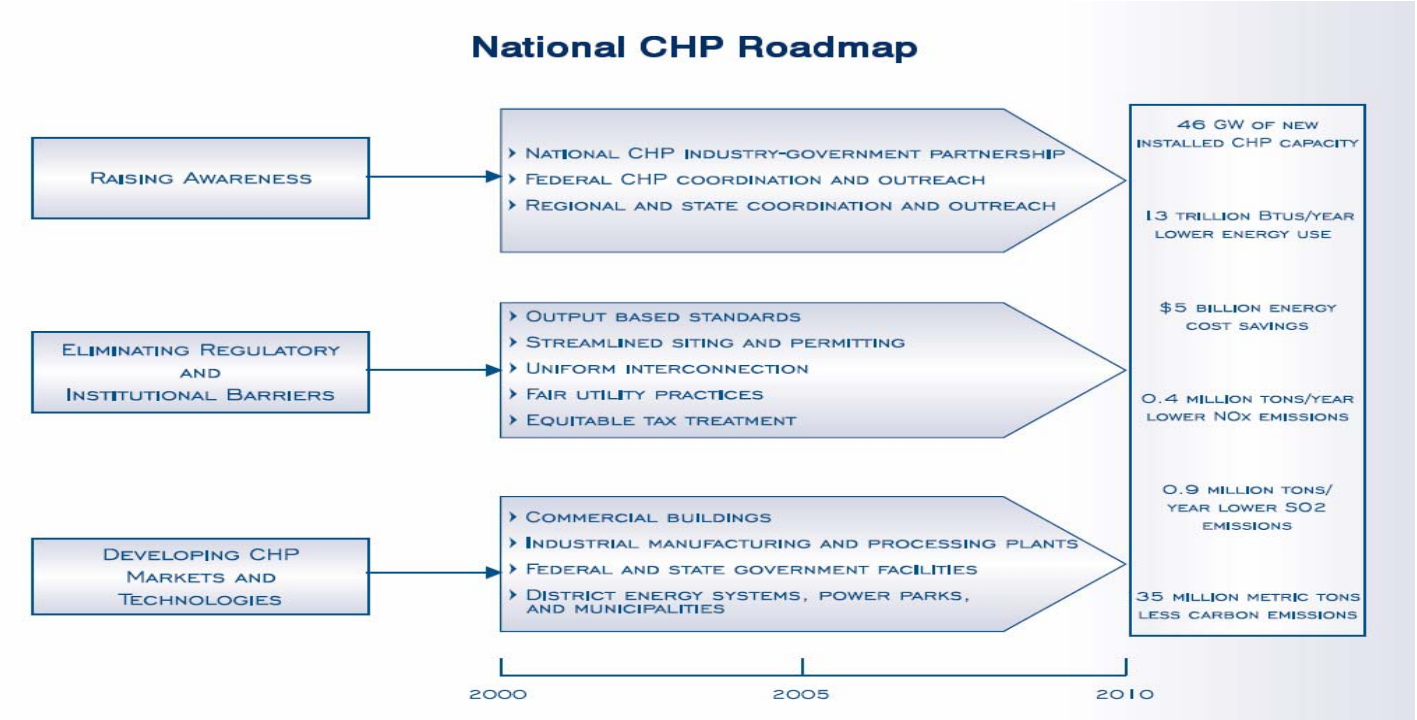

Accomplishments and Progress

ORNL has been working with EEA in the development of a CHP Installation Database, which has been the primary source for tracking progress to the 92 GW goal. The database currently has 2,960 operating sites representing over 82 GW of capacity. Since the development of the Roadmap, the most significant growth period was in the 2000-2003 timeframe. The past two years have seen a relatively low growth rate in CHP additions.

Additions by sector:

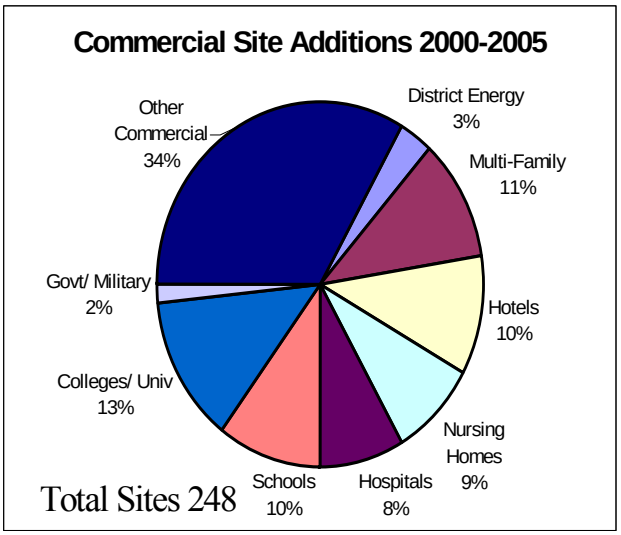

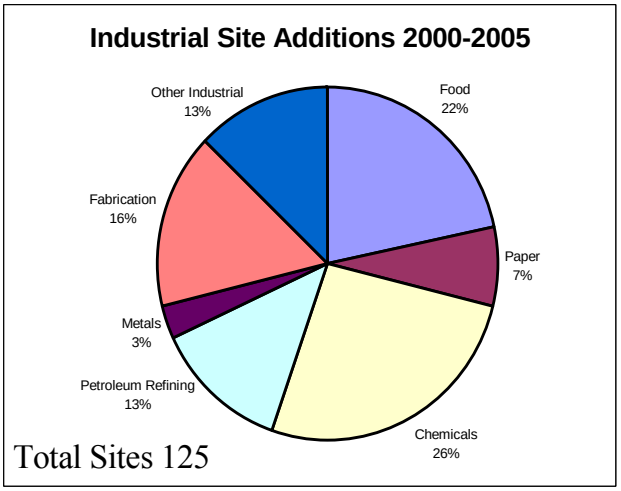

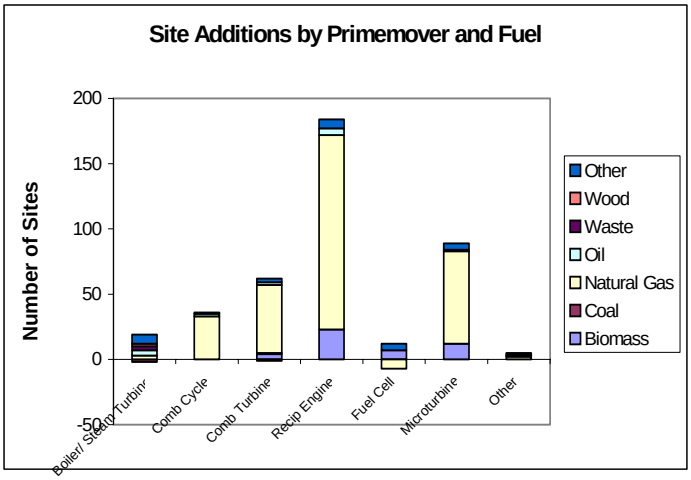

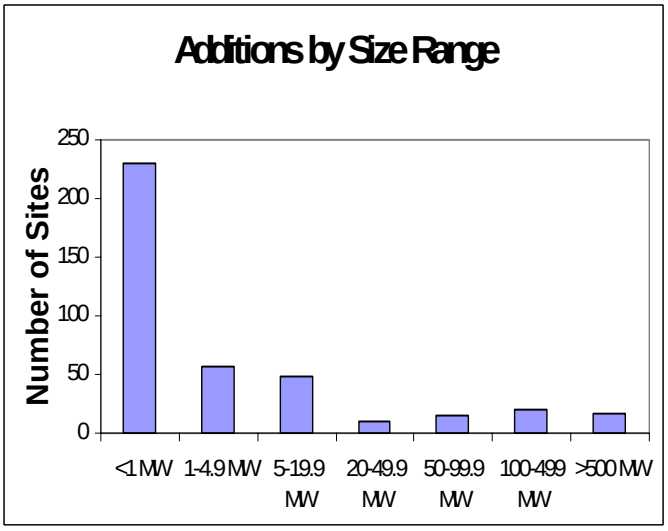

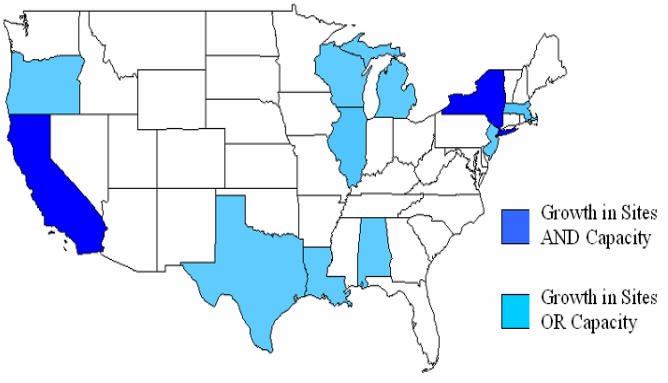

Conclusions and Recommendations

The 2001-2005 CHP market trends can be summarized as follows:

- Annual CHP site additions increased from 2001 to 2003 and then decreased in 2004 and 2005.
- There has been a decrease in CHP capacity (MW) additions every year since 2001.
- While commercial applications make up the majority of new CHP sites, capacity (MW) additions are dominated by industrial applications.
- Natural gas has continued to be the dominant fuel for CHP.
- The majority of site additions in the 2000-2005 timeframe have been natural gas-fired reciprocating engines less than 1 MW.
- The vast majority of recent CHP capacity additions have come from very large projects.
- With regard to geographical trends in new CHP, growth tends to be concentrated in the Northeast, Midwest, Gulf Coast, and West Coast. There has been high project activity in the Midwest, Northeast, and Pacific regions and the large capacity additions due to very large CHP projects in the Gulf Coast.

As the CHP community develops priority action items to achieve the 92 GW goal, these trends need to considered. Small commercial installations make up the majority of recent CHP activity but comprise just a small contribution to capacity additions. Continued focused activities and coordinated strategic planning sessions with industry need to continue to answer many questions that could include: What is the appropriate balance between commercial, institutional and industrial markets? What is the appropriate balance between small and large CHP applications? The price of natural gas is typically viewed as the primary contributor to the decrease in CHP market activity. What customer sectors or geographical markets provide the best opportunities to mitigate fuel price risk? States with historically favorable spark spreads and incentive programs for CHP, e.g., California and New York have experienced growth in both projects and capacity additions. What can be done to promote and accelerate the development and implementation of incentive programs in other states? What can be done to with regard to incentives in EPACT to improve CHP economics?

Subtasks

4.3.1 Facilitate CHP working group; review environmental models and utility interconnection and tariff practices with project partner ACEEE.

The project tasks are: 1) identify individual interconnection and tariff practices on a state-by-state basis, 2) conduct a review of existing emissions models to produce some basic rules of thumb for regulators, policy makers, and CHP system developers to estimate the general local environmental impact of a CHP system, and 3) facilitate the CHP Analysis Working Group. Status of tasks: 1) ACEEE is creating a database for 22 states. Utility companies related to expanded adoption of CHP in each state have been identified. A preliminary report on *State Opportunities for Action: Update of States' CHP Activities*can be found at: http://www.aceee.org/pubs/ie032full.pdf 2) Research has been completed on the methodologies of IPM and AMIGA. 3) Have held several meetings of the CHP Analysis Working Group. The next meeting will be on the topic of Small CHP.

4.3.2 Prepare market segment reports, trade show booth materials, conduct workshops with project partner AGF.

The project tasks are: 1) natural gas and energy price volatility study, and 2) market analysis of CHP potential in national account sectors. This project tasks are complete: 1) Prepared a 2-part report that presents a summary of an in-depth study of the issue of energy price volatility and the impact of volatility on consumers, industry participants, and the penetration of new technologies, and 2) in conjunction with AGF's National Accounts Energy Alliance, completed a report on market potential for advanced thermally activated BCHP in Five National Accounts Sectors.

4.3.3 Prepare database of CHP installations with turbine inlet cooling and/or thermal energy storage with project partner Cool Solutions.

This project is complete. A final summary report and database have been published and can be found on the DOE DE website. Many combined heat and power (CHP) systems can and do incorporate thermal energy storage (TES) and/or turbine inlet cooling (TIC) systems to improve the overall system economics. 56 CHP installations have been identified and entered into the database, each incorporating either TES or TIC, or both. 53 of these installations are in the U.S. The rated capacities of all combustion turbines are based on the standard ambient air conditions of 59 °F and 14.7 psia at sea level, as selected by the International Standards Organization (ISO). One unattractive characteristic of

all combustion turbines is that their power output decreases as the ambient air temperature increases, as shown in the following figure.

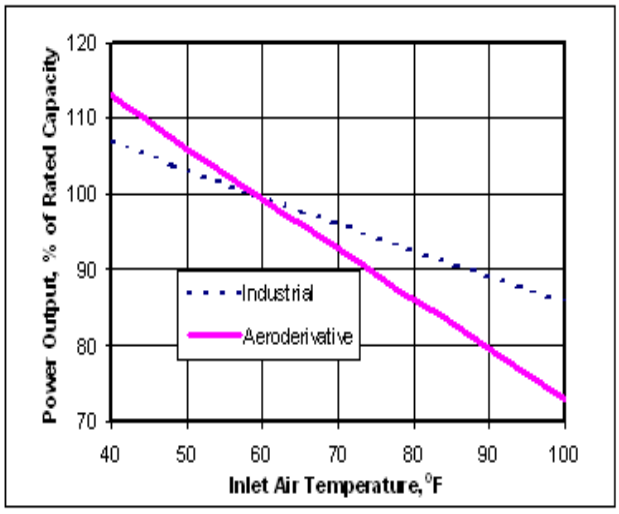

Effect of Ambient Temperature on the Output of Combustion Turbines

4.3.4 Preparation of CHP issue papers with project partner DUA.

The purpose of this project is to provide California Edison decision makers with input on policy and market opportunities to DER integration where it brings value to the customers and the grid. A draft report entitled: *The Value of Distributed Generation and Combined Heat and Power Resources in Wholesale Power Markets,* was completed in September 2005 and is currently undergoing review.

4.3.5 Coordination of CHP meetings and stakeholder outreach with project partner Energetics.

The project tasks are: 1) plan and coordinate the CHP Roadmap meeting, 2) Coordinate the CHP Team meetings, and 3) Coordinate education and outreach materials. Status of Tasks: 1) Task is ongoing, Implemented 2004 workshop in Austin, Texas. Coordinating 2005 workshop to be held in New York City. 2) Meetings are held on a quarterly basis in Washington DC. Stakeholder partners, including USCHPA, IDEA, HUD, EPA, VA, and industry partners participate in these meetings. and 3) Coordinated development and implementation of the IES Webcast held in September 2005. Approximately 581 persons viewed the webcast as individuals or in 29 viewing groups set up by CHP Regional Application Centers.

4.3.6a Analysis of Environmental Regulatory Barriers and Incentives for CHP with Project Partner Energy and Environmental Analysis.

This project tasks are: 1) Air quality permitting barriers to CHP, 2) CHP Emissions/Credit Calculator, 3) CHP Permitting and Regulatory Requirements Database, and 4) Environmental Regulatory Analysis on CHP/DG issues. Status of tasks: 1) The draft report has been completed and is undergoing review. 2) The CHP Emissions Calculator (EC) is a tool to estimate the net air pollution emissions from a small CHP system. The EC performs calculation for NOx, SO2, CO2 and mercury (Hg).

The EC is a Microsoft Excel spreadsheet that calculates net emissions based on information provided by the user and default information provided by the system. The net emissions are calculated from three primary components: onsite emissions from the CHP system, displaced emissions from onsite thermal production (i.e., steam boiler), and displaced emissions from offsite generation of electricity. The net emissions equal the emissions from CHP minus the displaced emissions from thermal production and electricity production. The emissions calculator can be found at: http://www.eea-inc.com/dgchp_reports/EEA-CHP-Calc4-05.xls.

3) The regulatory requirements database for small electric generators can be found at:

http://www.eea-inc.com/rrdb/DGRegProject/index.html

4) This task is a series of white papers for ORNL/DOE consumption only.

4.3.6b CHP Applications and Analytical Support with Project Partner Energy and Environmental Analysis.

Project tasks include: 1) Development of a CHP installation database, 2) installation cost analysis for small CHP, 3) DG/CHP financing options, and 4) electric rate primer. Status of tasks: 1) The CHP installation database is complete and is posted at: http://www.eea-inc.com/chpdata/index.html. A sort of the CHP installations have been made by state and then grouped into Regions consistent with the CHP Regional Application Centers. The RACs reviewed for accuracy the sites in the database and added sites that were not in the database. Reports against the CHP Goal of 92 GW are taken from this database. This database will be updated through FY2006. 2) A draft report was provided in August 2005 and is undergoing review. 3) two reports were drafted: *DG Financing Options* and *Industry Feedback on Financing Issues*. They are

undergoing review and will be published in 1st quarter FY06, and 4) a draft report *Impact of Electric Rate Structures on CHP Economics* was drafted and is undergoing review. It will be published in 1st quarter FYY06.

4.3.6c Analysis of Industrial and Commercial CHP Markets with project partner Energy and Environmental Analysis.

Project tasks include: 1) Inventory of existing industrial/commercial boiler population, 2) evolution in the demand for steam, 3) changing CHP applications, 4) forecast of new and conventional industrial CHP. The final report *Characterization of the U.S. Industrial/Commercial Boiler Population* can be found at:
http://www.eea-inc.com/natgas_reports/BoilersFinal.pdf
The U.S. industrial and commercial sectors consume large quantities of energy. Much of this energy is used in boilers to generate steam and hot water. EEA estimates that there are almost 163,000 industrial and commercial boilers in the U.S. with a total fuel input capacity of 2.7 million MMBtu/hr. These boilers consume about 8,100 TBtu per year, accounting for about 40 percent of all energy consumed in these sectors. This report characterizes the boilers in the industrial and commercial sector in terms of number of units, aggregate capacity, unit capacity, primary fuel, application and regional distribution. The report also includes analysis of boiler fuel consumption and the age of boiler units. It does not include an inventory of individual boilers. A think piece on the task 4 forecasting of the boiler population was drafted and is being vetted with the American Boiler Manufacturers Association.

4.3.6d DG Operational Reliability and Availability Database with project partner Energy and Environmental Analysis.

The increased deployment of Distributed Generation (DG)/Combined Heat and Power (CHP) has been identified as a means to enhance both individual customer reliability and electric transmission and distribution system reliability. DG/CHP reliability and availability performance relates to several significant issues affecting market development. The reliability/availability profiles for DG/CHP systems can affect electric standby charges and backup rates, the value of ancillary services offered to Independent Transmission System Operators (ISO), local grid stability and reliability, customer power delivery system reliability, and customer economics. Interest in power reliability has heightened in recent years in light of highprofile system. This project represents the first attempt to establish baseline operating and reliability data for DG/CHP systems in more than a decade. This project is complete with publication of two documents: 1) *Executive Summary Report: Distributed Generation Operational Reliability and Availability Database* that can be found at: http://www.eea-inc.com/dgchp_reports/DGRELExecSummaryReport.pdf, and 2) the final report, *Distributed Generation Operational Reliability and Availability Database*, can be found at the following url: http://www.eea-inc.com/dgchp_reports/FinalReportORNLDGREL.pdf.

4.3.7 Facilitation of CHP in the Northwest with project partner Energy International [now Energy and Environmental Analysis].

Project tasks include: 1) Market assessment of the opportunities for combined heat and power (CHP) in the Pacific Northwest, specifically in the states of Washington, Oregon, Idaho, and Alaska, including developing a baseline of existing CHP in each state, estimating the technical and economic market potential for CHP in each state, and providing a comprehensive review of market, regulatory and institutional impediments to CHP development in the Northwest, 2) case studies and a brochure for regulators and policy makers. 3) Adding Arizona and Nevada to the market assessment developed in task 1, and 4) Western States Summary Evaluation including a consolidated summary report of the CHP market potential in the eight states that represent the market focus of the DOE-WRO (Alaska, Hawaii, Idaho, Oregon, Washington, California, Arizona, and Nevada.). This project is complete. The final report summary titled: "CHP Market Potential in the Western States," can be found on the Pacific CHP Regional Application Centers website: www.chpcenterpr.org. The following case studies were completed and provided to the Pacific RAC for posting on their website:

- 525 kW Wind/Diesel Hybrid CHP Plant in Alaska
- 130 MW Gas Turbine Combined Cycle Power Plant at SP Newsprint Company
- Lewis and Clark College 30 kW microturbine CHP in Portland, Oregon
- Kimberly Clark 52 MW Wood-Chip Fired Steam-Turbine Generator in Washington

- Columbia Boulevard Wastewater Treatment 320 kW Fuel Cell and Microturbine Plant in Portland, Oregon
- Kenai Fjords National Park 5 kW solid oxide fuel cell in Seward, Alaska

4.3.8 Development of guide on sustainable metropolitan energy planning with project partner Gas Technology Institute

This project is complete. The guide was submitted as the official U.S. entry to the International Competition for Sustainable Urban System Design, the San Diego/Tijuana region was the subject for creation of an integrated energy, environmental, land-use, and transportation design for the year 2103. In addition, the entry included an information resources guide for all American cities that will describe innovative approaches to sustainable energy planning, derived from the seven finalist cities in the U.S. competition. The guide will provide information on clean power generation, distribution and use technologies, alternative transportation fuels/fleets, energy efficiency programs and practices, financing for municipal sustainability, and emerging technologies. Two documents were published: 1) Model *for Sustainable Urban Design*, and 2) *Blueprint for Urban Sustainability: Integrating Sustainable Energy Practices into Metropolitan Planning*.

For copies of these docuements, please see: http://www.gastechnology.org/webroot/app/xn/xd.aspx?it=enweb&xd=1researchcap\1_6distenergy\1_6_1_researchcapabilities\energyandenvironmentalhomepage.xml

4.3.9 Development of environmental permit screening tool with project partner I.C. Thomasson.

The draft report was complete in April 2005. The final report will be submitted in the 1st quarter of 2006, at which time it will be posted on the DOE DE website. The tool developed under this project will assist facilities that desire to install cogeneration plants to determine the air permitting process that would be required to meet applicable environmental regulations and standards. This Environmental Permitting and Screening Tool is applicable to facilities interested in installing a gas turbine between one and five megawatts and located in the EPA's Region IV located in the Southeastern United States [Mississippi, South Carolina, North Carolina, Tennessee, Georgia, Alabama, and Florida. The tool provides a brief overview of gas turbines, emissions produced by a cogeneration plant and how gas turbines are regulated, the applicable Code of Federal Regulations, and how to determine the type of permit required.

4.3.10 Screening and ranking of potential college and university campus sites for CHP with project partner IDEA.

This project is complete. The final report is provided in powerpoint format and can be foundon the DOE DE website. A presentation on consensus survey and lessons learned was provided by IDEA Executive Director Rob Thornton at IDEA's 15th College and University Conference held in 2002. For that presentation, see: http://www.eere.energy.gov/de/pdfs/chp_idea_survey.pdf

4.3.11 Coordination of regional initiatives and stakeholder activities with project partner NEMW Institute. The project tasks are: 1) Education and Outreach Briefings, 2) Manufacturing Sector Initiatives, and 3) CHP/DE Regional Initiatives. Task status: 1) The following capital hill briefings were held:

- On October 3, 2005, *Distributed Energy and the Energy Bill*, which addressed legislative solutions needed, even after the recent energy bill, to overcome the policy barriers to distributed electricity generation. Discussing those barriers and the benefits of distributed generation were representatives of the U.S. Combined Heat and Power Association, International District Energy Association, American Council for Energy-Efficient Economy, and Calpine Corporation.
- On September 19, 2005, *Multi-Family Housing: An Underserved Market for Combined Heat and Power.* Representatives of the Department of Housing and Urban Development, the Mid-Atlantic CHP Application Center, and Energy and Environmental Analysis reviewed the potential for cogeneration as well as the federal programs that could encourage its use in multi-family housing.
- On February 23, 2005, *Combined Heat and Power - Realizing the Promise***.** The session quantified cogeneration's potential, reviewed what's at stake, and outlined barriers that need to be addressed. Speakers were from Energy and Environmental Analysis, the New York City Economic

Development Corporation, and the U.S. Combined Heat and Power Association.

- On January 31, 2005, *CHP's Contribution to Alleviating Tight Natural Gas Markets.* Speakers were from Energy and Environmental Analysis, Inc., American Forest and Paper Association (AF&PA) and Cummins Inc.

The following guide was issued and can be found on the NEMW website: *Combined Heat and Power Education and Outreach Guide to State and Federal Government*, issued October 2005.

2) A Workshop to Identify CHP Opportunities in the NE Food and Beverage Processing Industries was held January 27, 2005, Syracuse New York, and 3) Coordination of the CHP Regional Initiatives continues. Quarterly calls are held and minutes are distributed to DOE, ORNL, USCHPA, PEA, and Regional Initiative Representatives. An end-of-year status report in powerpoint presentation is being posted to the DOE DE website.

4.3.12a A review of distributed generation siting procedures with project partner Resource Dynamics.
This project is complete. The final report was issued and is posted on the DOE DE website. The final report includes recommendations for state and local regulators to improve DG siting:

- Reducing permitting and interconnection times
- Mandating statewide utility business terms
- Standardizing and streamlining the interconnection process; consistent with IEEE 1547
- Considering the value of CHP thermal output and the DG state of the art in state air emissions requirements
- Providing incentive programs that give an early push towards market adoption of new DG technologies and energy efficient technologies such as CHP

The report also includes four siting principles to guide DG developers and customers in reducing siting costs and time:

- Careful up-front planning will avoid unnecessary risks
- Developers should budget for interconnection uncertainty, and try to get resolution on these issues as soon as possible
- To reduce costs, developers should consider DG equipment that has been pre-certified in states where that applies.
- Make use of existing government and utility providing siting tools.

4.3.12b Market potential of opportunity fuels in DER/CHP applications with project partner Resource Dynamics.
Phase I of this project included 3 tasks and is complete: 1) collect and evaluate opportunity fuel information, 2) explore DER/CHP technology options, and 3) develop potential market estimates and make recommendations. This work has been of much interest to the CHP community, as evidenced by the webcast request and the many invited presentations. The final report can be found on the DOE DE website. Phase II of this project will be complete in FY06. In the Phase II effort, a state-by-state analysis of the impact of state level renewable portfolio standards will be performed, using state target dates and impacts as well as emerging values of renewable energy certificates (RECs). This analysis builds off of the completed Task 3 opportunity fuel assessment. It will analyze the potential capacity from opportunity fuels that would satisfy the state renewable portfolio standards, based on availability of fuel, economics of opportunity fueled CHP, and prospects for wind and solar renewables.

4.3.13 Assessment of target markets (healthcare, education, data processing) with project partner University of Illinois, Chicago.
This project is complete. The final report has been published and can be found on the DOE DE website. This report defines the opportunity for CHP in three specific commercial building market segments

• Smaller Educational Facilities,
• Smaller Healthcare Facilities, and
• Data Centers/Server Farms/Telecom Switching Centers

Major issues affecting each of these markets are explored in the report in detail to provide guidance on the best manner to present the CHP concept to meet individual market concerns and needs.

4.3.14 Information dissemination, awareness campaigns, stakeholder meetings with project partner USCHPA.
This work is complete. It consisted of three tasks: 1) select and profile industrial market sectors with high potential for CHP utilization, 2) evaluate CHP technologies and applications, and 3) exchange information with stakeholder groups to promote the awareness and deployment of CHP.

The work was conducted in accordance with the earlier strategy that emerged from the "MARKET AND CROSS-CUTTING TECHNOLOGY ASSESSMENT FOR INDUSTRIAL SECTORS WITH HIGH POTENTIAL FOR CHP UTILIZATION," prepared during the first year of the contract. Three high-potential industrial markets were chosen by the USCHPA and its subcontractors, namely 1) Food processing, 2) Pharmaceutical, and 3) Wastewater treatment. Information on a. Industry Sector Analysis, b. CHP Market Potential, c. Industry-specific Technologies, and d. Key Industry Associations was characterized for each industrial market. Initial research indicated that the pharmaceutical industry was already relatively well developed in its CHP potential, so the project then focused on the remaining two sectors.

Food Processing outreach focused on consensus building, website coding, and workshop presentations. Deliverables included: a Website detailing nine promising food & beverage sectors, benefits, drivers, incentives, emerging technologies, thermal energy uses, etc. at http://www.sentech.org/CHP4foodprocessing/ and a 4-page brochure completed in conjunction with EEA. In addition to networking and exchanging information with above groups, USCHPA and SENTECH conducted information exchange activities with several other groups including Energy Solutions Center, Energy & Environmental Analysis, the National Food Processing Association, the California League of Food Processors, the American Meat Institute, as well as twenty-some other food and beverage industry associations.

Wastewater Treatment outreach focused on professional journal and conference presentation modes. The contract team participated integrally in planning and conducting a conference on "Environmental Issues for Energy Generation in the Non-Utility Sector" with the Air and Waste Management Association, in Arlington, Virginia, April 4-5, 2005. A CD of the conference proceedings WAS issued and distributed to all attendees; a copy could be provided at your request. The following articles were completed: APPA DEED Digest article--attached. Deliverable 9. BioEnergy Update article--attached. Power Magazine article draft (presented to Ken Wicker a few months ago, currently under final editing)--draft attached.

USCHPA worked closely with the Aspen Institute's Energy and Environmental Task Force to assure that CHP and clean distributed energy played a prominent role in the program for the Institute's annual Energy Policy Forum held July 1-5, 2005, which addressed the theme, "Who is Responsible for Future Power Supply." This included arranging for Tom Casten, CEO of Primary Energy, to participate in the keynote panel, for Michael Brown of WADE as well as John Jimison of USCHPA to be invited as participants. As a result of this participation, the potential role of CHP and other distributed generation in future power supply was a major theme of the discussions. The forthcoming conclusions of the Forum are likely to note the significant potential of CHP to provide clean power with security and other advantages.

4.3.16 Coordination of Regional CHP Application Centers with project partner Power Equipment Associates.

This project consists of multiple tasks including: 1) attend kickoff meetings of each Regional Application Center to provide: Input / guidance to application center approach, provide sources / clarification of existing application center processes and activities, provide guidance on startup or leveraging of industry coalitions and provide summary of strengths from other regions, 2) Develop Regional Application Center Steering Committee/Working Group, 3) plan and conduct quarterly application center working group conference calls, 4) issue annual regional application center coordination report and presentation. This report will provide a discussion of accomplishments and plans for the following year for US DOE's Regional Application Center Program, and 5) complete a CHP Tool Box, a resource guide for CHP Application Centers. Acoomplishments include: the end-of-year report that can be found on the DOE DE website, coordination of quarterly RAC calls, completion of two face-to-face RAC meetings, planning and facilitation of the RAC roadmap meetings in the Gulf Coast and the Southeast and completion of the RAC toolkit, which is being distributed to the RACs on a CD.

4.3.20 Technical support to HUD.

Under a work-for-others agreement with HUD in support of the HUD Energy Action Plan, ORNL is providing technical assistance in the area of CHP for multi-family housing. ORNL developed screening software for evaluating CHP potential in multi-family housing. This stand-alone program is based on an appendix attachment in the FY2005 *HUD CHP Guide #2 Feasibility Screening for Combined Heat and Power*

in Multi-Family Housing, whose audience is apartment building owners and managers. The program is being adapted to include CHP systems incorporating uses of recovered heat for space cooling in addition to space heating and hot water heating. ORNL is providing technical assistance on an as-needed basis to the eight DOE Regional CHP technical assistance centers who have been enlisted to reach and advise owners of apartment buildings on the opportunities for using CHP. A copy of the ORNL developed program can be downloaded from the following website: http://www.ornl.gov/sci/engineering_science_technology/cooling_heating_power/success_analysis_HUD.htm

4.3.21 Techncial support to LEED.

ORNL is an active participant on the LEED CHP subcommittee [hosted by the U.S. Green Buildings Council], which is ensuring that appropriate LEED credit is awarded for on-site power generation CHP. Objectives of ORNL are to participate in reviews, and model and evaluate CHP applications for incorporation into guidance issued by LEED. In addition, ORNL participation is encouraging development of LEED 3.0 to more fully incorporate benefits of CHP such as reduced air emissions and improved efficiency of fossil fuels. ORNL developed a model and analyzed example cases for how the calculation methodology, developed by the committee, would be applied. This model has been reviewed and approved by the committee and is being discussed with the full Technical Advisory Group (TAG) for LEED Environment and Atmosphere credit 1 for incorporation in guidance provided with LEED 2.2. The TAG has approved 3 of 4 cases for deploying CHP system. LEED credit available for the fourth case, third-party ownership of a district CHP system, is still being discussed with the TAG.

The LEED approach is to compare a 'baseline case' with a 'design case' where the design case improves the building's energy and environmental performance. Extensive and complex modeling of energy savings associated with a district CHP system would required to compare a design case with energy supplied from the district system to a base case with building boilers and chillers However, this is not practical, so a specific method for crediting the energy benefits of district CHP is provided in the recommended text for insertion into LEED NC 2.2 EA Credit 1 Reference Guide. Key factors for identifying structural issues associated with application of this performance review method include:

- Whether the CHP is internal or external to building;
- Whether the CHP output is purchased from another entity (usually correlated with ownership of the building vs. the CHP); and
- Whether all CHP output is used inside the building.

CHP cases are categorized as follows for the purpose of highlighting the key structural issues. These conceptual cases are summarized in the Table below

Case	**Ownership of CHP vs. building**	**Design heating source**	**Design cooling source**	**CHP location**	**Power**	**Thermal**
1a	Same	CHP + boilers	CHP + chillers	Inside building	All in building	All in building
1b	Same	CHP + boilers	CHP + chillers	Inside building	Some or all sold to grid	All in building
2	Different (3rd party CHP owner inside building)	CHP + boilers	CHP + chillers	Inside building	All in building	All in building
3a	Common ownership	Campus heating plant with CHP	Campus cooling plant with CHP	Campus energy plant	Campus power supply + district energy plant in-house use for thermal production	District energy plant production of heating & cooling
3b	Common ownership	Campus heating plant with CHP	Campus cooling plant with CHP	Campus energy plant	Some or all sold to grid	District energy plant production of heating & cooling
4a	Different (district energy plant)	District heating plant with CHP	District cooling plant with CHP	District energy plant	District energy plant in-house use for thermal production	District energy plant production of heating & cooling
4b	Different (district energy plant)	District heating plant with CHP	District cooling plant with CHP	District energy plant	Some or all sold to grid	District energy plant production of heating & cooling

Project Reports:
A description of reports published under this project are included within the above taks along with the appropriate urls.

Project Databases:
A description of databases developed under this project are included within the above tasks along with the appropriate urls.

FY05 Presentations:
1. P. W. Garland presented "Status of the DOE DE CHP Program Activities," at the Roadmap meeting of the Southeastern CHP Regional Application Center held in Atlanta, Georgia, September 2005.
2. J. Sand presented "Desiccant Dehumidification and Absorption Systems – Building Blocks for CHP," at the Roadmap meeting of the Southeastern CHP Regional Application Center held in Atlanta, Georgia, September 2005.
1. T. L. Bronson presented "CHP Application Center Basics," at the Roadmap meeting of the Southeastern CHP Regional Application Center held in Atlanta, Georgia, September 2005.
2. B. Hedman presented "Status and Potential of CHP in the Southeast," at the Roadmap meeting of the Southeastern CHP Regional Application Center held in Atlanta, Georgia, September 2005.
3. P. L. Lemar presented "Market Size – Market Opportunities," at the CHP and Bioenergy for Landfills and Wastewater Treatment Plants Workshop held in Salt Lake City, August 2005.
4. P. L. Lemar presented "CHP Systems for Landfills and Wastewater Treatment Plants," at the CHP and Bioenergy for Landfills and Wastewater Treatment Plants Workshop held in Salt Lake City, August 2005.

5. Fischer presented the ORNL BCHP Screening Tool overview at the CHP Regional Application Center Face-to-Face Meeting held in Washington, DC, May 2005.
6. Doug Hinrichs presented "Evaluating Energy Conservation Systems to Maximize Effectiveness Through the Manufacturing Process" at the Food and Beverage Summit held in LaQuinta, CA, May 2005.
7. T. L. Bronson presented "DOE's CHP RAC Program," at the Roadmap meeting of the Gulf Coast CHP Regional Application Center held in the Woodlands, Texas, April 2005.
8. B. Hedman presented "CHP Market Status: National and Regional Perspectives," at the Roadmap meeting of the Gulf Coast CHP Regional Application Center held in the Woodlands, Texas, April 2005.
9. P.W. Garland presented "Energy Security at Federal Buildings," in the Distributed Generation, CHP and Recycling Energy Track at Electric Power 2005, held in Chicago, in April, 2005.
10. Doug Hinrichs presented "Energy Production and Efficiency in Wastewater Treatment Facilities" at the Air and Waste Management Association meeting held in Arlington, Virginia, April, 2005.
11. P. W. Garland presented "Recycling Waste Heat – A CHP Alternative," at the Waste Heat to Power Generation Workshop held at the University of California Irvine, in March 2005.
12. J. J. Cuttica presented "Opportunity Fuels for CHP" at the CHP for Food and Beverage Processing Industries Workshop held in Syracuse, New York, January 2005.
13. P.L. Lemar presented a 3-hour webcast on "Opportunity Fuels for CHP," in December 2004.
14. B. Hedman and P. Bautista presented a 3-hour webcast titled "Update on ORNL/DOE DG/CHP Program," in October 2004. Webcast covered: DG Reliability Database, CHP Facilities Database, Regulatory Database, and CHP Emissions Calculator.
15. P. W. Garland presented "ORNL IES/CHP Research Activities" at CHP Regional Application Center Face-to-Face Meeting held annually, Austin, Texas, September 2004.

6.1 DE Crosscutting, Systems Integration, and Analysis

Therese Stovall
Engineering, Science and Technology Division
Oak Ridge National Laboratory
(865)574-0329; email: stovalltk@ornl.gov

DOE Manager: Patricia Hoffman
(202) 586-6074; email: patricia.hoffman@ee.doe.gov

Objective

- Provide the foundation for informed program management decisions, including the definition of program priorities, direction, effectiveness, and strategy.
- Facilitate the deployment of advanced technologies developed under the program mantle by conveying the full extent of potential benefits and the role of DE in the energy market.
- Support cooperation and partnership with other DOE offices and other government agencies, such as the EPA, FERC, and IRS. This cooperation will meet their needs, as well as facilitating the DE program's efforts to remove deployment barriers under the control of these agencies.

Approach

- Consider Distributed Energy benefits analyses on a national, regional and local basis. A broad national analysis will provide potential market penetration of DE. However, due to regionalized market and regulatory drivers, it is important to understand impacts within local and regional areas. Several SCE feeders were selected for a localized analysis.
- Analyze the expansion potential of DER in the customer-owned utility market.
- Quantify the value of DER in ancillary electricity markets such as reserves and reactive power. Coordinate DOE efforts with the Mid-Atlantic Distributed Resources Initiative (MADRI), with particular emphasis on advanced metering and improving the DE business case.

Accomplishments:

- Three articles were published in Public Utilities Fortnightly to disseminate the results of prior analyses. The full reports were placed on the DOE web site.
- A white paper describing the potential for DG in the customer-owned utility market was completed.
- The draft report describing the detailed SCE feeder study was completed.
- Inventoried the installed meter base in the five Mid-Atlantic states to assess advanced metering capability and conducted an advanced metering workshop for Mid-Atlantic utility commissioners and their staff.
- Developed a "tool box" to provide utility commissions and their staff easy access to background studies, technical reports and technical experts in the advanced metering area.
- Evaluated the DR business case in the Mid-Atlantic and identified several alternatives for Mid-Atlantic states to consider to improve the overall business case for DR.

Future Direction:

- Expand the efforts to define the DG benefits for customer-owned utility settings.
- Support the broad benefits study mandated by the 2005 Energy Policy Act.
- Support the National Research Council review of the End Use portion of the DE program.
- Coordinate the MADRI examination of the business case and advanced metering areas.
- Evaluate the possible definition and benefits of an optimal DE system.

Introduction

A large number of studies have been performed over the last 30 years that describe and quantify the benefits of Distributed Energy (DE) to system owners. These benefits typically include reduced utility expenses and the provision of back-up power. However, the establishment of a broader DE program at the Department of Energy (DOE) led to a number of questions regarding the benefits of DE to society in general, as well as to other stakeholders. These broader benefits are often poorly understood and difficult to quantify. In fact, the earliest analyses focused simply on listing possible benefits and their recipients. For example, total air emission reductions benefit society at large while voltage support may benefit only electric customers located in close proximity to the DE. The question becomes more complex as you try to assign monetary values to the benefits, and to address the issue that benefits to one group of stakeholders may involve added costs to other stakeholders. Over the past four years ORNL has studied the benefits of Distributed Energy Resources (DER) in several different areas. Case studies, quantification of market benefits to different stakeholders, an analysis of competing power sources, and a preliminary examination of DE benefits for customer-owned utilities were conducted, with reports and summary articles published for the broader industry. We have learned that broad national estimates must be supplemented with more localized studies and that defining a DE business case that is attractive to utilities can be most challenging. The most recent projects have examined the role of DE for municipal utilities and the ability of DE to defer T&D investment on specific circuits.

Accomplishments and Progress

One of this year's publications directly addressed a question that has been raised repeatedly regarding DE; will net emissions increase as DE displaces cleaner and more efficient central combined cycle (CC) power plants? This question is based on the premise that all the power produced by DE would have otherwise been produced at CC plants. However, the complex interactions within the market over time make it difficult to claim that DER displaces any single other capacity. A detailed examination was completed to look at a range of possible long-term market responses to DE: (1) no other change occurring in the rest of the system's capacity; (2) an equivalent amount of new gas-fired CC capacity not being built; and (3) the oldest and least-economical existing capacity retiring. It could be argued that the most likely scenario is a combination of these three bounding extreme cases. When the added emissions from the DER (with CHP) are summed with the reductions from the CC and thermal system, the result is a net lowering of emissions in all cases. As shown in Figure 1, the central station emissions actually increase in only one extreme scenario, that in which DE is only used for peaking, none of the DE includes waste heat recovery, and new CC capacity is canceled in an amount equal to the added DE capacity. In all of the other scenarios, and in all of the scenarios for baseload DER, the reduction in electric system NOX emissions alone is more than the increase from DER.

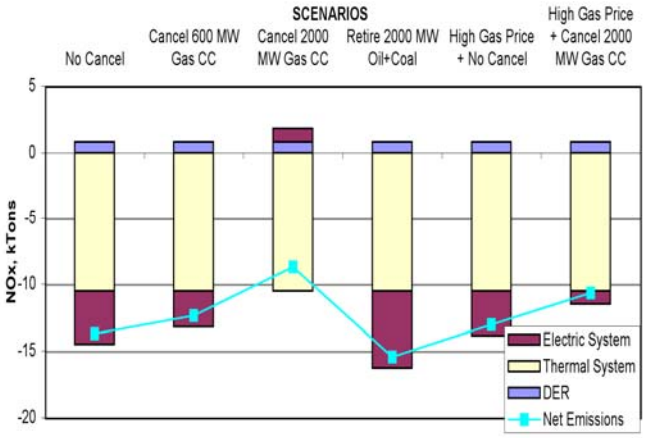

Figure 1. Net emissions from DER operating during weekdays only for different scenarios.
(Ref: http://www.eere.doe.gov/de/pdfs/genco.pdf)

Three assessments reported here share a common starting point, namely that energy cost savings for customers who operate DE often represent revenue reductions for the utility that serves that customer. Utilities have addressed this situation in a number of ways, few of which are conducive to the increased use of DE. These assessments are focused on finding mutually beneficial situations for the DE owner and the utility via: (1) examining utility market conditions unique to customer-owned utilities, (2) examining the DE potential to displace or defer T&D expansion investments, and (3) examining multiple business case models for DE.

Municipal utilities are actually owned by their customers, and may therefore offer one of the best opportunities to forge a DE implementation model that

benefits both the customers and the utility. Municipal utilities are also often motivated by energy security concerns and economic development objectives. During the initial stage of the assessment completed this year, we identified three municipal utilities with significant DE resources, but with very different operational paradigms. Heber Light & Power (HLP), the municipal utility in Heber City, UT, operates a combination of advanced gas-fired generators, diesel generators, and hydro with a total capacity of 12.5 MW, about half of the local peak demand (see Figure 2). They actively manage their equipment to interact with the market, dispatching power from their plants when hourly market prices rise above the operating cost. They are located on the end of a long 138 kV transmission line, so locating a portion of the power generation close to the load also improves the power quality. The McMinnville Electric System in McMinnville, Tennessee, operates a block of 11 diesel generators to provide peaking power to the TVA system and back-up power for the city of McMinnville. When operating, the 20 MW capacity of the installation provides approximately 40% of the city's total demand, and is tied into a critical care feeder circuit that services the local hospital and jail. In contrast to the HLP system, this system is only permitted to run a maximum of 350 h/year due to emissions limitations and is dispatched by TVA. The diesel generators provide voltage support to other power distributors 50 miles away. The Powell Valley Cooperative operates a system similar to that of McMinnville, but their system is also configured to provide black-start power if needed for a large central coal-fired station.

Figure 2. A portion of the Heber City complex

Another project examined whether DE could offer enough load relief to practically defer distribution system expansion costs, thereby reducing utility costs by an amount greater than the reduction in sales revenue associated with a DE installation. Two southern California feeders were selected, one in a suburban area and one in a rural area. The assessment sought to determine whether sufficient DE, at a price attractive to customers, could be installed to avoid the planned capacity expansion for these two circuits. With currently available California DE incentive payments, sufficient DE market penetration may indeed occur. A careful examination of the load profiles for the individual customers and for the circuit as a whole showed that the peak load could be reduced to a level that would eliminate the need to build additional distribution capacity, as shown in Figure 3. However, given current market prices and utility rates, the local utility would lose more in sales revenue than it would save in expansion costs, which are relatively low at these two locations. The assessment looked further to examine what types of changes to incentives or rates would change this outcome, for example by limiting the DE load relief to on-peak times only. It also summarized the broader spectrum of T&D expansion costs (which range from less than $100/kW to more than $1,000/kW) reported by utilities across the country over the last ten years. The assessment tool developed in this project could be used to define the minimum distribution expansion cost at which DE installations would be the preferred alternative from both the utility and customer perspective on any given circuit.

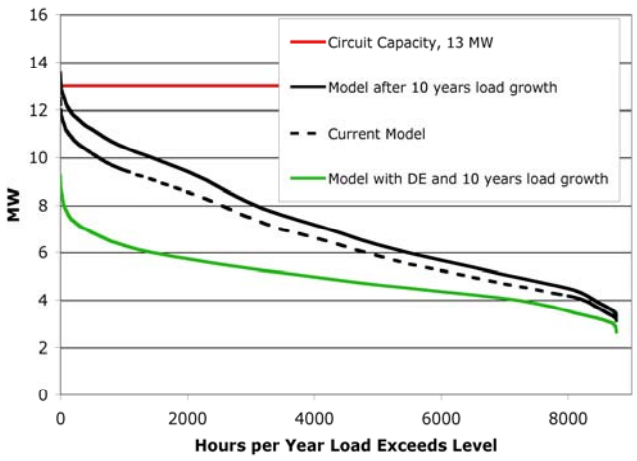

Fig. 3. Load duration curve shows ability of DE to defer T&D investments

The Mid-Atlantic Distributed Resources Initiative (MADRI) was established in June of 2004 to work with the states in the Mid-Atlantic region to enable self-

sustaining markets for distributed resources (DR). MADRI, with technical support from DOE, helps to coordinate state activities to remove barriers and create more favorable incentives to stimulate market activity for distributed resources. Two key focus areas for MADRI have been advanced metering and enhancement of the DR business case. One advanced metering project surveyed the installed meter base in the Mid-Atlantic to provide baseline data on the region's existing advanced metering capability. The survey revealed that most electric customers in the Mid-Atlantic region do not have advanced meters installed. This limits the development of dynamic pricing structures and subsequent deployment of distributed resources. Another project coordinated a workshop on advanced metering for state utility commissioners and developed the "MADRI AMI Toolbox" (shown in Figure 4) to provide utility commissioners and their staffs with easy access to business case evaluations, technical reports and technical experts in the advanced metering area.

For the MADRI DR business case task, coordination activities with the New Jersey/Pennsylvania STAC Distributed Resources Project revealed that the current business climate in the Mid-Atlantic poses significant challenges for DR and also revealed significant shortcomings or "gaps" in the revenues available to support the current DR business case. With the insights gained from this "gap" analysis, it became possible to identify specific types of actions state regulatory commissions could undertake to enhance the overall business case for DR. Several different options for states to consider are currently being developed and are to be presented to state utility commissioners in early 2006.

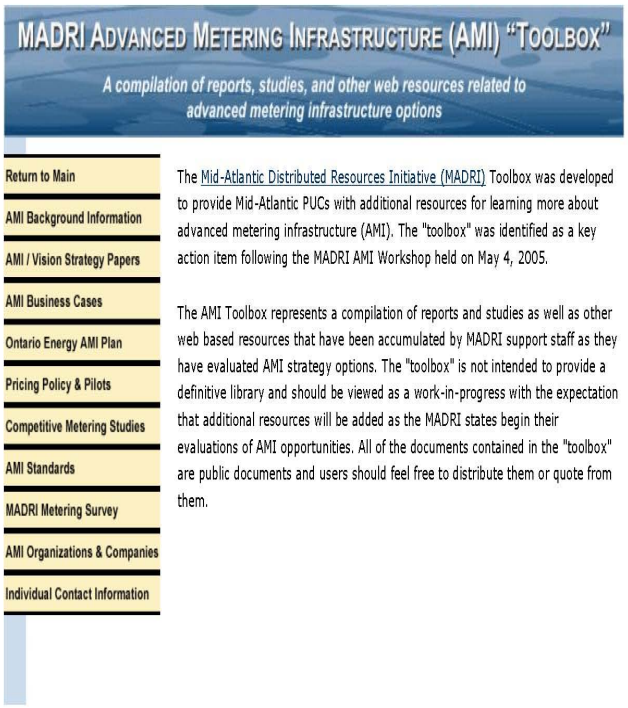

Figure 4. AMI Tool Box Graphic

Project Publications

(including those not covered in previous annual progress reports):

1. "Realizing the Full Potential of Distributed Resources," Brad Johnson, to be published.
2. "DER: Hastening Genco Obsolescence?," *Public Utilities Fortnightly*, May 2005.
3. "Distributed Generation: Benefit Values in Hard Numbers," *Public Utilities Fortnightly*, April 2005.
4. "Distributed Generation: Who Benefits?," *Public Utilities Fortnightly*, March 2005.
5. *The Effect of Distributed Energy Resource Competition With Centra,l* Oak Ridge National Laboratory, October 2003.
6. *Economic Potential of CHP In Detroit Edison Service Area: The Customer Perspective,* Oak Ridge National Laboratory, June 2003.
7. *Quantitative Assessment of Distributed Energy Resource Benefits,* Oak Ridge National Laboratory, May 2003.
8. *Connecting Distributed Energy Resources to the Grid: Their Benefits to the DER Owner/Customer,*

Other customers, the Utility, and Society, Oak Ridge National Laboratory, March 2002.

Presentations
(including those not covered in previous annual progress reports):

1. Rich Scheer, Energetics Inc., "Making a Business Case for Distributed Energy,"
2. Brad Johnson, consultant , "PJM Distributed Energy Market Opportunity Study."
3. Brad Johnson, "MADRI Business Models Subgroup Status Report," MADRI Working Group Meeting #9, Washington, DC.
4. Brad Johnson, "Business Model Abstracts,"Business Case Sub-Group Meeting, Philadelphia, PA.
5. Brad Johnson and Jim Torpey "Business model subgroup," MADRI Working Group Meeting #8, Washington, D.C.
6. Brad Johnson, , Key Summary Points and Action Items, MADRI Interconnection Sub Group Meeting, Philadelphia, PA.
7. Brad Johnson, "MADRI DR Business Case Task," MADRI Business Models Sub Group Meeting, Philadelphia, PA.
8. Brad Johnson, PAKey Summary Points and Action Items, MADRI Interconnection Sub Group Meeting, Philadelphia, PA.
9. Brad Johnson, "MADRI Interconnection Sub-Group Status Report," MADRI Working Group Meeting #7, Trenton, NJ.
10. Brad Johnson, Joe Kerecman, "MADRI Role in Developing Regional Interconnection Requirements," MADRI Steering Committee Meeting, Washington, DC.
11. Brad Johnson, Interconnection Discussion, MADRI Working Group Meeting #4, Newark, NJ.

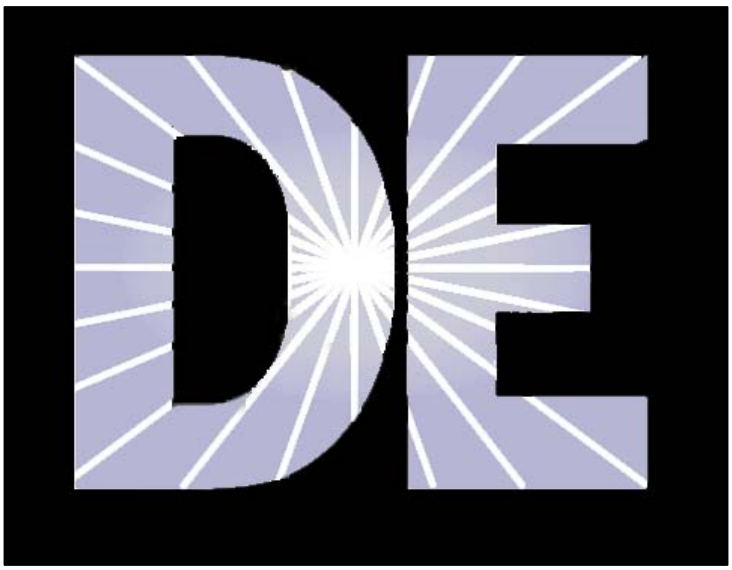

7.1 Fuels Combustion: Impact of Opportunity Fuel Combustion on Distributed Energy Platforms

John M. Storey[1], Peter Tortorelli[2]
[1]Fuels, Engines, and Emissions Research Center; [2]Corrosion Science and Technology Group
Oak Ridge National Laboratory
[1](865) 946-1232; fax: 946-1248; e-mail: storeyjm@ornl.gov
[2](865) 574-5119; fax: 865-241-0215; e-mail: tortorellipf@ornl.gov

DOE Technology Development Manager: Debbie Haught
(202) 586-2211; fax: 586-5860; e-mail: Debbie.Haught@EE.DOE.GOV
NETL Technical Monitor: William Cary Smith
(304) 285-4260; fax: 285-4403; e-mail: William.Smith@NETL.DOE.GOV
ORNL Technical Monitor: Tim Theiss
(865) 946-1348; fax: 946-1248; e-mail: theisstj@ornl.gov

Objectives

- Determine combustion characteristics and identify potential control parameters in accordance with the physical and chemical properties of selected fuels.
- Measure and analyze the emissions associated with the combustion of opportunity/ alternative fuels in multiple DE platforms, including unregulated emissions and hazardous air pollutants (HAPs) and assess the impact of these emissions on aftertreatment systems.
- Understand materials durability and reliability issues based on an assessment of the effects of the combustion of opportunity fuels.

Approach

- Measure and evaluate the combustion characteristics on a single cylinder reciprocating engine and a combustion burner operating on pre-determined opportunity fuels.
- Assess emissions, including criteria pollutants (e.g., nitrogen oxides) and HAPs, from engines operating on two opportunity/alternative fuels.
- For a given fuel, the relationships among materials behavior, the composition of the alloy or ceramic involved, the characteristic exhaust chemistry associated with combustion, thermodynamic predictions, and reaction kinetic parameters will be sought.
- Field evaluations of DE platforms using opportunity and alternative fuels will be compared with lab results for validation.

Accomplishments

- The opportunity fuel selected for future study in reciprocating engines will be as medium grade gaseous fuel with siloxane and H2S contaminants, simulating both landfill gas fuel and anaerobic digester gas. The opportunity fuel selected for turbine studies will be biodiesel.
- ORNL personnel visited Solar Turbine and University of California-Irvine (UC-I) to plan future turbine studies and collaborations. Input on opportunity fuel issues was also received from the reciprocating engine manufacturers.
- ORNL is collaborating with Brookhaven National Lab (BNL) in this work to compare results by using the same fuel in our turbine evaluations.

Future Direction

- Fabricate exhaust composition sampling device for use in follow up turbine and reciprocating engine studies.
- Conduct field evaluation of influence of biodiesel blends in a micro-turbine at UC-I.
- Develop degradation-erosion-corrosion models for turbine systems and reciprocating engines.
- Install and commission combustion rig and large bore gaseous-fueled single cylinder engine.
- Determine effects of fuel variables on combustion quality, emissions, and durability in single cylinder engine.
- Examine effects of liquid fuel on emissions and materials durability using burner rig.

Introduction

Opportunity and alternative fuels represent a largely untapped energy resource that could improve the energy security of the United States by providing a source of domestically available fuels for distributed generation systems. However, the lower quality of these fuels (i.e., lower heating value), operational and durability problems associated with contaminants in the fuels, and a lack of data on their emissions profiles have prevented their widespread use in conventional distributed energy (DE) platforms. Accordingly, Oak Ridge National Laboratory (ORNL) is performing combustion experiments on various opportunity and alternative fuels (real and simulated). Combustion measurements and/or analyses of byproduct chemistry will be used to, for a given fuel/platform, evaluate combustion quality, characterize the emissions profile, and examine materials issues limiting component lifetime (durability) (see Figure 1). The knowledge and understanding gained from such an approach can be used by industry to design and implement distributed generation systems capable of using opportunity/alternative fuels. Moreover, it will expand the potential for DE to provide the United States with secure, fuel-flexible, on-demand power (and heat).

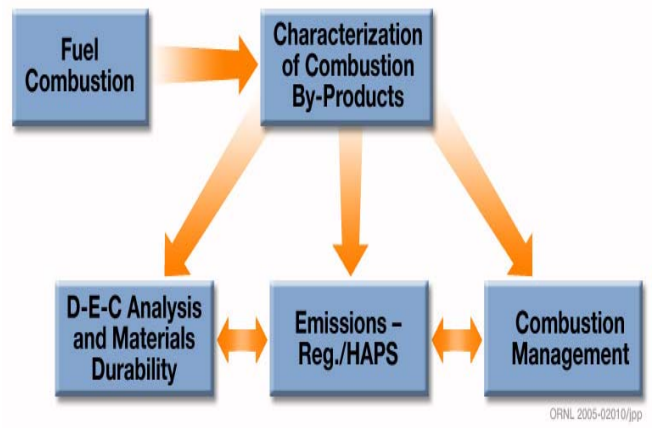

Figure 1. ORNL approach for a given fuel platform combination couples combustion, emissions, and materials interactions.

Uncertainties about the combustion characteristics and emissions resulting from the use of opportunity fuels are key barriers to their implementation. The combustion byproducts can lead to durability problems in engine materials. Therefore, effective utilization of opportunity fuels, and market viability of DE platforms using them, will require a thorough understanding of the combustion characteristics and emissions of these fuels. These fuels often contain large amounts of contaminants, which may form toxic and/or corrosive byproducts and limit their use in turbine and reciprocating engines.

In addressing materials concerns regarding the use of DE platforms operating on opportunity or alternative fuels, this project is motivated by the potential heightened threat of deposition, erosion, and corrosion (often designated, in the aggregate, as D-E-C[1]) caused by fuel contaminants, combustion byproducts, and/or significant changes in heat flux to the combustor and gas-path structures resulting from changes in ignition/firing conditions. D-E-C can lead to problems with materials durability and reliability and associated derating of engine/turbine systems (with potential substantial decreases in energy efficiency), combustion problems, fouling, and/or increased operating and maintenance costs.

A recent survey identified four of the most promising domestic opportunity fuel sources: landfill gas, anaerobic digester gas, gasified biomass fuels, and wood waste from the pulp and paper industry.[2] In recent years, the technology for collecting landfill gas has improved so that this opportunity fuel is starting to see more widespread utilization. However, the effectiveness of this resource would be enhanced through improved knowledge and control of the fuel combustion processes and resulting emissions. Anaerobic digester gas is currently used as a low-quality heating fuel but has potential for efficient use in distributed generation. Biomass fuels are typically associated with high collection and transport costs; thus distributed generation systems would need to be located at the collection points and the energy exported as electricity to realize the full potential of this fuel. Similarly, wood waste is often used to provide process heat for the originating paper plant; efficient co-generation at the site would improve the efficiency and economics of this resource.

Diesel fuel and biodiesel will become important as an alternative to natural gas when economic or gas availability/volatility concerns necessitate its use. Being able to quickly switch from NG to an alternative fuel (such as diesel) allows customers to negotiate significantly lower NG rates. Under such circumstances, it is desirable to maintain recent advances in efficiency and/or emissions reduction for NG-fired reciprocating engines, microturbines, and industrial turbines when using diesel fuel. Each of the fuels described earlier can alter combustion sufficiently that existing engines and

turbines will not economically burn them. The exact fuel selected for future use is detailed in the Results Section below.

Approach

Combustion Analysis

ORNL will measure and evaluate the combustion characteristics for two DE platforms operating on pre-determined opportunity fuels. The platforms will include a single-cylinder reciprocating research engine and a burner to simulate turbine combustion. The combustion process will be characterized using in-cylinder pressure transducers, as well as by applying powerful analytical methods to the chemical constituents of the exhaust gases. The combination of thermodynamic and exhaust chemistry information will result in a more complete description of the combustion process than is usually available. This level of insight is important for evaluating the platform-specific combustion characteristics of opportunity fuels, as well as for providing insight into pathways for improved operation in conventional and, eventually, advanced combustion modes. Experimental combustion analysis will be coupled with analytical combustion models for comparison.

We anticipate the wide-ranging properties of opportunity fuels will have significant effects on the combustion process. These effects will include issues associated with ignitability, combustion phasing, stability, and materials effects, which will be discussed in a later section. ORNL will experimentally address the combustion issues through detailed characterization as described. Note that this investigation will be limited to production-type geometries and control parameters but will provide insight into potential modifications (e.g., compression ratio) that would result in improved operation with these fuels for the long term. ORNL also has experience in high-speed adaptive control of inherently unstable cyclic combustion processes. While it is beyond the scope of the proposed activity, the experimental results of this investigation will be useful in addressing the suitability of control techniques for this application. The expected outcome of this portion of the investigation is improved insight into combustion management methods for enabling the use of these fuels in DE platforms.

Assessment of Emissions and Combustion Byproducts

ORNL will assess emissions, including criteria pollutants (e.g., nitrogen oxides) and HAPs, from engines operating on at least two opportunity/alternative fuels. The emissions from opportunity fuels are a potential barrier to their use; the poor combustion may result in excessive emissions, and fuel contaminants may result in poisons for catalytic aftertreatment devices. In addition, the information gathered can be used for engine/combustion model validation as well as for improving the understanding of the combustion process. An understanding of the emissions can also help to identify potential emissions controls technologies (including combustion modification techniques and exhaust aftertreatment).

HAPs were measured in a large NG reciprocating engine and found to depend heavily on combustion parameters such as air–fuel ratio.[3] We expect that the combustion of opportunity fuels will result in HAPs, some of which may not have been observed in exhaust previously, because of the unusual chemistry associated with the fuels themselves. In another study,[4] contaminants in exhaust were compared with microstructural analysis of the catalyst (see Figure 2). A significant finding was that the extent and type of catalyst poisoning was dependent on the chemical form of the contaminant in the exhaust. The combustion of opportunity/alternative fuels will likely result in byproducts that can similarly poison catalysts. ORNL has a unique capability and reputation for detailed characterization of exhaust emissions; this understanding will be used to help enable the adoption of opportunity/alternative fuels.

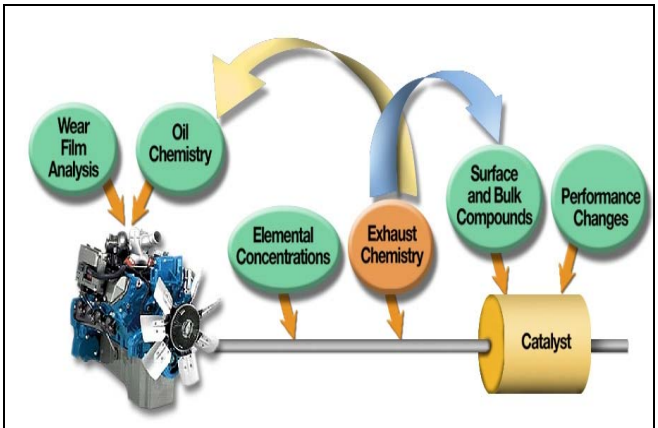

Figure FC.2. Exhaust chemistry measurements can provide a link among fuel chemistry, engine-related effects, and catalyst effects.

Materials Durability
For a given fuel, the relationships among materials behavior, the composition of the alloy or ceramic involved, the characteristic exhaust chemistry associated with combustion, thermodynamic predictions, and reaction kinetic parameters will be sought. With this approach, some aspects of materials selection and lifetime prediction/reliability can be addressed for the specific cases studied. The understanding developed as part of this work can then be used to predict the responses of alloys and ceramics in engines/turbines operating on different fuels or with modified fuel pretreatments/combustor designs, and used as input into materials development for improved performance.

For each fuel/platform combination, this work will consist of (1) use of the data from the in-situ analysis of combustion byproducts for thermochemical and kinetic evaluation of the potential for deposition (including coking) and corrosion in the combustor and along the exhaust gas path and (2) characterization of the effects of exposure on specimens (from rigs or field tests) or components (from field tests). This effort will include various methods of microstructural analysis and determination of retained properties that affect reliability.

The in-situ gas analysis will provide valuable real-time environmental data for evaluating the potential for D-E-C. Post-exposure materials characterization work can use such chemical information, when linked to appropriate thermochemical models, to better define the underlying mechanisms of observed degradation or deposition and, in some cases, to correlate results with specific reactive species and their concentrations in the gas phases and/or to particular operational procedures. (This will be of great value in comparing results from the laboratory environment with those from the field.) The gas analyses can also provide information about time-dependent processes and, with sampling along the gas path, about temperature and flow effects on D-E-C.

Standard thermochemical modeling (principally involving FACTSage™) will be used to examine the potential for deposition and corrosion product formation based on key environmental variables—reactant activities derived from the gas analysis, pressures, and temperatures as a function of position along the gas path. Differences between what is predicted from this equilibrium thermodynamics approach and what is observed from the materials characterization efforts will yield crucial information about kinetic limitations and can bound what is possible in terms of extrapolation to/prediction about other fuel-platform systems. In addition, kinetic modeling using, for example, Chemkin™ can be applied to address time-dependent aspects of deposition and corrosion.

Laboratory and Field Studies
For combustion studies, opportunity fuels will be simulated with synthetic gas mixtures so that the energy content can be carefully controlled and studied. Key contaminants will be included so that a simulated gas is representative of opportunity fuels with respect to their lower quality, potential HAPS, and material durability. We will conduct field evaluations of DE platforms using opportunity and alternative fuels to compare with lab results. This comparison will provide the necessary materials compatibility and gas composition data for validation of the laboratory evaluations. Field tests will include at least one reciprocating engine company and a diesel-fired microturbine system operating at the University of California–Irvine. In-situ combustion byproduct analysis will be conducted during these field tests, and post-exposure microstructural characterization will be used to examine possible materials degradation modes.

ORNL is procuring a large-bore single-cylinder engine designed to match the new ARES Waukesha engine (APG). The single cylinder engine will be the workhorse for combustion quality studies for the duration of this project. In addition, we are purchasing a combustor rig which will be able to simulate turbine systems and allow for the exposure of coupons in the exhaust. Both of these systems are expected in the first quarter of FY2006.

Results
The ARES (Advanced Reciprocating Engine System) manufacturers (Caterpillar, Cummins, and Waukesha) and others knowledgeable in the field were polled about the use of opportunity fuels and the optimum gaseous fuel for use in our future examinations of reciprocating engines. Through these interviews and literature surveys, the following observations are offered:

- Although reciprocating engines operate on a variety of opportunity fuels today, there are still significant gaps in their operation and additional development is

necessary before engines are capable of operating optimally on these low quality fuels.
- The market needs established equipment protocols so that fuel clean-up devices and engines can be designed to mate to each other.
- Landfill gas (LFG) is considered one of the more difficult opportunity fuels to deal with due to the high siloxane content, the sulfur contamination, and lower heating value or quality.

Based on this input and our literature review, ORNL has decided that the gaseous opportunity fuel for future use will simulate landfill gas and anaerobic digester gas (ADG). The market pull for these fuels is very strong now and understanding their combustion will aid all other opportunity fuels. Medium quality fuels (~500 Btu/ft^3) with siloxane and H_2S contamination will simulate LFG and ADG well (landfills are considered poor anaerobic digesters anyway). The exact contaminant level will be set as the engine evaluations begin.

ORNL is also interacting with Dr. C. R. Krishna at Brookhaven National Lab (BNL) in order to collaborate with them on our fuels combustion projects. BNL is investigating biodiesel blends in micro-turbines, which can couple well with our project. Based in part on this interaction, ORNL has decided to use biodiesel as the liquid fuel for use in turbine systems in this project. The exact blend will be selected with input from UC-I and BNL.

ORNL personnel visited Solar Turbines and University of California-Irvine (UC-I) to learn more about their work and interests in the fuel flexibility of turbines and micro-turbines. The following directions resulted from these collaborations:

- Turbine end-users are placing a very high value on fuel flexibility and demanding the ability to quickly switch between gaseous and liquid fuels.
- Solar is interested in adapting their Mercury 50 turbine to burn opportunity fuels. They are converting it to burn landfill gas now and are hoping the collaboration with ORNL will help them convert the unit to diesel and biodiesel.
- There is a need for measuring unregulated emissions in turbine systems burning opportunity fuels.
- UCI is using Capstone 30 & 60 and is very interested in biodiesel fuel. They will be helping with the characterization of the fuel spray and are willing to assist ORNL with coupon exposures and materials,

Conclusion

The use of opportunity fuels in today's energy market is growing and the market is providing significant "pull" for inclusion of these types of fuels. Transportation costs will limit the use of these fuels in large-scale power plants but the use of these fuels in distributed generation systems is ideal. However, engines and turbines today need additional expensive equipment for clean up, processing and burning these fuels, which creates unsustainable market. DE platforms need to be able to operate effectively under wide ranges of fuel variability rather than "backing off" of optimum control points. This investigation will lead to improvements in the ability of engines and turbines to economically and effectively use these abundant, low quality fuels providing a hedge against NG volatility and improving energy security.

References

1. R. A. Wenglarz and I. G. Wright, "Alternative Fuels for Land-Based Turbines," pp. 4–45 to 4–64 in *Proceedings of the Workshop on Materials and Practices to Improve Resistance to Fuel-Derived Environmental Damage in Land- and Sea-Based Turbines*, EPRI No. 1009173, October 2003.
2. "Combined Heat and Power Market Potential for Opportunity Fuels—Tasks 1 & 2," draft report prepared by Resource Dynamics Corporation, August 2004.
3. J. M. Storey et al., "Regulated and Unregulated Emissions from a Stoichiometric 250-kW Natural Gas Engine," ASME ICEF 2004-987, 2004.
4. B. G. Bunting, K. More, S. Lewis, and T. Toops, "Exhaust Phosphorous Chemistry and Catalyst Poisoning," presented at 2004 Diesel Engine Emissions Reduction Conference, Coronado, California, August 2004.